

Chemistry of the Trifluoromethoxy Group: From Nucleophilic Transfer Reagents to Fluorinated Sulfur Compounds

Inaugural-Dissertation
to obtain the academic degree
Doctor rerum naturalium (Dr. rer. nat.)

submitted to the Department of Biology, Chemistry,
Pharmacy
of Freie Universität Berlin

by

Paul Golz

2024

The work for this thesis has been conducted between Mai 2019 and July 2024 under the supervision of Prof. Dr. Sebastian Hasenstab-Riedel at the Institute of Chemistry and Biochemistry of Freie Universität Berlin.

1st reviewer: Prof. Dr. Sebastian Hasenstab-Riedel, Freie Universität Berlin

2nd reviewer: Prof. Dr. Berthold Hoge, Universität Bielefeld

Date of defense: 08.11.2024

Acknowledgement

First of all, I would like to thank Prof. Dr. Sebastian Hasenstab-Riedel for giving me the opportunity to work on this interesting and future-oriented topic. His support and guidance were invaluable in completing this thesis.

I would also like to thank Prof. Dr. Berthold Hoge for kindly accepting the role of second reviewer.

My gratitude goes to Lilian Maas, Kamar Shakeri, Stefan Dix, and Gesa Dreyhsig for their fruitful collaboration. I would also like to thank all the people from the Solvay project for their help.

I am especially grateful to Dr. Helmut Beckers for his support, insightful discussions, and lessons throughout my work until his retirement. I would also like to thank Dr. Simon Steinhauer, Dr. Julia Bader, Dr. Günther Thiele, and Dr. Merlin Kleoff for their scientific guidance, valuable discussions, and help in writing the manuscripts. Special thanks go to Dr. Patrick Voßnacker and Dr. Marlon Winter, who became mentors of sorts during this journey. Both of you always had an open ear for my problems and worries, and I deeply appreciate your mental and scientific support. Thomas Drews, thank you for the practical discussions and support.

I would like to thank my students Clara Schritt, Helen Kemmler, Paul Maruska, Marius Balizs, Nils Gerwien, Pascal dos Santos Vieira, and Gesa Dreyhsig for their excellent work and the wonderful time we spent together in the lab.

I am grateful for the support of the entire AC, including the secretariats, workshops, and materials management, as well as BioSupraMol and ZEDAT for their work and support.

Thanks to the the whole AG Riedel for the wonderful time, the memorable moments and the many evenings spent together, as well as the social activities and the movie evening(s), especially during the COVID pandemic. My thanks also go to all the people I shared the lab with in U408 and later in U308 - Thomas Drews, Holger Pernice, Dr. Marlon Winter, Johanna Schlögl, and Gesa Dreyhsig.

Over the years, some colleagues have become friends. Marlon, Vossi, Jonas, Luise, Benny, Tyler, Karsten, Gene, Helen, Jan, Freddy, Maite, Lili, Gesa, Niklas, Johanna, Marius. I am deeply grateful for so many unforgettable moments, activities and travels together. I am especially grateful for the sports evenings in the bouldering/climbing gym and on the squash and tennis courts.

Finally, I am grateful to my family for their support over the years and their belief in me.

Declaration of Authorship

I hereby declare that I alone am responsible for the content of my doctoral dissertation and that I have only used the sources or references cited in the dissertation.

Berlin, 30.07.2024

Paul Golz _____

List of Abbreviations

BDEs	Bond dissociation energies
CF ₃ OSF ₅	Trifluoromethoxy sulfur pentafluoride
CF ₃ OSO ₂ F	Trifluoromethyl fluorosulfonate
CFCs	Chlorofluorocarbons
COF ₂	Carbonyl fluoride
DNTFB	2,4-Dinitro(trifluoromethoxy)benzene
DS	Dielectric strength
ECHA	European Chemicals Agency
FDMI	2-Fluoro-1,3-dimethylimidazolidinium
F-Gas	Fluorinated gases
GC-IR	Gas chromatography – infrared spectroscopy
GED	Gasphase electron diffraction
GWP	Global warming potential
HFC-1234yf	2,3,3,3-Tetrafluoropropane
HFC-134a	1,1,1,2-Tetrafluoroethane
HFCs	Hydrofluorocarbons
IR	Infrared
LC	Lethal concentration
Nf ⁻	Nonaflate anion
NHCs	<i>N</i> -Heterocyclic carbenes
-OCF ₃	Trifluoromethoxy group
ODP	Ozone Depleting Potential
PCAs	Perfluoroalkyl carboxylic acids
PEMs	Proton exchange membranes
PFA	Perfluoroalkoxy alkane
PFAS	Poly and perfluorinated alkyl substances
PFCs	Perfluorocarbons
PFHS	Perfluorohexanesulfonic acid
PFOA	Perfluorooctanoic acid
PFOS	Perfluorooctanesulfonic acid
pip ⁺	1,1,3,3,5,5-Hexamethylpiperidinium
PMVE	Perfluoromethyl vinyl ether
POPs	Persistent Organic Pollutants

PSAs	Perfluoroalkyl sulfonic acids
PTFE	Polytetrafluoroethylene
PVDF	Polyvinylidene difluoride
REACH	Registration, Evaluation, Authorization, and Restriction of Chemicals
TEMPO	(2,2,6,6-Tetramethylpiperidin-1-yl)oxyl
TFA	Trifluoroacetic acid
TFE	Tetrafluoroethylene
TFMBz	Trifluoromethyl benzoate
TFMNf	Trifluoromethyl nonaflate
TFMS	Trifluoromethyl sulfonates
TFMTf	Trifluoromethyl triflate
UNFCCC	United Nations Framework Convention on Climate Change
XRD	X-ray diffraction
ΔH	Reaction enthalpy

Table of Contents

1	Introduction	1
1.1	The Element Fluorine	2
1.2	Natural Organic Molecules Containing Fluorine	3
1.3	Stability of the C–F Bond and Properties of Fluorinated Molecules	4
1.4	Environmental Concerns Related to Fluorinated Compounds	6
1.4.1	Persistent Fluorinated Compounds	8
1.4.2	Extensive PFAS Regulation in the European Union	8
1.4.3	Regulation of SF ₆ , its Applications and its Regulation	9
1.4.4	Environmental Impact of Potential SF ₆ Alternatives	10
1.5	Possible Solutions for a More Sustainable Fluorine Chemistry	13
1.6	Approaches for Synthesizing –OCF ₃ Compounds.....	15
1.6.1	Construction of the –OCF ₃ Group - Indirect Approach	15
1.6.2	Radical Trifluoromethoxylation.....	17
1.6.3	Trifluoromethoxylation-Halogenation with Trifluoromethyl Hypohalites.....	19
1.6.4	Nucleophilic Substitution.....	20
2	Objectives	25
3	Publications	26
3.1	Silver(I) Perfluoroalcoholates: Synthesis, Structure, and their Use as Transfer Reagents	26
3.2	Trifluoromethyl Fluorosulfonate (CF ₃ OSO ₂ F) and Trifluoromethoxy Sulfur Pentafluoride (CF ₃ OSF ₅) – Two Gaseous Sulfur(VI) Compounds with Insulating Properties	36
4	Conclusion and Outlook	44
4.1	Conclusion.....	44
4.2	Outlook.....	48
5	References	50
6	Publications, Patents and Conference Contributions	58
6.1	Publications	58
6.2	Patents	59
6.3	Conference Contributions – Oral and Poster Presentations	59
7	Curriculum Vitae	60
8	Appendix	61
8.1	SI of Silver(I) Perfluoroalcoholates: Synthesis, Structure, and their Use as Transfer Reagents	61
8.2	SI of Trifluoromethyl Fluorosulfonate (CF ₃ OSO ₂ F) and Trifluoromethoxy Sulfur Pentafluoride (CF ₃ OSF ₅) – Two Gaseous Sulfur(VI) Compounds with Insulating Properties	138

Abstract

In this work, a general and direct method for the synthesis of silver(I) perfluoroalcoholates has been investigated, including an examination of their structural properties in both solid state and solution, as well as an evaluation of their effectiveness as transfer reagents. The synthesis was performed by reaction of AgF with corresponding perfluorinated carbonyl compounds in acetonitrile (MeCN). The obtained silver(I) perfluoroalcoholates in MeCN were found to be stable at $-18\text{ }^{\circ}\text{C}$ over months. X-ray crystallographic analysis of the perfluoroalcoholate single crystals revealed a structure characterized by silver centers bridged by alcoholate ligands, while two alcohol ligands coordinate to one silver center. In acetonitrile solutions, $\text{Ag}[\text{OCF}_3]$ adopts a variety of structural forms as shown by IR spectroscopy. Furthermore, these silver(I) perfluoroalcoholates were found to be valuable as user-friendly transfer reagents, facilitating the synthesis of $\text{Cu}[\text{OCF}_3]$, $\text{Cu}[\text{OC}_2\text{F}_5]$, $[\text{PPh}_4][\text{Au}(\text{CF}_3)_3(\text{OCF}_3)]$, and various fluorinated alkyl ethers.

Trifluoromethyl fluorosulfonate ($\text{CF}_3\text{OSO}_2\text{F}$) and trifluoromethoxysulfur pentafluoride (CF_3OSF_5), both bearing the $-\text{OCF}_3$ moiety, were investigated regarding their dielectric behavior. Both compounds exhibit higher breakdown voltages compared to sulfur hexafluoride (SF_6), with averaged relative breakdown voltages of 1.3 ± 0.2 for $\text{CF}_3\text{OSO}_2\text{F}$ and 1.4 ± 0.2 for CF_3OSF_5 , compared to 1.0 for SF_6 . This makes them promising candidates for dielectric applications where higher voltage tolerance is necessary. During an electrical breakdown, both compounds, $\text{CF}_3\text{OSO}_2\text{F}$ and CF_3OSF_5 , decompose in a rate similar to that of the dielectric $(\text{CF}_3)_2\text{CFCN}$. The decomposition behavior was analyzed using IR spectroscopy and GC-IR techniques to identify the decomposition products. Moreover, the molecular structures of these compounds were successfully obtained using *in situ* crystallization methods. In addition, evaluations of their physical properties, including vapor pressure, critical parameters, and melting points, were performed. These assessments further demonstrated the viability and performance of these materials as dielectric materials.

Kurzzusammenfassung

In dieser Arbeit wurden eine generelle Methode zur Synthese von Silber(I)-perfluoroalkoholaten, ihre strukturellen Eigenschaften, sowohl im festen Zustand als auch in Lösung, sowie eine Bewertung ihrer Wirksamkeit als Transferreagenzien untersucht. Die Synthese wurde durch die Reaktion von AgF mit entsprechenden perfluorierten Carbonylverbindungen in Acetonitril durchgeführt. Es wurde festgestellt, dass diese Verbindungen bei -18 °C über mehrere Monate stabil gelagert werden können. Die Röntgenkristallanalyse der Perfluoralkoholat-Einkristalle zeigte Ag(I)-Zentren, welche durch Alkoholat-Liganden verbunden sind. Die IR-spektroskopische Analyse wies darauf hin, dass Ag[OCF₃] eine Vielzahl von Strukturformen in Acetonitrillösung aufweist. Darüber hinaus erwiesen sich diese Silber(I)-perfluoroalkoholate als besonders wertvolle und benutzerfreundliche Transferreagenzien, welche die Synthese von Cu[OCF₃], Cu[OC₂F₅], [PPh₄][Au(CF₃)₃(OCF₃)] und verschiedenen fluorierten Alkylethern erleichtern.

Trifluormethylfluorosulfonat (CF₃OSO₂F) und Trifluormethoxyschwefelpentafluorid (CF₃OSF₅), die beide die –OCF₃ Einheit enthalten, wurden hinsichtlich ihres dielektrischen Verhaltens untersucht. Beide Verbindungen wiesen im Vergleich zu Schwefelhexafluorid (SF₆) höhere Durchschlagsspannungen auf, mit durchschnittlichen Werten von $1,3 \pm 0,2$ für CF₃OSO₂F und $1,4 \pm 0,2$ für CF₃OSF₅, verglichen mit 1,0 für SF₆. Dies macht sie zu vielversprechenden Kandidaten für dielektrische Anwendungen, für die höhere Spannungstoleranzen erforderlich sind. Bei einem elektrischen Durchschlag zersetzen sich beide Verbindungen, CF₃OSO₂F und CF₃OSF₅, mit einer ähnlichen Geschwindigkeit wie das Dielektrikum (CF₃)₂CFCN. Das Zersetzungsverhalten wurde mittels IR-Spektroskopie und GC-IR-Techniken analysiert, um die Zersetzungsprodukte zu identifizieren. Darüber hinaus wurden die Molekülstrukturen der Verbindungen mit Hilfe von In-situ-Kristallisationsmethoden erfolgreich ermittelt. Außerdem wurden ihre physikalischen Eigenschaften, einschließlich Dampfdruck, kritischer Parameter und Schmelzpunkte, ermittelt. Diese Untersuchungen haben die Eignung und Leistungsfähigkeit dieser Materialien als Dielektrikum weiter belegt.

"The most exciting phrase to hear in science, the one that heralds new discoveries, is not -Eureka!- (I found it!) but -That's funny ...-"

— Isaac Asimov

1 Introduction

Fluorinated compounds have emerged as important components in various sectors due to their unique chemical properties derived from the substitution of hydrogen with fluorine. Molecules with fluorine substituents or fluorinated groups at specific positions can exhibit enhanced metabolic stability, lipophilicity, and bioactivity, making them highly valuable in pharmaceuticals and agrochemicals. Molecules with high fluorine content also possess remarkable properties such as high stability, low-reactivity, and resistance to heat and chemicals. Moreover, these compounds exhibit water and dirt repellency, rendering them optimal for incorporation into fabrics, carpets, and paper products. Fluorinated polymers, used in non-stick cookware, gaskets, seals, and bearings, are appreciated for their high chemical resistance and durability, making them suitable for coatings, cables, and hoses. Hydrofluorocarbons (HFCs) and perfluorocarbons (PFCs) are widely used as refrigerants due to their high efficiency and low flammability. In the electronics industry, fluorinated compounds are essential in the manufacturing of semiconductors, display panels, and other components due to their excellent insulating properties and chemical resistance. They are also used as etchants for the preparation of electrical boards.^[1-5]

However, the widespread use and persistence of fluorinated compounds has raised concerns regarding their environmental effects, human exposure, and potential adverse effects on ecosystems and health. Poly- and perfluorinated alkyl substances (PFAS) have garnered particular attention due to their persistence in the environment and bioaccumulative tendencies. Understanding the behavior, fate, and impacts of fluorinated compounds is crucial for developing sustainable strategies to mitigate their environmental footprint and safeguard human and environmental health. Over the time regulations like the Montreal protocol (1987),^[6] the Kyoto protocol (1997),^[7] the Stockholm Convention on Persistent Organic Pollutants,^[8] and restrictions under REACH^[5,9] have been made or are planned.^[10,11]

For some applications different technologies have already been found, which do not use PFAS. However, for applications where the technical solutions are no suitable alternatives, chemical solutions are required. Therefore, we need to understand the properties of fluorinated molecules especially of carbon-based organic molecules, where the nature of the C–F bond influences the properties and adopt concepts to find substances, which have similar properties, but are better decomposable to replace environmental unfriendly fluorinated compounds.

1.1 The Element Fluorine

Fluorine, known for its high reactivity and high oxidizing power, forms compounds with all elements except helium and neon. Therefore, the toxic gas does not occur in its elemental form on Earth, except for areas with high energy irradiation, like from the decay of uranium. Normally fluorine would react immediately with the surrounding but trapped in the inert fluorite mineral called stinkspar, the element is stable.^[12,13]

Elemental fluorine was isolated for the first time by Henry Moissan in 1886 by the electrolysis of a mixture of HF and KF. Over the time the process was improved, while fluorine is nowadays produced at a rate of approximately 27 kilotons per year by electrolysis of HF, which is mainly derived from fluorite minerals and sulfuric acid. Despite the high reactivity, some metals, such as nickel, copper, or stainless steel, can withstand fluorine due to passivation, where a stable fluorinated surface layer forms. However, this passivation is not effective under high temperatures or high pressure. For instance, iron alloys, including stainless steel, react with fluorine when the temperature exceeds 200 °C or the fluorine pressure surpasses approximately 30 bar. Consequently, fluorine production facilities are typically integrated directly with downstream equipment because elemental fluorine is challenging to store and handle due to its reactive nature. The produced fluorine is primarily used (Figure 1) to manufacture the insulating gas SF₆ (32 %), various compounds such as COF₂, CF₄, WF₆, or IF₅ (10 %), and the largest portion is used to produce UF₆ (58 %).^[1,3]

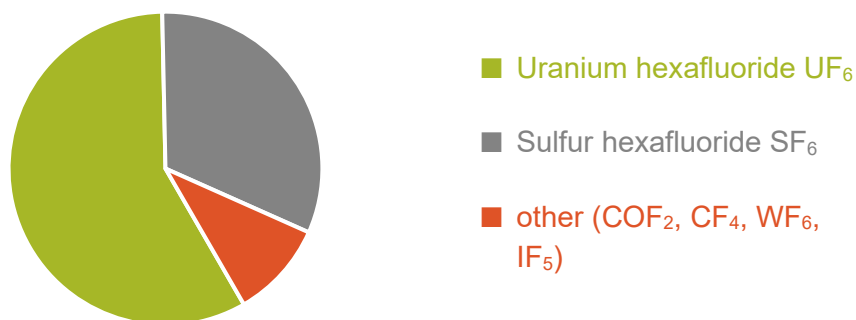


Figure 1: Use of elemental fluorine for the preparation of follow-up products. Data were taken from literature^[1].

UF₆ plays a central role in the uranium enrichment process, serving as the essential intermediate compound that facilitates the separation of the fissile isotope ²³⁵U from the non-fissile isotope ²³⁸U. Its volatility makes it suitable for use in enrichment technologies such as gas diffusion and gas centrifuge process. These processes rely on the slight mass difference between ²³⁵U and ²³⁸U isotopes, since fluorine is a monoisotopic element. This leads to a mass difference of about 0.85 % between the main isotopologues ²³⁵UF₆ and ²³⁸UF₆, allowing for the gradual increase in the concentration of ²³⁵UF₆. Beside these inorganic fluorine compounds, fluorine substituents are also very important moieties in especially carbon-based organic substances.^[1,3]

1.2 Natural Organic Molecules Containing Fluorine

Nowadays a huge number of fluorinated organic molecules exist, while there is only a small number of natural occurring fluorinated organic molecules known, which are mainly bioactive. The incorporation of fluorine substituents into organic molecules can dramatically alter the chemical and biological behavior due to fluorine's small atomic size and high electronegativity. For example, fluoroacetate, after conversion to (2*R*,3*R*)-2-fluorocitrate, inhibits the enzyme aconitase and therefore the whole citrate cycle, a fundamental process in the production of cellular energy. This inhibition is toxic to animals and serves as a potent defense mechanism for the plants that produce it. Other examples include monofluorinated ω -fatty acids, nucleocidin, and 4-fluorothreonine (Figure 2). In these compounds, the introduction of a fluorine atom notably alters their properties and actions. The presence of fluorine can affect molecular shape, polarity, and stability, leading to diverse effects on biological processes. These examples underscore the importance of understanding the role of fluorine in nature and its potential applications in fields such as medicine and agriculture.^[3,14] However, this implies that all of the other substances that occur in the environment have been created by humans.

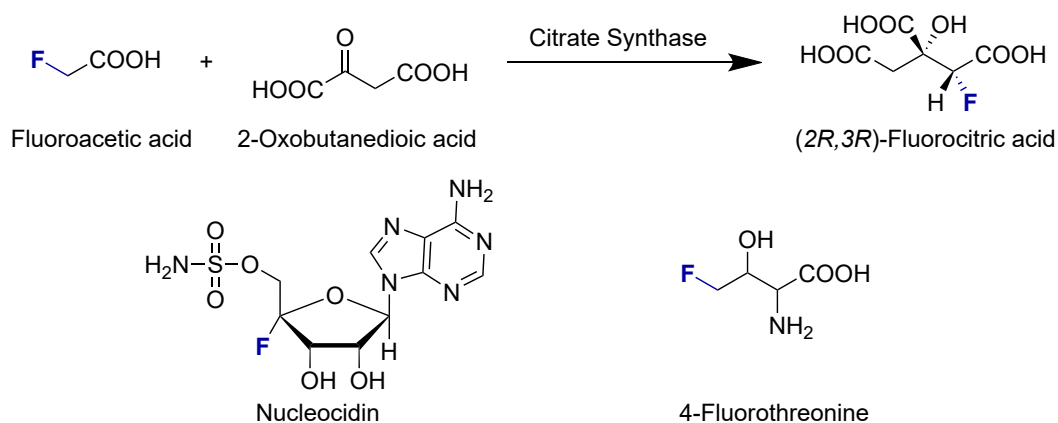


Figure 2: Natural bioactive compounds containing one fluorine atom.

1.3 Stability of the C–F Bond and Properties of Fluorinated Molecules

The properties of fluoroorganic compounds are based to a large extent on the C–F bond, which is the strongest single carbon-element bond with an energy of 481 kJ mol^{-1} in CH_3F . This bond is considerably stronger than the C–H bond (439 kJ mol^{-1} in CH_4) and C–Cl bond (350 kJ mol^{-1} in CH_3Cl).^[15] Moreover, the C–F bond energy increases with fluorine content, from 481 kJ mol^{-1} in CH_3F to 550 kJ mol^{-1} in CF_4 . A similar trend is observed with the decrease in the C–F bond length, from 140 pm in CH_3F to 130 pm in CF_4 (Figure 3). The strong C–F bond can be explained by the good orbital overlap of the $2s$ and $2p$ orbitals of fluorine and carbon. As a result, perfluorocarbons are very stable compounds that decompose only at high temperatures. For instance, the perfluorinated polymer polytetrafluoroethylene (PTFE) decomposes above $400 \text{ }^\circ\text{C}$, shorter perfluoroalkanes such as C_2F_6 decompose above $1000 \text{ }^\circ\text{C}$, and CF_4 does not decompose until temperatures above $2000 \text{ }^\circ\text{C}$. The difference in the decomposition temperatures is based on the decomposition pathway. In CF_4 only the very stable C–F bonds can be cleaved at extreme temperatures, while the longer perfluoroalkanes can decompose via the C–C bond cleavage.^[3,4] This can also be used for the depolymerization of PTFE under reduced pressure yielding mainly the monomer tetrafluoroethylene (TFE).^[16]

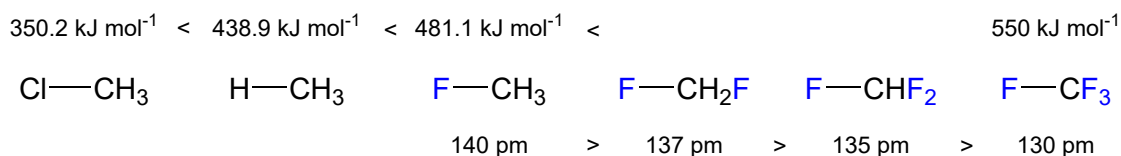


Figure 3: Comparison of bond enthalpies and C–F bond lengths of methane derivatives. Data were taken from literature.^[3,15]

The larger size of the fluorine atom compared to the hydrogen atom is responsible for the difference in structure between fluorinated and non-fluorinated molecules. The perfluorinated carbon chains are slightly twisted into a helical structure due to the steric repulsion of the fluorine substituents, while the similar hydrocarbon chains are zigzagged (Figure 4, top). The high electronegativity of fluorine additionally results in an inverted polarization of the C–F bond compared to the C–H bond. This can lead to a different charge distribution in the molecules as it is known for the fluorinated benzene derivatives. In hexafluorobenzene, the negative partial charge is predominantly localized on the fluorine atoms, resulting in a relatively positive charge on the central carbon ring. In contrast, in benzene, the hydrogen atoms bear a positive charge, while the carbon ring carries a negative charge (Figure 4, bottom). This also results in a different reactivity. The non-fluorinated benzene is usually attacked by electrophiles, while the fluorinated benzene is attacked by nucleophiles.^[3,4]

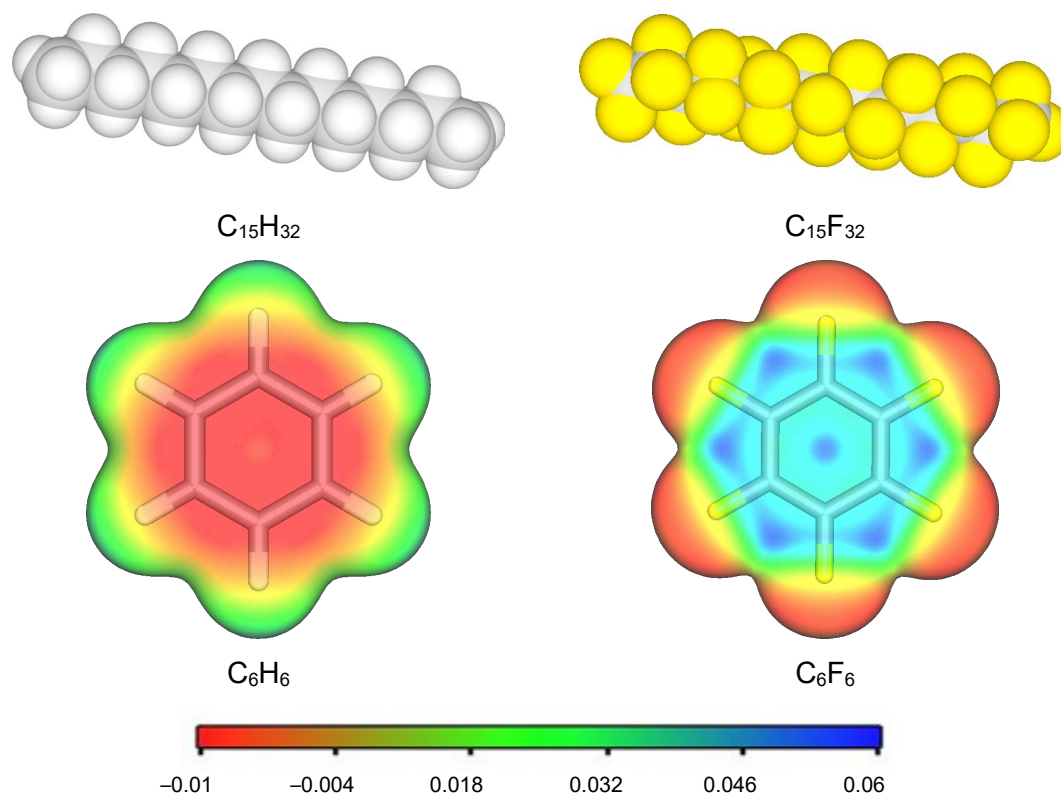


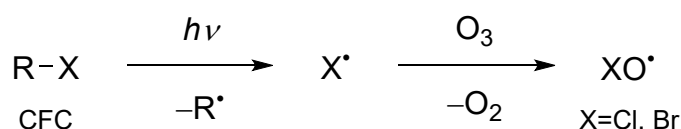
Figure 4: Comparison of the chain structure of pentadecane (top left) vs. the helical structure of perfluoropentadecane (top right) modeled on the PM3 level of theory (Orca 5.0.3), and the electrostatic potential of benzene (bottom left) vs perfluorobenzene (bottom right) in the range of -0.01 a.u. (red) to 0.06 a.u. (blue) mapped onto their electron densities (isosurface value 0.0035 a.u.); calculated at the B3LYP-D3(BJ)/aug-cc-pvtz level of theory (Gaussian 16) in the gas phase and visualized with VMD 1.9.3.

The highly polarized C–F bond results also in polarized molecules when the fluorine content is low, while in highly fluorinated molecules the polarizations cancel each other out, resulting in very unpolar molecules. In addition, highly fluorinated compounds have a low ability to induce dipole interactions, resulting in relatively weak attractive forces between molecules. This results in interesting properties such as the formation of distinct fluorinated phases, as observed in the heptane/perfluoro(methylcyclohexane) system,^[3,17] and the dirt, water and oil repellency of fluorinated surfaces. In addition, this effect results in lower boiling points and increased volatility compared to similar non-fluorinated compounds.^[1–4,12]

1.4 Environmental Concerns Related to Fluorinated Compounds

One of the main sources of emissions of fluorinated compounds is the use of fluorinated gases and volatile compounds.^[6] Together with their stability and inertness, these compounds are suitable for use as blowing agents for foams, fire extinguishers, propellants, and solvents. Due to their relatively high heat of vaporization, they are also utilized as refrigerants.^[4] Although generally not toxic, these compounds can have substantial environmental impacts, primarily in three areas of concern.

Ozone Depleting Properties: Many gaseous fluorocarbons are stable enough to pass through the troposphere, while especially chlorofluorocarbons (CFCs) and other halogen derivatives, become unstable when exposed to extraterrestrial radiation in the stratosphere. This instability leads to the formation of chlorine and bromine radicals through electromagnetic radiation. These radicals are known to react with ozone, contributing to a large extent to the ozone layer depletion (Scheme 1).^[18] The ozone depleting potential (ODP) quantifies a substance's ability to deplete the ozone layer. The ozone hole over Antarctica, observed in the early 1980s, is a consequence of the extensive use of CFCs since the 1930s.^[19]



Scheme 1: Decay of CFCs in the stratosphere via the irradiation with UV light and ozone depletion reaction of the formed radicals. Data were taken from literature^[18].

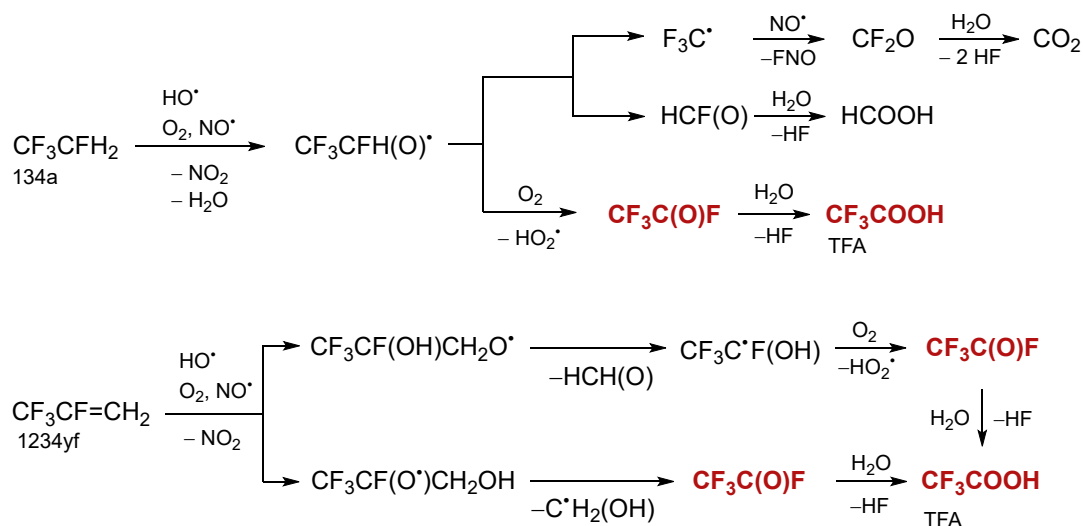
The recognition of the ozone-depleting effects of various halogenated compounds led to a series of multilateral environmental agreements in the 1980s. The Vienna Convention of 1985 established the first international framework for regulating ozone-depleting substances.^[20] Following this, the Montreal Protocol of 1987 regulated and banned many ozone-depleting chemicals, primarily chlorinated and brominated fluorocarbons.^[6]

Contribution to the Greenhouse Effect: Another considerable but concerning effect of fluorocarbons is their ability to absorb extraterrestrial IR radiation, trapping energy that would otherwise be reflected into space. This process contributes to the greenhouse effect. The global warming potential (GWP), a measure of the ability of substances to trap heat, is a function of their IR absorption and atmospheric lifetime.^[21] Both properties are often higher for fluorinated molecules than for non-fluorinated derivatives. Due to the alarming impact on global warming, the United Nations Framework Convention on Climate Change (UNFCCC) of 1992 aims to reduce and regulate anthropogenic greenhouse gases in order to limit global warming. This framework was later expanded by the Kyoto Protocol in 1997, which specifically lists greenhouse gases such as PFCs, HFCs, and SF₆.^[7] The Paris Agreement, another UNFCCC framework, aims to limit global warming to a maximum of 1.5 °C.^[22]

Since 1987, the Montreal Protocol has been ratified by 198 countries and improved several times. The Kigali Amendment extended the protocol's coverage to include non-ozone-depleting HFCs in 2016.^[23] In order to implement this amendment, the European Parliament and the Council of the European Union issued the F-Gas Regulation EU 517/2014, which was designed to reduce the emission of fluorinated greenhouse gases, including sulfur hexafluoride (SF₆).^[24] This regulation was updated in 2022 to increase the regulation and phase-out these gases.^[9]

Formation of Persistent Decomposition Products: The third area of concern is the impact of decomposition products. Many partially fluorinated compounds can decompose into moieties which are persistent in nature. For example, HFC-134a (1,1,1,2-tetrafluoroethane) and HFC-1234yf (2,3,3,3-tetrafluoropropane) have zero ODP and are used as refrigerants for example in air conditioning systems for cars. However, while HFC-134a has a high GWP of 1430, HFC-1234yf has a low GWP (<1). Despite this, both substances degrade in the atmosphere to form trifluoroacetic acid (TFA) (Scheme 2).^[18,25]

TFA is not the only example of persistent fluorinated compounds. In general, PFAS exhibit high persistence in nature. PFAS are defined as substances containing at least one fully fluorinated –CF₃ or –CF₂ group.^[26] Fluorinated molecules often lack the same degradation pathways as their non-fluorinated counterparts due to the high binding energy of the carbon-fluorine (C–F) bond (for details, see Section 1.3) which is responsible for their remarkable stability.^{[3,4][27]}



Scheme 2: Degradation of HFC-134a (top) and HFC-1234yf (bottom) in the atmosphere into the persistent compound TFA. The complete pathways are only shown for the fluorinated compounds. Data were taken from literature.^[18,25]

1.4.1 Persistent Fluorinated Compounds

PFAS are widely used due to their unique properties. One class of PFAS are fluorinated polymers which are used to provide nonstick surfaces due to the weak interaction with other substances. PTFE, commonly known by its brand name Teflon™, is an important example. PTFE is used in nonstick cookware, as a grease additive in lubricating oils, and in manufacturing water and dirt-repellent materials such as Gore-Tex. PTFE and similar polymers, like perfluoroalkoxy alkane (PFA) or polyvinylidene difluoride (PVDF), are also valuable for creating corrosion-resistant reaction vessels and insulating materials for electronics and cables due to their high dielectric constants.^[3,4]

The manufacturing of PTFE surfaces often employs emulsion polymerization, stabilized by highly fluorinated surfactants such as perfluoroalkyl carboxylic acids (PCAs) and their salts. PCAs and the similar class of perfluoroalkyl sulfonic acids (PSAs) serve as fluorophilic analogues of classical surfactants, with their fluorinated chains acting as the lipophilic or fluorophilic site, and their carboxylate or sulfonate groups providing hydrophilicity. Compared to non-fluorinated compounds, fluorinated surfactants offer lower surface tension, enhanced chemical resistance, and high thermal stability. This high stability is one reason these substances are used in firefighting foams, a key emission pathway. However, the main disadvantages of these compounds are their toxicity and environmental persistence. Perfluorooctanoic acid (PFOA) and perfluorooctanesulfonic acid (PFOS) have been linked to thyroid disease, liver damage, kidney cancer, lower birth weight, breast cancer, testicular cancer, and other health issues.^[10,11] Additionally, these short-chain compounds are volatile and water-soluble, making them extremely mobile and widely dispersed by the water cycle.^[5]

1.4.2 Extensive PFAS Regulation in the European Union

Because of their concerning properties such as toxicity, bioaccumulation, water solubility and persistence, some PFAS are already banned under the Stockholm Convention on Persistent Organic Pollutants (POPs). Examples for these compounds are perfluorohexanesulfonic acid (PFHS), PFOA, and PFOS.^[8] Other PCAs and PSAs are subject to restrictions under REACH (Registration, Evaluation, Authorization, and Restriction of Chemicals). In 2023, the European Chemicals Agency (ECHA) published a proposal to restrict PFAS using a new approach. This proposal includes an outright ban on all PFAS, with specific use authorizations required. The proposal also discusses specific exemptions for certain uses, including $-CF_3$ or $-CF_2-$ groups attached to certain heteroatoms, while complete exemptions are made for pharmaceutical and agrochemical research, which are regulated under different laws. The report indicates that the majority of PFAS emissions are related to fluorinated gases (about 60 %) and fluorinated polymers (about 30 %), with major use in the textile industry for applications

such as textiles, upholstery, carpets, and leather.^[5] Not only are carbon-based PFASs of high environmental concern, but the inorganic compounds mentioned above can also have substantial environmental impacts.

1.4.3 Regulation of SF₆, its Applications and its Regulation

Fluorinated gases of concern include SF₆, which is also very problematic due to its high stability, persistence in nature and therefore enormous GWP. It is strongly regulated by multi-lateral agreements such as the Kyoto Protocol^[7] and the Kigali Amendment^[23] of the Montreal Protocol.^[6] In the EU, its regulation and phase-out, specifically prohibiting the use of SF₆ in new electrical equipment by 2031 is covered by the Update in 2022^[9] of the F-Gas Regulation EU 517/2014.^[24]

SF₆ is the second most produced chemical from elemental fluorine (for details, see Section 1.1), renowned for its remarkable properties that make it invaluable in various applications, especially in electrical engineering. Its low sublimation point (−63.8 °C), high chemical stability, and thermal conductivity contribute to its effectiveness as an insulating medium. One of the most notable properties of SF₆ is its high dielectric strength (DS), which allows it to withstand high voltages without electrical breakdown. This property makes SF₆ an ideal insulating medium for high-voltage applications such as switchgear, circuit breakers, and transformers. Additionally, SF₆ has excellent arc-quenching properties, meaning it can quickly extinguish electrical arcs that may occur in switchgear during fault conditions. This property helps to protect equipment and ensure the safe operation of electrical systems. Furthermore, the low thermal conductivity of SF₆ enhances its effectiveness as an insulating medium by reducing heat transfer within electrical equipment. This property helps to maintain stable operating temperatures and prevents overheating, which can lead to equipment failure. Overall, the combination of these properties makes sulfur hexafluoride a highly desirable insulating medium for various electrical applications, particularly in switchgear where reliable performance and safety are paramount.^[3,28–30]

The unique properties of SF₆, primarily due to its saturation with fluorine atoms, make it valuable for various industrial applications beyond electrical engineering. In the production of magnesium, SF₆ serves as an inert blanket gas to prevent oxidation of the molten metal, ensuring the quality of the final product. Similarly, in semiconductor manufacturing, SF₆ is utilized as a plasma etchant due to its chemical inertness and ability to effectively remove material from semiconductor surfaces, when activated.^[29] The high molecular weight and density of SF₆ make it advantageous for applications where diffusion through materials is undesired. For instance, it has been used to insulate windows and fill tires, where its low diffusion through rubber helps maintain tire pressure. The use of SF₆ in products like Nike's Air brand shoes resulted in the use of 277 tons of SF₆ in these sports shoes alone in 1997.^[29] However, the environmental

impact of SF₆ is a substantial concern. Its long atmospheric lifetime (3200 years) and ability to absorb infrared radiation contribute to its substantial GWP of 23500 over a period of 100 years, making it one of the most potent greenhouse gases known so far.^[3,28,30]

The concentration of SF₆ in the atmosphere experienced a noteworthy increase, where it has more than doubled from 4.73 parts per trillion (ppt) in 2001 to 9.59 ppt in 2018. In this year alone, global emissions of SF₆ were estimated at 9 kilotons, equivalent to approximately 0.22 gigatons of CO₂, roughly 0.6 % of the global CO₂ emissions for the same year, which totaled 36.6 gigatons.^[30,31] Despite SF₆ contributing relatively modest to overall greenhouse gas emissions, the European Parliament and the Council of the European Union (EU) recognized the environmental concerns associated with SF₆ and other fluorinated gases. Consequently, measures were implemented to address the impact of these gases, aiming for their reduction. An update in 2022 further emphasized the urgency of addressing SF₆ emissions by calling for an accelerated phase-out of SF₆ in all new electricity transmission equipment by 2031.^[9] This initiative reflects a proactive approach towards mitigating the environmental impact of SF₆ and aligns with broader efforts to transition towards more sustainable practices in energy infrastructure.^[5]

1.4.4 Environmental Impact of Potential SF₆ Alternatives

In many applications, like window filling or sports shoes, SF₆ can be replaced by alternative compounds or different technical solutions. However, finding suitable replacements in the energy sector poses challenges. The criteria for such alternative dielectrics are stringent. Firstly, they must be environmentally friendly, with low GWP and no ODP. The compound should be safe to handle, non-toxic, and non-flammable, with decomposition products that are also non-harmful. To ensure a long operating life expectancy, it should be thermally and chemically stable, resistant to decomposition during arc events, yet decomposable when emitted. Additionally, it should possess high dielectric strength and arc quenching properties, equaling or surpassing those of SF₆. High to moderate thermal conductivity is desirable to manage heat flow effectively, with fast recovery after an arc event. Compatibility with equipment materials is crucial, along with a low boiling point to facilitate applications in low-temperature environments.^[32–36]

Natural gases such as dry air or its individual components N₂, O₂, and CO₂ fulfill many of the desired requirements (Figure 5). They are environmentally friendly, abundant, and easy to obtain. However, their dielectric strength is only one-third that of SF₆, making them less effective as dielectrics. As a result, they are suitable for low to medium voltage applications but inadequate for high voltage applications. For these higher voltage applications, different technical solutions or synthetic gases with appropriate properties are necessary. Examples for these gases are shown in Figure 5, with values for their dielectric strength, boiling points and GWP.

Compounds with high dielectric strength often contain considerable amounts of fluorine, due to fluorine's high electronegativity, which leads to high breakdown voltages. Additionally, fluorine forms strong bonds, resulting in stable compounds. The shielding effect of fluorine atoms also reduces molecular interactions, often leading to lower boiling points. Consequently, many compounds currently being studied as SF₆ substitutes contain fluorine atoms. While the high fluorine content enhances dielectric strength, it also leads to environmental persistence of highly fluorinated carbon chains. [3,28,37–39]

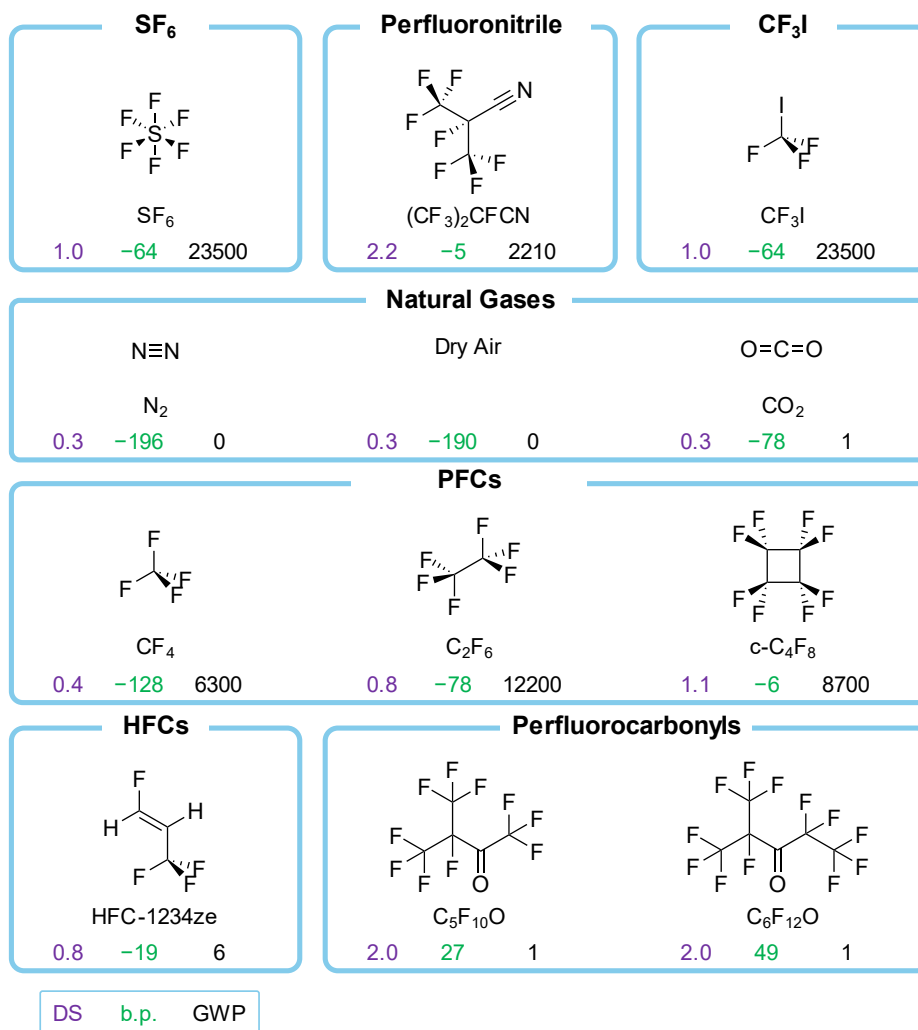


Figure 5: Selected compounds considered and used as SF₆ replacements with their relative dielectric strength (DS) in lilac, boiling points (b.p.) [°C] in green and GWP in black. Data were taken from literature^[33,36]. Note that some values, especially the ones for the GWP vary between references.

During the switching processes of higher voltages, arcs can occur when the breakdown voltage of the insulation medium is exceeded. These arcs ionize the molecules within, increasing electrical conductivity and forming a plasma that can reach temperatures up to 10000 K.^[33] Even SF₆ decomposes under these conditions, primarily into F[•] radicals and several sulfur fluoride species such as [SF₅][•] and SF₄. The advantage of SF₆ is that a significant portion of these compounds recombine after the arc is extinguished to form SF₆ again. This recombination is rapid and thermodynamically favored. Only small amounts react with H₂O or O₂, forming

toxic compounds like SF₄, SO₂F₂, or HF. Additionally, some [SF₅][•] radicals can recombine to form the highly toxic S₂F₁₀.^[33,36,40]

The overall decomposition of SF₆ is relatively minor compared to other dielectrics in use. Experiments testing the decomposition behavior of the recently adopted replacement (CF₃)₂CFCN compared to SF₆ showed that SF₆ performed much better. Only a small amount (1.6 %) of SF₆ decomposed after 200 electrical discharges of approximately 10 ms each, while a comparable mixture of (CF₃)₂CFCN (53 %) in air (47 %) showed a degradation of 61.7 % of the nitrile under the same conditions. The nitrile has more complex decomposition pathways due to its intricate structure. The list of possible decomposition products is extensive and includes toxic compounds like CF₃CN, C₄F₈, C₃F₆, and HF, as well as greenhouse gases like CF₄, C₂F₆, C₃F₈, and C₂N₂. The (CF₃)₂CFCN (53 %) in air (47 %) mixture is notably more toxic, with an LC₅₀(4 h) of 2035 ppm, compared to SF₆, which has an LC₅₀(4 h) of >80 %. However, the decomposed mixture of (CF₃)₂CFCN has an LC₅₀(4 h) value of only 31 ppm for male mice. In comparison, the decomposed SF₆ mixture has an LC₅₀(4 h) of around 3 %, drastically (1100 times) higher than that of (CF₃)₂CFCN.^[41,42] Therefore, compounds such as (CF₃)₂CFCN which have already been adopted as replacements, pose environmental concerns because both the compounds and their decomposition products are persistent and harmful to the environment.

For the assessment of the dielectric strength of possible new replacement candidates, basic descriptors are required. A very rough approach is the connection of the adiabatic electron affinity to its ability to absorb free electrons and therefore to the dielectric strength.^[28,38,43] A more precise method was developed by Rabie *et al.* to predict values of the dielectric strengths based on quantum chemical calculations. Values for the electric dipole moment (μ), the average static electronic polarizability (α), the adiabatic ionization energy (ϵ_i) are obtained by calculating anionic, neutral, and cationic species by DFT methods. Together with the number of electrons (N_e) these values are used to predict the dielectric strength with the use of empiric equations.^[44]

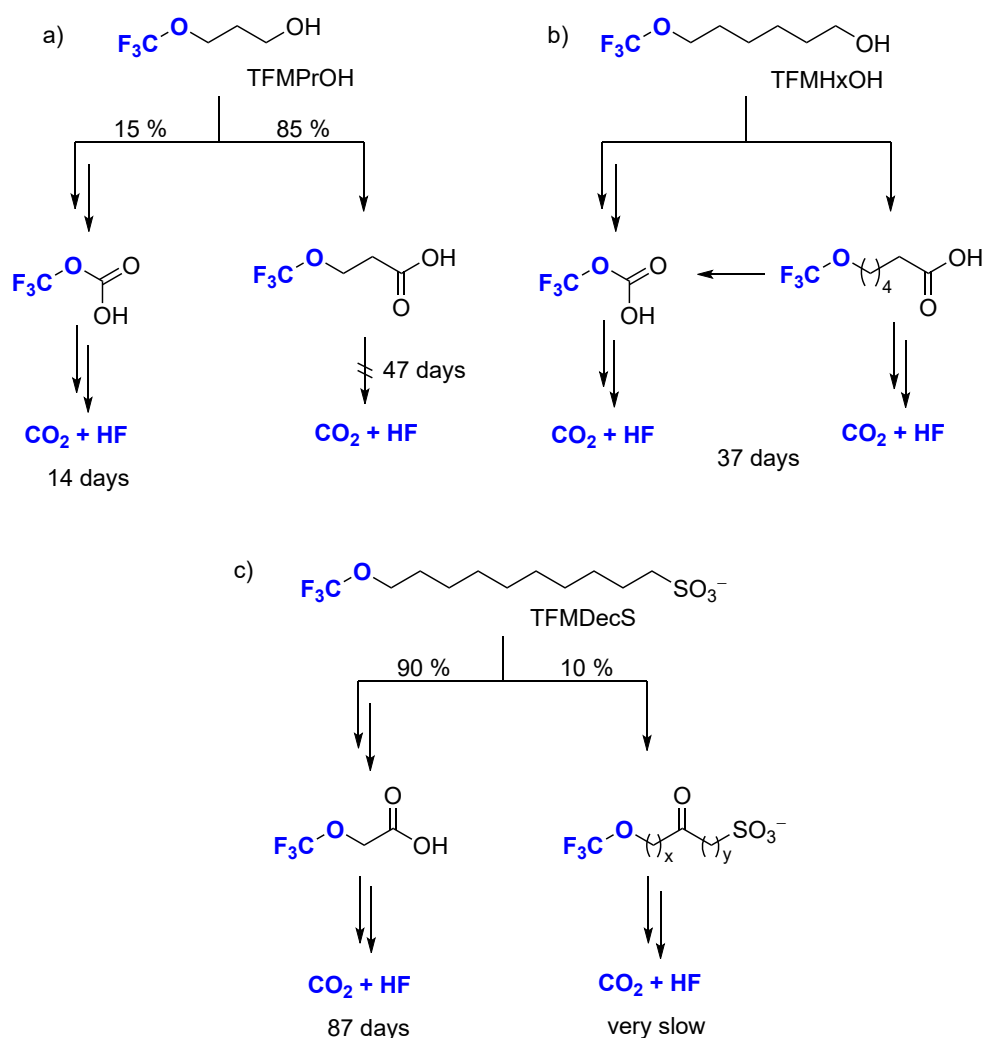
1.5 Possible Solutions for a More Sustainable Fluorine Chemistry

Fluorine and its compounds have driven numerous innovations across various fields. Presently, fluorinated compounds play a crucial role in energy production and conversion technologies. Notable examples include SF₆ as insulation gas and proton exchange membranes (PEMs) made from Nafion, a fluorinated polymer, which are essential components in fuel cells. Additionally, fluorinated compounds are integral to lithium- and sodium-ion batteries, serving as fluorinated cathodes, electrolytes, or interfaces.^[45] Despite their technological benefits, the persistence and environmentally unfriendly nature of fluorinated compounds necessitate a more sustainable approach to their use. In some instances, non-fluorinated alternatives have been identified; however, such substitutions are not universally feasible. One strategy to address these challenges involves incorporating more breaking points into chemical structures, as observed in alternatives to fluorinated surfactants.^[10,46] Moreover, fluorochemical research is increasingly focusing on developing more easily degradable groups. These degradable groups typically feature either a single perfluorinated carbon atom bonded to a heteroatom, such as in –OCF₃, or –OCF₂O– groups. Generally, these compounds should exhibit substantially lower persistence than longer per- and polyfluoroalkyl substances (PFASs). Consequently, the –OCF₃ group, among others, has been excluded from the initial draft of the EU's proposed ban on PFAS.^[5] However, the decomposition of molecules bearing the OCF₃ group has only been partially researched so far. Moreover, –SF₅ or –OSF₅ groups can also be interesting as alternatives.

Many reports and publications mention the easy decomposability of –OCF₃ compounds. However, some investigations based on their stability in biological systems have been made by testing the stability of the desired bio-active compounds or their desired activity. Depending on the substance these compounds show sometimes more sometimes less stability compared to similar compounds without the –OCF₃ moiety. Moreover, there is a lack of investigations regarding to the lifetimes and decomposition pathways of –OCF₃ compounds especially of the fluorinated parts. Only a few publications provide an experimental examination. The decomposition of fluorinated surfactants, such as 3-(trifluoromethoxy)-propan-1-ol (TFMPrOH), 6-(trifluoromethoxy)-hexan-1-ol (TFMHxOH) and 10-(trifluoromethoxy)decane-1-sulfonate (TFMDecS) could be explored in effluent or surface water. All three compounds showed biodegradation under these conditions. Unfortunately only 15 % of TFMPrOH decompose into CO₂, HF and a non-fluorinated organic rest within 14 days, while 85 % of TFMPrOH were only oxidized to the corresponding carboxylic acid (TFMPrA), which was stable under these conditions (Scheme 3a).^[47] In contrast, the –OCF₃ moiety in TFMHxOH decomposed nearly quantitative into CO₂ and HF within 37 days (Scheme 3b).^[47] Similar results were obtained for TFMDecS, which degraded 89 % in 87 days (Scheme 3c).^[48]

These results show that $-\text{OCF}_3$ compounds can be in principle biodegraded, whereas the split of the $-\text{OCF}_3$ group is the critical step. Depending on the organic rest these compounds show different stabilities and decomposition pathways. The poor decomposability of TFMPPrA demonstrates that some compounds bearing the $-\text{OCF}_3$ group could be more stable than expected. Nonetheless, it is advisable to conduct much more degradation studies on different organic compounds, as the $-\text{OCF}_3$ group can influence compound stability, with the critical step being the cleavage of the $-\text{OCF}_3$ group.^[3,4,47–53]

In recent years, the $-\text{OCF}_3$ group has emerged as a prominent entity in the field of fluorine chemistry. In organic molecules, this group is often characterized by its lipophilicity (Hansch parameter 1.04), electron-withdrawing properties, enhanced metabolic stability, and its ability to influence molecular conformation.^[51] This group plays crucial roles in medicinal chemistry,^[51,54] agrochemicals,^[55] and materials science.^[56]

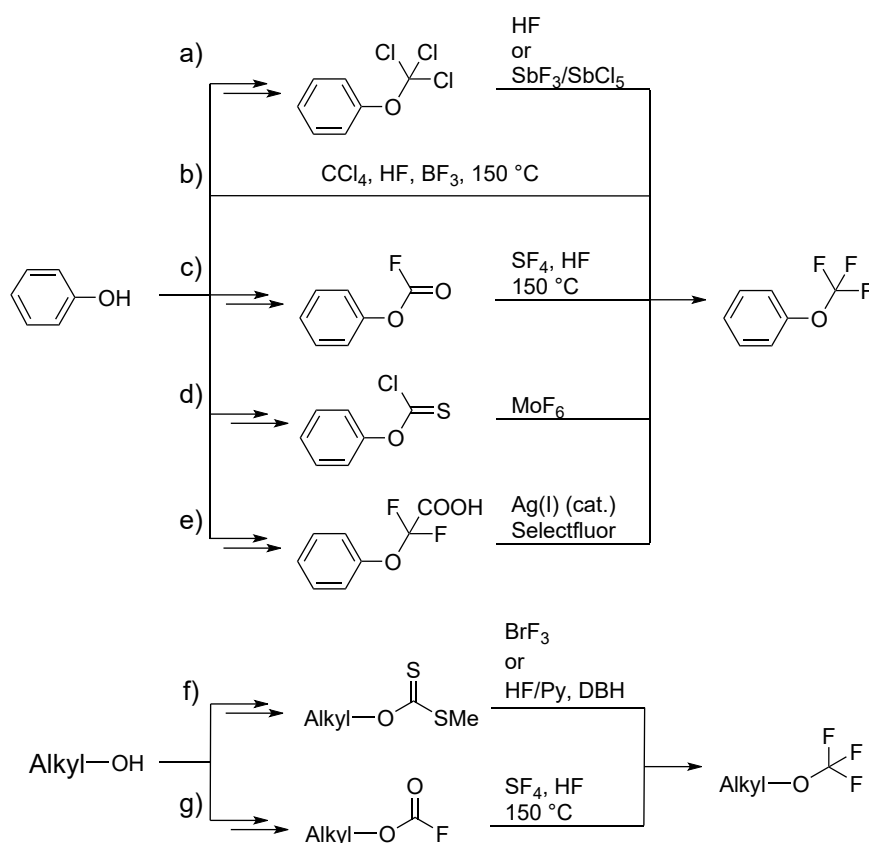


Scheme 3: Biodegradation of a) HFBPrOH, b) TFMPPrOH, and c) TFMHxOH in surface or effluent water. Decomposition products are only shown for the $-\text{OCF}_3$ group. Data were taken from literature.^[47,48]

1.6 Approaches for Synthesizing $-OCF_3$ Compounds

1.6.1 Construction of the $-OCF_3$ Group - Indirect Approach

There are several ways known to incorporate the $-OCF_3$ group into molecules. One possibility is the synthesis of this group in the desired molecule. An important method within this framework is the *de novo* synthesis, which starts from fundamental and simple starting materials. Although this method is constrained to a narrow spectrum of substrates and exhibits limited functional group compatibility, it provides the notable benefit of scalability at comparatively low costs. Consequently, the reaction predominantly yields building blocks that necessitate additional functionalization processes. Despite the inherent advantages of this approach, the development of transformations within this framework remains limited. Furthermore, the used reagents are most likely highly reactive, toxic and corrosive.



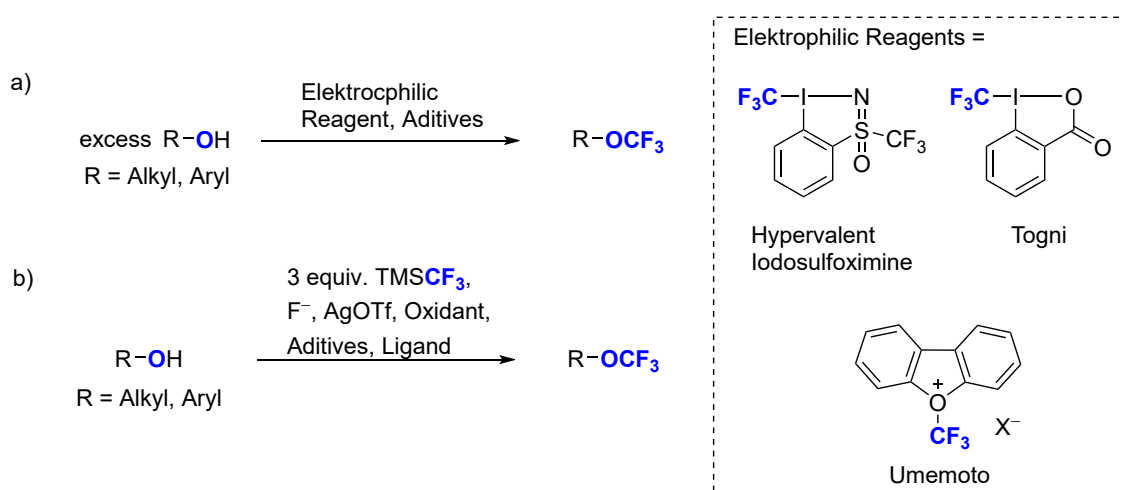
Scheme 4: *De novo* synthesis of trifluoromethoxylated alkyl or aryl compounds starting from simple alcohols or phenols. Data were taken from literature.^[50,57–64]

Initially, this method was based on the transfer of phenols into the corresponding trichloromethyl ether followed by halogen exchange (HalEx) into fluorine substituents (Scheme 4a).^[3,50,57] Alternatively, phenols can be reacted directly with CCl_4 and HF in the presence of the Lewis acid BF_3 (Scheme 4b).^[58] Later synthetic strategies such as the formation of fluoroformates, followed by the deoxyfluorination with SF_4 in HF at $150\text{ }^\circ\text{C}$ (Scheme 4c),^[59] the

fluorination of O-aryl-substituted carbonochloridothioates with MoF_6 (Scheme 4d),^[60] were developed. Furthermore, phenols can be converted into the difluoroacetic acid, followed by the decarboxylation-fluorination with Selectfluor II and a silver(I) catalyst (Scheme 4e).^[61] For alcohols also some *de novo* pathways are known, such as the formation of xanthates, followed by the oxidative desulfurization-fluorination with BrF_3 ^[62] or HF/Py and DBH (Scheme 4f),^[63] or the deoxyfluorination with SF_4 in HF of fluoroformates (Scheme 4g).^[64]

Transferring a $-\text{CF}_3$ group to an alcohol or phenyl group is another method for constructing the $-\text{OCF}_3$ functionality. However, this strategy is similar to the *de novo* synthesis limited to substrates that contain an $-\text{OH}$ group. The utilization of different electrophilic reagents, such as the Umemoto reagent,^[65] Togni reagent,^[66] and hypervalent iodine reagents (Scheme 5a),^[67] facilitates this transformation. Furthermore, nucleophilic reagents such as TMSCF_3 can be used under oxidative conditions for the trifluoromethylation (Scheme 5b).^[68] These reactions exhibit good functional group compatibility and are valuable in drug synthesis. This versatility makes them valuable tools in organic synthesis, particularly in medicinal chemistry and drug discovery efforts.^[3,57] Nevertheless, the reagents are not very atom economic.

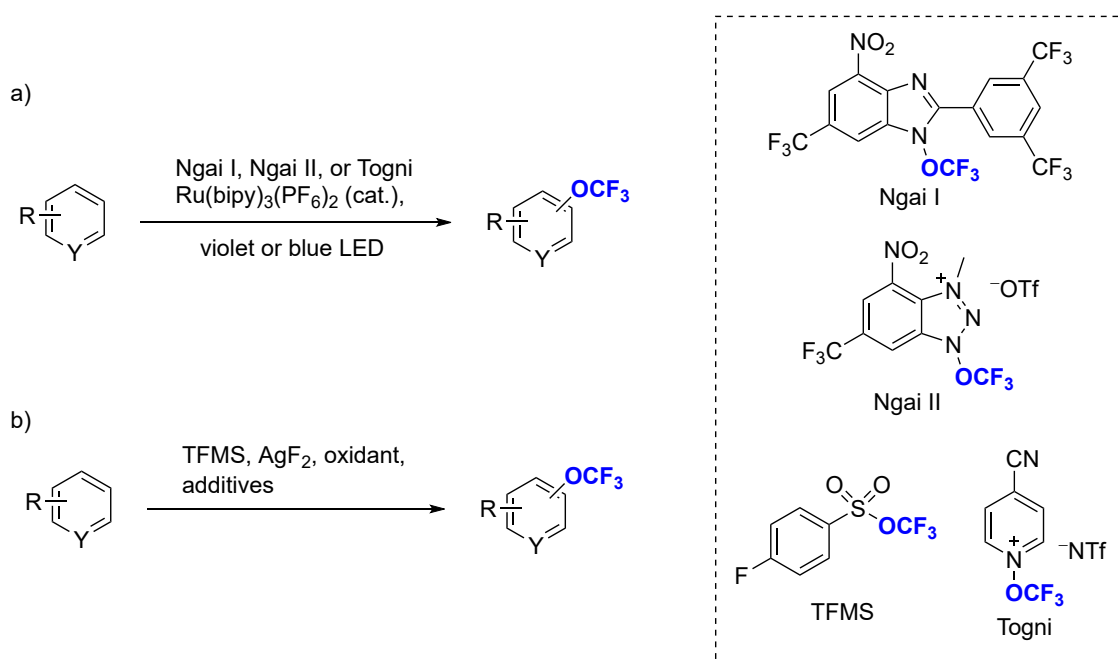
Overall, these Methods based on the construction of the $-\text{OCF}_3$ group can be profitable and valuable, especially for simple building blocks or molecules with $-\text{OH}$ groups at the desired places. Therefore, methods for the direct introduction of $-\text{OCF}_3$ moieties were developed. These can be very important for mid- to late-stage functionalization.



Scheme 5: a) Electrophilic trifluoromethylation of alcohols or phenols with Umemoto, Togni, or hypervalent iodine reagents, and b) oxidative nucleophilic trifluoromethylation of alcohols or phenols with TMSCF_3 . Data were taken from literature.^[65–68]

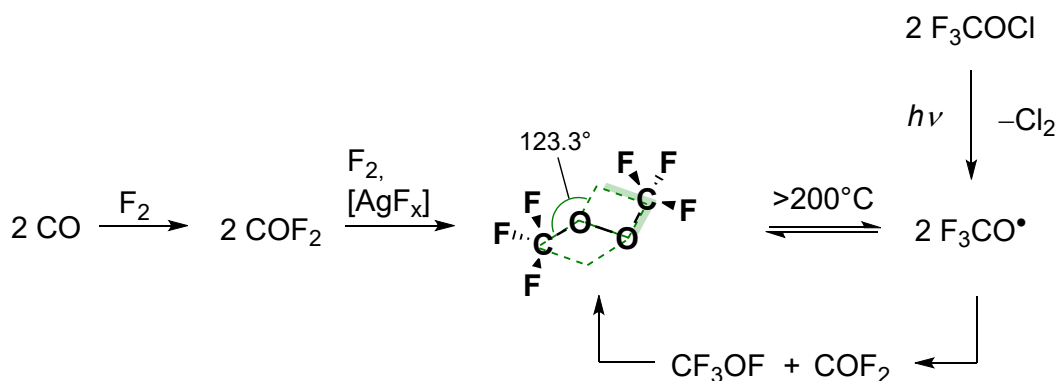
1.6.2 Radical Trifluoromethoxylation

A direct method for introducing the $-\text{OCF}_3$ group is the radical pathway. This method is particularly beneficial for the introduction of $-\text{OCF}_3$ groups into (hetero)aromatic positions but is also applicable to a variety of other substrates. A crucial step for this pathway is the *in situ* formation of the relative instable $[\text{OCF}_3]^\bullet$ radical. Suitable reagents such as nitrogen-based $-\text{OCF}_3$ compounds can be activated by a photo-redox catalyst under the formation of the reactive $[\text{OCF}_3]^\bullet$ radical (Scheme 6a).^[69–71] Alternatively, a silver mediated reaction starting from TFMS can be performed transferring the $-\text{OCF}_3$ group to arenes or pyridine derivatives (Scheme 6b).^[72] These reagents possess distinct advantages such as bench stability and ease of handling, which contribute to their appeal in practical synthetic applications. Their ease of use and compatibility with various reaction conditions make them valuable tools in the synthesis of $-\text{OCF}_3$ -containing compounds.



Scheme 6: Radical trifluoromethoxylation of (hetero)arenes with Ngai I, Ngai II, or Togni reagent. Data were taken from literature.^[69–72]

A major drawback of these reagents is again the circumstantial preparation and the lack of atom economy. A valuable alternative is the use of bis(trifluoromethyl) peroxide, a gas with a boiling point of $-37\text{ }^\circ\text{C}$ ^[73] and remarkable stability up to $200\text{ }^\circ\text{C}$, beyond which it decomposes into two $[\text{OCF}_3]^\bullet$ radicals.^[74] This contrasts with the non-fluorinated dimethyl peroxide, which is an explosive. The bond dissociation energy of the O–O bond in $(\text{CF}_3\text{O})_2$ ($199 \pm 2\text{ kJ mol}^{-1}$)^[73,75] is slightly higher than in $(\text{CH}_3\text{O})_2$ ($157 \pm 8\text{ kJ mol}^{-1}$)^[76,77]. Moreover, the decomposition of the $[\text{OCF}_3]^\bullet$ radical into CF_2O and CF_3OF (Scheme 7) is endothermic and slow, while the decomposition of the non-fluorinated $[\text{OCH}_3]^\bullet$ radical is exothermic and rapid. This results in a chain propagation of the decomposition reaction of $(\text{CH}_3\text{O})_2$ and explosion.^[74,78,79]



Scheme 7: Synthesis and decomposition reactions of bis(trifluoromethyl)peroxide (CF_3O)₂. Data were taken from literature.^[74,80–84]

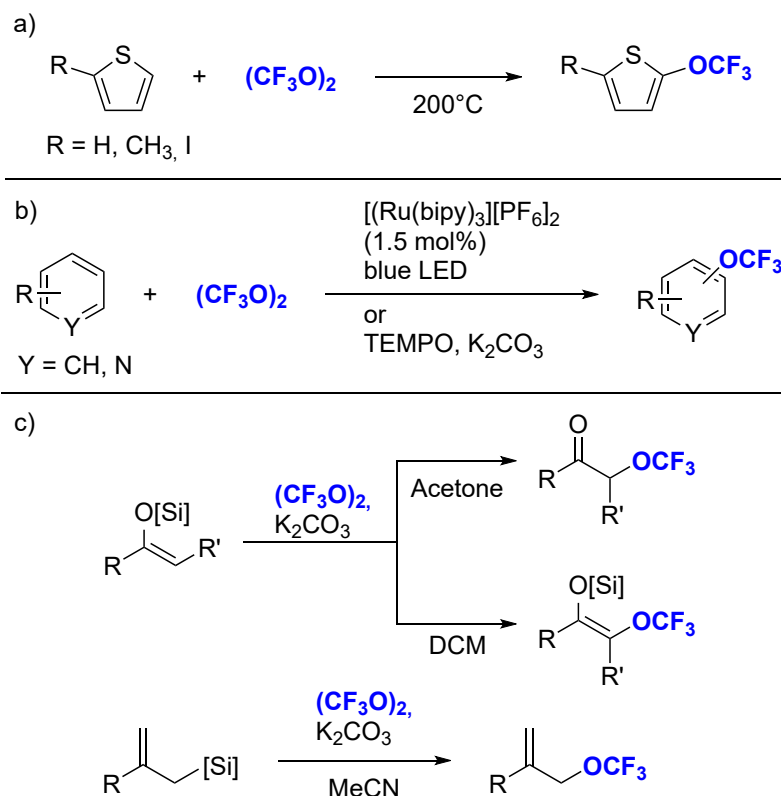
The structure of the $(\text{CF}_3\text{O})_2$ obtained by GED analysis (Scheme 7) show a COOC dihedral angle of 123.3° ,^[85] while the non-fluorinated counterpart $(\text{CH}_3\text{O})_2$ has dihedral angle of 180° ,^[86] and FOOF of 88° . In contrast to FOOF, which has a very short (121 pm)^[87,88] and therefore strong O–O bond and long and weak O–F bond (158 pm)^[87,88], due to negative hyperconjugation, the O–O bond in $(\text{CF}_3\text{O})_2$ is with 142 pm comparatively long.

$(\text{CF}_3\text{O})_2$ can be formed by the recombination reaction of two $[\text{OCF}_3]^\bullet$ radicals, which are obtained from the photolysis of CF_3OCl (Scheme 7).^[80] Alternative routes for the formation of $(\text{CF}_3\text{O})_2$ include the reaction of CF_3OF with CF_2O ^[81] and the reaction of CF_2O with fluorine in the presence of a catalyst (Scheme 7) such as silver fluoride.^[82]

First, $(\text{CF}_3\text{O})_2$ was used as a source of the $[\text{OCF}_3]^\bullet$ radical by thermolysis at 200°C in the gas phase (Scheme 8a),^[89] or activation by irradiation.^[90] Nevertheless, recent improvements in synthetic methodology have facilitated the development of alternative approaches to the activation of $(\text{CF}_3\text{O})_2$. For instance, the utilization of photocatalysts, the radical initiator TEMPO (Scheme 8b), or reactions with specific silylated substrates (Scheme 8c) has emerged as promising strategies, expanding the repertoire of accessible substrates beyond traditional aromatic systems to include (hetero)arenes, silyl enol ethers, and allyl silanes. This diversification of substrates enhances the versatility and scope of the radical trifluoromethoxylation reaction.^[91,92]

A notable advantage of utilizing $(\text{CF}_3\text{O})_2$ as a radical source lies in its atom-economic nature, as it can be synthesized from fluorine and CF_2O , which can be obtained from the reaction of carbon monoxide with fluorine, or from silver(II) fluoride or cobalt(III) fluoride.^[83,84]

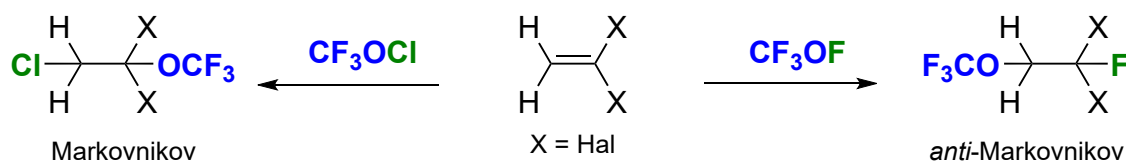
Overall, the radical trifluoromethoxylation reaction represents a powerful strategy for the synthesis of diverse $-\text{OCF}_3$ -containing organic molecules, offering synthetic chemists a versatile and efficient means of functionalizing a wide range of substrates for applications in medicinal chemistry, materials science, and beyond. Overall, the diversity of radical sources allows for exploration of various potential products, offering flexibility in synthesis strategies.^[3,57]



Scheme 8: Radical trifluoromethoxylation with $(\text{CF}_3\text{O})_2$ a) with thermal activation and b) with activation by photocatalysts, c) direct reaction of silylated substrates with $(\text{CF}_3\text{O})_2$ under the formation of trifluoromethoxylation products. Data were taken from literature.^[89,91,92]

1.6.3 Trifluoromethoxylation-Halogenation with Trifluoromethyl Hypohalites

The reactions of CF_3OCl and CF_3OF with olefins is another method to produce fluoro- or chloro-trifluoromethyl ethers. Both compounds react very differently. CF_3OF reacts notably faster and at lower temperatures than CF_3OCl , predominantly yielding *anti*-Markovnikov products through a free radical mechanism with limited stereoselectivity and regioselectivity. In contrast, CF_3OCl primarily produces Markovnikov products via *syn*-addition, consistent with a polar electrophilic addition mechanism that exhibits higher stereoselectivity (Scheme 9).^[93] Fluorinated vinyl ethers such as perfluoromethyl vinyl ether (PMVE) can also be synthesized by addition of a hypofluorite to a fluorinated olefin and subsequent halogen elimination reaction. Copolymerization of PMVE with tetrafluoroethylene then produces the widely used polymer PFA.^[94–96]



Scheme 9: Compared reactions of a substituted olefin with trifluoromethyl hypochlorite and trifluoromethyl hypofluorite. Data were taken from literature.^[93]

Trifluoromethyl hypohalites with the general formula CF_3OX , where $\text{X} = \text{F}^{[97]}$, $\text{Cl}^{[98]}$, or $\text{Br}^{[99]}$ display, similar to $(\text{CF}_3\text{O})_2$, a greater stability than non-fluorinated hypohalites. A fact exemplified by the observation that CF_3OF is a stable gas while CH_3OF is an unstable explosive.^[100] The formal charge of the halogen, X, in these hypohalites is +1, except in CF_3OF , where the fluorine carries a formal charge of -1 .^[101,102] A comparative analysis of the atomic charges in CF_3OCl and CF_3OF reveals that the CF_3 unit's atoms have similar charges in both compounds (Figure 6). However, the chlorine in CF_3OCl is positively charged (0.26), while the fluorine in CF_3OF (-0.11) is negatively charged. Furthermore, the oxygen in CF_3OCl is more negatively charged (-0.54) than the oxygen in CF_3OF (-0.18).^[102]

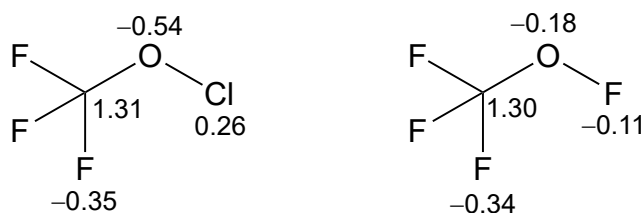


Figure 6: Comparison of the atomic charges of trifluoromethyl hypofluorite (left) and trifluoromethyl hypochlorite (right). Data were taken from the literature.^[102]

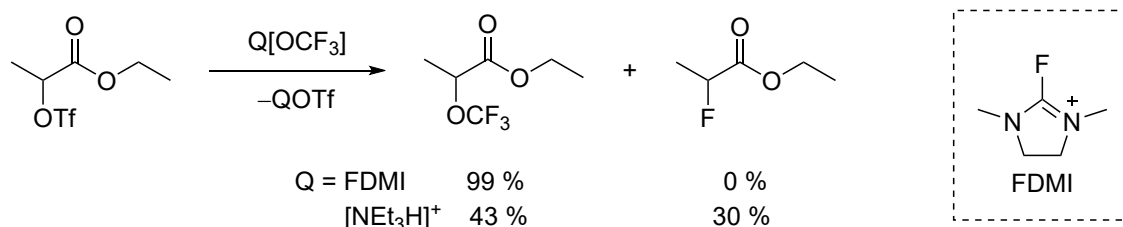
The distinct polarities of CF_3OCl and CF_3OF lead to different reactivities. Fluorinated hypochlorites, such as CF_3OCl , react with negatively charged chlorine substituents or anions to form elemental chlorine and transfer the alkoxide group. This works well for loosely bound chlorides like in coordination compounds.^[103,104]

Furthermore, due to the relatively low bond dissociation energies (BDE) of the O-X bond in CF_3OF ($184.2 \text{ kJ mol}^{-1}$) and CF_3OCl ($220.9 \text{ kJ mol}^{-1}$), small molecules can react with the hypohalites by inserting into the O-X bond.^[75] This reactivity enables the synthesis of compounds such as fluoroformates $\text{R}^{\text{F}}\text{OC}(\text{O})\text{F}^{[105-107]}$, chloroformates $\text{R}^{\text{F}}\text{OC}(\text{O})\text{Cl}^{[80,108,109]}$ and chlorosulfates $\text{R}^{\text{F}}\text{OSO}_2\text{Cl}^{[110]}$. Both, CF_3OCl and CF_3OF , can be prepared by reacting COF_2 with ClF and F_2 , respectively, in the presence of a metal fluoride catalyst such as CsF . Similarly, other fluorinated hypohalites can be obtained, when the corresponding carbonyl compounds are reacted with ClF or F_2 . Furthermore, this can be done in continuous process for the synthesis of trifluoromethyl hypochlorite (CF_3OCl).^[111] Both CF_3OCl and CF_3OF are gases with low boiling points of $-47 \text{ }^\circ\text{C}^{[98]}$ and $-95 \text{ }^\circ\text{C}^{[97]}$, respectively. The O-F bond length in CF_3OF ($142.4 \text{ pm}^{[112]}$ in the gas phase) is comparable to that of OF_2 ($140.9 \text{ pm}^{[113]}$ in the gas phase) or HOF ($144.2 \text{ pm}^{[114]}$ in the solid phase).

1.6.4 Nucleophilic Substitution

A common method for the early to late-stage trifluoromethylation of primarily alkyl derivatives is the nucleophilic substitution by the $[\text{OCF}_3]^-$ anion, while the choice of corresponding cation

and reaction conditions impacts reactivity and yield. For instance, in the conversion of ethyl-2-(triflate)propanoate into ethyl-2-(trifluoromethoxy)propanoate, it has been reported that using the 2-fluoro-1,3-dimethylimidazolium (FDMI) cation results in quantitative conversion, while employing $[\text{NEt}_3\text{H}]^+$ as the cation yields only a 43 % of the trifluoromethoxylated and 30 % of the fluorinated product (Scheme 10).^[115]



Scheme 10 Nucleophilic substitution of ethyl-2-(trifluoromethoxy)propanoate with FDMI[OCF₃] and [NEt₃H][OCF₃]. Data were taken from literature.^[115]

The corresponding alcohol, CF₃OH, is only stable at low temperatures, while some of its salts are room temperature stable compounds.^[116,117] Among alkali metal [OCF₃]⁻ salts, stability decreases from heavier to lighter cations due to the increasing lattice energy of the fluoride. Specifically, lithium and sodium salts are not stable at room temperature, whereas stability increases progressively from potassium to rubidium and cesium (K < Rb < Cs).^[118] These salts can be synthesized by the reaction of the metal fluoride with COF₂ making this approach an atom economic and effective source of -OCF₃ compounds. Furthermore the structures of different salts have been determined, including M⁺ (M = K, Rb, and Cs),^[118] pip⁺ (1,1,3,3,5,5-hexamethylpiperidinium),^[119] and [S(NMe₂)₃]⁺.^[120]

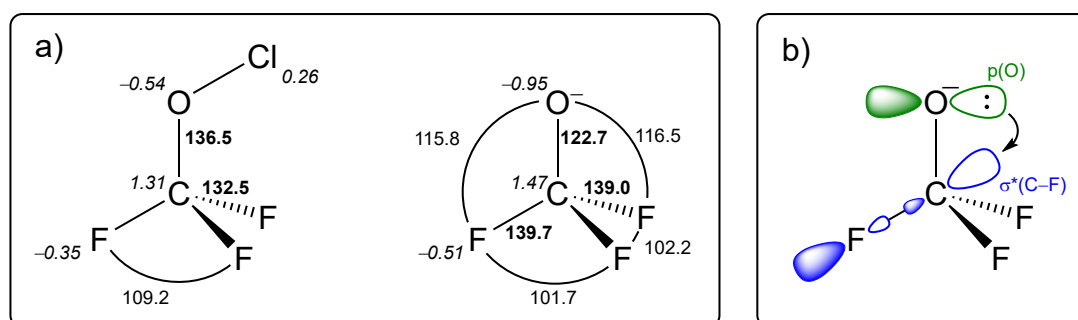
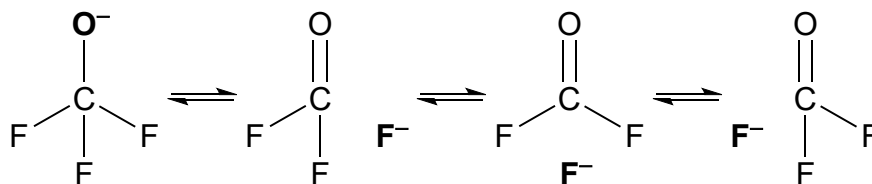


Figure 7: a) Structural parameters by the GED of CF₃OCl and the X-ray diffraction of [S(NMe₂)₃][OCF₃] as well as their calculated atomic charges for the -OCF₃ moieties. Bond lengths are given in bold, angles in plain and atomic charges in italic. Data were taken from literature.^[102,120,121] b) negative hyperconjugation in the [OCF₃]⁻ anion.

The structure of the free [OCF₃]⁻ anion exhibits substantial deviations from -OCF₃ moieties, which are bound to other entities. In [S(NMe₂)₃][OCF₃], the anion adopts a distorted tetrahedral configuration, characterized by F-C-F angles of 101.7° and 102.2° and O-C-F angles of 116.5° and 115.8° (Figure 7a). This contrasts sharply with the -OCF₃ group in gaseous

CF_3OCl , which approximates an ideal tetrahedral geometry, with F-C-F angles of 109.2° (Figure 7a). Additionally, the bond lengths in CF_3OCl are relatively uniform, with C-F and C-O bond lengths measuring 132.5 pm and 136.5 pm, respectively. However, in the $[\text{OCF}_3]^-$ anion, the C-F bonds are elongated, measuring 139.0 pm and 139.7 pm, while the C-O bond is notably shorter at 122.7 pm (Figure 7a). This length of the C-O bond is intermediate between that of a double bond as seen in COF_2 (117.2 pm) and a single bond as in CF_3OCl . However, it more closely approximates the double bond, suggesting a partial double bond character. These structural differences highlight the unique structural and electronic characteristics of the $[\text{OCF}_3]^-$ anion compared to other $-\text{OCF}_3$ -containing species.^[120–122]

The pronounced double bond character and the very short C-O bond in the $[\text{OCF}_3]^-$ anion can be attributed to negative hyperconjugation, wherein electron density from a $\text{p}(\text{O})$ orbital is delocalized into a $\sigma^*(\text{C-F})$ orbital (Figure 7b). Consequently, the $[\text{OCF}_3]^-$ anion can be partially described as a separated fluoride ion coordinating to a COF_2 molecule, stabilized by resonance structures (Scheme 11). This explanation aligns with the calculated higher atomic charge at the fluorine atoms in the anion (-0.51) compared to CF_3OCl (-0.35) (Figure 7a).^[102, 120]



Scheme 11: Resonance structures of the $[\text{OCF}_3]^-$ anion. Data were taken from literature.^[120]

This perspective of a preformed fluoride ion coordinating to carbonyl fluoride provides also an explanation for the decomposition pathway of the isolated $[\text{OCF}_3]^-$ anion, the $[\text{OCF}_3]^\cdot$ radical, and various element $-\text{OCF}_3$ compounds into COF_2 and a fluoride ion, a fluoride radical, or the corresponding element- F .^[47,78,123,124] In contrast, bound $-\text{OCF}_3$ groups can exhibit a better stability due to the lower electron density at the oxygen caused by the bond to another moiety. Transition metal complexes containing the $[\text{OCF}_3]^-$ anion, such as $\text{M}[\text{OCF}_3]$, can be stabilized through coordination with ligands or solvation. Solvation with acetonitrile overcomes the lattice energy of silver fluoride, stabilizing the $-\text{OCF}_3$ compound.

Alternatively, the coordination of transition metal compounds with N-heterocyclic carbenes (NHCs), bidentate amines, or phosphine ligands is utilized to stabilize these $-\text{OCF}_3$ compounds (Figure 8). This coordination can lead to the formation of stable compounds such as $[(\text{SIPr})\text{M}(\text{OCF}_3)]$ ($\text{M} = \text{Cu}$ or Au),^[128] $[\text{Ag}(\text{bpy})(\text{PPh}^t\text{Bu}_2)(\text{OCF}_3)]$,^[125] $[\text{Ag}(\text{PPh}^t\text{Bu}_2)(\text{OCF}_3)]_2$,^[126] or $[\text{Ag}(\text{Aryl-BIAN})(\text{THF})(\text{OCF}_3)]$ ^[127] (Figure 8). Another approach involves the reaction of COF_2 with a metal fluoride complex. This pathway was employed to synthesize the species $[\text{AuF}_2(\text{OCF}_3)(\text{SIMes})]$ through the reaction of $[\text{AuF}_3(\text{SIMes})]$ and COF_2 .^[129] These strategies

underscore the versatility of fluorine chemistry in forming stable complexes, expanding the utility of the $[\text{OCF}_3]^-$ anion in various chemical applications.^[129]

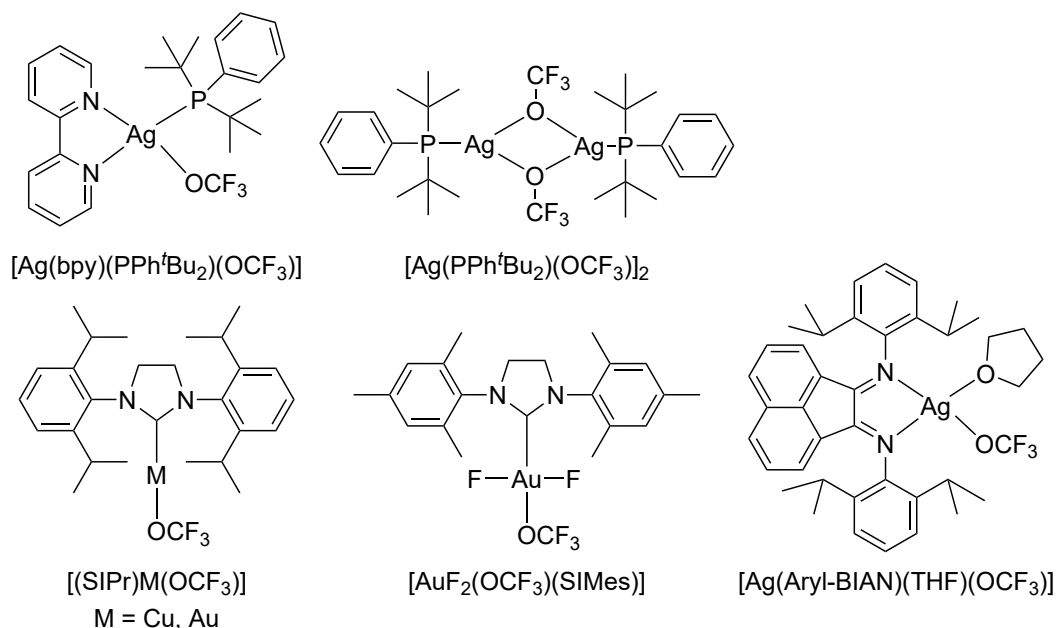
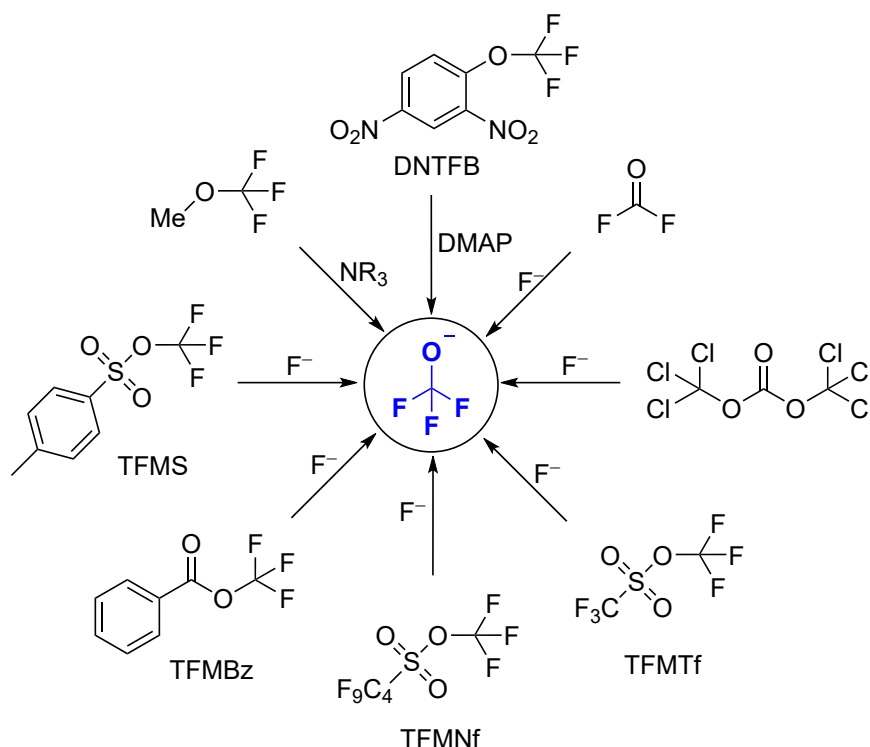


Figure 8: Examples for isolated coordination compounds bearing the $[\text{OCF}_3]^-$ anion. Data were taken from literature.^[125–129]

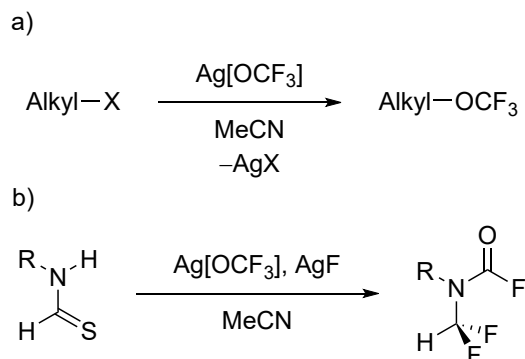
The utilization of COF_2 as a source of the $[\text{OCF}_3]^-$ anion is limited due to its toxicity, necessitating the demand for a bench-stable and easily handled reagent. Consequently, various alternative pathways for the preparation of the active $[\text{OCF}_3]^-$ anion have been explored (Scheme 12), such as the conversion of triphosgene (bis(trichloromethyl)carbonate) with an *in situ* fluoride ion source.^[130–132] Additionally, other sources of nucleophilic $[\text{OCF}_3]^-$ include $-\text{OCF}_3$ -containing compounds that can be activated by fluoride sources, such as trifluoromethyl triflate (TFMTf),^[115] trifluoromethyl nonaflate (TFMNf),^[133] trifluoromethyl benzoate (TFMBz),^[130] trifluoromethyl sulfonates (TFMS),^[134] or with amines like trifluoromethyl methyl ether,^[135] or 2,4-dinitro(trifluoromethoxy)benzene (DNTFB)^[136].

A major drawback of these reagents is their lack of atom economy. Additionally, synthesizing these molecules often involves generating the $[\text{OCF}_3]^-$ anion. For example, TFMBz is commonly prepared from $\text{K}[\text{OCF}_3]$ and benzoyl bromide,^[130] TFMS from benzenesulfonic acid and Togni's reagent,^[137] and DNTFB through the nitration of trifluoromethoxy benzene.^[59] Moreover, the use of TFMNf yields the nonaflate (Nf^-) anion,^[133] a PFAS, and generating COF_2 from triphosgene and AgF produces 2 equiv. AgCl for 1 equiv. of $\text{Ag}[\text{OCF}_3]$.^[132]



Scheme 12: Overview of synthetic pathways to the nucleophilic $[\text{OCF}_3]^-$ anion. Data were taken from literature.^[115,130,130–135]

To foster more sustainable and atom-economic fluorine chemistry, a more direct approach is desired. Given the relatively low nucleophilicity of the $[\text{OCF}_3]^-$ anion, activated substrates such as diazonium or arynes are commonly employed.^[50] Another effective strategy involves the use of AgOCF_3 with alkyl bromides or iodides, facilitating the formation of the corresponding sparingly soluble silver halides (Scheme 13a). Consequently, this active species is documented in numerous publications.^[131–133,138–142] Moreover, AgOCF_3 can also serve as a reagent, as it remains stable in acetonitrile solution when stored at lower temperatures.^[132] The research group led by Schoenebeck demonstrated that AgOCF_3 can be utilized as a reagent for synthesizing *N*-difluoromethyl amides (Scheme 13b).^[142]



Scheme 13: a) Nucleophilic substitution of alkyl bromides or iodides with $\text{Ag}[\text{OCF}_3]$ and b) reaction of thioformamide with $\text{Ag}[\text{OCF}_3]$ under the formation of *N*-difluoromethyl amide. Data were taken from literature.^[132,142]

2 Objectives

The extensive use of PFAS has led to substantial environmental concerns over the past few decades. Consequently, the focus has shifted to the trifluoromethoxy group in fluorine chemistry. This group is stable when connected to organic molecules but can decompose into CO_2 and HF when split off. One method to incorporate this group into organic molecules is through nucleophilic substitution. $\text{Ag}[\text{OCF}_3]$ is a commonly used active species for this purpose, typically prepared *in situ* from organic molecules with a labile $-\text{OCF}_3$ group. However, this process generates substantial organic waste and is not very efficient or atom economical.

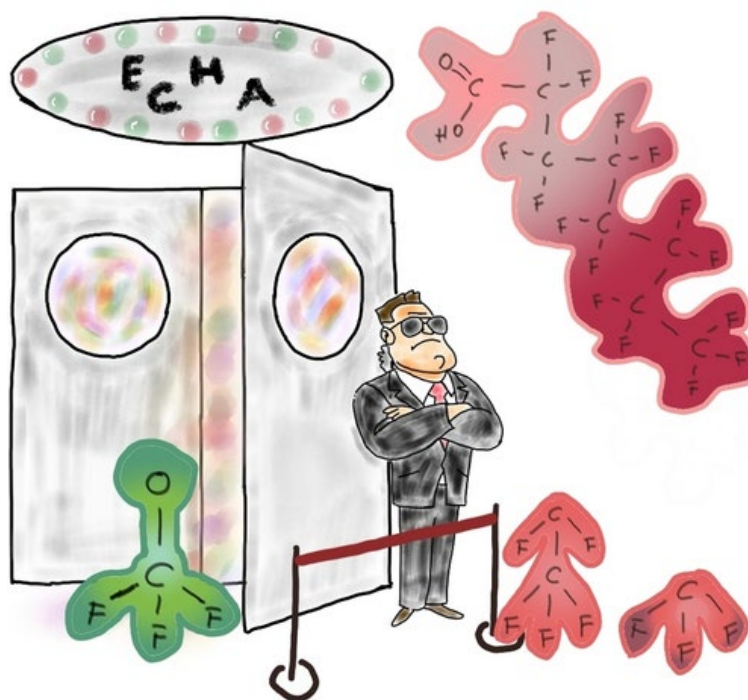
To make the use of $\text{Ag}[\text{OCF}_3]$ more economical and attractive for industrial applications, a direct synthesis approach involving the reaction of AgF with COF_2 is being investigated. Structural analysis of $\text{Ag}[\text{OCF}_3]$ is also being pursued to gain insights into subsequent chemistry. Additionally, the expansion of this reactivity to higher fluorinated carbonyls is being explored, which could be beneficial for applications where the advantages of higher groups outweigh the disadvantages of fluorinated moieties, such as in pharmaceuticals or as reference materials for PFAS analysis.

Another aspect of modern fluorine chemistry is finding a replacement for SF_6 in high-voltage applications as a dielectric medium. In other applications like tire fillings, window glazing, or as insulators in low to mid-voltage electric equipment, SF_6 can be replaced with other compounds or technical solutions. However, most compounds considered as SF_6 replacements are highly fluorinated substances and often fall into the PFAS category. Addressing the use of SF_6 , which has an enormous global warming potential (GWP), and finding sustainable alternatives is crucial. Compounds bearing the $-\text{OCF}_3$ group could be promising in this regard, as they are potentially degradable in nature, reducing both GWP and persistence while retaining the advantages of fluorinated molecules.

Preliminary work by Prof. Dr. Hasenstab-Riedel's group suggests that sulfur(VI)-based compounds such as trifluoromethyl fluorosulfonate ($\text{CF}_3\text{OSO}_2\text{F}$) and trifluoromethoxy sulfur pentafluoride (CF_3OSF_5) containing the $-\text{OCF}_3$ group, could show noteworthy dielectric strengths. Therefore, these two candidates are investigated for their properties and dielectric strengths, as well as improving their accessibility.

3 Publications

3.1 Silver(I) Perfluoroalcoholates: Synthesis, Structure, and their Use as Transfer Reagents



Paul Golz, Kamar Shakeri, Lilian Maas, Marius Balizs, Alberto Pérez-Bitrián, Helen D. Kemmler, Merlin Kleoff, Patrick Voßnacker, Mathias Christmann, and Sebastian Riedel*

Chem. Eur. J. **2024**, *30*, e202400861.

<https://doi.org/10.1002/chem.202400861>

© 2024 The Authors. Published by Wiley-VCH Verlag GmbH. This is an open access article under the terms of the [Creative Commons Attribution License \(CC BY 4.0\)](#), which permits use, distribution and reproduction in any medium, provided the original work is properly cited.

Author contributions

Paul Golz designed the project, performed experiments and wrote the manuscript. Kamar Shakeri and Lilian Maas performed experiments with organic substrates and revised the manuscript. Marius Balizs performed experiments during his Bachelor's thesis with supervision of Paul Golz. Alberto Pérez-Bitrián co-designed the project. Helen D. Kemmler performed experiments during her research internship under supervision of Paul Golz. Merlin Kleoff co-designed the project and revised the manuscript. Patrick Voßnacker performed the XRD measurements. Mathias Christmann and Sebastian Riedel managed the project and revised the manuscript

Silver(I) Perfluoroalcoholates: Synthesis, Structure, and their Use as Transfer Reagents

Paul Golz,^[a] Kamar Shakeri,^[a] Lilian Maas,^[a] Marius Balizs,^[a] Alberto Pérez-Bitrián,^[a] Helen D. Kemmler,^[a] Merlin Kleoff,^[a] Patrick Voßnacker,^[a] Mathias Christmann,^[a] and Sebastian Riedel^{*[a]}

Herein we report a general access to silver(I) perfluoroalcoholates, their structure in the solid state and in solution, and their use as transfer reagents. The silver(I) perfluoroalcoholates are prepared by the reaction of AgF with the corresponding perfluorinated carbonyl compounds in acetonitrile and are stable for a prolonged time at -18°C . X-ray analysis of single crystals of perfluoroalcoholate species showed that two Ag(I)

centers are bridged by the alcoholate ligands. In acetonitrile solution, $\text{Ag}[\text{OCF}_3]$ forms different structures as indicated by IR spectroscopy. Furthermore, the silver(I) perfluoroalcoholates can be used as easy-to-handle transfer reagents for the synthesis of $\text{Cu}[\text{OCF}_3]$, $\text{Cu}[\text{OC}_2\text{F}_5]$, $[\text{PPh}_4][\text{Au}(\text{CF}_3)_3(\text{OCF}_3)]$, and fluorinated alkyl ethers.

Introduction

In recent years, the trifluoromethoxy group ($-\text{OCF}_3$) gained importance as a unique functional group in medicinal research,^[1,2] materials science,^[3] and coordination chemistry.^[4–7] Particularly, trifluoromethoxylation is a useful tool to tune the lipophilicity and metabolic stability, and to influence the conformation of bioactive compounds.^[2] Unlike other fluorinated groups, the $-\text{OCF}_3$ group has the advantage of being degradable into non-persistent compounds, like CO_2 and HF .^[8–10] Due to the high stability, mobility, and toxicity of some PFAS (per- and polyfluorinated alkyl substances), the EU demands a ban of these PFAS with some exceptions, especially for substances with $-\text{OCF}_3$ groups and for agrochemicals and pharmaceuticals.^[11] This shifts the focus even more to the research towards valuable and economical methods to introduce the $-\text{OCF}_3$ group into organic molecules. Important examples for $-\text{OCF}_3$ containing drugs include Pretomanid^[12] or the recently developed SARS-CoV-2 MPro inhibitor MI-09,^[13] while Triflumuron^[14] is a common insecticide (Figure 1).

In contrast to the well-established $-\text{OCF}_3$ group, higher perfluoroalkoxy groups remain underutilized despite their potential. For instance, the pentafluoroethoxy-substituted derivative of Riluzole shows a higher “antiglutamate” activity ($\text{ED}_{50} = 2.5 \text{ mg/kg}$) compared to Riluzole ($\text{ED}_{50} = 3.2 \text{ mg/kg}$),

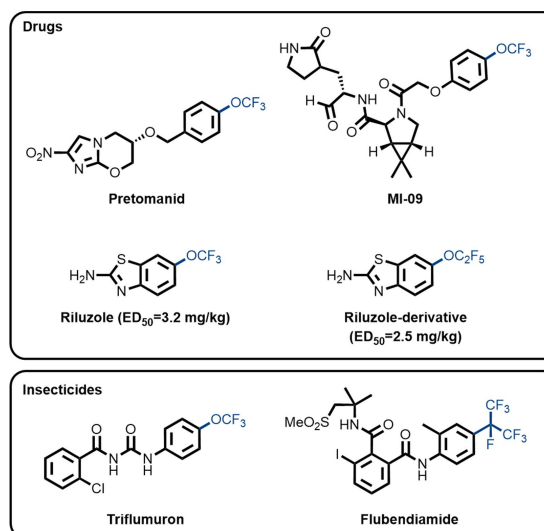


Figure 1. Examples of bioactive substances containing $-\text{OCF}_3$, $-\text{OC}_2\text{F}_5$, or $-i\text{-C}_3\text{F}_7$ groups under development or used as drugs or insecticides.

which is used for the treatment of amyotrophic lateral sclerosis (ALS).^[15] Similarly, Flubendiamide, an insecticide for controlling lepidopterous insects, is functionalized with a perfluorinated *iso*-propyl group which highlights the potential of larger perfluorinated groups.^[16] Therefore, it can be anticipated that higher perfluoroalkoxy groups such as $-\text{OC}_2\text{F}_5$, $-\text{O}(i\text{-C}_3\text{F}_7)$, and $-\text{O}(n\text{-C}_3\text{F}_7)$ could complement the toolbox of fluorinated moieties for the finetuning of pharmacological properties of drugs and for agrochemicals.

However, although several reagents have been developed that allow the convenient preparation of trifluoromethoxylated compounds, there are only a few suitable reagents for the introduction of higher perfluoroalkoxy groups.^[17–19] While most

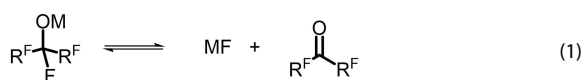
[a] P. Golz, K. Shakeri, L. Maas, M. Balizs, Dr. A. Pérez-Bitrián, H. D. Kemmler, Dr. M. Kleoff, Dr. P. Voßnacker, Prof. Dr. M. Christmann, Prof. Dr. S. Riedel
Fachbereich Biologie, Chemie, Pharmazie
Institut für Chemie und Biochemie—Anorganische Chemie
Fabeckstr. 34/36, 14195 Berlin (Germany)
E-mail: s.riedel@fu-berlin.de

Supporting information for this article is available on the WWW under <https://doi.org/10.1002/chem.202400861>

© 2024 The Authors. Chemistry - A European Journal published by Wiley-VCH GmbH. This is an open access article under the terms of the Creative Commons Attribution License, which permits use, distribution and reproduction in any medium, provided the original work is properly cited.

perfluoroalkoxylation reagents are bench-stable and easy-to-handle,^[20,21] they also present some drawbacks. These include high cost, complex preparations, and poor atom economy. In addition, many reagents require stoichiometric amounts of silver(I) salts to promote the desired perfluoroalkoxylation reaction. Very recently, Schoenebeck and coworkers developed a valuable method for the simple preparation of a stable solution of Ag[OCF₃] in acetonitrile via the reaction of bis(trichloromethyl)carbonate (BTC) with AgF.^[22] Additionally they could show that Ag[OCF₃] can be used for the effective synthesis of *N*-difluoromethyl amides.^[23]

Stable salts of the trifluoromethoxide anion [OCF₃][−] are reported and structurally analyzed for different cations like M⁺ (M=K, Rb, and Cs),^[24] Py⁺ ((2,4-dinitrophenyl)(dimethylamino)pyridinium),^[25] [NR₄]⁺ (R=alkyl),^[19] pip⁺ (1,1,3,3,5,5-hexamethylpiperidinium),^[26] and [(Me₂N)₃S]⁺.^[27] Cu[OCF₃] is also known in solution^[28] and was crystallized as side product from the attempted synthesis of [(SIPr)Cu(OCF₃)].^[6] For the pentafluoroethoxide anion [OC₂F₅][−], salts with cations such as M⁺ (M=Rb and Cs),^[29,30] [NR₄]⁺,^[19] and pip⁺^[26] form stable compounds, while for other primary and secondary perfluorinated alkoxides only few examples are reported. Hexafluoroacetone reacts with CsF, KF, and AgF in acetonitrile under formation of the corresponding [*i*-OC₃F₇][−] salts. By metathesis reaction of the potassium salt with [NEt₄][ClO₄] the [NEt₄][O(*i*-C₃F₇)] salt can be obtained.^[31] Similarly, the pip⁺^[26] and [(Me₂N)₃S]⁺^[27] salts could be synthesized and structurally analyzed. Also oxalyl fluoride is known to react with one equivalent of [NMe₄]F forming the mono alkoxide [NMe₄][F(C(O)CF₂O)].^[26]



Metal salts of perfluorinated tertiary alcoholates like the Ag[t-OC₄F₉] or Li[t-OC₄F₉] are relatively stable compounds,^[32,33] while the metal alcoholates with an α -fluorine (M[OC(R^F)₂F]) are in an equilibrium with the carbonyl ((O)C(R^F)₂) and the corresponding metal fluoride (MF) (1). This equilibrium is shifted to M[OR^F] if the lattice energy of the MF is comparably low. In the row of the alkaline metal fluorides the lattice energy decreases from Li to Cs while the stability of the corresponding M[OR^F] species is increasing.^[24] M[OC(R^F)₂F] species with the tendency to decompose can be stabilized by overcoming the lattice energy of MF by dissolution in a suitable solvent.^[22] Alternatively, M[OCF₃] species like [(SIPr)M(OCF₃)] (M=Cu or Au),^[6] [Ag(bpy)(PPh^tBu₂)(OCF₃)],^[4] [Ag(PPh^tBu₂)(OCF₃)],^[7] or [Ag(AryI-BIAN)(THF)(OCF₃)]^[5] are stabilized by using, e.g., phosphines, NHC or bidentate nitrogen ligands. Therefore, we envisaged to prepare and investigate an array of silver(I) salts of perfluoroalkoxy groups that could be used as atom-economic reagents for the introduction of perfluoroalkoxy groups into organic and inorganic molecules.

Results and Discussion

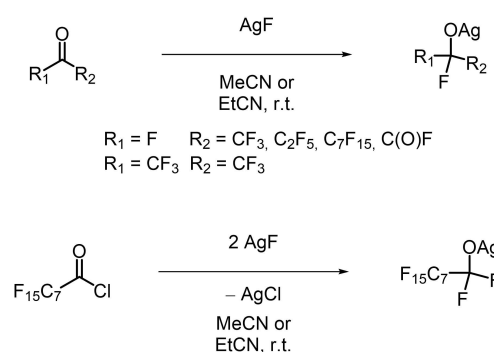
Silver(I) Trifluoromethoxide

At the outset, we envisioned the direct synthesis of Ag[OCF₃] from carbonyl fluoride and silver(I) fluoride as the simplest and most atom-economic starting materials. In a first experiment, we exposed a suspension of AgF in acetonitrile to an atmosphere of carbonyl fluoride providing Ag[OCF₃] in a quantitative yield according to ¹⁹F NMR spectroscopy after only 15 minutes (Scheme 1). After filtration of the reaction mixture, a clear solution of Ag[OCF₃] in acetonitrile was obtained, which is in accordance with previous results.^[22]

This solution decomposes slowly and showed a 15 % lower Ag[OCF₃] content after 6 days and had completely decomposed after one month at room temperature, while at −18 °C no significant decomposition was observed even after 15 months.

Structure

Single crystals of Ag[OCF₃] were obtained by cooling an acetonitrile solution to −40 °C. X-ray analysis of these crystals reveals the formation of polymeric chains of [Ag(MeCN)₂(OCF₃)]_n (Figure 2). In this structure, the silver cation is distorted trigonally pyramidal ($\tau_4=0.80$) coordinated by two acetonitrile molecules and two [OCF₃][−] anions, while the [OCF₃][−] anion coordinates as a bridging ligand via the oxygen atom to two silver centers. Due to the disorder of the −CF₃ group we do not discuss the C–F bond lengths. However, this does not affect so much the C–O bond, which shows a bond length of 123.28(19) pm and is similarly short as in [(Me₂N)₃S][OCF₃] (122.7(4) pm)^[27] due to its high double bond character, despite the coordination of the [OCF₃][−] anion to the silver atom. In the similar ligand-stabilized compounds [Ag(bpy)(PPh^tBu₂)(OCF₃)] (128.1(3) pm)^[4] and [Ag(AryI-BIAN)(THF)(OCF₃)] (131.5(6) pm)^[5] the C–O bonds are significantly longer. When warming up these crystals to room temperature, decomposition under evolution of a gas was observed, indicating the formation of COF₂, AgF, and MeCN.



Scheme 1. Synthesis of silver(I) perfluoroalcoholates starting from silver fluoride and fluorinated carbonyl compounds.

By adding 2 equivalents of 2,2'-bipyridine (bpy) to a solution of $\text{Ag}[\text{OCF}_3]$ the room-temperature-stable compound $[\text{Ag}(\text{bpy})_2][\text{OCF}_3]$ can be isolated (2). X-ray analysis of single crystals obtained similarly to the ones of $\text{Ag}[\text{OCF}_3]$ revealed an ion separation in the solid state (Figure 2). The exchange of the acetonitrile ligands by the stronger bpy ligands leads to the formation of the $[\text{Ag}(\text{bpy})_2]^+$ cation, in which the coordination sphere of Ag is saturated by bpy ligands. The $[\text{OCF}_3]^-$ anion is slightly distorted ($\tau_4=0.90$) like in $\text{Ag}[\text{OCF}_3]$ and the bond lengths are similar to the corresponding ones in $\text{Ag}[\text{OCF}_3]$ and $[(\text{Me}_2\text{N})_3\text{S}][\text{OCF}_3]$.^[27]

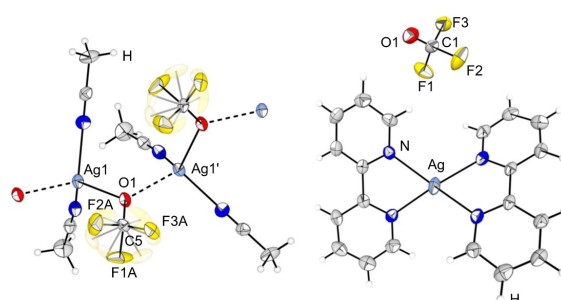
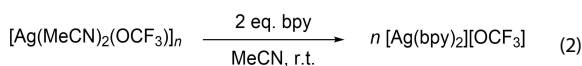


Figure 2. Polymeric chain structure of $[\text{Ag}(\text{MeCN})_2(\text{OCF}_3)]_n$ (left) and molecular structure of $[\text{Ag}(\text{bpy})_2][\text{OCF}_3]$ (right) in the solid state. Thermal ellipsoids are set at 50% probability. Disorder of the CF_3 group (left) and solvent and second molecule (right) are omitted for clarity. Selected bond lengths [pm] and angles $[\circ]$ of $[\text{Ag}(\text{MeCN})_2(\text{OCF}_3)]_n$: 133.9(8) (C5–F1 A), 138.3(8) (C5–F2 A), 136.6(9) (C5–F3 A), 123.28(19) (C5–O1), 234.17(12) (O1–Ag1), 239.98(12) (O1–Ag1'), 116.5(6) (O1–C5–F1 A), 102.2(7) (F1 A–C5–F2 A), 102.2(7) (F1 A–C5–F3 A). Selected bond lengths [pm] and angles $[\circ]$ of $[\text{Ag}(\text{bpy})_2][\text{OCF}_3]$: 122.5(5) (C1–O1), 137.9(5) (C1–F1), 137.5(5) (C1–F2), 137.9(5) (C1–F3), 116.2(4) (O1–C1–F1), 102.5(3) (F1–C1–F2).

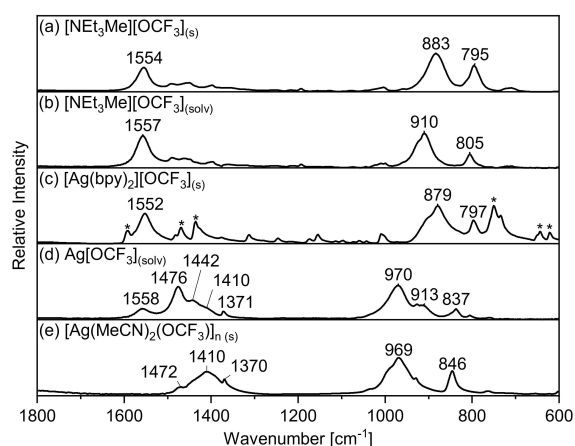


Figure 3. ATR infrared spectra between 600 and 1800 cm^{-1} of solid (s) or dissolved in acetonitrile (solv) $[\text{OCF}_3]^-$ compounds. (a): solid $[\text{NET}_3\text{Me}][\text{OCF}_3]$ at r.t., (b): $[\text{NET}_3\text{Me}][\text{OCF}_3]$ 0.65 M solution in acetonitrile at r.t., (c): $[\text{Ag}(\text{bpy})_2][\text{OCF}_3]$ solid at r.t. (* = $[\text{Ag}(\text{bpy})_2]^+$), (d): $[\text{Ag}][\text{OCF}_3]$ 0.65 M solution in acetonitrile at r.t., (e) crystals of $[\text{Ag}(\text{MeCN})_2(\text{OCF}_3)]_n$ at $T = -40^\circ\text{C}$.

IR Spectroscopic Investigations

To get more insights into the nature and especially the stability of $\text{Ag}[\text{OCF}_3]$ in solution and their effects on the reactivity we compared the ATR infrared spectra of different $[\text{OCF}_3]^-$ containing compounds in the solid state or in acetonitrile solution (Figure 3). Quaternary ammonium cations like $[\text{NET}_3\text{Me}]^+$ are known for their weak interactions with anions.^[34] Therefore, we anticipated that the ion interactions in $[\text{NET}_3\text{Me}][\text{OCF}_3]$ should be weak as well. The ATR IR spectrum of solid $[\text{NET}_3\text{Me}][\text{OCF}_3]$ (a) obtained by reacting $[\text{NET}_3\text{Me}]\text{Cl}$ with $\text{Ag}[\text{OCF}_3]$, shows a strong band for the C–O stretching ($\nu(\text{C–O})$) at 1554 cm^{-1} and at 883 and 795 cm^{-1} for the antisymmetric ($\nu_{\text{as}}(\text{C–F})$) and symmetric ($\nu_{\text{s}}(\text{C–F})$) C–F stretching mode, respectively. In solution (MeCN) the C–F stretching bands are slightly blue shifted (b). The ATR IR spectrum of solid $[\text{Ag}(\text{bpy})_2][\text{OCF}_3]$ (c) shows bands of the $[\text{OCF}_3]^-$ anion similar to the corresponding ones in $[\text{NET}_3\text{Me}][\text{OCF}_3]$. Since the ion separation in $[\text{Ag}(\text{bpy})_2][\text{OCF}_3]$ crystals is known from the X-ray analysis the weak ion interactions in $[\text{NET}_3\text{Me}][\text{OCF}_3]$ can be confirmed from the IR spectra. However, the ATR IR spectrum of $\text{Ag}[\text{OCF}_3]$ in solution (d) show bands for different $[\text{OCF}_3]^-$ anion species. Besides smaller bands for the isolated $[\text{OCF}_3]^-$ anion, bands for different oligo and polymeric structures are observed. In the case of the solid $[\text{Ag}(\text{MeCN})_2(\text{OCF}_3)]_n$ the $\nu(\text{C–O})$ appear as a broad band with a red shifted maximum at 1472 cm^{-1} and minor bands at 1410 and 1370 cm^{-1} . Contrary to the similar C–O bond lengths in $[\text{Ag}(\text{MeCN})_2(\text{OCF}_3)]_n$ and $[\text{Ag}(\text{bpy})_2][\text{OCF}_3]$, the $\nu(\text{C–O})$ is significantly shifted in solid $[\text{Ag}(\text{MeCN})_2(\text{OCF}_3)]_n$ to lower wavenumbers indicating a lower bond strength. This mismatch is most likely due to effects regarding the polymeric structure. The comparison of IR spectra of different $[\text{OCF}_3]^-$ species cannot fully clarify the structure of $\text{Ag}[\text{OCF}_3]$ in MeCN solution. The observation of different species indicates an equilibrium between isolated $[\text{OCF}_3]^-$ anions and those bound to silver cations. The occurrence of many species can also be an explanation for the very broad ^{19}F NMR signal of $\text{Ag}[\text{OCF}_3]$. Nevertheless, the partially isolated $[\text{OCF}_3]^-$ anions should have a higher nucleophilicity than those bound to silver centers, while the coordination to silver can facilitate reactivities over the coordination sphere of the metal.

Reaction Energy of $\text{Ag}[\text{OCF}_3]$ Synthesis

During the synthesis of $\text{Ag}[\text{OCF}_3]$ we noticed an exothermic reaction when adding carbonyl fluoride to AgF . To quantify the released energy, we investigated the thermodynamic properties of the reaction by heat flow calorimetry. The reaction enthalpy was determined to be $\Delta_{\text{r}}H = -66.7 \text{ kJ mol}^{-1}$. This is in good agreement with the solvation corrected (MeCN) fluoride ion affinity $\text{FIA}_{\text{solv}}(\text{MeCN}) = 71 \text{ kJ mol}^{-1}$ of COF_2 obtained from the experimental FIA (208.8 kJ mol^{-1})^[35] and the calculated solvation energy at PW6B95-D3(BJ)/def2-QZVPP level of theory. However, the value for the FIA disregards the interaction of the $[\text{OCF}_3]^-$ anion with the silver cations or the energy contribution of the solvation of AgF in acetonitrile.

Higher Silver(I) Alkoxides

Intrigued by the easy and clean formation of $\text{Ag}[\text{OCF}_3]$ we anticipated that this reactivity could be extended to further carboxylic acid fluorides. The calculated solvation (MeCN) corrected FIA values at PW6B95-D3(BJ)/def2-QZVPP level of theory of trifluoroacetyl fluoride ($\text{CF}_3\text{C}(\text{O})\text{F}$, 69 kJ mol^{-1}), pentafluoropropionyl fluoride ($\text{C}_2\text{F}_5\text{C}(\text{O})\text{F}$, 68 kJ mol^{-1}), hexafluoroacetone ($\text{CF}_3\text{C}(\text{O})\text{CF}_3$, 74 kJ mol^{-1}), oxalyl fluoride ($\text{F}(\text{O})\text{CC}(\text{O})\text{F}$, 60 kJ mol^{-1}), and perfluorooctanoic acid fluoride ($\text{C}_7\text{F}_{15}\text{C}(\text{O})\text{F}$, 49 kJ mol^{-1}) show only a small difference to the value of COF_2 (See Experimental Section for Details). Indeed, the reaction of AgF with these fluorinated carbonyls gave the corresponding AgOR^f compounds in quantitative yields within 15 minutes (Scheme 1). $\text{F}(\text{O})\text{CC}(\text{O})\text{F}$ was found to react with only one equivalent of AgF forming the monoanion. Instead of $\text{C}_7\text{F}_{15}\text{C}(\text{O})\text{F}$ the corresponding acid chloride was used together with 2 equiv. of AgF (Scheme 1).

The ^{19}F NMR spectra of the silver(I) perfluoroalcoholates show a broad signal for the α -fluorine atom with shifts of $\delta(\text{ppm}) = -0.3 \text{ ppm}$ ($\text{Ag}[\text{OCF}_2\text{C}(\text{O})\text{F}]$), -25.9 ppm ($\text{Ag}[\text{OCF}_3]$), -33.2 ppm ($\text{Ag}[\text{OC}_8\text{F}_{17}]$), -34.5 ppm ($\text{Ag}[\text{O}(n\text{-C}_3\text{F}_7)]$), -41.0 ppm ($\text{Ag}[\text{OC}_2\text{F}_5]$), and -80.8 ppm ($\text{Ag}[\text{O}(i\text{-C}_3\text{F}_7)]$). The other $-\text{CF}_2-$ and $-\text{CF}_3$ groups have relatively sharp signals in the normal region for these groups. Notably, $\text{Ag}[\text{OCF}_2\text{C}(\text{O})\text{F}]$ shows only one signal for all three fluorine atoms indicating a fast exchange of the fluoride between the two sides.

X-ray Analysis

$\text{Ag}[\text{OC}_2\text{F}_5]$ and $\text{Ag}[\text{O}(i\text{-C}_3\text{F}_7)]$ were crystallized by cooling propionitrile solution to -77°C . In contrast to the polymeric chain structure of $\text{Ag}[\text{OCF}_3]$, the X-ray diffraction analysis of both colorless crystals reveals the formation of dimeric species $[\text{Ag}(\text{EtCN})_2(\text{OC}_2\text{F}_5)]_2$ and $[\text{Ag}(\text{EtCN})_2(\text{O}(i\text{-C}_3\text{F}_7))]_2$ (Figure 4). Even though these structures differ from the polymeric structure of $\text{Ag}[\text{OCF}_3]$ there are several similarities. In $[\text{Ag}(\text{EtCN})_2(\text{OC}_2\text{F}_5)]_2$ and $[\text{Ag}(\text{EtCN})_2(\text{O}(i\text{-C}_3\text{F}_7))]_2$ the silver atoms are coordinated by two propionitrile molecules and two bridging alcoholate

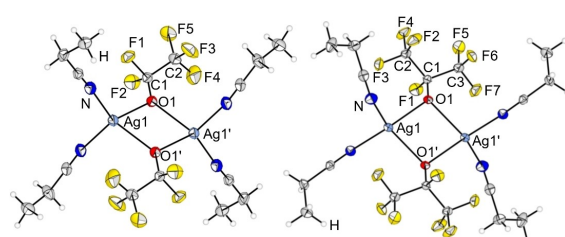


Figure 4. Molecular structure of $[\text{Ag}(\text{EtCN})_2(\text{OC}_2\text{F}_5)]_2$ (left) and $[\text{Ag}(\text{EtCN})_2(\text{O}(i\text{-C}_3\text{F}_7))]_2$ (right) in the solid state. Thermal ellipsoids are set at 50% probability. Co-crystallized solvent molecules are omitted for clarity. Selected bond lengths [pm] and angles [$^\circ$] of $[\text{Ag}(\text{EtCN})_2(\text{OC}_2\text{F}_5)]_2$: $140.1(2)$ ($\text{C}1-\text{F}1$), $141.4(2)$ ($\text{C}1-\text{F}2$), $124.8(2)$ ($\text{C}1-\text{O}1$), $235.45(13)$ ($\text{O}1-\text{Ag}1$), $238.73(13)$ ($\text{O}1-\text{Ag}1'$), $114.90(15)$ ($\text{O}1-\text{C}1-\text{F}1$), $100.82(14)$ ($\text{F}1-\text{C}1-\text{F}2$). Selected bond lengths [pm] and angles [$^\circ$] of $[\text{Ag}(\text{EtCN})_2(\text{O}(i\text{-C}_3\text{F}_7))]_2$: $143.19(13)$ ($\text{C}1-\text{F}1$), $129.07(14)$ ($\text{C}1-\text{O}1$), $231.21(9)$ ($\text{O}1-\text{Ag}1$), $242.05(9)$ ($\text{O}1-\text{Ag}1'$), $114.16(9)$ ($\text{O}1-\text{C}1-\text{F}1$).

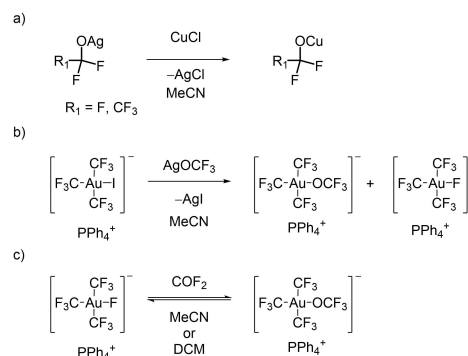
ligands in a trigonal pyramidal ($\tau_4 = 0.82$) and distorted seesaw geometry ($\tau_4 = 0.73$), respectively.

The C–F bond lengths at the α carbon atom are in good agreement with those in the corresponding pip salts.^[26] The C–O bond lengths are in the typical range^[26] and increase from $\text{Ag}[\text{OCF}_3]$ ($123.28(19) \text{ pm}$) to $[\text{Ag}(\text{EtCN})_2(\text{OC}_2\text{F}_5)]_2$ ($124.8(2) \text{ pm}$) and to $[\text{Ag}(\text{EtCN})_2(\text{O}(i\text{-C}_3\text{F}_7))]_2$ ($129.07(14) \text{ pm}$), possibly due to the exchange of fluorine atoms by the slightly less electro-negative CF_3 groups, resulting in a higher electron density at the central carbon atom.

Transmetalation Reactions and Coordination

Besides the perfluoroalcoholates of silver(I), the transfer to other metal centers is of interest with respect to new pathways for the incorporation of these groups into organic molecules. Therefore, we re-evaluated the less described $\text{Cu}[\text{OCF}_3]$ by the transmetalation reaction of $\text{Ag}[\text{OCF}_3]$ with CuCl (Scheme 2a). The ^{19}F NMR spectrum shows a very broad signal at $\delta = -24.2 \text{ ppm}$ ($\text{fwhm} = 1500 \text{ Hz}$) for the $[\text{OCF}_3]^-$ anion. In the same manner $\text{Cu}[\text{OC}_2\text{F}_5]$ can be obtained starting from $\text{Ag}[\text{OC}_2\text{F}_5]$ and CuCl (Scheme 2a). The ^{19}F NMR spectrum shows a very broad signal at $\delta = -39.4 \text{ ppm}$ ($\text{fwhm} = 1600 \text{ Hz}$) for the fluorine atoms at the α carbon and a singlet at $\delta = -83.9 \text{ ppm}$ for the CF_3 group. Both substances are stable for a short time in MeCN solution but decompose upon removal of the solvent. Crystals of $[\text{Cu}(\text{MeCN})_4][\text{OCF}_3]$ and $[\text{Cu}(\text{MeCN})_4][\text{OC}_2\text{F}_5]$ suitable for X-ray diffraction could be obtained by slowly cooling the corresponding acetonitrile solutions to -40°C . In contrast to the silver(I) derivatives, $[\text{Cu}(\text{MeCN})_4][\text{OCF}_3]$ and $[\text{Cu}(\text{MeCN})_4][\text{OC}_2\text{F}_5]$ show a different connectivity (Figure 5). The Cu atoms are coordinated by four MeCN molecules, while the $[\text{OR}^f]^-$ anions are isolated. In $[\text{Cu}(\text{MeCN})_4][\text{OCF}_3]$ one of the three crystallographically independent $[\text{OCF}_3]^-$ anions in the unit cell is disordered. The C–F and C–O bond lengths are similar to the ones in the corresponding silver(I) perfluoroalcoholates.

In contrast, attempts to crystallize $\text{Cu}[\text{O}(n\text{-C}_3\text{F}_7)]$ and $\text{Cu}[\text{O}(i\text{-C}_3\text{F}_7)]$, obtained by transmetalation reactions, failed, although



Scheme 2. a) Transmetalation reaction of $\text{Ag}[\text{OCF}_3]$ with CuCl under formation of $\text{Cu}[\text{OCF}_3]$, b) reaction of $[\text{PPh}_4][\text{Au}(\text{CF}_3)_3]$ with $\text{Ag}[\text{OCF}_3]$ and c) reaction of $[\text{PPh}_4][\text{Au}(\text{CF}_3)_3]$ with COF_2 .

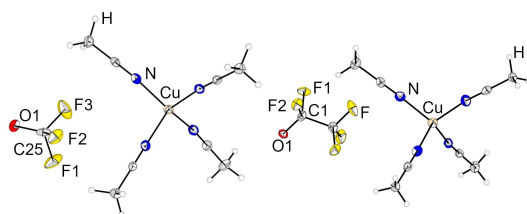


Figure 5. Molecular structure of $[\text{Cu}(\text{MeCN})_4][\text{OCF}_3]$ (left) and $[\text{Cu}(\text{MeCN})_4][\text{OC}_2\text{F}_5]$ (right) in the solid state. Thermal ellipsoids are set at 50% probability. Co-crystallized solvent molecules are omitted for clarity. Selected bond lengths [pm] and angles $^\circ$ of $[\text{Cu}(\text{MeCN})_4][\text{OCF}_3]$: 124.0(6) (C25–O1), 138.8(7) (C25–F1), 139.4(7) (C25–F2), 137.2(7) (C25–F3), 115.8(6) (O1–C25–F1), 102.6(4) (F1–C25–F2). Selected bond lengths [pm] and angles $^\circ$ of $[\text{Cu}(\text{MeCN})_4][\text{OC}_2\text{F}_5]$: 126.2(5) (C1–O1), 143.3(3) (C1–F1), 140.1(5) (C1–F2), 111.8(3) (O1–C1–F1), 104.0(3) (F1–C1–F2).

The ^{19}F NMR spectra showed signals for perfluoroalcoholate species. Instead of the desired Cu(I) compounds, crystals of mixed valent Cu(I/II) species were obtained. From an experiment to synthesize $\text{Cu}[\text{O}(i\text{-C}_3\text{F}_7)]$ in propionitrile solution, crystals could be obtained showing a species with a Cu(II) center coordinated by the chelating ligand $[\text{OC}(\text{CF}_3)_2\text{O}(\text{C}(\text{CF}_3)_2\text{O})_2]^{2-}$ and $[\text{Cu}(\text{MeCN})_4]^+$ cations (SI, Figure S1).

Very recently our group synthesized the first Au(III) complex with $[\text{OCF}_3]^-$ as a ligand, $[\text{AuF}_2(\text{OCF}_3)(\text{SIMes})]$, by the reaction of $[\text{AuF}_3(\text{SIMes})]$ and COF_2 .^[36] Herein we report the formation of the anionic Au(III) complex $[\text{Au}(\text{CF}_3)_3(\text{OCF}_3)]^-$. The well understood system $[\text{PPh}_4][\text{Au}(\text{CF}_3)_3\text{X}]$ where X is an anionic ligand, mostly a halogen or similar behaving system is easily accessible from the iodide complex $[\text{PPh}_4][\text{Au}(\text{CF}_3)_3\text{I}]$ and a silver salt (AgX).^[37,38] Transferring this reactivity to our $\text{Ag}[\text{OCF}_3]$ system led to the formation of $[\text{PPh}_4][\text{Au}(\text{CF}_3)_3(\text{OCF}_3)]$ in solution (Scheme 2b). ^{19}F NMR spectroscopy of the reaction mixture revealed the formation of the species $[\text{PPh}_4][\text{Au}(\text{CF}_3)_3(\text{OCF}_3)]$, with ^{19}F NMR shifts of $\delta = -28.0$ ppm (sept) for *trans*- CF_3 , $\delta = -36.8$ ppm (br, s) for the $[\text{OCF}_3]^-$ ligand and $\delta = -39.4$ ppm (q) for the *cis*- CF_3 groups. The signals for the $-\text{CF}_3$ groups show no resolved coupling to the broad signal for the OCF_3 . Additionally the fluoride complex $[\text{PPh}_4][\text{Au}(\text{CF}_3)_3\text{F}]$ (δ (ppm) = -28.5 (dsept, $\text{CF}_3\text{-Au-X}$), -40.8 (dq, $\text{CF}_3\text{-Au-CF}_3$), and -250.0 (qsept, Au-F) is formed.^[38] During the NMR experiments we noticed the decomposition of $[\text{PPh}_4][\text{Au}(\text{CF}_3)_3(\text{OCF}_3)]$, even when storing the solution at lower temperatures. ESI mass spectrometry of a freshly prepared sample of $[\text{PPh}_4][\text{Au}(\text{CF}_3)_3(\text{OCF}_3)]$ confirmed the formation of the $[\text{Au}(\text{CF}_3)_3(\text{OCF}_3)]^-$ anion with a molecule peak at 488.9429 m^{-1} (calc. 488.94286). The species $[\text{Au}(\text{CF}_3)_3\text{F}]^-$ with a molecule peak at 422.9569 m^{-1} (calc. 422.95113) is not only formed during the synthesis reaction, but also during the mass spectrometry experiments. This could be confirmed by a MSMS experiment isolating the $[\text{Au}(\text{CF}_3)_3(\text{OCF}_3)]^-$ anion. Attempts to crystallize $[\text{PPh}_4][\text{Au}(\text{CF}_3)_3(\text{OCF}_3)]$ failed due to decomposition. To further investigate the desired product, we reacted the fluoride complex $[\text{PPh}_4][\text{Au}(\text{CF}_3)_3\text{F}]$ in MeCN or DCM with an atmosphere of carbonyl fluoride (Scheme 2c), as it was already described for the similar $[\text{AuF}_2(\text{OCF}_3)(\text{SIMes})]$.^[36] In both solvents the ^{19}F NMR spectra showed a mixture of the $[\text{OCF}_3]^-$ and the F^-

complex and carbonyl fluoride. In the case where MeCN was the solvent, decomposition of $[\text{Au}(\text{CF}_3)_3(\text{OCF}_3)]^-$ was observed. In DCM solution it was stable for a few days, but the conversion of $[\text{PPh}_4][\text{Au}(\text{CF}_3)_3\text{F}]$ into the product was lower. The ^{19}F NMR spectrum revealed the formation of a 1:1.2:2.4 mixture of $[\text{PPh}_4][\text{Au}(\text{CF}_3)_3(\text{OCF}_3)]$, $[\text{PPh}_4][\text{Au}(\text{CF}_3)_3\text{F}]$ and COF_2 in DCM-d_2 , while giving sufficiently resolved signals to determine the coupling constant $^5J(^{19}\text{F}, ^{19}\text{F}) = 2.3$ Hz between the fluorine atoms of the $-\text{OCF}_3$ and the $-\text{CF}_3$ groups. This is in good agreement with the known complex $[\text{AuF}_2(\text{OCF}_3)(\text{SIMes})]$, which shows a quartet signal at -40.2 ppm ($^4J(^{19}\text{F}, ^{19}\text{F}) = 1.9$ Hz) for the $[\text{OCF}_3]^-$ ligand.^[36] Crystallization attempts failed from the DCM mixture.

Transfer Reactions to Organic Halides

As the introduction of fluorinated groups is one of the key techniques in contemporary medicinal chemistry to tune properties such as lipophilicity and stability of potential drugs, we investigated the application of the prepared silver(I) perfluoroalcoholates as transfer reagents (Figure 6). Assuming that silver(I) perfluoroalcoholates would behave as relatively weak nucleophiles, our experiments concentrated on highly reactive benzyl bromides and alkyl iodides. During the reaction,

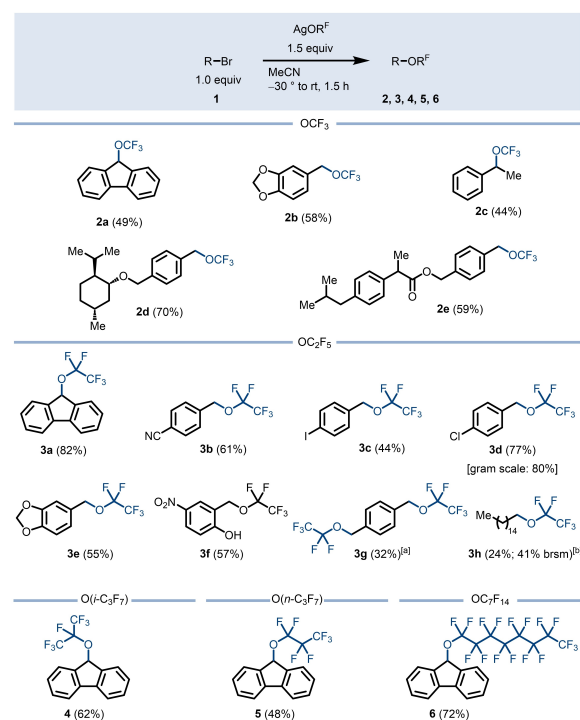


Figure 6. Scope of organic compounds for the introduction of perfluoroalkyl ether groups to alkyl bromides. Conditions: alkyl bromide (1.0 equiv), silver(I) perfluoroalcoholate (2.5 equiv), MeCN, -30 $^\circ\text{C}$ to r.t., 1 h.^[a] 2.5 equiv. of $\text{Ag}[\text{OC}_2\text{F}_5]$.^[b] The corresponding alkyl iodide was used. Brsm = based on recovered starting material.

these substrates would precipitate silver(I) bromide or silver(I) iodide, respectively, thereby further activating the substrates. By treating various alkyl bromides **1** with silver(I) perfluoroalcoholates at -30°C , the corresponding fluorinated ethers **2–6** were obtained in up to 82% yield. Following this procedure, trifluoromethoxylation of the corresponding benzyl bromides afforded the products **2a–2e** in 44% to 70% yield. Interestingly, this reaction was also successful for the (–)-menthol derivative **2d** (70% yield) and the trifluoromethoxylated ibuprofen ester **2e** (59% yield) (See the Supporting Information for limitations of this protocol).

As there are only few protocols for the introduction of $-\text{OC}_2\text{F}_5$ groups by substitution,^[19] we explored the usage of the silver salt $\text{Ag}[\text{OC}_2\text{F}_5]$ to realize this desirable transformation. Following the same procedure, the fluorenyl ether **3a** was obtained in a yield of 82%. This method accommodates various functional groups, including nitriles (**3b**, 61% yield), aryl halides (**3c**, 44%; **3d**, 77%), acetals (**3e**, 55% yield), and nitrophenols (**3f**, 57% yield). To demonstrate the scalability of this reaction, we performed the synthesis of fluorinated alkyl ether **3d** on a gram scale in a slightly better yield of 80%. Notably, by using 2.5 equiv. of $\text{Ag}[\text{OC}_2\text{F}_5]$ also a twofold substitution could be realized providing product **3g** (38% yield). In addition, this method is also applicable for alkyl compounds as shown for the fluorinated alkyl ether **3h**, although the reaction proceeded slower in this case (24% yield).

Finally, we tested the higher silver(I) alcoholates for the substitution reaction with fluorenyl bromide providing the corresponding $-i\text{-OC}_3\text{F}_7$ ether **4** in 62% yield, the $-n\text{-C}_3\text{F}_7$ ether **5** in 48% yield, and the highly fluorinated $-\text{OC}_7\text{F}_{14}$ ether **6** in 72% yield.

These experiments demonstrate that the prepared silver(I) alcoholates are versatile and easy-to-handle reagents for the transfer of fluorinated ether moieties to various substrates with short reaction times.

Conclusions

In conclusion, we disclosed a general access to silver(I) perfluoroalcoholates by the reaction of AgF with the corresponding perfluorinated carbonyl compounds in acetonitrile including $\text{Ag}[\text{OCF}_3]$, $\text{Ag}[\text{OC}_2\text{F}_5]$, $\text{Ag}[\text{O}(i\text{-C}_3\text{F}_7)]$, $\text{Ag}[\text{O}(n\text{-C}_3\text{F}_7)]$, and $\text{Ag}[\text{OC}_8\text{F}_{17}]$. These silver(I) perfluoroalcoholates are stable for months when stored at -18°C . Investigation of the molecular structures by X-ray diffractometry revealed that the perfluorinated alcoholates serve as bridging ligands coordinating to two Ag(I) centers for dimeric and polymeric structures. In contrast, when dissolved in acetonitrile various structures of $\text{Ag}[\text{OCF}_3]$ could be observed by IR spectroscopy.

Notably, we found that the acetonitrile solutions of the silver(I) perfluoroalcoholates serve as easy-to-handle reagents for the transfer of perfluoroalcoholates. We first investigated transmetalation reactions to other coinage metals providing $\text{Cu}[\text{OCF}_3]$, $\text{Cu}[\text{OC}_2\text{F}_5]$, and $[\text{PPh}_4][\text{Au}(\text{CF}_3)_3(\text{OCF}_3)]$. In contrast to the corresponding silver(I) salts, in the molecular structures of $[\text{Cu}(\text{MeCN})_4][\text{OCF}_3]$ and $[\text{Cu}(\text{MeCN})_4][\text{OC}_2\text{F}_5]$ the perfluoroalcoholate

late anions are separated from the metal centers. Additionally, we demonstrated that acetonitrile solutions of the prepared silver(I) perfluoroalcoholates can be used to introduce perfluoroalkoxy groups into organic molecules. We anticipate that these metal perfluoroalcoholates will become valuable reagents in future.

Experimental Section

Experiments with air sensitive compounds were conducted under exclusion of moisture and air using standard Schlenk techniques. Sensitive solids were handled inside an MBRAUN UNILab plus glovebox with an argon atmosphere ($\text{c}(\text{O}_2) < 0.5$ ppm, $\text{c}(\text{H}_2\text{O}) < 0.5$ ppm). All purchased chemicals were used without further treatment. Pentane used for column chromatography was redistilled prior to use. Solvents were dried using an MBRAUN SPS-800 solvent system and stored over 3 Å molecular sieves. Thin-layer chromatography was performed on silica gel coated aluminium plates ALUGRAM® Xtra SIL G/UV254 (Macherey-Nagel). The product spots were detected by UV light (254 nm) or as permanganate stains. Flash column chromatography was performed with silica gel 60 M (0.040–0.063 mm, 230–400 mesh, Macherey-Nagel). $[\text{PPh}_4][\text{Au}(\text{CF}_3)_3\text{F}]$ and $[\text{PPh}_4][\text{Au}(\text{CF}_3)_3]$ were prepared via literature-known procedures.^[38] IR spectra of moisture and temperature sensitive solids were measured under a cooled nitrogen stream using a Nicolet iS50 FTIR spectrometer with a diamond ATR attachment with 32 scans and a resolution of 4 cm^{-1} . IR spectra of air insensitive solids were measured with a NICOLET iS10 FTIR spectrometer equipped with an ATR unit (NICOLET SMART DuraSamplIR) and only diagnostic absorption bands are reported. IR spectra of air sensitive solutions were measured at room temperature using a Vertex70 with external MCT detector and an ATR Fiber Probe IN-350-T. IR spectra were processed using OPUS 7.5 and Origin 2022 was used for their graphical representation. NMR spectra were recorded using a Varian INOVA 600 (600 MHz), JEOL (ECZ-R 400, ECS 400, ECA 400, ECX 400, ECP 500, ECZ 600), or BRUKER (AVANCE III 500, AVANCE III 700) spectrometer and all chemical shifts are referenced using the δ values given in the IUPAC recommendations of 2008 and the ^2H signal of the deuterated solvent as internal reference.^[39] For external locking, acetone- d_6 was flame sealed in a glass capillary and the lock oscillator frequency was adjusted to give $\delta(^1\text{H}) = 7.26$ ppm for a CHCl_3 sample locked on the capillary. MestReNova 14.2 was used for processing the spectra and for their graphical representation. ^1H NMR yields were measured using CH_2Br_2 as an internal standard. X-ray diffraction measurements were performed on a Bruker D8 Venture diffractometer with $\text{MoK}\alpha$ ($\lambda = 0.71073\text{ \AA}$) radiation at 100 K. Single crystals were picked in perfluoroether oil at -40°C under a nitrogen atmosphere and mounted on a 0.15 mm Mitegen micromount. They were solved using the ShelXT structure solution program with intrinsic phasing and were refined with the refinement package ShelXL using least squares minimizations by using the program OLEX2 Diamond 3 and POV-Ray 3.7 were used for their graphical representation. ESI mass spectrum of $[\text{PPh}_4][\text{Au}(\text{CF}_3)_3(\text{OCF}_3)]$ was recorded using a Synapt G2-S HDMS mass spectrometer by Waters Co., MA, USA. The ionization and transfer conditions of the mass spectrometer were optimized for maximal intensity of instable inorganic molecules. Negative ESI with a capillary voltage of 1.6 kV was used. The source temperature was set to 40°C , the desolvation temperature was set to 80°C . Sampling cone and source offset voltages were set to 25 and 50 V. The desolvation gas flow was 350.0 L/hr. For the analysis, dry acetonitrile and Pressurized Sample Infusion ESI^[40] was used to establish inert source conditions. LockSpray correction (LeuEnk, m/z

554.27) was used for exact mass measurement / internal recalibration mass spectra only since the lock spray solvent contained 0.1% Formic acid and led to fast degradation of the analysts. High-resolution mass spectra of organic substrates were measured with an Agilent (6210 ESI-TOF; 4 μ L/min, 1.0 bar, 4 kV) or EI-MS (MAT 711, 80 eV). Quantum-chemical calculations were conducted using the HPC system provided by the ZEDAT (Freie Universität Berlin, Curta).^[41] The program Orca 5.0.3^[42] was used with PW6B95^[43] or B3LYP^[44] as functional and the basis sets def2-QZVPP^[45,46]. The FIA values were calculated from the optimized structures at PW6B95-D3(BJ)/def2-QZVPP level of theory similar to the literature procedure.^[35] For the solvation correction the difference of the single point energies at PW6B95-D3(BJ)/def2-QZVPP level of theory between the ones with solvation (c-pcm, MeCN) and without were used. (See Supporting Information for structures) Calorimetric measurements were performed with an EasyMax 102 Thermostat System by Mettler Toledo (100 mL glass reactor, temperature sensor: Pt100 FEP-coated) using the HFCal upgrade kit. (for details, see SI)

Preparation of Ag[OR^F] Solutions

AgF (1.27 g, 10 mmol) was suspended in MeCN or EtCN (10 mL). After degassing the suspension, an excess of the gaseous fluorinated acid fluoride or ketone was added at r.t. until the vessel retained a constant pressure (0.5–1.0 bara, normally less than 15 min.). Any excess of gas was removed by pumping off for 15 sec. After pressurizing the vessel with argon again, the solution was filtered with a syringe filter (PTFE, 0.45 μ m). The obtained Ag[OR^F] solution (1 M) was stored in a glass vessel at -20°C .

Ag[OCF₃]

¹⁹F NMR (377 MHz, MeCN-d₃, 20 $^{\circ}\text{C}$): $\delta = -25.9$ ppm (s, fwhm = 310 Hz, 3F).

Ag[OC₂F₅]

¹⁹F NMR (377 MHz, MeCN-d₃, 16 $^{\circ}\text{C}$): $\delta = -41.0$ (s, fwhm = 240 Hz, 2F, OCF₂), -84.5 ppm (s, 3F, CF₃).

Ag[O(i-C₃F₇)]

¹⁹F NMR (377 MHz, MeCN-d₃, 21 $^{\circ}\text{C}$): $\delta = -80.8$ (s, fwhm = 85 Hz, 1F, OCF), -82.0 ppm (s, 6F, CF₃).

Ag[O-nC₃F₇]

¹⁹F NMR (377 MHz, MeCN-d₃, 21 $^{\circ}\text{C}$): $\delta = -34.5$ (s, fwhm = 530 Hz, 2F, OCF₂), -82.0 (s, 3F, CF₃), -126.3 ppm (s, 2F, CF₂).

Preparation of Ag[OCF₂C(O)F]

AgF (0.25 g, 2 mmol, 1 eq.) was suspended in MeCN (2 mL) and FC(O)C(O)F (2 mmol, 1 eq.) was condensed into the reaction vessel at -196°C . After warming up to r.t. the suspension was stirred for 15 min. The obtained Ag[OCF₂C(O)F] solution (1 M) was stored in a glass vessel at -20°C .

¹⁹F NMR (377 MHz, MeCN-d₃, 18 $^{\circ}\text{C}$): $\delta = -0.3$ ppm (s, fwhm = 130 Hz).

Preparation of Ag[OC₈F₁₇] Solution

AgF (1.27 g, 10 mmol, 1 equiv) was suspended in MeCN (5 mL) and ClC(O)C₇F₁₅ (2.16 g, 5 mmol, 0.5 equiv) was added at r.t. After stirring the suspension for 15 min, the precipitate was filtered off with a syringe filter (PTFE, 0.45 μ m). The obtained Ag[OC₈F₁₇] solution (1 M) was stored in a glass vessel at -20°C .

¹⁹F NMR (377 MHz, MeCN-d₃, 21 $^{\circ}\text{C}$): $\delta = -33.2$ (s, fwhm = 400 Hz, 2F, OCF₂), -81.7 (s, 3F, CF₃), -122.1 (m, 2F, CF₂), -122.5 (m, 6F, CF₂), -123.3 (m, 2F, CF₂), -126.7 (m, 2F, CF₂) ppm.

Preparation of [Ag(bpy)₂][OCF₃]

Bpy (0.6 g, 4 mmol, 2 equiv) was added to an Ag[OCF₃] solution in MeCN (2 mL, 2 mmol, 1 equiv). After stirring the suspension for 30 min the solvent was removed in vacuum resulting in an off-white crystalline powder of [Ag(bpy)₂][OCF₃] (1.0 g, 99%).

¹⁹F NMR (377 MHz, DCM-d₂, 19 $^{\circ}\text{C}$): $\delta = -21.6$ ppm (s, fwhm = 200 Hz).

¹H NMR (401 MHz, DCM-d₂, 19 $^{\circ}\text{C}$): $\delta = 8.64 - 8.55$ (m, 4H), $8.35 - 8.23$ (m, 4H), $8.10 - 7.97$ (m, 4H), $7.60 - 7.46$ (m, 1H) ppm.

Preparation of [NEt₃Me][OCF₃]

A solution of Ag[OCF₃] in MeCN (1 M, 21 mL, 21 mmol, 1.06 equiv) was added to a solution of [NEt₃Me]Cl (3.01 g, 19.8 mmol, 1 equiv) in MeCN, and a colorless precipitate formed. After the filtration with a syringe filter (PTFE, 0.45 μ m) the solvent was removed in vacuum resulting in an off-white crystalline powder of [NEt₃Me][OCF₃] (99%).

¹⁹F NMR (377 MHz, DCM-d₂, 19 $^{\circ}\text{C}$): $\delta = -22.1$ ppm (s, 3F).

¹H NMR (401 MHz, DCM-d₂, 19 $^{\circ}\text{C}$): $\delta = 1.33$ (pseudo-tt, 3F, ³J(¹H, ¹H) = 7.3 Hz, ³J(¹H, ¹⁴N) = 1.9 Hz), 3.02 (s, 3F), 3.38 (q, 2F, ³J(¹H, ¹H) = 7.3 Hz) ppm.

Preparation of Cu[OR^F] Solutions

CuCl (97.9 mg, 1 mmol, 1 equiv) was dissolved in MeCN (1 mL) and an Ag[OR^F] stock solution (1 M, 1 mL, 1 equiv) was added. After stirring for 10 min the solution was filtered with a syringe filter (PTFE, 0.45 μ m). The obtained Cu[OR^F] solution (0.5 M) was analysed directly.

Cu[OCF₃]

¹⁹F NMR (377 MHz, MeCN-d₃, 21 $^{\circ}\text{C}$): $\delta = -24.2$ ppm (s, fwhm = 1500 Hz, 3F).

Cu[OC₂F₅]

¹⁹F NMR (377 MHz, MeCN-d₃, 21 $^{\circ}\text{C}$): $\delta = -39.4$ (s, fwhm = 1600 Hz, 2F, OCF₂), -83.9 ppm (s, 3F, CF₃).

PPh₄[Au(CF₃)₃(OCF₃)]

a) from PPh₄[Au(CF₃)₃] and AgOCF₃ in MeCN

PPh₄[Au(CF₃)₃] (261.0 mg, 0.3 mmol, 1 equiv) was dissolved in MeCN (1 mL) and an Ag[OR^F] stock solution (1 M, 0.3 mL, 1 equiv)

was added at -30°C . After stirring for 15 min the solution was filtered with a syringe filter (PTFE, $0.45\ \mu\text{m}$).

^{19}F NMR (377 MHz, MeCN, 20°C): $\delta = -28.0$ (hept, 3F, CF_3 , $^4J(^{19}\text{F}, ^{19}\text{F}) = 6.3$ Hz), -36.8 (br, s, 3F, OCF_3), -39.4 (q, 6F, CF_3 , $^4J(^{19}\text{F}, ^{19}\text{F}) = 6.3$ Hz) ppm.

MS (ESI $^-$): $m\ z^{-1} = 488.9429$ ($[\text{Au}(\text{CF}_3)_3(\text{OCF}_3)]^-$, calc. 488.94286, $< 1\%$), 422.9569 ($[\text{Au}(\text{CF}_3)_3\text{F}]^-$, calc. 422.95113, 100%).

b) from $\text{PPh}_4[\text{Au}(\text{CF}_3)_3\text{F}]$ and COF_2

$\text{PPh}_4[\text{Au}(\text{CF}_3)_3\text{F}]$ (76 mg, 0.1 mmol, 1 equiv) was dissolved in DCM or MeCN (0.6 mL) and the vessel was pressurized with exc. COF_2 (1 bara) at r.t. The mixture was agitated over 5 min and then analyzed by NMR spectroscopy.

^{19}F NMR (377 MHz, DCM- d_2 , 19°C): $\delta = -28.2$ (hept, 3F, CF_3 , $^4J(^{19}\text{F}, ^{19}\text{F}) = 6.3$ Hz), -37.5 (br, pseudo-quint, 3F, OCF_3 , $^5J(^{19}\text{F}, ^{19}\text{F}) = 2.3$ Hz), -39.6 (qq, 6F, CF_3 , $^4J(^{19}\text{F}, ^{19}\text{F}) = 6.3$ Hz, $^5J(^{19}\text{F}, ^{19}\text{F}) = 2.3$ Hz) ppm.

Reactions with Organic Halides

A solution of $\text{Ag}[\text{OR}]^+$ in MeCN (1.0 M, 0.750 mL, 0.750 mmol, 1.5 equiv) was added to a heat gun-dried Schlenk tube and cooled to -30°C . The alkyl halide (0.500 mmol, 1.0 equiv) was added to the solution and the mixture was stirred for 30 min at -30°C . The solution was allowed to warm to r.t. over 1 h by removing the cooling bath. The suspension was filtered and washed with Et_2O , the filtrate was concentrated under reduced pressure, and the products **2a-6** were purified by flash column chromatography (SiO_2 , *n*-pentane/ Et_2O). The products were analysed by NMR spectroscopy and HRMS spectrometry.

(For details see SI).

Supporting Information

The authors have cited additional references within the Supporting Information.^[47–54]

Deposition Number(s) 2326777 (for $[\text{Ag}(\text{MeCN})_2(\text{OCF}_3)]_n$), 2326778 (for $[\text{Ag}(\text{bpy})_2][\text{OCF}_3]$), 2326776 (for $[\text{Ag}(\text{EtCN})_2(\text{OC}_2\text{F}_3)]_2$), 2326775 (for $[\text{Ag}(\text{EtCN})_2(\text{O}^i\text{C}_3\text{F}_7)]_2$), 2326772 (for $[\text{Cu}(\text{MeCN})_4][\text{OCF}_3]$), 2326773 (for $[\text{Cu}(\text{MeCN})_4][\text{OC}_2\text{F}_5]$), 2326774 (for $[\text{Cu}^{\text{I}}(\text{MeCN})_4][\text{Cu}^{\text{II}}\{\text{OC}(\text{CF}_3)_2-\text{O}-\text{C}(\text{CF}_3)_2\text{O}\}_2]$) contain the supplementary crystallographic data for this paper. These data are provided free of charge by the joint Cambridge Crystallographic Data Centre and Fachinformationszentrum Karlsruhe Access Structures service.

Acknowledgements

The authors would like to thank the HPC Service of ZEDAT, Freie Universität Berlin, for computing time and gratefully acknowledge the assistance of the Core Facility BioSupraMol supported by the DFG. Further support is acknowledged by the Deutsche Forschungsgemeinschaft (DFG, German Research Foundation) – Project-ID 387284271-SFB 1349. We thank Solvay Fluor for providing COF_2 . P.G. thanks Jonas R. Schmid (FU Berlin) for help with quantum-chemical calculations and Gesa Dreyhsig (FU

Berlin) for help designing the TOC graphic. Open Access funding enabled and organized by Projekt DEAL.

Conflict of Interests

The authors declare no conflict of interest.

Data Availability Statement

The data that support the findings of this study are available from the corresponding author upon reasonable request.

Keywords: Trifluoromethoxy · Perfluoroalcoholates · Metal Salts · Fluorine Chemistry · Solvent Effects

- [1] C. Ghiazza, T. Billard, C. Dickson, A. Tlili, C. M. Gampe, *ChemMedChem* **2019**, *14*, 1586.
- [2] A. Tlili, F. Toulgoat, T. Billard, *Angew. Chem. Int. Ed.* **2016**, *55*, 11726.
- [3] M. Hird, *Chem. Soc. Rev.* **2007**, *36*, 2070.
- [4] D. Chen, L. Lu, Q. Shen, *Org. Chem. Front.* **2019**, *6*, 1801.
- [5] S. Chen, Y. Huang, X. Fang, H. Li, Z. Zhang, T. S. A. Hor, Z. Weng, *Dalton Trans.* **2015**, *44*, 19682.
- [6] C.-P. Zhang, D. A. Vivic, *Organometallics* **2012**, *31*, 7812.
- [7] D. Chen, Y. Luo, L. Lu, Q. Shen, *Organometallics* **2024**, DOI: 10.1021/acs.organomet.4c00073.
- [8] T. Frömel, T. P. Knepper, *J. Fluor. Chem.* **2015**, *177*, 80.
- [9] I. G. Logvinenko, Y. Markushyna, I. S. Kondratov, B. V. Vashchenko, M. Kliachyna, Y. Tokaryeva, V. Pivnytska, O. O. Grygorenko, G. Haufe, *J. Fluor. Chem.* **2020**, *231*, 109461.
- [10] L. P. Wackett, *Microorganisms* **2022**, *10*, 1664.
- [11] BAuA (DE), RIVM (NL) KEM (SE), NEA (NO), DEPA (DK), *Annex XV Restriction Report Per- and Polyfluoroalkyl Substances (PFAS)*, Helsinki, 2023.
- [12] M. A. Marsini, P. J. Reider, E. J. Sorensen, *J. Org. Chem.* **2010**, *75*, 7479.
- [13] J. Qiao, Y.-S. Li, R. Zeng, F.-L. Liu, R.-H. Luo, C. Huang, Y.-F. Wang, J. Zhang, B. Quan, C. Shen, X. Mao, X. Liu, W. Sun, W. Yang, X. Ni, K. Wang, L. Xu, Z.-L. Duan, Q.-C. Zou, H.-L. Zhang, W. Qu, Y.-H.-P. Long, M.-H. Li, R.-C. Yang, X. Liu, J. You, Y. Zhou, R. Yao, W.-P. Li, J.-M. Liu, P. Chen, Y. Liu, G.-F. Lin, X. Wang, J. Zou, L. Li, Y. Hu, G.-W. Lu, W.-M. Li, Y.-Q. Wei, Y.-T. Zheng, J. Lei, S. Yang, *Science* **2021**, *371*, 1374.
- [14] R. Timoumi, I. Amara, I. B. Salem, G. Souid, S. Abid-Essefi, *J. Biochem. Mol. Toxicol.* **2023**, *37*, e23341.
- [15] P. Jimonet, F. Audiau, M. Barreau, J. C. Blanchard, A. Boireau, Y. Bour, M. A. Coléno, A. Doble, G. Doerflinger, C. D. Huu, M. H. Donat, J. M. Duchesne, P. Ganil, C. Guérémy, E. Honor, B. Just, R. Kerphirique, S. Gontier, P. Hubert, P. M. Laduron, J. Le Blevac, M. Meunier, J. M. Miquet, C. Nemecek, S. Mignani, *J. Med. Chem.* **1999**, *42*, 2828.
- [16] M. Tohnishi, H. Nakao, T. Furuya, A. Seo, H. Kodama, K. Tsubata, S. Fujioka, H. Kodama, T. Hirooka, T. Nishimatsu, *J. Pestic. Sci.* **2005**, *30*, 354.
- [17] S. Fujioka, K. Hirano, N. Hoshiya, A. Yamauchi, Y. Kishikawa, M. Uchiyama, *Chem. Commun.* **2023**, *59*, 8290.
- [18] B. J. Jelier, J. L. Howell, C. D. Montgomery, D. B. Leznoff, C. M. Friesen, *Angew. Chem. Int. Ed.* **2015**, *54*, 2945.
- [19] J. J. Newton, B. J. Jelier, M. Meanwell, R. E. Martin, R. Britton, C. M. Friesen, *Org. Lett.* **2020**, *22*, 1785.
- [20] Z. Lu, T. Kumon, G. B. Hammond, T. Umemoto, *Angew. Chem. Int. Ed.* **2021**, *60*, 16171.
- [21] P. Tang, X. Jiang in *Emerging fluorinated motifs. Synthesis, properties and applications* (Eds.: D. Cahard, J.-A. Ma), Wiley-VCH, Weinheim, **2020**, pp. 207–224.
- [22] A. Turksyoy, T. Scattolin, S. Bouayad-Gervais, F. Schoenebeck, *Chem. Eur. J.* **2020**, *26*, 2183.
- [23] F. G. Zivkovic, G. Wycich, L. Liu, F. Schoenebeck, *J. Am. Chem. Soc.* **2024**, *146*, 1276.
- [24] M. E. Redwood, C. J. Willis, *Can. J. Chem.* **1965**, *43*, 1893.

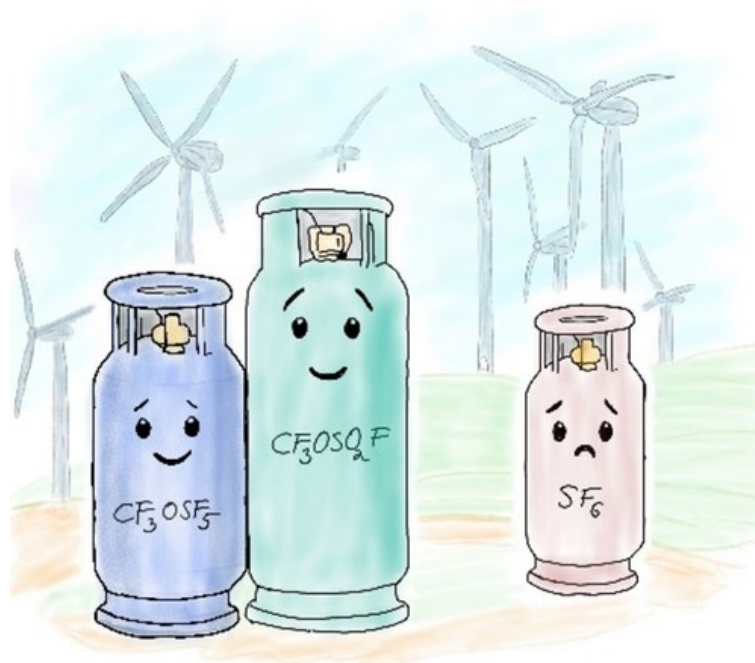
- [25] G. Duran-Camacho, D. M. Ferguson, J. W. Kampf, D. C. Bland, M. S. Sanford, *Org. Lett.* **2021**, *23*, 5138.
- [26] X. Zhang, K. Seppelt, *Inorg. Chem.* **1997**, *36*, 5689.
- [27] W. B. Farnham, B. E. Smart, W. J. Middleton, J. C. Calabrese, D. A. Dixon, *J. Am. Chem. Soc.* **1985**, *107*, 4565.
- [28] A. A. Kolomeitsev, M. Vorobyev, H. Gillandt, *Tetrahedron Lett.* **2008**, *49*, 449.
- [29] M. E. Redwood, C. J. Willis, *Can. J. Chem.* **1967**, *45*, 389.
- [30] F. Seel, M. Pimpl, *Justus Liebigs Ann. Chem.* **1975**, *1975*, 1700.
- [31] F. W. Evans, M. H. Litt, A. M. Weidler-Kubanek, F. P. Avonda, *J. Org. Chem.* **1968**, *33*, 1837.
- [32] A. Reisinger, D. Himmel, I. Krossing, *Angew. Chem. Int. Ed.* **2006**, *45*, 6997.
- [33] A. Reisinger, N. Trapp, I. Krossing, *Organometallics* **2007**, *26*, 2096.
- [34] S. H. Dempsey, S. R. Kass, *J. Org. Chem.* **2022**, *87*, 15466.
- [35] P. Erdmann, J. Leitner, J. Schwarz, L. Greb, *ChemPhysChem* **2020**, *21*, 987, and references therein.
- [36] M. Winter, M. A. Ellwanger, N. Limberg, A. Pérez-Bitrián, P. Voßnacker, S. Steinhauer, S. Riedel, *Chem. Eur. J.* **2023**, e202301684.
- [37] A. Pérez-Bitrián, M. Baya, J. M. Casas, L. R. Falvello, A. Martín, B. Menjón, *Chem. Eur. J.* **2017**, *23*, 14918.
- [38] A. Pérez-Bitrián, S. Martínez-Salvador, M. Baya, J. M. Casas, A. Martín, B. Menjón, J. Orduna, *Chem. Eur. J.* **2017**, *23*, 6919.
- [39] R. K. Harris, E. D. Becker, S. M. Cabral de Menezes, P. Granger, R. E. Hoffman, K. W. Zilm, *Pure Appl. Chem.* **2008**, *80*, 59.
- [40] K. L. Vikse, M. P. Woods, J. S. McIndoe, *Organometallics* **2010**, *29*, 6615.
- [41] L. Bennett, B. Melchers, B. Proppe, *Curta: A General-purpose High-Performance Computer at ZEDAT, Freie Universität Berlin, Freie Universität Berlin, Berlin*, **2020**, DOI: 10.17169/refubium-26754.
- [42] F. Neese, *WIREs Comput. Mol. Sci.* **2012**, *2*, 73.
- [43] Y. Zhao, D. G. Truhlar, *J. Phys. Chem. A* **2005**, *109*, 5656.
- [44] A. D. Becke, *J. Chem. Phys.* **1993**, *98*, 5648.
- [45] F. Weigend, R. Ahlrichs, *Phys. Chem. Chem. Phys.* **2005**, *7*, 3297.
- [46] F. Weigend, M. Häser, H. Patzelt, R. Ahlrichs, *Chem. Phys. Lett.* **1998**, *294*, 143.
- [47] A. López-Pérez, J. Adrio, J. C. Carretero, *Org. Lett.* **2009**, *11*, 5514.
- [48] C. J. J. Hall, I. S. Marriott, K. E. Christensen, A. J. Day, W. R. F. Goundry, T. J. Donohoe, *Chem. Commun.* **2022**, *58*, 4966.
- [49] X. Zhu, M. Jiang, X. Li, E. Zhu, Q. Deng, X. Song, J. Lv, D. Yang, *Org. Chem. Front.* **2022**, *9*, 347.
- [50] M. Yang, J. Fang, H. Liu, X. Lu, J. Zhou, Z. Mou, H. Wang, *Adv. Synth. Catal.* **2023**, *365*, 1806.
- [51] W. Zhang, J. Chen, J.-H. Lin, J.-C. Xiao, Y.-C. Gu, *iScience* **2018**, *5*, 110.
- [52] O. Marrec, T. Billard, J.-P. Vors, S. Pazenok, B. R. Langlois, *J. Fluor. Chem.* **2010**, *131*, 200.
- [53] M.-L. Fu, J.-B. Liu, X.-H. Xu, F.-L. Qing, *J. Org. Chem.* **2017**, *82*, 3702.
- [54] D. Louvel, A. Chelagha, J. Rouillon, P.-A. Payard, L. Khrouz, C. Monnereau, A. Tlili, *Chem. Eur. J.* **2021**, *27*, 8704.

Manuscript received: February 29, 2024

Accepted manuscript online: April 12, 2024

Version of record online: May 22, 2024

3.2 Trifluoromethyl Fluorosulfonate ($\text{CF}_3\text{OSO}_2\text{F}$) and Trifluoromethoxy Sulfur Pentafluoride (CF_3OSF_5) – Two Gaseous Sulfur(VI) Compounds with Insulating Properties



Paul Golz[†], Gesa H. Dreyhsig[†], Holger Pernice, Thomas Drews, Jan H. Nissen, Helmut Beckers, Simon Steinhauer, Anja Wiesner, and Sebastian Riedel*

[†] These authors have contributed equally.


Chem. Eur. J. **2024**, *30*, e202400258.

<https://doi.org/10.1002/chem.202400258>

© 2024 The Authors. Published by Wiley-VCH Verlag GmbH. This is an open access article under the terms of the [Creative Commons Attribution License \(CC BY 4.0\)](#), which permits use, distribution and reproduction in any medium, provided the original work is properly cited.

Author contributions

Paul Golz designed the project, performed experiments and wrote the manuscript. Gesa H. Dreyhsig performed experiments analyzed data and co-wrote the manuscript. Holger Pernice and Thomas Drews improved the synthesis of $\text{CF}_3\text{OSO}_2\text{F}$ and CF_3OSF_5 . Jan H. Nissen and Helmut Beckers designed the arcing experimental setup. Helmut Beckers revised the manuscript. Simon Steinhauer and Anja Wiesner performed the XRD measurements. Sebastian Riedel managed the project and revised the manuscript.

 Hot Paper

Trifluoromethyl Fluorosulfonate (CF₃OSO₂F) and Trifluoromethoxy Sulfur Pentafluoride (CF₃OSF₅) – Two Gaseous Sulfur(VI) Compounds with Insulating Properties

Paul Golz,^[a] Gesa H. Dreyhsig,^[a] Holger Pernice,^[a] Thomas Drews,^[a] Jan H. Nissen,^[a] Helmut Beckers,^[a] Simon Steinhauer,^[a] Anja Wiesner,^[a] and Sebastian Riedel^{*[a]}

In this work, we analyzed trifluoromethyl fluorosulfonate (CF₃OSO₂F) and trifluoromethoxy sulfur pentafluoride (CF₃OSF₅) regarding their potential use as dielectrics by investigating some of their intrinsic and extrinsic properties. Both compounds show a higher breakdown voltage than SF₆ with averaged relative breakdown voltages of 1.3 ± 0.2 for CF₃OSO₂F and 1.4 ± 0.2 for CF₃OSF₅, compared to SF₆ with 1.0. Like the dielectric

(CF₃)₂CFCN, both compounds decompose during the breakdown process. The decomposition products were analyzed by IR spectroscopy and GCIR methods. Furthermore, the molecular structures of both gaseous compounds CF₃OSO₂F and CF₃OSF₅ have been determined by in situ crystallization, and their physical properties were determined as well.

Introduction

Sulfur hexafluoride (SF₆) is one of the most potent greenhouse gases due to its extreme stability in the atmosphere. Most of its emission is human-made and mostly related to its usage as a dielectric.^[1,2] In applications like sound insulating glazing, car tires or in sport shoes, SF₆ has been replaced, by air, nitrogen or argon, but it is still used in various industrial processes due to its distinct properties.^[3,4] The European Parliament and the Council of the European Union (EU) have ordered the reduction of artificially produced fluorinated gases, particularly SF₆, in an EU regulation. An update in 2022 called for an increased phase out of SF₆ in all new electricity transmission equipment by 2031.^[5] However, this phase out proved challenging, as the industrially favored properties of SF₆ are also the reason for its exceptionally long atmospheric lifetime of about 3200 years and the resulting global warming potential (GWP) of around 23900 over a 100 year period.^[6–8] The high GWP value is based on the lifetime in the environment and on the ability to absorb IR irradiation. The absorption cross section for fluorinated molecules is often relatively high. Therefore, short lifetimes and low GWP values are becoming important properties in the search for gaseous dielectric media. SF₆ is a colorless, odorless,

and non-toxic gas at room temperature, with a high density, a high thermal conductivity, and a low viscosity. These properties enable an effective heat transfer through different media.^[3,8,9] Additionally, SF₆ is very temperature stable and shows a remarkably low reactivity towards other chemical compounds and is thus considered to be chemically inert.^[10,11]

A valuable approach to replace SF₆ in low (LV) and middle (MV) voltage applications is the use of nitrogen or dry air. Due to their low dielectric strengths, these replacements do not work for high voltage (HV) applications like gas-insulated switchgears (GISs) or gas-insulated transmission lines (GILs). The effective ability of SF₆ to suppress and extinguish electric arcs is based on its high dielectric strength and breakdown voltage, which are directly related to the electronegativity of its elements.^[12–14]

Fluorine, the element with the highest electronegativity, forms very stable compounds, and its gaseous compounds often show a high electrical resistance^[15] and high breakdown voltage.^[12] Consequently, various compounds which are nowadays studied as SF₆-substitutes mostly contain fluorine atoms e.g. CF₃I, C₂F₆, heptafluoroisobutyronitrile ((CF₃)₂CFCN, *Novec 4710*), heptafluoroisopropyl trifluoromethyl ketone ((CF₃)₂CFC(O)CF₃, *Novec 5110*) and heptafluoroisopropyl pentafluoroethyl ketone ((CF₃)₂CFC(O)CF₂CF₃, *Novec 1230*).^[3,6] Although these gases provide very high dielectric strengths, some of their properties, such as high boiling points, their decomposition products and possible toxicity, limit their usage on an industrial scale.^[16] Furthermore, such PFAS (per- and polyfluorinated alkyl substances) are environmentally problematic due to their unique properties. Therefore, the EU is considering a ban of PFAS with use-specific exemptions and some exclusions where –CF₃ or –CF₂– groups are bound to specific heteroatoms.^[17]

Accordingly, it is necessary for future dielectrics to be environmentally friendly by enabling a degradation of the compound in the atmosphere into harmless compounds.^[3,18] In

[a] P. Golz, G. H. Dreyhsig, H. Pernice, T. Drews, Dr. J. H. Nissen, Dr. H. Beckers, Dr. S. Steinhauer, Dr. A. Wiesner, Prof. Dr. S. Riedel
Fachbereich Biologie, Chemie, Pharmazie
Institut für Chemie und Biochemie – Anorganische Chemie
Freie Universität Berlin
Fabeckstr. 34/36, 14195 Berlin (Germany)
E-mail: s.riedel@fu-berlin.de

Supporting information for this article is available on the WWW under <https://doi.org/10.1002/chem.202400258>

© 2024 The Authors. Chemistry - A European Journal published by Wiley-VCH GmbH. This is an open access article under the terms of the Creative Commons Attribution License, which permits use, distribution and reproduction in any medium, provided the original work is properly cited.

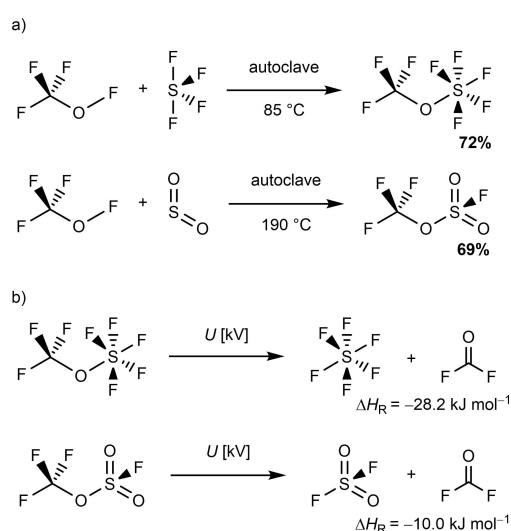
addition, they must be safe to use, harmless to the used infrastructure and facilitate a well-known industrial handling.^[2,19] Furthermore, specific intrinsic and extrinsic properties are required, including basic chemical and physical properties like high dielectric strength (DS), low boiling point and suitable reactivity, including the formation of harmless by-products.^[2,13,20] The required high dielectric strength depends on the ability to absorb free electrons and to form anions and thus on the compound-related electron affinity.^[12,21,22]

At the outset of this work, we were looking for gaseous compounds with insulating properties that would extend the range of dielectrics and could be considered as substituents for SF₆. Trifluoromethoxy sulfur pentafluoride (CF₃OSF₅) and trifluoromethyl fluorosulfonate (CF₃OSO₂F) are promising candidates as both compounds have high predicted DS values and high adiabatic electron affinities based on quantum chemical evaluations. Furthermore, these compounds show interesting properties such as boiling points of −10 °C^[23] (CF₃OSF₅) and −4.2 °C^[24] (CF₃OSO₂F) and are accessible from starting materials such as CF₃OF and SF₄^[23] or CF₃OF and SO₂^[24] respectively.

Results and Discussion

Synthesis

CF₃OSF₅ and CF₃OSO₂F were prepared by modified literature procedures^[23,24] starting from CF₃OF and SF₄ or CF₃OF and SO₂ in a stainless steel autoclave (Scheme 1, a). Reactive species were quenched with soda lime. The gases were obtained in good yields (72% and 69%, respectively) by isothermal distillation. IR spectra recorded in the gas phase of both compounds are consistent with those in the literature.^[23,24]



Scheme 1. a) Synthesis of CF₃OSF₅ and CF₃OSO₂F starting from CF₃OF and SF₄ or SO₂, respectively, b) Arc plasma decomposition reactions of CF₃OSO₂F and CF₃OSF₅.

Solid State Structure

Both substances have low melting points (−156.5 °C for CF₃OSO₂F and −161.6 °C for CF₃OSF₅, Table 1). Crystals suitable for X-ray analysis were obtained by in situ crystallization. Their recorded molecular structures are in accordance with DFT-calculations. In CF₃OSO₂F (Figure 1, top), both the sulfur and the carbon atoms show a slightly distorted tetrahedral coordination environment with a geometry index of $\tau_4 = 0.96$ for carbon and $\tau_4 = 0.89$ for sulfur.^[25] Both moieties are connected via O1 with a C1–O1–S1 bond angle of 122.0(2)° and C1–O1 and O1–S1 bond distances of 141.7(4) and 157.3(2) pm. The distortion of the sulfur-based tetrahedron might be caused by the repulsion of the lone pairs of F1 with those of O2 and O3. This assumption is corroborated by the slightly longer S1–O2, S1–O3 and S1–F1 bond distances of 139.9(3), 139.0(3), and 152.7(2) pm, respectively, compared to the molecular structure of solid sulfuranyl fluoride (SO₂F₂) with 138.6(2) for the S–O bonds and 151.4(2) pm for the S–F bonds.^[26] In the structurally related molecule CF₃OSO₂CF₃, the two terminal S–O bonds and the bridging S–O bond are with distances of 141.1(3), 141.4(4) and 160.7(3) pm, respectively, longer than in CF₃OSO₂F. On the other hand, the C1–O1 bond of CF₃OSO₂F is with 141.7(4) pm longer than the C–O bond in CF₃OSO₂CF₃ with 139.9(5) pm. Additionally, the bond angle O2–S1–O3 of 124.2(2)° shows similar values to the corresponding angles in SO₂F₂ and CF₃OSO₂CF₃ with 124.6(1)°

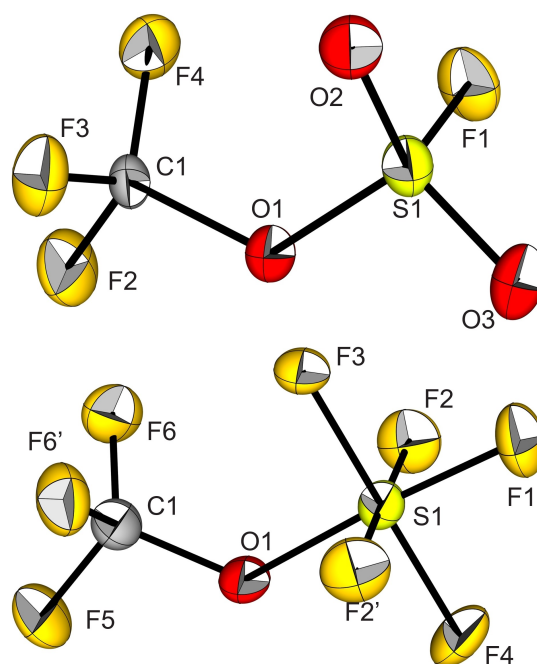


Figure 1. Molecular structures in the solid state of CF₃OSO₂F (top) and CF₃OSF₅ (bottom). Thermal ellipsoids are set at 50% probability. Selected bond lengths [pm] and angles [°] of CF₃OSO₂F: 141.7(4) (C1–O1), 157.3(2) (O1–S1), 139.9(3) (S1–O2), 139.0(3) (S1–O3), 152.7(2) (S1–F1), 121.9(2) (C1–O1–S1), 124.2(2) (O2–S1–O3), 106.8(2) (O2–S1–F1). Selected bond lengths [pm] and angles [°] of CF₃OSF₅: 137.2(3) (C1–O1), 163.8(2) (O1–S1), 125.1(2) (C1–O1–S1).

and $123.5(2)^\circ$, respectively. This is also the case for the O2–S1–F1 bond angle of $106.8(2)^\circ$ when compared to this angle in SO_2F_2 with $107.6(1)^\circ$ ^[26] and for the C1–O1–S1 bond angle of $121.9(2)^\circ$ compared to $\text{CF}_3\text{OSO}_2\text{CF}_3$ with a value of $122.0(3)^\circ$ ^[27]

The molecular structure of CF_3OSF_5 (Figure 1, bottom) shows a carbon-based tetrahedron ($\tau_4=0.95$) and a sulfur-based octahedron, both connected by O1. The C1–O1–S1 bond angle of $125.1(2)^\circ$ is widened, the O1–S1 bond distance of $163.8(2)$ pm longer and the C1–O1 bond of $137.2(3)$ pm shorter than that in $\text{CF}_3\text{OSO}_2\text{F}$. However, the C–F bonds of the CF_3 group and the S–F bonds show almost the same lengths in both compounds. Additionally, these S–F bond distances are similar to those in SF_6 ^[28]

Gas Phase Data

The vapor pressures of $\text{CF}_3\text{OSO}_2\text{F}$ and CF_3OSF_5 were measured in two temperature ranges by using different setups. The Antoine-parameters A, B and C (see Table S7) were determined using a multiple linear regression of the measured vapor pressure curves. The parameters are valid for the Antoine-equation using p [bara] and T [K].^[29] The first range was chosen in a temperature window around the boiling points known from the literature, -4.2°C ^[24] ($\text{CF}_3\text{OSO}_2\text{F}$) and -10°C ^[23] (CF_3OSF_5). The measurements carried out led to a re-evaluation of the boiling points at -5.5°C ($\text{CF}_3\text{OSO}_2\text{F}$) and -10.5°C (CF_3OSF_5). In comparison, SF_6 has a sublimation point of -63.8°C ^[10] and is therefore used as dielectric even at low temperatures. $\text{CF}_3\text{OSO}_2\text{F}$ and CF_3OSF_5 , like the Novec compounds, are more limited to higher temperatures. Using a setup for the determination of critical parameters (see SI, Figure S11), we measured the vapor pressures in a larger temperature range from low temperatures to temperatures above the critical points of the substances.

We were able to determine the critical points due to the visible change from the two-phase system (gas and liquid phase) into a supercritical fluid. The critical points were reached at $T_{\text{crit}} = 110.7 \pm 0.7^\circ\text{C}$, and $p_{\text{crit}} = 28.7 \pm 0.1$ bara for $\text{CF}_3\text{OSO}_2\text{F}$ and at $T_{\text{crit}} = 123.5 \pm 0.8^\circ\text{C}$, and $p_{\text{crit}} = 32.2 \pm 0.1$ bara for CF_3OSF_5 (Table 1). Knowing the critical point of a substance, its *van der Waals*-constants a and b were estimated (see Table S4) using the *van der Waals*-equation.^[29]

The gas densities ρ_{gas} were determined to be 7.1 ± 0.1 kg m^{-3} ($\text{CF}_3\text{OSO}_2\text{F}$) and 8.9 ± 0.1 kg m^{-3} (CF_3OSF_5) at 26.0°C

	$\text{CF}_3\text{OSO}_2\text{F}$	CF_3OSF_5
$T_{\text{m,p}}$ [$^\circ\text{C}$]	-116.4 ± 2.0	-142.0 ± 2.0
$T_{\text{b,p}}$ [$^\circ\text{C}$]	-5.5 ± 0.5	-10.5 ± 0.5
$\rho_{\text{gas}}(26.0^\circ\text{C})$ [kg m^{-3}]	7.1 ± 0.1	8.9 ± 0.1
T_{crit} [$^\circ\text{C}$]	110.7 ± 0.7	123.5 ± 0.8
p_{crit} [bara]	28.7 ± 0.1	32.2 ± 0.1

and a pressure of 1013 mbar (Table 1). These gas phase densities are higher than those of SF_6 (6.0 ± 0.1 kg m^{-3}).

Quantum Chemistry

Quantum chemical calculations were performed to support the experimental data. Geometry optimizations of the structures on the B3LYP–D3/def2-TZVP level of theory provided consistent structures to those obtained by X-ray analysis and enabled the assignments of the gas-phase IR bands (see Table S1). Both optimized structures were used for a NBO analysis. Furthermore, evaluations at the BP86–D3/def2-QZVPP level of theory were used to predict DS values by the method of Rabie *et al.*^[30] Obtained by DFT calculations of anionic, neutral, and cationic species, values for the electric dipole moment (μ), the average static electronic polarizability (α), the adiabatic ionization energy (ϵ_i) and the number of electrons (N_e), showing high relative DS of 1.7 and 2.1 for $\text{CF}_3\text{OSO}_2\text{F}$ and CF_3OSF_5 , respectively, compared to SF_6 (1.0). In addition, higher adiabatic electron affinity values (ϵ_a) of -2.9 eV (CF_3OSF_5) and -2.4 eV ($\text{CF}_3\text{OSO}_2\text{F}$) compared to SF_6 (-2.1 eV) were also obtained.

Dielectric Strength and Decomposition Behavior

Based on calculated predictions, high DS values are expected for both compounds. One method to analyze the DS of a compound, is the determination of its breakdown voltage U_{BD} . Therefore, we developed a simplified method to determine the U_{BD} of different gases. The setup was realized by using a 250 mL flask with a Young valve and two electrodes with an adjustable distance facing each other. After filling the flask with a certain pressure of the gas, a voltage (AC, 230 V–10.5 kV, 50 Hz) was applied and increased, until an arc became visible between the electrodes (Figure 2). Measurements of the breakdown voltages U_{BD} as a function of the electrode spacing (Figure 3) were carried out with the gaseous dielectrics at an initial pressure of 0.1 bara and electrode distances between 0.2 and 1.0 cm. The U_{BD} of CF_3OSF_5 and $\text{CF}_3\text{OSO}_2\text{F}$ showed better results compared to SF_6 , demonstrating higher electrical resistances and thus higher dielectric strengths. The averaged relative insulation

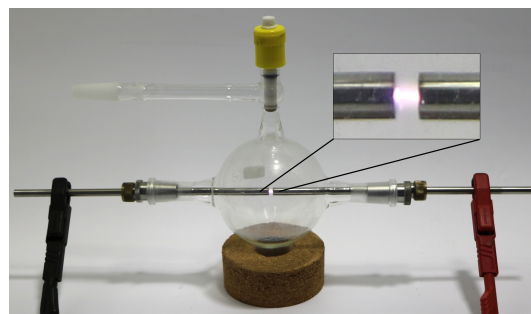


Figure 2. Experimental setup for the determination of dielectric properties during an arc event.

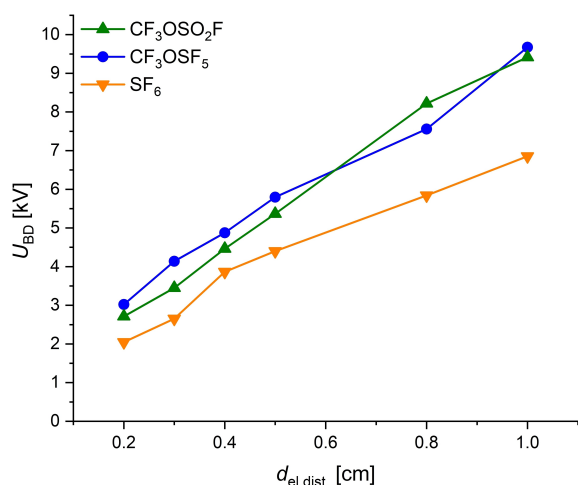


Figure 3. Breakdown voltages U_{BD} [kV] as a function of the distance between the electrodes $d_{el.dist.}$ [cm] used for CF₃OSO₂F (▲), CF₃OSF₅ (●) and SF₆ (▼) at an initial pressure of $p_i = 0.1$ bara.

strength of CF₃OSF₅ (1.4 ± 0.2) and CF₃OSO₂F (1.3 ± 0.2) are lower than the predicted ones. Nevertheless, the values are higher than for SF₆, which is set to 1 by definition. The higher DS values are in accordance with the higher gas densities compared to SF₆, as the electrical resistance of a gas is roughly proportional to its density.^[31] Potential SF₆ substitutes with higher insulation characteristics than SF₆, such as (CF₃)₂CFCN (2.2) and (CF₃)₂CFC(O)CF₃ (2.0), already exist.^[3] However, potential SF₆ substitutes must also provide adequate decomposition characteristics.

As already mentioned, electric arcs can appear during switching operations of high voltages. These are high energy events where the dielectric medium gets ionized and temperatures around 10,000 K are possible.^[16] Under these extreme conditions, SF₆ splits into several sulfur fluoride species like [SF₅]^{*} or SF₄ and mainly F^{*} radicals inside the arc plasma. Extinguishing this arc will lead to a rapid, thermodynamically favored recombination of these molecules to SF₆. To a lesser extent, [SF₅]^{*} radicals can recombine to the highly toxic S₂F₁₀, and in the presence of H₂O or O₂, other toxic compounds like SF₄, SO₂F₂, or HF can be formed. Due to the favored recombination to SF₆, the overall decomposition is rather low.^[3,16] For other dielectrics such as (CF₃)₂CFCN, the decomposition is much more favored. A mixture of (CF₃)₂CFCN (53%) in air (47%) shows a degradation of the nitrile of 61.7% after 200 breakdown processes with a duration of ~10 ms each, while only a small amount (1.6%) of SF₆ is decomposed under the same conditions.^[32] This can be explained by a lower recombination rate of the more complex nitrile and the thermodynamically favored formation of other reaction products. Some of the decomposition products like CF₄, C₂F₆, or C₂N₂ have a high GWP, while several are also highly toxic like CF₃CN, C₄F₈, and HF. This leads to a drastically increased acute toxicity with a lethal concentration (LC₅₀) of the nitrile mixture that is around 1100

times lower than that of pure SF₆ after 200 breakdown processes.^[32]

To analyze the decomposition behavior of CF₃OSO₂F and CF₃OSF₅, experiments were conducted at their breakdown voltages. The gas was exposed to a stable arc over a period of 10 s at an initial pressure of $p_i = 0.1$ bara, which corresponds to 1000 breakdown processes with a duration of 10 ms each. IR spectra of the gas phase after the arc revealed the partial decomposition of CF₃OSF₅ and CF₃OSO₂F. The undecomposed portion φ of the dielectric determined after discharge depends on the electrode distance (Figure 4). At larger distances between the electrodes, φ decreases in breakdown processes, which corresponds to Paschen's law.^[21,33] While the decomposition of CF₃OSF₅ with $\varphi = 19\%$ is already well advanced at electrode distances of ≥ 0.8 cm, the decomposition of CF₃OSO₂F is less favored, as the undecomposed portion was $\varphi = 42\%$ at the largest electrode spacing of 1.0 cm used (Figure 4).

IR spectra of the gas mixture after the electrical breakdown in gaseous CF₃OSF₅ revealed CF₂O and SF₆ as main decomposition products (Scheme 1, b). The formation of SF₆ during the decomposition process significantly limits the suitability of this compound as an SF₆ substitute. CF₃OSO₂F shows similar properties in terms of boiling point and a good DS value as CF₃OSF₅, but the tendency to form SF₆ during arcing events should be lower due to the lower fluorine but higher oxygen content. IR spectra of the gas mixture formed after the electrical breakdown revealed CF₂O and SO₂F₂ as the main decomposition products (Scheme 1, b). Both compounds are toxic while SO₂F₂ is also a greenhouse gas. However, as rather reactive species, these products can be hydrolyzed, especially with basic media like soda lime. CF₃OSO₂F itself is quite stable towards hydrolysis and was only partially hydrolyzed after contact to 5 M NaOH at 100 °C for 39 h, as reported by Wayne et al.^[24] This gives CF₃OSO₂F a clear advantage over other SF₆ substitutes currently

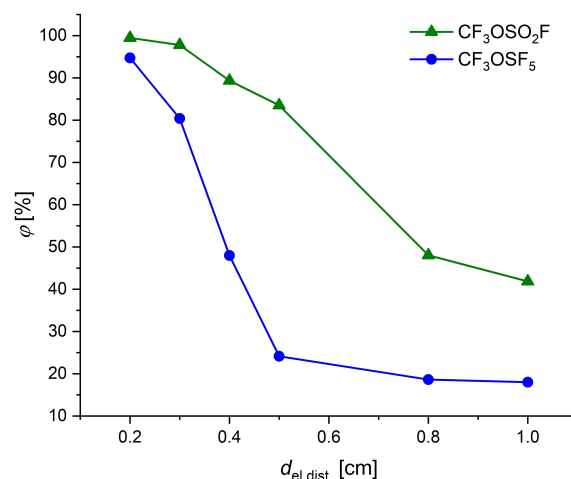


Figure 4. Undecomposed amount of dielectric φ [%] after arc-exposition as a function of the electrode distance $d_{el.dist.}$ [cm] for CF₃OSO₂F (▲) and CF₃OSF₅ (●).

in use, whose decomposition products can mostly not be hydrolyzed.

Decomposition Pathways

CF_3OSF_5 and $\text{CF}_3\text{OSO}_2\text{F}$ decompose in a similar way during arcing events into two main species each (cf. Scheme 1, b). For $\text{CF}_3\text{OSO}_2\text{F}$, this can mainly be explained by a labile S–O bond. NBO analysis shows that the lowest unoccupied molecular orbital can be regarded as the σ^* -bond orbital between the sulfur atom and the bridging oxygen atom (Figure 5, left). The formation of $[\text{CF}_3\text{O}]^*$ and $[\text{SO}_2\text{F}]^*$ radicals seems to be feasible. These can either recombine, or the $[\text{CF}_3\text{O}]^*$ radical eliminates an F^* radical which then reacts with the $[\text{SO}_2\text{F}]^*$ radical under formation of SO_2F_2 (Scheme 2, a). Transferring this tentative mechanism to CF_3OSF_5 would also explain the decomposition products SF_6 and CF_2O . However, NBO analysis of CF_3OSF_5 reveals a LUMO mainly localized at the σ^* -bond orbital between the sulfur atom and the apical fluorine atom (Figure 5, right). This suggests a mechanism in which the dissociation into F^* and $[\text{CF}_3\text{OSF}_4]^*$ radicals is favored. $[\text{CF}_3\text{OSF}_4]^*$ could then decay into $[\text{CF}_3\text{O}]^*$ radicals and SF_4 . The reaction between these two species could lead to the formation of SF_6 and CF_2O (Scheme 2, b).

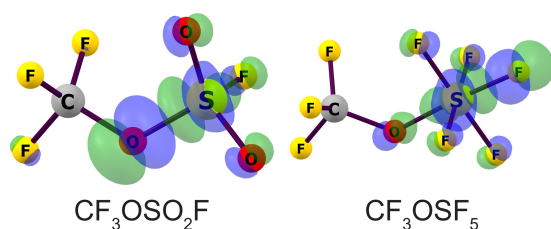
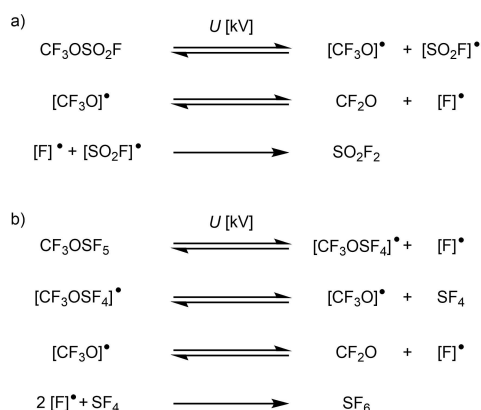


Figure 5. Quantum chemical calculations of the lowest unoccupied natural bond orbitals (NBO) at B3LYP–D3/def2-TZVP level of theory of $\text{CF}_3\text{OSO}_2\text{F}$ (left) and CF_3OSF_5 (right).



Scheme 2. Tentative decomposition reaction pathways of a) $\text{CF}_3\text{OSO}_2\text{F}$ and b) CF_3OSF_5 .

Quantum chemical calculations at the B3LYP–D3/def2-TZVP level of theory provide reaction enthalpies of $-10.0 \text{ kJ mol}^{-1}$ and $-28.2 \text{ kJ mol}^{-1}$ for these decomposition pathways of $\text{CF}_3\text{OSO}_2\text{F}$ and CF_3OSF_5 , respectively (cf. Scheme 1). Although both reaction sequences are slightly exothermic, the activation barrier for their decomposition appears to be high. However, it can be overcome in an arc with high energy.

Conclusions

Trifluoromethyl fluorosulfonate ($\text{CF}_3\text{OSO}_2\text{F}$) and trifluoromethoxy sulfur pentafluoride (CF_3OSF_5) were (re-)evaluated with regard to their intrinsic and extrinsic properties in the solid, liquid and gas phase. We were able to determine the molecular structures in the solid state for both $\text{CF}_3\text{OSO}_2\text{F}$ (b.p.: -5.5°C) and CF_3OSF_5 (b.p.: -10.5°C). Measurements of the liquid and the gas phase led to the determination of their critical parameters (T_{crit} and p_{crit}), their *van der Waals*-constants a and b , and their *Antoine*-parameters A , B , and C . With averaged relative breakdown voltages of 1.3 ($\text{CF}_3\text{OSO}_2\text{F}$) and 1.4 (CF_3OSF_5), both substances show better insulation properties than SF_6 and are comparable to $(\text{CF}_3)_2\text{CFCN}$.^[16] All three substances ($\text{CF}_3\text{OSO}_2\text{F}$, CF_3OSF_5 , and $(\text{CF}_3)_2\text{CFCN}$) show higher decomposition rates than SF_6 during arcing events. CF_3OSF_5 decomposes into SF_6 which affects its potential use as an SF_6 replacement. In contrast, $\text{CF}_3\text{OSO}_2\text{F}$ is more stable and decomposes into the hydrolysable compounds CF_2O and SO_2F_2 during arcing events. Due to the short perfluorinated chains, $\text{CF}_3\text{OSO}_2\text{F}$ and CF_3OSF_5 can be considered as degradable materials and are exempt from the planned PFAS ban. For their potential use as dielectrics, further studies will be conducted to evaluate their toxicity, GWP, or their compatibility with materials.

Experimental Section

Reagents and Analytical Techniques

All gases were handled using standard Schlenk techniques and oil pump vacuum up to 10^{-3} mbar. Commercially available SO_2 (Linde), SF_4 (abcr), SF_6 (Linde) and R134a (Linde) were used without further purification. CF_3OF was prepared according to a literature procedure.^[34]

X-ray diffraction measurements were performed on a Bruker D8 Venture diffractometer with a CMOS area detector using $\text{CuK}\alpha$ radiation. Single crystals were obtained using in situ crystallization and selectively melting of the substances in capillaries installed on the diffractometer in a cooled nitrogen stream at -148°C . The structures were solved using the ShelXT structure solution program using intrinsic phasing and refined with the ShelXL refining package using least-squares minimization by using OLEX2. For graphical representations, the programs Diamond 4 and POV-Ray 3.7 were used. IR spectra were recorded with eight scans and a resolution of 4 cm^{-1} using a Bruker Vector 22 FTIR spectrometer or a Thermo Fisher Scientific Nicolet™ i550 FTIR spectrometer in combination with a Thermo Fisher Scientific TRACE™ 1310 GC-Analyzer gas chromatograph. The programs OPUS 7.5 and OMNIC 48 were used for the evaluation of the recorded spectra, and Origin 2022 for the graphical representation. NMR spectra were recorded

using a JEOL 400 MHz ECZR or ECS spectrometer and all chemical shifts are referenced using the δ values given in the IUPAC recommendations of 2008 and the ^2H signal of the deuterated solvent as internal reference.^[35] For external locking, acetone- d_6 was flame sealed in a glass capillary and the lock oscillator frequency was adjusted to give $\delta(^1\text{H}) = 7.26$ ppm for a CHCl_3 sample locked on the capillary. For strongly coupled spin systems all chemical shifts and coupling constants are reported as simulated in gNMR.^[36] MestReNova 14.2 was used for processing the spectra and for their graphical representation. Quantum chemical calculations were conducted using program Orca 5.0.3^[37] on the HPC system provided by the ZEDAT (Freie Universität Berlin, Curta).^[38] The B3LYP^[39] or BP86^[40] functionals (with D3BJ^[41]) were used with the basis sets def2-TZVP or def2-QZVPP.^[42] For the NBO analysis the software extension NBO 7.0.4^[43] was used.

General Synthesis: Reactions were carried out in a 500 mL stainless steel autoclave (Model IV, Carl Roth) of 740 mL (gas) capacity equipped with a 100 bar bursting disk. The autoclave was tempered by a silicon oil bath and an electric magnetic stirrer (IKA® RCT standard safety control, IKA-Werke, Staufen im Breisgau, Germany) for stirring and heating. After the reaction the autoclave was cooled to room temperature and the gaseous material was released through an U-shaped stainless-steel tube filled with soda lime into a dry ice cooling trap. To prevent the product from decomposition the temperature of the soda lime was kept below 60 °C. The raw material was then condensed into a liquid nitrogen cooled trap by applying a vacuum (1×10^{-3} mbar). The products were obtained by fractional isothermal distillation and stored in stainless steel vessels.

CF_3OSF_5

54 g (0.5 mol, 1 eq.) SF_4 and 53 g (0.51 mol, 1.02 eq.) CF_3OF were condensed into the autoclave and after warming to room temperature it was heated to 85 °C for 48 h. The product (76.1 g, 0.36 mmol, 72%) was obtained as colorless gas via distillation. $T_{\text{b.p.}} = -10.5$ °C. ^{19}F NMR (377 MHz, neat, external $[\text{D}_6]\text{acetone}$, 21 °C): δ (ppm) = 66.1 (m, $4F_{\text{Br}}$, $^2J(^{19}\text{F}_{\text{Br}}, ^{19}\text{F}_{\text{A}}) = 153.1$ Hz, $^4J(^{19}\text{F}_{\text{Br}}, ^{19}\text{F}_{\text{CF}}) = 10.0$ Hz), 58.9 (m, $1F_{\text{Ar}}$, $^2J(^{19}\text{F}_{\text{Ar}}, ^{19}\text{F}_{\text{B}}) = 153.1$ Hz, $^4J(^{19}\text{F}_{\text{Ar}}, ^{19}\text{F}_{\text{CF}}) = 1.4$ Hz), -59.5 (dq, $3F$, OCF_3 , $^4J(^{19}\text{F}_{\text{Ar}}, ^{19}\text{F}_{\text{CF}}) = 1.4$ Hz, $^4J(^{19}\text{F}_{\text{Br}}, ^{19}\text{F}_{\text{CF}}) = 10.0$ Hz, $^1J(^{19}\text{F}_{\text{CF}}, ^{13}\text{C}) = 266$ Hz). ^{13}C NMR (101 MHz, neat, external $[\text{D}_6]\text{acetone}$, 21 °C): δ (ppm) = 119.6 (q, $^1J(^{13}\text{C}, ^{19}\text{F}_{\text{CF}}) = 266$ Hz, $^3J(^{13}\text{C}, ^{19}\text{F}) = 2.1$ Hz). ^{17}O NMR (54 MHz, neat, external $[\text{D}_6]\text{acetone}$, 21 °C): δ (ppm) = 212 (s). ^{33}S NMR (31 MHz, neat, external $[\text{D}_6]\text{acetone}$, 21 °C): δ (ppm) = -182 (sext, $^1J(^{33}\text{S}, ^{19}\text{F}) = 250$ Hz).

$\text{CF}_3\text{OSO}_2\text{F}$

4.6 g (72 mmol, 1 eq.) SF_4 and 13.8 g (133 mmol, 1.85 eq.) CF_3OF were condensed into the autoclave and after warming to room temperature it was heated to 190 °C for 48 h. The product (8.4 g, 50 mmol, 69%) was obtained as a colorless gas via distillation. $T_{\text{b.p.}} = -5.5$ °C. ^{19}F NMR (377 MHz, neat, external $[\text{D}_6]\text{acetone}$, 21 °C): δ (ppm) = 45.0 (q, $1F_{\text{S}}$, $^4J(^{19}\text{F}, ^{19}\text{F}) = 6.7$ Hz), -58.4 (d, $3F_{\text{C}}$, $^4J(^{19}\text{F}, ^{19}\text{F}) = 6.7$ Hz, $^1J(^{19}\text{F}, ^{13}\text{C}) = 273$ Hz). ^{13}C NMR (101 MHz, neat, external $[\text{D}_6]\text{acetone}$, 21 °C): δ (ppm) = 118.8 (q, $^1J(^{13}\text{C}, ^{19}\text{F}) = 273$ Hz). ^{17}O NMR (54 MHz, neat, external $[\text{D}_6]\text{acetone}$, 21 °C): δ (ppm) = 191 (s, OCF_3), 164 (d, 2O, SO_2F , $^2J(^{17}\text{O}, ^{19}\text{F}) = 35$ Hz).

Determination of Intrinsic Properties

Densities were analyzed by weighing the mass of the gas in a defined volume depending on its pressure and temperature. Critical points were determined optically by observing an opalescence between the coexisting phases of the substance using a pressure-

resistant fused quartz tube inside a temperature-adjustable autoclave with quartz windows. The same setup was used for measurements of vapor pressure curves above 1 bara while measurements at lower pressures were performed using a classical Schlenk tube. Melting points were determined by placing the sample, in a sealed glass ampoule, in a beaker containing liquid nitrogen and liquified propane which was slowly heated so that the substance liquified evenly.

Determination of Extrinsic Properties

Electrical discharge properties were determined by measuring the breakdown voltages of the substance of interest at an initial pressure of $p_i = 0.1$ bara and at different distances between two electrodes. Insulation strengths of the investigated gases relative to SF_6 were calculated as a function of the electrode distance. Decomposition products of $\text{CF}_3\text{OSO}_2\text{F}$ and CF_3OSF_5 were analyzed by IR spectroscopy after exposure to an electrical arc for a defined period of ten seconds. In addition to measuring IR spectra of the product mixtures immediately after the electrical discharge, these mixtures were also analyzed with a GCIR system by separating them into their individual components and characterizing them using IR spectroscopy.

Deposition Numbers 2308232 (for $\text{CF}_3\text{OSO}_2\text{F}$) and 2308230 (for CF_3OSF_5) contain the supplementary crystallographic data for this paper. These data are provided free of charge by the joint Cambridge Crystallographic Data Centre and Fachinformationszentrum Karlsruhe Access Structures service.

Supporting Information

The authors have cited additional references within the Supporting Information.^[44]

Acknowledgements

The authors would like to thank the HPC Service of ZEDAT, Freie Universität Berlin, for computing time and gratefully acknowledge the assistance of the Core Facility BioSupraMol supported by the DFG. P.G. and G.D. thank Nils Wehowsky for help designing the TOC graphic. Open Access funding enabled and organized by Projekt DEAL.

Conflict of Interests

This work was carried out partly in cooperation with Solvay Fluor GmbH, Hannover. At the time this work was carried out, H. Pernice was employed by Solvay Fluor GmbH. This collaboration resulted in a patent,^[45] in which the Solvay Fluor GmbH, FU-Berlin, as well as the authors S. Riedel, H. Beckers, S. Steinhauer, and H. Pernice hold shares. All other authors declare no conflict of interest.

Data Availability Statement

The data that support the findings of this study are available from the corresponding author upon reasonable request.

Keywords: trifluoromethoxylated sulfur(VI) fluorides · SF₆ substitutes · dielectric properties · decomposition pathways · solid state structures

- [1] a) L. Stuart, J. Luterbacher, L. Paterson, R. Devillier, S. Castonguay, *United in Science 2022. A multi-organization high-level compilation of the most recent science related to climate change, impacts and responses*, 2022; b) L. K. Gohar, K. P. Shine, *Weather* 2007, 62, 307; c) P. Widger, A. Haddad, *Energies* 2018, 11, 2037.
- [2] L. G. Christophorou, J. K. Olthoff, R. J. van Brunt, *IEEE Electr. Insul. Mag.* 1997, 13, 20.
- [3] S. Tian, X. Zhang, Y. Cressault, J. Hu, B. Wang, S. Xiao, Y. Li, N. Kabbaj, *AIP Adv.* 2020, 10, 050702.
- [4] a) J. Harnisch, W. Schwarz, *Costs and the impact on emissions of potential regulatory framework for reducing emissions of hydrofluorocarbons, perfluorocarbons and sulphur hexafluoride*, 2003; b) P. G. Simmonds, M. Rigby, A. J. Manning, S. Park, K. M. Stanley, A. McCulloch, S. Henne, F. Graziosi, M. Maione, J. Arduini, S. Reimann, M. K. Vollmer, J. Mühle, S. O'Doherty, D. Young, P. B. Krummel, P. J. Fraser, R. F. Weiss, P. K. Salameh, C. M. Harth, M.-K. Park, H. Park, T. Arnold, C. S. Rennick, L. P. Steele, B. Mitrevski, R. H. J. Wang, R. G. Prinn, *Atmos. Chem. Phys.* 2020, 20, 7271.
- [5] a) European Commission - Press release Green Deal: Phasing down fluorinated greenhouse gases and ozone depleting substances, Brussels, 2022; b) Regulation (EU) No 517/2014 on fluorinated greenhouse gases and repealing Regulation (EC) No 842/2006, *Off. J. Eur. Communities: Legis.* 2014, L150, 195.
- [6] J. Owens, A. Xiao, J. Bonk, M. DeLorme, A. Zhang, *Energies* 2021, 14, 5051.
- [7] M. Melinda, M. Manning, D. Qin, S. Solomon, K. Averyt, M. Tignor, H. L. Miller, Jr., Z. Chen, *IPCC, 2007: Climate Change 2007. The Physical Science Basis*, Cambridge (UK) and New York (USA), 2007.
- [8] T. F. Stocker, D. Qin, G.-K. Plattner, M. Tignor, S. K. Allen, J. Boschung, A. Nauels, Y. Xia, V. Bex and P. M. Midgley, *IPCC, 2013: Climate Change 2013. The Physical Science Basis*, Cambridge (UK) and New York (USA), 2013.
- [9] A. A. Lindley, A. McCulloch, *J. Fluorine Chem.* 2005, 126, 1457.
- [10] A. F. Holleman, N. Wiberg, *Lehrbuch der Anorganischen Chemie*, de Gruyter, Berlin, 2007.
- [11] a) E. Riedel, C. Janiak, *Anorganische Chemie*, de Gruyter, Berlin, Boston, 2015; b) P. W. Atkins, T. L. Overton, J. P. Rourke, M. T. Weller, F. A. Armstrong, *Shriver & Atkins' inorganic chemistry*, Oxford Univ. Press, Oxford, 2010.
- [12] W. M. Leeds, T. E. Browne, A. P. Strom, *Trans. Am. Inst. Electr. Eng. Part 3* 1957, 76, 906.
- [13] L. G. Christophorou, *Electron-Molecule Interactions and Their Applications. Volume 2*, Elsevier Science, Burlington, 1984.
- [14] E. E. Kunhardt, L. H. Luessen (Eds.) *NATO Advanced Science Institutes Series, 89a*, Springer, Boston, MA, 1983.
- [15] a) A. Haupt (Ed.) *Organic and Inorganic Fluorine Chemistry*, de Gruyter, Berlin, Boston, 2021; b) P. R. Howard, *Proc. Inst. Electr. Eng., Part A UK* 1957, 104, 139.
- [16] X. Li, H. Zhao, A. B. Murphy, *J. Phys. D* 2018, 51, 153001.
- [17] BAUA (DE), RIVM (NL) KEM (SE), NEA (NO), DEPA (DK), *Annex XV Restriction Report Per- and Polyfluoroalkyl Substances (PFAS)*, Helsinki, 2023.
- [18] M. Rabie, C. M. Franck, *Environ. Sci. Technol.* 2018, 52, 369.
- [19] C. M. Franck, J. Engelbrecht, M. Muratović, P. Pietrzak, P. Simka, *B&H Electrical Engineering* 2021, 15, 19.
- [20] R. C. Tolman, *Phys. Rev.* 1917, 9, 237.
- [21] M. S. Naidu, V. Kamaraju, *High voltage engineering*, McGraw-Hill, New York, 1996.
- [22] A. Chachereau, A. Hösl, C. M. Franck, *J. Phys. D* 2018, 51, 495201.
- [23] G. Pass, H. L. Roberts, *Inorg. Chem.* 1963, 2, 1016.
- [24] W. P. van Meter, G. H. Cady, *J. Am. Chem. Soc.* 1960, 82, 6005.
- [25] L. Yang, D. R. Powell, R. P. Houser, *Dalton Trans.* 2007, 955.
- [26] D. Mootz, A. Merschenz-Quack, *Acta Crystallogr. Sect. C* 1988, 44, 924.
- [27] T. Knuplez, L. N. Schneider, T. Preitschopf, Y. K. J. Bejaoui, L. Zapf, N. Schopper, K. A. M. Maibom, J. A. P. Sprenger, F. Gehrke, S. Lorenzen, R. Graf, R. Bertermann, I. Fischer, N. V. Ignat'ev, M. Finze, *Chem. Eur. J.* 2023, 29, e202302701.
- [28] L. S. Bartell, S. K. Doun, *J. Mol. Struct.* 1978, 43, 245.
- [29] P. W. Atkins, J. de Paula, *Atkins' Physical chemistry*, Oxford University Press, Oxford, New York, 2006.
- [30] M. Rabie, D. A. Dahl, S. M. A. Donald, M. Reiher, C. M. Franck, *IEEE Trans. Dielectr. Electr. Insul.* 2013, 20, 856.
- [31] L. G. Christophorou, J. K. Olthoff, *Gaseous Dielectrics VIII*, Springer, Boston, MA, 1998.
- [32] F. Ye, X. Zhang, Y. Li, Q. Wan, J.-M. Bauchire, D. Hong, S. Xiao, J. Tang, *High Volt.* 2022, 7, 856.
- [33] L. Ledernez, F. Olcaytug, G. Urban, *Contrib. Plasma Phys.* 2012, 52, 276.
- [34] R. C. Kennedy, G. H. Cady, *J. Fluorine Chem.* 1973, 3, 41.
- [35] R. K. Harris, E. D. Becker, S. M. Cabral de Menezes, P. Granger, R. E. Hoffman, K. W. Zilm, *Pure Appl. Chem.* 2008, 80, 59.
- [36] Adept Scientific, *gNMR V 5.0*, 2005.
- [37] F. Neese, *WIREs Comput. Mol. Sci.* 2012, 2, 73.
- [38] L. Bennett, B. Melchers, B. Proppe, *Curta: A General-purpose High-Performance Computer at ZEDAT, Freie Universität Berlin*, 2020, Freie Universität Berlin, DOI:10.17169/refurbium-26754.
- [39] A. D. Becke, *J. Chem. Phys.* 1993, 98, 5648.
- [40] A. D. Becke, *Phys. Rev. A* 1988, 38, 3098.
- [41] a) S. Grimme, S. Ehrlich, L. Goerigk, *J. Comput. Chem.* 2011, 32, 1456; b) S. Grimme, J. Antony, S. Ehrlich, H. Krieg, *J. Chem. Phys.* 2010, 132, 154104.
- [42] F. Weigend, R. Ahlrichs, *Phys. Chem. Chem. Phys.* 2005, 7, 3297.
- [43] E. D. Glendening, J. K. Badenhop, A. E. Reed, J. E. Carpenter, J. A. Bohmann, C. M. Morales, P. Karafiloglou, C. R. Landis, F. Weinhold, *NBO 7.0*, Theoretical Chemistry Institute, University of Wisconsin, Madison, WI, 2018.
- [44] a) D. Attack, W. G. Schneider, *J. Phys. Chem.* 1951, 55, 532; b) A. Diefenbacher, M. Türk, *Fluid Phase Equilib.* 2001, 182, 121; c) K. Morofuji, K. Fujii, M. Uematsu, K. Watanabe, *Int. J. Thermophys.* 1986, 7, 17.
- [45] J. Fabre, F. Hardinghaus, H. Pernice, S. Hasenstab-Riedel, H. Beckers, S. Steinhauer, T. Schlöder PCT Int. Appl. (2017), WO 2017093510 A1.

Manuscript received: January 20, 2024
 Accepted manuscript online: February 8, 2024
 Version of record online: February 27, 2024

4 Conclusion and Outlook

4.1 Conclusion

Poly- and perfluorinated alkyl substances (PFAS) possess desirable features such as high stability, non-sticking and insulation properties and have a wide range of applications. However, their persistence and bioaccumulation make their use problematic. As a result, there is an ongoing revision of fluorinated compounds focusing on small, fluorinated groups connected to heteroatoms, which are more easily degradable. Among these groups, the trifluoromethoxy ($-\text{OCF}_3$) group is particularly notable for its degradability. One method to incorporate this group into organic molecules is the use of nucleophilic $-\text{OCF}_3$ reagents. Typically, these reagents require complex preparation methods and generate substantial organic waste. Therefore, developing a strategy to obtain a nucleophilic $-\text{OCF}_3$ reagent in a direct and atom-economic way was a primary goal.

In this work, a new and straightforward method for the synthesis of the commonly used reagent $\text{Ag}[\text{OCF}_3]$ for the nucleophilic incorporation of the $-\text{OCF}_3$ group is presented. The reaction of COF_2 with AgF in acetonitrile or propionitrile yields a solution of $\text{Ag}[\text{OCF}_3]$ through a fast conversion. These solutions can be stored at $-18\text{ }^\circ\text{C}$ for months. The heat released during the formation of an $\text{Ag}[\text{OCF}_3]$ acetonitrile solution was determined using reaction calorimetry, with $\Delta H = -66.7\text{ kJ mol}^{-1}$. Despite the use of the toxic gas COF_2 , this method is considered to be the most atom-economic way to synthesize $\text{Ag}[\text{OCF}_3]$, making its synthesis more sustainable and suitable for industrial applications. X-ray crystallographic analysis of single crystals revealed a polymeric chain structure of $\text{Ag}[\text{OCF}_3]$ in the solid state. In this structure, each silver ion is connected to two bridging alcoholate ligands with acetonitrile molecules further coordinating to the silver centers completing their coordination sphere. Although the $[\text{OCF}_3]^-$ anion coordinates to silver centers, the bond lengths and bond angles are found to be similar to $[\text{S}(\text{NMe}_2)_3][\text{OCF}_3]$, where the ions are separated.

The reaction of $\text{Ag}[\text{OCF}_3]$ with two equivalents of bipyridine resulted in the formation of $[\text{Ag}(\text{bipy})_2][\text{OCF}_3]$, a compound stable at room temperature once the solvent was removed. This demonstrates the possibility to stabilize normally unstable $-\text{OCF}_3$ compounds through saturation by coordinating them with suitable ligands. X-ray crystallographic analysis revealed a structure where the silver is saturated by two bipyridine ligands, while the $[\text{OCF}_3]^-$ anion is separated in the solid state. By comparing the IR spectra of solid $-\text{OCF}_3$ compounds with ones in solution, as well as with the spectrum of $\text{Ag}[\text{OCF}_3]$ in acetonitrile, insights into the nature of $\text{Ag}[\text{OCF}_3]$ were obtained. The IR spectrum exhibited bands corresponding to isolated $[\text{OCF}_3]^-$ anions, alongside bands likely representing oligomeric or polymeric structures similar to those observed in solid $[\text{Ag}(\text{MeCN})_2(\text{OCF}_3)]_n$. This indicates that the reactivity of $\text{Ag}[\text{OCF}_3]$ can be

influenced not only by the nucleophilicity of the $[\text{OCF}_3]^-$ anion but also by interactions between silver centers and the anions in solution. This interaction can potentially activate the $[\text{OCF}_3]^-$ anion. Furthermore, the formation of silver halides is a driving force for the substitution reaction.

Inspired by the direct synthesis of $\text{Ag}[\text{OCF}_3]$, the reaction was extended to higher perfluoroalcoholates, which are of interest for bioactive substances such as pharmaceuticals or agrochemicals. Following the reactivity of COF_2 and AgF , a range of higher silver(I) perfluoroalcoholates, $\text{Ag}[\text{OC}_2\text{F}_5]$, $\text{Ag}[\text{O}(i\text{-C}_3\text{F}_7)]$, $\text{Ag}[\text{O}(n\text{-C}_3\text{F}_7)]$, and $\text{Ag}[\text{OC}_8\text{F}_{17}]$, was obtained as solutions using the corresponding fluorinated carbonyl compounds. These silver(I) perfluoroalcoholate solutions are stable for months when stored at $-18\text{ }^\circ\text{C}$. Investigations of the molecular structures by X-ray diffraction revealed that the perfluorinated alcoholates serve as bridging ligands coordinating to two silver(I) centers in a dimeric structure similar to the polymeric structure of $[\text{Ag}(\text{MeCN})_2(\text{OCF}_3)]_n$. Remarkably, acetonitrile solutions of silver(I) perfluoroalcoholates function as user-friendly reagents for transferring perfluoroalcoholates. Initial transmetalation reactions with other coinage metals produced $\text{Cu}[\text{OCF}_3]$, $\text{Cu}[\text{OC}_2\text{F}_5]$, and $[\text{PPh}_4][\text{Au}(\text{CF}_3)_3(\text{OCF}_3)]$ in solution. Unlike their silver(I) counterparts, the perfluoroalcoholate anions in the molecular structures of solid $[\text{Cu}(\text{MeCN})_4][\text{OCF}_3]$ and $[\text{Cu}(\text{MeCN})_4][\text{OC}_2\text{F}_5]$ are not directly associated with the metal centers. Additionally, it has been demonstrated that an acetonitrile solution of the synthesized $\text{Ag}[\text{OCF}_3]$ can be employed from $[\text{NEt}_3\text{Me}][\text{OCF}_3]$. These acetonitrile solutions of silver(I) perfluoroalcoholates are also useful for incorporating perfluoroalkoxy groups into organic molecules. Various reagents were reacted with fluorenyl bromide, providing the corresponding ethers. Additionally, $\text{Ag}[\text{OCF}_3]$ and $\text{Ag}[\text{OC}_2\text{F}_5]$ solutions were reacted with reactive benzyl bromides and alkyl iodides, demonstrating that the higher ethoxide can be used similarly to $\text{Ag}[\text{OCF}_3]$ to incorporate the pentafluoroethoxy group. It is anticipated that these metal perfluoroalcoholates will become valuable reagents in the future.

In this first part of the work, a general protocol for the synthesis of silver(I) perfluoroalcoholates stabilized in acetonitrile or propionitrile solutions has been developed. The higher alcoholates are interesting for the design of bioactive compounds or the preparation of reference materials, while the straightforward and atom-economic preparation of $\text{Ag}[\text{OCF}_3]$ is a step forward for its use on an industrial scale as a nucleophilic trifluoromethylation reagent. In contrast, other methods typically use complex organic molecules, which sometimes require the already nucleophilic $[\text{OCF}_3]^-$ anion for synthesis and are thus producing a large amount of organic waste. Furthermore, the silver(I) perfluoroalcoholates can be used to synthesize other metal alcoholates and coordination compounds with the alcoholates as ligands, leading to new reagents for the transfer of these groups. The exploration of the structure of the silver(I) perfluoroalcoholates, especially of $\text{Ag}[\text{OCF}_3]$ in the solid state and, more importantly, in solution, is a step forward to a better understanding of the reactivity of these compounds. In the future, this

information can help to tune the reactivity by optimizing the reaction conditions for subsequent chemistry.

In the second part of this thesis, the gases trifluoromethyl fluorosulfonate ($\text{CF}_3\text{OSO}_2\text{F}$) and trifluoromethoxy sulfur pentafluoride (CF_3OSF_5) were re-examined regarding their dielectric properties. Both gases contain the $-\text{OCF}_3$ moiety and are therefore considered to be decomposable. The predicted dielectric strengths are relatively high, with values of 1.7 and 2.1 for $\text{CF}_3\text{OSO}_2\text{F}$ and CF_3OSF_5 , respectively, compared to the commonly used dielectric sulfur hexafluoride (SF_6) (1.0). Because of its enormous GWP, SF_6 is part of many regulations and will be banned as soon as possible. Therefore, alternative technical and chemical replacements must be found (for details, see Section 1.4.3).

The synthesis of both gases from CF_3OF and SF_4 , or CF_3OF and SO_2 , was optimized. *In situ* crystallization techniques were employed to investigate their molecular structures in the solid state. Measurements of the liquid and gas phases allowed the determination of critical parameters, including critical temperature and critical pressure. Additionally, the van der Waals constants (a and b) and Antoine parameters (A , B , and C) were determined for both gases. These findings provide a comprehensive understanding of the physical and chemical properties of $\text{CF}_3\text{OSO}_2\text{F}$ and CF_3OSF_5 , contributing valuable data for their potential applications in various fields.

The dielectric properties of these gases were examined using a newly developed, easy-to-perform method. Averaged relative breakdown voltages of 1.3 for $\text{CF}_3\text{OSO}_2\text{F}$ (boiling point: $-5.5\text{ }^\circ\text{C}$) and 1.4 for CF_3OSF_5 (boiling point: $-10.5\text{ }^\circ\text{C}$) were observed. This indicates that both substances exhibit better insulation properties than sulfur hexafluoride and are comparable to the already-used replacement $(\text{CF}_3)_2\text{CFCN}$, which is a PFAS based on the current regulations making, its future application in accordance with the discussed PFAS ban questionable. In addition, higher decomposition rates during arc events were noted for these substances ($\text{CF}_3\text{OSO}_2\text{F}$ and CF_3OSF_5) compared to SF_6 , while being in the same range as $(\text{CF}_3)_2\text{CFCN}$. However, CF_3OSF_5 decomposes into SF_6 , which affects its potential use as an SF_6 replacement. In contrast, $\text{CF}_3\text{OSO}_2\text{F}$ is more stable and decomposes into hydrolysable compounds such as carbonyl fluoride and sulfonyl fluoride during arcing events. These findings suggest that while both $\text{CF}_3\text{OSO}_2\text{F}$ and CF_3OSF_5 have promising dielectric properties, their decomposition under arc conditions presents a challenge. The decomposition can be partially counteracted by the higher dielectric strength and therefore smaller amount needed for the same application. $\text{CF}_3\text{OSO}_2\text{F}$ shows potential as a dielectric due to its more stable decomposition products, which may be advantageous for certain applications requiring robust insulation materials.

This thesis has made a substantial contribution to modern fluoroorganic chemistry, which is driven by the need for a more sustainable approach, while at the same time providing already possible applications. The concerns about the harmful effects of PFAS and their persistence

in nature are the subject of many discussions and ongoing regulation proceedings. The enormous stability of the C–F bond, which even increases with the fluorine content, inhibits an easy decomposition of highly fluorinated compounds in nature. Even organic molecules with only small perfluorinated groups leave the fluorinated moieties as persistent compounds after decomposition (for details, see Section 1.4). A ban on all PFAS is an option and is part of the proposed ban of all PFAS in the EU, but there are some applications such as insulating gases in high voltage electrical applications, which require most likely fluorinated molecules for high voltage applications. Therefore, compounds with better decomposable fluorinated groups are considered to replace existing PFAS. The $-\text{OCF}_3$ group, which is part of this work, is expected to be easier decomposable than classic PFAS. The bond between the oxygen of the $-\text{OCF}_3$ group and the organic residue is much weaker than the C–F bond and is therefore prone to get split. Once the $-\text{OCF}_3$ group gets split off the molecule in the form of an anion or radical the group can decompose more easily. The negative hyperconjugation, wherein electron density from a p(O) orbital is delocalized into a $\sigma^*(\text{C}-\text{F})$ orbital destabilizes the C–F bond, while stabilizing the C–O bond. The resulting decomposition pathway involves the formation of COF_2 , which is easily hydrolyzed into CO_2 and HF, followed by the mineralization of the HF. In contrast, the $-\text{OCF}_3$ group is much more stable in organic molecules due to the absence of this kind of hyperconjugation. The $-\text{OCF}_3$ moieties in organic molecules show similar short C–F and long C–O bond distances to the ones in CF_3OCl (for details, see Section 1.6.4).^[143]

As part of this thesis a new atom economic access to the reagent $\text{Ag}[\text{OCF}_3]$, an analysis of the structure in the solid state and solution as well as the use to transfer the $-\text{OCF}_3$ group were presented. Moreover, the synthesis could be extended to higher silver(I) perfluoroalcoholates and the investigations revealed their similar reactivity to $\text{Ag}[\text{OCF}_3]$. The direct synthesis of silver(I) perfluoroalcoholates and especially $\text{Ag}[\text{OCF}_3]$ makes these reagents more interesting for industrial applications.

Beside fundamental research on $-\text{OCF}_3$ moieties it is also of high importance to find suitable substitutes for the greenhouse gas SF_6 . The implementation of the $-\text{OCF}_3$ moiety into small molecules provides volatile compounds which are expected to decompose more easily and therefore be excluded from the PFAS ban. Two of those molecules were investigated in this work regarding their insulating properties. Even if a final assessment cannot yet be made due to the complex requirements of SF_6 replacements, the compounds presented are examples of new possibly degradable dielectric media. Both compounds possess higher dielectric strengths than SF_6 and could be used as suitable and more sustainable replacements in high voltage applications for the greenhouse gas SF_6 .

Overall, this work contributes to the growing field of sustainable fluorine chemistry by offering new and atom economic synthetic route to trifluoromethoxylated compounds, insights into their

structures and reactivity as well as potential sustainable substitutes for SF₆ addressing research and industry.

4.2 Outlook

Silver(I) perfluoroalcoholates are crucial compounds for the formation of corresponding perfluoroalkyl ethers. Higher alcoholates are particularly interesting for applications in bioactive substances within pharmaceuticals and agrochemicals, as their activity and performance can be influenced by chain length and structure. Additionally, they can be used for synthesizing reference materials and model compounds to investigate the distribution and degradation of PFAS, an area requiring further examination.

Ag[OCF₃] plays a special role since the –OCF₃ group is considered a fluorinated group with low environmental impact. To realize new synthetic pathways, the coordination chemistry of these compounds could be further investigated, with copper(II) species presenting intriguing possibilities. By exploring these avenues, innovative compounds with beneficial properties and minimal environmental consequences can be developed.

The –OCF₃ group is highly important in modern fluorine chemistry due to the positive and unique properties of fluorinated alkyl groups. Unlike other fluorinated compounds, the –OCF₃ group is expected not to have the drawback of being highly persistent in the environment and is therefore excluded from the mentioned ban of PFAS in the EU.^[5] However, there are only few studies addressing the degradation pathways of –OCF₃-bearing compounds in nature (for details, see Section 1.5). Therefore, it is essential to thoroughly examine the degradation behavior of various –OCF₃-containing compounds. This necessity also applies to trifluoromethyl fluorosulfonate (CF₃OSO₂F) and trifluoromethoxy sulfur pentafluoride (CF₃OSF₅), which exhibit dielectric properties superior to sulfur hexafluoride (SF₆). However, the requirements for SF₆ replacements are diverse and multifaceted (for details, see Section 1.4.4). Consequently, it is crucial to investigate other properties such as global warming potentials (GWP), toxicities, and material compatibilities.

Further research into the decomposition pathways of these compounds is necessary to fully understand the byproducts formed during their electrical breakdown as well as the potential environmental and health impacts of the formed byproducts. Additionally, the dielectric properties should be tested using more complex, established test frameworks. This includes determining swarm parameters and evaluating arc extinguishing properties. Such comprehensive testing will ensure a thorough understanding of these compounds and their suitability as SF₆ replacements in various applications. Furthermore, it is imperative to evaluate other compounds for high voltage applications, ideally those containing –OCF₃ groups, which can potentially degrade in the environment. By exploring a wider range of degradable compounds, it is possible to identify environmentally friendly alternatives with desirable properties for industrial

and commercial use. This approach is particularly important in scenarios where other technical solutions are insufficient to replace SF₆ as a dielectric medium. Additionally, the feasibility of large-scale synthesis and practical application in electrical insulation and other industries should be explored to provide valuable insights into the potential for these compounds to replace more harmful substances currently in use.

5 References

- [1] M. Jaccaud, R. Faron, D. Devilliers, R. Romano, S. Riedel, H. Pernice (Eds.) *Ullmann's Encyclopedia of Industrial Chemistry (Fluorine)*, Wiley-VCH Verlag GmbH & Co. KGaA, Weinheim, **2020**.
- [2] D. M. Lemal, *J. Org. Chem.* **2004**, 69, 1.
- [3] A. Haupt (Ed.), *Organic and Inorganic Fluorine Chemistry*, de Gruyter, Berlin, Boston, **2021**.
- [4] P. Kirsch, *Modern Fluoroorganic Chemistry, Synthesis, Reactivity, Applications*, Wiley-VCH, Weinheim, **2004**.
- [5] BAuA (DE), RIVM (NL) KEM (SE), NEA (NO), DEPA (DK), *Annex XV Restriction Report Per- and Polyfluoroalkyl Substances (PFAS)*, Helsinki, **2023**.
- [6] *2. a Montreal Protocol on Substances that Deplete the Ozone Layer*, United Nations, New York, **1989**, as available on <http://treaties.un.org/Pages/CTCs.aspx>, accessed 11.07.2024.
- [7] *7. a Kyoto Protocol to the United Nations Framework Convention on Climate Change*, United Nations, New York, **1997**, as available on <http://treaties.un.org/Pages/CTCs.aspx>, accessed 11.07.2024.
- [8] *15. Stockholm Convention on Persistent Organic Pollutants*, United Nations, New York, **2009**, as available on <http://treaties.un.org/Pages/CTCs.aspx>, accessed 11.07.2024.
- [9] *European Commission - Press release Green Deal: Phasing down fluorinated greenhouse gases and ozone depleting substances*, Brussels, **2022**.
- [10] R. A. Dickman, D. S. Aga, *J. Hazard. Mater.* **2022**, 436, 129120.
- [11] S. E. Fenton, A. Ducatman, A. Boobis, J. C. DeWitt, C. Lau, C. Ng, J. S. Smith, S. M. Roberts, *Environ. Toxicol. Chem.* **2021**, 40, 606.
- [12] A. F. Holleman, N. Wiberg (Eds.), *Lehrbuch der Anorganischen Chemie*, 102. ed, de Gruyter, Berlin, **2007**.
- [13] J. Schmedt auf der Günne, M. Mangstl, F. Kraus, *Angew. Chem. Int. Ed.* **2012**, 51, 7847.
- [14] D. O'Hagan, *Chem. Soc. Rev.* **2008**, 37, 308.
- [15] S. J. Blanksby, G. B. Ellison, *Acc. Chem. Res.* **2003**, 36, 255.
- [16] I. J. van der Walt, O. S. L. Bruinsma, *J. Appl. Polym. Sci.* **2006**, 102, 2752.

-
- [17] A. Endres, G. Maas, *Chem. Unserer Zeit* **2000**, *34*, 382.
- [18] J. B. Burkholder, R. A. Cox, A. R. Ravishankara, *Chem. Rev.* **2015**, *115*, 3704.
- [19] J. C. Farman, B. G. Gardiner, J. D. Shanklin, *Nature* **1985**, *315*, 207.
- [20] *2. Vienna Convention for the Protection of the Ozone Layer*, United Nations, New York, **1985**, as available on <http://treaties.un.org/Pages/CTCs.aspx>, accessed 11.07.2024.
- [21] M. Melinda, M. Manning, D. Qin, S. Solomon, K. Averyt, M. Tignor, H. L. Miller, Jr., Z. Chen, *IPCC, 2007: Climate Change 2007, The Physical Science Basis*, Cambridge (UK) and New York (USA), **2007**.
- [22] *7. d Paris Agreement, Treaty Series*, United Nations, New York, **2015**, as available on <http://treaties.un.org/Pages/CTCs.aspx>, accessed 11.07.2024.
- [23] *2. f Amendment to the Montreal Protocol on Substances that Deplete the Ozone Layer*, United Nations, New York, **2016**, as available on <http://treaties.un.org/Pages/CTCs.aspx>, accessed 11.07.2024.
- [24] Regulation (EU) No 517/2014 on fluorinated greenhouse gases and repealing Regulation (EC) No 842/2006, *Off. J. Eur. Communities: Legis.* **2014**, *L150*, 195.
- [25] D Behringer, F. Heydel, B. Gschrey, S. Osterheld, W. Schwarz, K. Warncke, F. Freeling, K. Nödler, S. Henne, S. Reimann, M. Blepp, W. Jörß, R. Liu, S. Ludig, I. Rüdener, S. Gartiser, *Persistent degradation products of halogenated refrigerants and blowing agents in the environment: type, environmental concentrations, and fate with particular regard to new halogenated substitutes with low global warming potential*, UBA, **2021**.
- [26] OECD, *Reconciling Terminology of the Universe of Per- and Polyfluoroalkyl Substances: Recommendations and Practical Guidance*, OECD Series on Risk Management, Paris, **2021**.
- [27] Z. Zhang, D. Sarkar, J. K. Biswas, R. Datta, *Bioresour. Technol.* **2022**, *344*, 126223.
- [28] W. M. Leeds, T. E. Browne, A. P. Strom, *Trans. Am. Inst. Electr. Eng., Part 3* **1957**, *76*, 906.
- [29] J. Harnisch, W. Schwarz, *Costs and the impact on emissions of potential regulatory framework for reducing emissions of hydrofluorocarbons, perfluorocarbons and sulphur hexafluoride*, **2003**.
- [30] P. G. Simmonds, M. Rigby, A. J. Manning, S. Park, K. M. Stanley, A. McCulloch, S. Henne, F. Graziosi, M. Maione, J. Arduini, S. Reimann, M. K. Vollmer, J. Mühle, S. O'Doherty, D. Young, P. B. Krummel, P. J. Fraser, R. F. Weiss, P. K. Salameh, C. M.
-

- Harth, M.-K. Park, H. Park, T. Arnold, C. S. Rennick, L. P. Steele, B. Mitrevski, R. H. J. Wang, R. G. Prinn, *Atmos. Chem. Phys.* **2020**, *20*, 7271.
- [31] P. Friedlingstein, M. W. Jones, M. O'Sullivan, R. M. Andrew, J. Hauck, G. P. Peters, W. Peters, J. Pongratz, S. Sitch, C. Le Quéré, D. C. E. Bakker, J. G. Canadell, P. Ciais, R. B. Jackson, P. Anthoni, L. Barbero, A. Bastos, V. Bastrikov, M. Becker, L. Bopp, E. Buitenhuis, N. Chandra, F. Chevallier, L. P. Chini, K. I. Currie, R. A. Feely, M. Gehlen, D. Gilfillan, T. Gkritzalis, D. S. Goll, N. Gruber, S. Gutekunst, I. Harris, V. Haverd, R. A. Houghton, G. Hurtt, T. Ilyina, A. K. Jain, E. Joetzjer, J. O. Kaplan, E. Kato, K. Klein Goldewijk, J. I. Korsbakken, P. Landschützer, S. K. Lauvset, N. Lefèvre, A. Lenton, S. Lienert, D. Lombardozzi, G. Marland, P. C. McGuire, J. R. Melton, N. Metzli, D. R. Munro, J. E. M. S. Nabel, S.-i. Nakaoka, C. Neill, A. M. Omar, T. Ono, A. Peregón, D. Pierrot, B. Poulter, G. Rehder, L. Resplandy, E. Robertson, C. Rödenbeck, R. Séférian, J. Schwinger, N. Smith, P. P. Tans, H. Tian, B. Tilbrook, F. N. Tubiello, G. R. van der Werf, A. J. Wiltshire, S. Zaehle, *Earth Syst. Sci. Data* **2019**, *11*, 1783.
- [32] J. Owens, A. Xiao, J. Bonk, M. DeLorme, A. Zhang, *Energies* **2021**, *14*, 5051.
- [33] X. Li, H. Zhao, A. B. Murphy, *J. Phys. D: Appl. Phys.* **2018**, *51*, 153001.
- [34] M. Rabie, C. M. Franck, *Environ. Sci. Technol.* **2018**, *52*, 369.
- [35] L. G. Christophorou, J. K. Olthoff, R. J. van Brunt, *IEEE Electr. Insul. Mag.* **1997**, *13*, 20.
- [36] S. Tian, X. Zhang, Y. Cressault, J. Hu, B. Wang, S. Xiao, Y. Li, N. Kabbaj, *AIP Adv.* **2020**, *10*, 50702.
- [37] P. R. Howard, *Proc. IEE A Power Eng. UK* **1957**, *104*, 139.
- [38] A. Chachereau, A. Hösl, C. M. Franck, *J. Phys. D: Appl. Phys.* **2018**, *51*, 495201.
- [39] L. G. Christophorou, J. K. Olthoff, *Gaseous Dielectrics VIII*, Springer, Boston, **1998**.
- [40] E. E. Kunhardt, L. H. Luessen (Eds.), *NATO Advanced Science Institutes Series, 89a*, Springer, Boston, **1983**.
- [41] F. Ye, X. Zhang, Y. Li, Q. Wan, J.-M. Bauchire, D. Hong, S. Xiao, J. Tang, *High Volt.* **2022**, *7*, 856.
- [42] B. Zhang, C. Li, J. Xiong, Z. Zhang, X. Li, Y. Deng, *AIP Adv.* **2019**, *9*, 115212.
- [43] M. S. Naidu (Ed.), *High voltage engineering, 2. ed.*, McGraw-Hill, New York, **1996**.
- [44] M. Rabie, D. A. Dahl, S. M. A. Donald, M. Reiher, C. M. Franck, *IEEE Trans. Dielect. Electr. Insul.* **2013**, *20*, 856.

- [45] T. Nakajima, H. Groult (Eds.) *Fluorinated materials for energy conversion*, Elsevier, Amsterdam, **2005**.
- [46] S. M. S. Hussain, A. A. Adewunmi, A. Mahboob, M. Murtaza, X. Zhou, M. S. Kamal, *Adv. Colloid Interface Sci.* **2022**, *303*, 102634.
- [47] T. Frömel, T. P. Knepper, *J. Fluorine Chem.* **2015**, *177*, 80.
- [48] M. Peschka, N. Fichtner, W. Hierse, P. Kirsch, E. Montenegro, M. Seidel, R. D. Wilken, T. P. Knepper, *Chemosphere* **2008**, *72*, 1534.
- [49] M. Inoue, Y. Sumii, N. Shibata, *ACS Omega* **2020**, *5*, 10633.
- [50] B.-Y. Hao, Y.-P. Han, Y. Zhang, Y.-M. Liang, *Org. Biomol. Chem.* **2023**, *21*, 4926.
- [51] A. Tlili, F. Toulgoat, T. Billard, *Angew. Chem. Int. Ed.* **2016**, *55*, 11726.
- [52] P. Jimonet, F. Audiau, M. Barreau, J. C. Blanchard, A. Boireau, Y. Bour, M. A. Coléno, A. Doble, G. Doerflinger, C. D. Huu, M. H. Donat, J. M. Duchesne, P. Ganil, C. Guérémy, E. Honor, B. Just, R. Kerphirique, S. Gontier, P. Hubert, P. M. Laduron, J. Le Blevec, M. Meunier, J. M. Miquet, C. Nemecek, S. Mignani, *J. Med. Chem.* **1999**, *42*, 2828.
- [53] J. Qiao, Y.-S. Li, R. Zeng, F.-L. Liu, R.-H. Luo, C. Huang, Y.-F. Wang, J. Zhang, B. Quan, C. Shen, X. Mao, X. Liu, W. Sun, W. Yang, X. Ni, K. Wang, L. Xu, Z.-L. Duan, Q.-C. Zou, H.-L. Zhang, W. Qu, Y.-H.-P. Long, M.-H. Li, R.-C. Yang, X. Liu, J. You, Y. Zhou, R. Yao, W.-P. Li, J.-M. Liu, P. Chen, Y. Liu, G.-F. Lin, X. Yang, J. Zou, L. Li, Y. Hu, G.-W. Lu, W.-M. Li, Y.-Q. Wei, Y.-T. Zheng, J. Lei, S. Yang, *Science* **2021**, *371*, 1374.
- [54] C. Ghiazza, T. Billard, C. Dickson, A. Tlili, C. M. Gampe, *ChemMedChem* **2019**, *14*, 1586.
- [55] R. Timoumi, I. Amara, I. B. Salem, G. Soud, S. Abid-Essefi, *J. Biochem. Mol. Toxicol.* **2023**, *37*, e23341.
- [56] M. Hird, *Chem. Soc. Rev.* **2007**, *36*, 2070.
- [57] P. Kirsch (Ed.), *Modern Fluoroorganic Chemistry*, 2. ed., Wiley-VCH, Weinheim, **2013**.
- [58] A. E. Feiring, *J. Org. Chem.* **1979**, *44*, 2907.
- [59] W. A. Sheppard, *J. Org. Chem.* **1964**, *29*, 1.
- [60] F. Mathey, J. Bensoam, *Tetrahedron Lett.* **1973**, *14*, 2253.
- [61] M. Zhou, C. Ni, Z. He, J. Hu, *Org. Lett.* **2016**, *18*, 3754.
- [62] I. Ben-David, D. Rechavi, E. Mishani, S. Rozen, *J. Fluorine Chem.* **1999**, *97*, 75.

- [63] M. Kuroboshi, K. Suzuki, T. Hiyama, *Tetrahedron Lett.* **1992**, 33, 4173.
- [64] P. E. Aldrich, W. A. Sheppard, *J. Org. Chem.* **1964**, 29, 11.
- [65] T. Umemoto, K. Adachi, S. Ishihara, *J. Org. Chem.* **2007**, 72, 6905.
- [66] R. Koller, K. Stanek, D. Stolz, R. Aardoom, K. Niedermann, A. Togni, *Angew. Chem. Int. Ed.* **2009**, 48, 4332.
- [67] J. Kalim, T. Duhail, T.-N. Le, N. Vanthuynne, E. Anselmi, A. Togni, E. Magnier, *Chem. Sci.* **2019**, 10, 10516.
- [68] L. Chu, F.-L. Qing, *Acc. Chem. Res.* **2014**, 47, 1513.
- [69] B. J. Jelier, P. F. Tripet, E. Pietrasiak, I. Franzoni, G. Jeschke, A. Togni, *Angew. Chem. Int. Ed.* **2018**, 57, 13784.
- [70] J. W. Lee, S. Lim, D. N. Maienshein, P. Liu, M.-Y. Ngai, *Angew. Chem. Int. Ed.* **2020**, 59, 21475.
- [71] W. Zheng, J. W. Lee, C. A. Morales-Rivera, P. Liu, M.-Y. Ngai, *Angew. Chem. Int. Ed.* **2018**, 57, 13795.
- [72] Z. Deng, M. Zhao, F. Wang, P. Tang, *Nat. Commun.* **2020**, 11, 2569.
- [73] H. L. Roberts, *J. Chem. Soc.* **1964**, 4538.
- [74] B. Descamps, W. Forst, *Can. J. Chem.* **1975**, 53, 1442.
- [75] W. Reints, D. A. Pratt, H.-G. Korth, P. Mulder, *J. Phys. Chem. A* **2000**, 104, 10713.
- [76] L. Batt, K. Christie, R. T. Milne, A. J. Summers, *Int. J. Chem. Kinet.* **1974**, 6, 877.
- [77] A. Rieche, *Ber. Dtsch. Chem. Ges. A/B* **1928**, 61, 951.
- [78] J. H. Nissen, T. Stüker, T. Drews, S. Steinhauer, H. Beckers, S. Riedel, *Angew. Chem. Int. Ed.* **2019**, 58, 3584.
- [79] R. C. Kennedy, J. B. Levy, *J. Phys. Chem.* **1972**, 76, 3480.
- [80] C. J. Schack, W. Maya, *J. Am. Chem. Soc.* **1969**, 91, 2902.
- [81] R. S. Porter, G. H. Cady, *J. Am. Chem. Soc.* **1957**, 79, 5628.
- [82] R. C. Kennedy, G. H. Cady, *J. Fluorine Chem.* **1973**, 3, 41.
- [83] O. Ruff, G. Miltschitzky, *Z. Anorg. Allg. Chem.* **1934**, 221, 154.
- [84] L. Yapi, J. B. Wagener, J. Le Roux, P. Crouse, *J. Fluorine Chem.* **2022**, 254, 109933.
- [85] C. J. Marsden, L. S. Bartell, F. P. Diodati, *J. Mol. Struct.* **1977**, 39, 253.

-
- [86] O. Ferchichi, N. Derbel, N.-E. Jaidane, T. Cours, A. Alijah, *Phys. Chem. Chem. Phys.* **2017**, *19*, 21500.
- [87] L. Hedberg, K. Hedberg, P. G. Eller, R. R. Ryan, *Inorg. Chem.* **1988**, *27*, 232.
- [88] R. H. Jackson, *J. Chem. Soc.* **1962**, 4585.
- [89] W. J. Peláez, G. A. Argüello, *Tetrahedron Lett.* **2010**, *51*, 5242.
- [90] C. Kelly, H. W. Sidebottom, J. Treacy, O. J. Nielsen, *Chem. Phys. Lett.* **1994**, *218*, 29.
- [91] S. Dix, P. Golz, J. R. Schmid, S. Riedel, M. N. Hopkinson, *Chem. Eur. J.* **2021**, *27*, 11554.
- [92] L. M. Maas, C. Fasting, P. Voßnacker, N. Limberg, P. Golz, C. Müller, S. Riedel, M. N. Hopkinson, *Angew. Chem. Int. Ed.* **2023**, *63*, e202317770.
- [93] K. K. Johri, D. D. DesMarteau, *J. Org. Chem.* **1983**, *48*, 242.
- [94] W. Navarrini, V. Tortelli, A. Russo, S. Corti, *J. Fluorine Chem.* **1999**, *95*, 27.
- [95] J. L. Cook, T. Fukushi, W. M. A. Grootaert, A. Verschuere, WO2011084404A2, **2010**.
- [96] E. Antenucci, V. Tortelli, S. Millefanti, WO2019110710A1, **2019**.
- [97] K. B. Kellogg, G. H. Cady, *J. Am. Chem. Soc.* **1948**, *70*, 3986.
- [98] D. E. Gould, L. R. Anderson, D. E. Young, W. B. Fox, *Chem. Commun.* **1968**, 1564.
- [99] R. Minkwitz, R. Bröchler, A. Kornath, R. Ludwig, F. Rittner, *Inorg. Chem.* **1997**, *36*, 2147.
- [100] M. Kol, S. Rozen, E. Appelman, *J. Am. Chem. Soc.* **1991**, *113*, 2648.
- [101] E. Riedel, C. Janiak (Eds.), *Anorganische Chemie*, 9. ed., de Gruyter, Berlin, Boston, **2015**.
- [102] O. Kwon, Y. Kwon, *Comput. Theor. Chem.* **1999**, *489*, 119.
- [103] R. Minkwitz, R. Bröchler, *Z. Naturforsch., B: Chem. Sci.* **1997**, *52*, 401.
- [104] J. M. Canich, G. L. Gard, J. M. Shreeve, *Inorg. Chem.* **1984**, *23*, 441.
- [105] P. J. Aymonino, *Chem. Commun.* **1965**, 241.
- [106] L. Du, D. D. DesMarteau, V. Tortelli, M. Galimberti, *J. Fluorine Chem.* **2009**, *130*, 830.
- [107] L. Du, D. D. DesMarteau, *J. Fluorine Chem.* **2008**, *129*, 1044.
- [108] D. E. Young, D. E. Gould, L. R. Anderson, W. B. Fox, US3627799A, **1971**.
- [109] D. E. Young, L. R. Anderson, D. E. Gould, W. B. Fox, US 3732274, **1973**.

- [110] D. E. Young, L. R. Anderson, D. E. Gould, W. B. Fox, *J. Am. Chem. Soc.* **1970**, *92*, 2313.
- [111] G. Guglielmo, G. Gregorio, P. Calani, EP0259818, **1991**.
- [112] F. P. Diodati, L. S. Bartell, *J. Mol. Struct.* **1971**, *8*, 395.
- [113] L. Pierce, R. Jackson, N. DiCianni, *J. Chem. Phys.* **1961**, *35*, 2240.
- [114] W. Poll, G. Pawelke, D. Mootz, E. H. Appelman, *Angew. Chem. Int. Ed.* **1988**, *27*, 392.
- [115] A. A. Kolomeitsev, M. Vorobyev, H. Gillandt, *Tetrahedron Lett.* **2008**, *49*, 449.
- [116] K. O. Christe, J. Hegge, B. Hoge, R. Haiges, *Angew. Chem. Int. Ed.* **2007**, *46*, 6155.
- [117] K. Seppelt, *Angew. Chem. Int. Ed.* **1977**, *16*, 322.
- [118] M. E. Redwood, C. J. Willis, *Can. J. Chem.* **1965**, *43*, 1893.
- [119] X. Zhang, K. Seppelt, *Inorg. Chem.* **1997**, *36*, 5689.
- [120] W. B. Farnham, B. E. Smart, W. J. Middleton, J. C. Calabrese, D. A. Dixon, *J. Am. Chem. Soc.* **1985**, *107*, 4565.
- [121] H. Oberhammer, T. Mahmood, J. M. Shreeve, *J. Mol. Struct.* **1984**, *117*, 311.
- [122] M. Nakata, K. Kohata, T. Fukuyama, K. Kuchitsu, C. J. Wilkins, *J. Mol. Struct.* **1980**, *68*, 271.
- [123] I. G. Logvinenko, Y. Markushyna, I. S. Kondratov, B. V. Vashchenko, M. Kliachyna, Y. Tokaryeva, V. Pivnytska, O. O. Grygorenko, G. Haufe, *J. Fluorine Chem.* **2020**, *231*, 109461.
- [124] L. P. Wackett, *Microorganisms* **2022**, *10*, 1664.
- [125] D. Chen, L. Lu, Q. Shen, *Org. Chem. Front.* **2019**, *6*, 1801.
- [126] D. Chen, Y. Luo, L. Lu, Q. Shen, *Organometallics* **2024**, 10.1021/acs.organomet.4c00073.
- [127] S. Chen, Y. Huang, X. Fang, H. Li, Z. Zhang, T. S. A. Hor, Z. Weng, *Dalton Trans.* **2015**, *44*, 19682.
- [128] C.-P. Zhang, D. A. Vacic, *Organometallics* **2012**, *31*, 7812.
- [129] M. Winter, M. A. Ellwanger, N. Limberg, A. Pérez-Bitrián, P. Voßnacker, S. Steinhauer, S. Riedel, *Chem. Eur. J.* **2023**, *29*, e202301684.
- [130] M. Zhou, C. Ni, Y. Zeng, J. Hu, *J. Am. Chem. Soc.* **2018**, *140*, 6801.
- [131] J. Saiter, T. Guérin, M. Donnard, A. Panossian, G. Hanquet, F. R. Leroux, *Eur. J. Org. Chem.* **2021**, *2021*, 3139.

-
- [132] A. Turksoy, T. Scattolin, S. Bouayad-Gervais, F. Schoenebeck, *Chem. Eur. J.* **2020**, *26*, 2183.
- [133] Z. Lu, T. Kumon, G. B. Hammond, T. Umemoto, *Angew. Chem. Int. Ed.* **2021**, *60*, 16171.
- [134] M. Lei, H. Miao, X. Wang, W. Zhang, C. Zhu, X. Lu, J. Shen, Y. Qin, H. Zhang, S. Sha, Y. Zhu, *Tetrahedron Lett.* **2019**, *60*, 1389.
- [135] J. J. Newton, B. J. Jelier, M. Meanwell, R. E. Martin, R. Britton, C. M. Friesen, *Org. Lett.* **2020**, *22*, 1785.
- [136] C. Bonnefoy, E. Chefdeville, A. Panosian, G. Hanquet, F. R. Leroux, F. Toulgoat, T. Billard, *Chem. Eur. J.* **2021**, *27*, 15986.
- [137] R. Koller, Q. Huchet, P. Battaglia, J. M. Welch, A. Togni, *Chem. Commun.* **2009**, 5993.
- [138] J. Barbion, S. Pazenok, J.-P. Vors, B. R. Langlois, T. Billard, *Org. Process Res. Dev.* **2014**, *18*, 1037.
- [139] X. Jiang, P. Tang, *Chin. J. Chem.* **2021**, *39*, 255.
- [140] P. Tang, X. Jiang in *Emerging fluorinated motifs. Synthesis, properties and applications* (Eds.: D. Cahard, J.-A. Ma), Wiley-VCH, Weinheim, **2020**, 207.
- [141] F. Wang, P. Xu, F. Cong, P. Tang, *Chem. Sci.* **2018**, *9*, 8836.
- [142] F. G. Zivkovic, G. Wycich, L. Liu, F. Schoenebeck, *J. Am. Chem. Soc.* **2024**, *146*, 1276.
- [143] B. Manteau, P. Genix, L. Brelot, J.-P. Vors, S. Pazenok, F. Giornal, C. Leuenberger, F. R. Leroux, *Eur. J. Org. Chem.* **2010**, *2010*, 6043.

6 Publications, Patents and Conference Contributions

6.1 Publications

- 1) Silver(i) Perfluoroalcoholates: Synthesis, Structure, and their Use as Transfer Reagents**
Paul Golz, Kamar Shakeri, Lilian Maas, Marius Balizs, Alberto Pérez-Bitrián, Helen D. Kemmler, Merlin Kleoff, Patrick Voßnacker, Mathias Christmann, Sebastian Riedel, *Chem. Eur. J.* **2024**, *30*, e202400861, <https://doi.org/10.1002/chem.202400861>
- 2) Trifluoromethyl Fluorosulfonate (CF₃OSO₂F) and Trifluoromethoxy Sulfur Pentafluoride (CF₃OSF₅) – Two Gaseous Sulfur(VI) Compounds with Insulating Properties**
Paul Golz, Gesa H. Dreyhsig, Holger Pernice, Thomas Drews, Jan H. Nissen, Helmut Beckers, Simon Steinhauer, Anja Wiesner, Sebastian Riedel, *Chem. Eur. J.* **2024**, *30*, e202400258, <https://doi.org/10.1002/chem.202400258>
- 3) Catalyst-Free Trifluoromethoxylation of Silyl Enol Ethers and Allyl Silanes with Bis(trifluoromethyl)peroxide**
Lilian M. Maas, Carlo Fasting, Patrick Voßnacker, Niklas Limberg, Paul Golz, Carsten Müller, Sebastian Riedel, Matthew N. Hopkinson, *Angew. Chem. Int. Ed.* **2024**, *63*, e202317770, <https://doi.org/10.1002/anie.202317770>
- 4) Radical C–H Trifluoromethoxylation of (Hetero)arenes with Bis(trifluoromethyl)peroxide**
Stefan Dix, Paul Golz, Jonas R. Schmid, Sebastian Riedel, Matthew N. Hopkinson, *Chem. Eur. J.* **2021**, *27*, 11554, <https://doi.org/10.1002/chem.202101621>
- 5) N-Heterocyclic Carbene Catalyzed Photoenolization/Diels–Alder Reaction of Acid Fluorides**
Andreas Mavroskoufis, Keerthana Rajes, Paul Golz, Arush Agrawal, Vincent Ruß, Jan P. Götze, Matthew N. Hopkinson, *Angew. Chem. Int. Ed.* **2019**, *59*, 3190, <https://doi.org/10.1002/anie.201914456>
- 6) Stabilization of Lewis Acidic AuF₃ as an N-Heterocyclic Carbene Complex: Preparation and Characterization of [AuF₃(SIMes)]**
Mathias A. Ellwanger, Simon Steinhauer, Paul Golz, Thomas Braun, Sebastian Riedel, *Angew. Chem. Int. Ed.* **2018**, *57*, 7210, <https://doi.org/10.1002/anie.201802952>

7) Taming the High Reactivity of Gold(III) Fluoride: Fluorido Gold(III) Complexes with N-Based Ligands

Mathias A. Ellwanger, Simon Steinhauer, **Paul Golz**, Helmut Beckers, Anja Wiesner, Beatrice Braun-Cula, Thomas Braun, Sebastian Riedel, *Chem. Eur. J.* **2017**, *23*, 13501, <https://doi.org/10.1002/chem.201702663>

6.2 Patents

1) Catalytic method for the preparation of perfluoroalkoxy substituted arenes and heteroarenes

Sebastian Hasenstab-Riedel, Matthew Hopkinson, Stefan Dix, **Paul Golz**, Jonas Rachid Schmid, Holger Pernice, Sebastian Gutmann, PCT Int. Appl. (**2021**) **WO2022175508 A1**.

6.3 Conference Contributions – Oral and Poster Presentations

1) New Perfluorinated Silver(I) and Copper(I) Alcoholates

Paul Golz, Marius Balizs, Helen Kemmler, Patrick Voßnacker, Sebastian Riedel, *20th European Symposium on Fluorine Chemistry*, Berlin Germany, **2022**.

2) New Perfluorinated Silver(I) and Copper(I) Alcoholates

Paul Golz, Sebastian Riedel, *19. Deutscher Fluortag*, Schmiten Germany, **2022**

3) New Perfluorinated Silver(I) and Copper(I) Alcoholates

Paul Golz, Marius Balizs, Helen Kemmler, Patrick Voßnacker, Sebastian Riedel, *21th Conference on Inorganic Chemistry (Wöhler-Vereinigung)*, Marburg Germany, **2022**.

4) New Perfluorinated Silver(I) Alcoholates – Versatile Transfer Reagents

Paul Golz, Marius Balizs, Helen Kemmler, Lilian M. Maas, Kamar Shakeri, Patrick Voßnacker, Merlin Kleoff, Sebastian Riedel, *23rd International Symposium on Fluorine Chemistry (23rd ISFC) and 9th International Symposium on Fluorous Technologies (ISoFT'23)*, Quebec Canada, **2023**

5) New Perfluorinated Silver(I) Alcoholates – Versatile Transfer Reagents

Paul Golz, Marius Balizs, Helen Kemmler, Lilian M. Maas, Kamar Shakeri, Patrick Voßnacker, Merlin Kleoff, Sebastian Riedel, *23. Norddeutsches Doktorandenkolloquium*, Berlin Germany, **2023**

7 Curriculum Vitae

The curriculum vitae is not included for reasons of data protection.

8 Appendix

8.1 SI of Silver(I) Perfluoroalcoholates: Synthesis, Structure, and their Use as Transfer Reagents

Paul Golz, Kamar Shakeri, Lilian Maas, Marius Balizs, Alberto Pérez-Bitrián, Helen D. Kemmler, Merlin Kleoff, Patrick Voßnacker, Mathias Christmann, and Sebastian Riedel*

Chem. Eur. J. **2024**, *30*, e202400861.

<https://doi.org/10.1002/chem.202400861>

© 2024 The Authors. Published by Wiley-VCH Verlag GmbH.

Chemistry–A European Journal

Supporting Information

Silver(I) Perfluoroalcoholates: Synthesis, Structure, and their Use as Transfer Reagents

Paul Golz, Kamar Shakeri, Lilian Maas, Marius Balizs, Alberto Pérez-Bitrián,
Helen D. Kemmler, Merlin Kleoff, Patrick Voßnacker, Mathias Christmann, and
Sebastian Riedel*

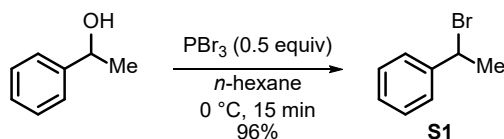
Table of Contents

Synthesis of Bromides S1 – S4.....	4
(1-bromoethyl)benzene S1	4
5-(bromomethyl)benzo[d][1,3]dioxole S2	4
1-(bromomethyl)-4-(((1 <i>R</i> ,2 <i>S</i> ,5 <i>R</i>)-2-isopropyl-5-methylcyclohexyl)oxy)methyl)benzene S3	5
4-(bromomethyl)benzyl 2-(4-isobutylphenyl)propanoate S4	5
General Procedure for the Perfluoroalkoxylation.....	6
9-(trifluoromethoxy)-9 <i>H</i> -fluorene 2a	6
5-((trifluoromethoxy)methyl)benzo[d][1,3]dioxole 2b	7
(1-(trifluoromethoxy)ethyl)benzene 2c	7
1-(((1 <i>R</i> ,2 <i>S</i> ,5 <i>R</i>)-2-isopropyl-5-methylcyclohexyl)oxy)methyl)-4-((trifluoromethoxy)methyl)benzene 2d	8
4-((trifluoromethoxy)methyl)benzyl 2-(4-isobutylphenyl)propanoate 2e	8
9-(perfluoroethoxy)-9 <i>H</i> -fluorene 3a	9
4-((perfluoroethoxy)methyl)benzotrile 3b	9
1-iodo-4-((perfluoroethoxy)methyl)benzene 3c	10
1-chloro-4-((perfluoroethoxy)methyl)benzene 3d	10
5-((perfluoroethoxy)methyl)benzo[d][1,3]dioxole 3e	11
4-nitro-2-((perfluoroethoxy)methyl)phenol 3f	11
1,4-bis((perfluoroethoxy)methyl)benzene 3g	12
1-(perfluoroethoxy)hexadecane 3h	12
9-((perfluoropropan-2-yl)oxy)-9 <i>H</i> -fluorene 4	13
9-(perfluoropropoxy)-9 <i>H</i> -fluorene 5	13
9-((perfluorooctyl)oxy)-9 <i>H</i> -fluorene 6	14
Limitation of the scope.....	14
X-Ray Crystallography.....	16
Crystallographic Data	16
Quantum Chemical Calculations - Optimized Minimum Structures	20
xyz-Coordinates [Å] of CF ₂ O on PW6B95-D3BJ/def2-QZVPP Level	20
xyz-Coordinates [Å] of [CF ₃ O] ⁻ on PW6B95-D3BJ/def2-QZVPP Level	20
xyz-Coordinates [Å] of CF ₃ CF(O) on PW6B95-D3BJ/def2-QZVPP Level.....	20
xyz-Coordinates [Å] of [C ₂ F ₅ O] ⁻ on PW6B95-D3BJ/def2-QZVPP Level	20
xyz-Coordinates [Å] of CF ₃ CF ₂ CF(O) on PW6B95-D3BJ/def2-QZVPP Level	21
xyz-Coordinates [Å] of [<i>n</i> -C ₃ F ₇ O] ⁻ on PW6B95-D3BJ/def2-QZVPP Level.....	21
xyz-Coordinates [Å] of CF ₃ C(O)CF ₃ on PW6B95-D3BJ/def2-QZVPP Level	21
xyz-Coordinates [Å] of [<i>i</i> -C ₃ F ₇ O] ⁻ on PW6B95-D3BJ/def2-QZVPP Level.....	22

xyz-Coordinates [\AA] of $\text{C}_7\text{F}_{15}\text{CF}(\text{O})$ on PW6B95-D3BJ/def2-QZVPP Level	22
xyz-Coordinates [\AA] of $[\eta\text{-C}_8\text{F}_{16}\text{O}]^-$ on PW6B95-D3BJ/def2-QZVPP Level.....	23
Calorimetric Measurements.....	25
Setup.....	25
Solvation Enthalpy of COF_2 in Acetonitrile	25
Reaction of AgF with COF_2 in Acetonitrile.....	32
NMR Spectra.....	38
$\text{Ag}[\text{OCF}_3]$	38
$[\text{Ag}(\text{bpy})_2][\text{OCF}_3]$	38
$\text{Ag}[\text{OC}_2\text{F}_5]$	39
$\text{Ag}[\text{O}^i\text{C}_3\text{F}_7]$	40
$\text{Ag}[\text{O}^o\text{C}_3\text{F}_7]$	40
$\text{Ag}[\text{OC}_8\text{F}_{17}]$	41
$\text{Ag}[\text{OCF}_2\text{C}(\text{O})\text{F}]$	41
$\text{Cu}[\text{OCF}_3]$	42
$\text{Cu}[\text{OC}_2\text{F}_5]$	42
$[\text{PPh}_4][\text{Au}(\text{CF}_3)_3(\text{OCF}_3)]$ from AgOCF_3	43
$[\text{NEt}_3\text{Me}][\text{OCF}_3]$	44
(1-bromoethyl)benzene S1	45
5-(bromomethyl)benzo[d][1,3]dioxole S2	46
1-(bromomethyl)-4-(((1 <i>R</i> ,2 <i>S</i> ,5 <i>R</i>)-2-isopropyl-5-methylcyclohexyl)oxy)methyl)benzene S3	47
4-(bromomethyl)benzyl 2-(4-isobutylphenyl)propanoate S4	48
9-(trifluoromethoxy)-9 <i>H</i> -fluorene 2a	49
5-((trifluoromethoxy)methyl)benzo[d][1,3]dioxole 2b	50
(1-(trifluoromethoxy)ethyl)benzene 2c	52
1-(((1 <i>R</i> ,2 <i>S</i> ,5 <i>R</i>)-2-isopropyl-5-methylcyclohexyl)oxy)methyl)-4-((trifluoromethoxy)methyl)benzene 2d	53
4-((trifluoromethoxy)methyl)benzyl 2-(4-isobutylphenyl)propanoate 2e	55
9-(perfluoroethoxy)-9 <i>H</i> -fluorene 3a	56
4-((perfluoroethoxy)methyl)benzotrile 3b	58
1-iodo-4-((perfluoroethoxy)methyl)benzene 3c	59
1-chloro-4-((perfluoroethoxy)methyl)benzene 3d	61
5-((perfluoroethoxy)methyl)benzo[d][1,3]dioxole 3e	62
4-nitro-2-((perfluoroethoxy)methyl)phenol 3f	64
1,4-bis((perfluoroethoxy)methyl)benzene 3g	65
1-(perfluoroethoxy)hexadecane 3h	67

9-((perfluoropropan-2-yl)oxy)-9 <i>H</i> -fluorene 4	68
9-(perfluoropropoxy)-9 <i>H</i> -fluorene 5	70
9-((perfluorooctyl)oxy)-9 <i>H</i> -fluorene 6	71
2-nitrobenzenesulfonyl fluoride S5	73
References	75

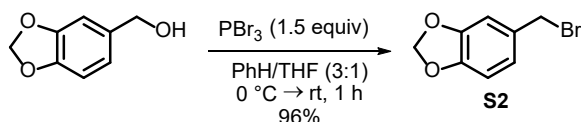
Synthesis of Bromides S1 – S4

(1-bromoethyl)benzene **S1**

To a stirred solution of 1-phenylethanol (1.00 g, 8.20 mmol, 1.0 equiv) in *n*-hexane (30 mL) at 0 °C, placed in a dry Schlenk tube, was added dropwise PBr₃ (1.14 g, 4.10 mmol, 0.5 equiv). After 15 min, the reaction mixture was slowly poured into 50 mL of ice water. The organic phase was washed with NaHCO₃ (sat. aq., 2 x 30 mL), HCl (aq. 1 M, 1 x 30 mL), and brine (3 x 30 mL), dried over MgSO₄, filtered and concentrated under reduced pressure. Product **S1** (1.45 g, 7.83 mmol, 96%) was obtained as a colorless liquid.

¹H NMR (400 MHz, CDCl₃): δ = 7.46 – 7.43 (m, 2H), 7.35 (tt, *J* = 6.5, 1.0 Hz, 2H), 7.29 – 7.26 (m, 1H), 5.22 (q, *J* = 6.9 Hz, 1H), 2.06 (d, *J* = 6.9 Hz, 3H) ppm. **¹³C{¹H} NMR** (151 MHz, CDCl₃): δ = 143.6, 129.0, 128.7, 127.1, 49.9, 27.2 ppm.

The spectroscopic data are in accordance with those reported in literature.^[47]

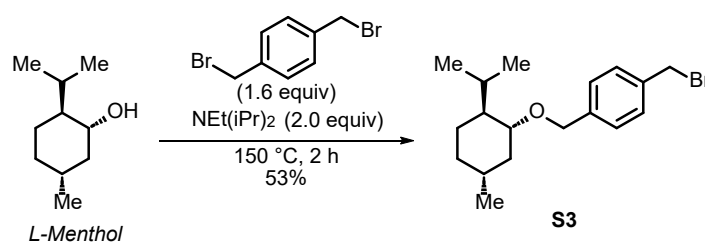
5-(bromomethyl)benzo[d][1,3]dioxole **S2**

Benzo[d][1,3]dioxol-5-ylmethanol (1.00 g, 6.57 mmol, 1.0 equiv) was placed in a dry Schlenk tube and dissolved in dry THF (5 mL) and dry PhH (15 mL). At 0 °C, PBr₃ (2.67 g, 9.86 mmol, 1.5 equiv) was added dropwise. The cooling bath was removed and the colorless solution was stirred at rt for 1 h. Then, the solution was poured on ice and extracted with Et₂O (3 x 30 mL). The combined organic layers were washed with brine (30 mL), dried over Na₂SO₄, filtered and concentrated under reduced pressure. The residue was dissolved in cyclohexane/EtOAc (1:1) and filtered over a pad of silica. The filtrate was concentrated under reduced pressure affording the product **S2** (1.35 g, 6.27 mmol, 96%) as a pale brown oil that solidified upon storage at 8 °C.

¹H NMR (400 MHz, CDCl₃): δ = 6.90 – 6.83 (m, 2H), 6.74 (d, *J* = 7.8 Hz, 1H), 5.96 (s, 2H), 4.45 (s, 2H) ppm. **¹³C{¹H} NMR** (176 MHz, CDCl₃): δ = 148.2, 148.1, 131.8, 123.1, 109.8, 108.7, 101.7, 34.5 ppm.

The spectroscopic data are in accordance with those reported in literature.^[48]

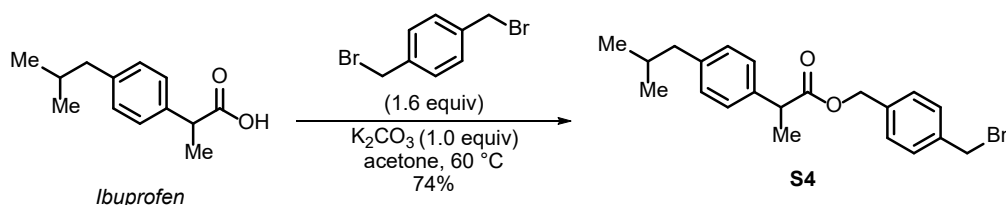
1-(bromomethyl)-4-((((1*R*,2*S*,5*R*)-2-isopropyl-5-methylcyclohexyl)oxy)methyl)benzene **S3**



S3 was synthesized according to a literature procedure.^[49] Menthol (500 mg, 3.20 mmol, 1.0 equiv), diisopropylethylamine (0.827 g, 1.09 mL, 6.40 mmol, 2.0 equiv) and 1,4-bis(bromomethyl)benzene (1.35 g, 5.12 mmol, 1.6 equiv) were placed into a heat-gun dried Schlenk flask equipped with a reflux condenser under argon atmosphere. The reaction mixture was stirred at 150 °C for 2 h before it was cooled to room temperature. Then, EtOAc (10 mL) and a solution of sodium bisulphate (10% aq., 10mL) were added to the mixture. The two phases were separated, the aqueous one was extracted with EtOAc (2 x 10 mL), the combined organic phases were dried over MgSO₄, filtered and the solvent was evaporated under reduced pressure. The product **S3** (578 mg, 1.70 mmol, 53%) was purified by flash column chromatography (SiO₂, Cy → EtOAc/Cy 10%) and obtained as a colorless oil.

¹H NMR (500 MHz, CDCl₃): δ = 7.31 – 7.28 (m, 2H), 7.27 – 7.24 (m, 2H), 4.58 (d, *J* = 11.6 Hz, 1H), 4.43 (s, 2H), 4.31 (d, *J* = 11.6 Hz, 1H), 3.10 (td, *J* = 10.6, 4.1 Hz, 1H), 2.21 (septd, *J* = 7.0, 2.8 Hz, 1H), 2.11 (dtd, *J* = 12.1, 3.8, 1.9 Hz, 1H), 1.62 – 1.53 (m, 2H), 1.34 – 1.25 (m, 1H), 1.22 (m, 1H), 0.96 – 0.73 (m, 9H), 0.64 (d, *J* = 6.9 Hz, 3H) ppm. ¹³C{¹H} NMR (151 MHz, CDCl₃): δ = 139.9, 137.2, 129.4, 128.5, 79.3, 70.3, 48.7, 40.6, 34.9, 33.8, 31.9, 25.9, 23.6, 22.7, 21.4, 16.4 ppm. IR (ATR): $\tilde{\nu}$ = 2954, 2920, 2867, 1455, 1342, 1226, 1107, 1084, 1071, 907, 731 cm⁻¹. HRMS (EI): *m/z* calculated for [C₂₁H₂₅BrO₂]⁺ ([M]⁺): 388.1032, measured: 339.1313.

4-(bromomethyl)benzyl 2-(4-isobutylphenyl)propanoate **S4**



S4 was synthesized according to a literature procedure.^[50] Ibuprofen (500 mg, 2.42 mmol, 1.0 equiv), K₂CO₃ (334 mg, 2.42 mmol, 1.0 equiv) and 1,4-bis(bromomethyl)benzene (1.02 g, 3.88 mmol, 1.6 equiv) and acetone (12 mL) were stirred in a sealed tube at 60 °C for 18 h. The reaction mixture was cooled to room temperature and a solution of CH₂Cl₂/EtOAc (1:1, 30 mL) was added. The reaction mixture was filtered through a plug of celite and rinsed with a solution of CH₂Cl₂/EtOAc (1:1). The solvent was evaporated under reduced pressure. The product **S4** was purified by flash column chromatography (SiO₂, Cy → EtOAc/Cy 15%) and obtained as colorless oil (696 mg, 1.79 mmol, 74%).

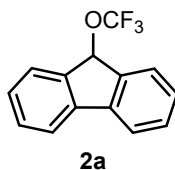
¹H NMR (500 MHz, CDCl₃): δ = 7.34 – 7.31 (m, 2H), 7.21 – 7.17 (m, 5H), 7.09 (dd, *J* = 8.2, 2.1 Hz, 3H), 5.09 (s, 1H), 4.47 (s, 2H), 3.77 – 3.72 (m, 1H), 2.45 (d, *J* = 7.0 Hz, 3H), 1.91 – 1.80 (m, 1H), 1.51 (dd, *J* = 7.1, 2.5 Hz, 4H), 0.91 (d, *J* = 1.9 Hz, 5H), 0.89 (d, *J* = 1.9 Hz, 5H) ppm. **¹³C NMR{¹H}** (151 MHz, CDCl₃): δ = 174.8, 141.0, 137.9, 136.8, 129.7, 129.5, 128.5, 128.2, 127.5, 66.1, 45.5, 45.4, 33.4, 30.5, 22.7, 18.7 ppm.

The spectroscopic data are in accordance with those reported in literature.^[41]

General Procedure for the Perfluoroalkoxylation

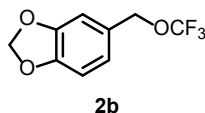
A solution of AgOR^F in MeCN (1.0 M, 0.750 mL, 0.750 mmol, 1.5 equiv) was added to a heat gun-dried Schlenk tube and cooled to –30 °C (dry ice/acetone). The halide (0.500 mmol, 1.0 equiv) was added to the solution and the mixture was stirred for 30 min at –30 °C. The solution was allowed to warm to rt over 1 h by removing the cooling bath. The suspension was filtered (rinsed with Et₂O), the filtrate was concentrated under reduced pressure, and the products **2a-6** were purified by flash column chromatography (SiO₂, *n*-pentane/Et₂O).

9-(trifluoromethoxy)-9*H*-fluorene **2a**



Product **4a** (61.0 mg, 0.240 mmol, 49%) was prepared according to the general procedure from 9-bromofluorene (127 mg, 0.500 mmol, 1.5 equiv) and obtained after flash column chromatography (SiO₂, *n*-pentane 100%) as a white solid.

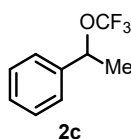
¹H NMR (400 MHz, CDCl₃): δ = 7.66 (d, *J* = 7.6 Hz, 2H), 7.62 (d, *J* = 7.5 Hz, 2H), 7.45 (t, *J* = 7.5 Hz, 2H), 7.35 (t, *J* = 7.5 Hz, 2H), 6.05 (s, 1H) ppm. **¹⁹F NMR** (376 MHz, CDCl₃): δ = –57.0 (s, 3F, OCF₃) ppm. **¹³C{¹H} NMR** (151 MHz, CDCl₃): δ = 140.9, 140.2, 130.3, 128.3, 126.0, 122.6 (q, *J* = 255 Hz), 120.3, 79.0 (q, *J* = 4 Hz) ppm. **IR (ATR):** $\tilde{\nu}$ = 3276, 2940, 1207, 1084 cm⁻¹. **HRMS (EI):** *m/z* calculated for [C₁₄H₉F₃O]⁺ ([M]⁺): 250.0600, measured: 250.0608.

5-((trifluoromethoxy)methyl)benzo[d][1,3]dioxole **2b**

Product **4b** (64.0 mg, 0.290 mmol, 58%) was prepared according to the general procedure from 5-(bromomethyl)benzo[d][1,3]dioxole **S2** (107 mg, 0.500 mmol, 1.0 equiv) and obtained after flash column chromatography (SiO₂, *n*-pentane 100%) as a colorless liquid.

¹H NMR (600 MHz, CDCl₃): δ = 6.87 – 6.79 (m, 4H), 5.99 (s, 2H), 4.88 (s, 2H) ppm. **¹⁹F NMR** (565 MHz, CDCl₃): δ = –60.0 (s, 3F, OCF₃) ppm. **¹³C{¹H} NMR** (151 MHz, CDCl₃): δ = 148.4, 148.2, 127.6, 122.5, 121.7 (q, *J* = 258 Hz), 109.0, 108.5, 101.5, 69.4 (q, *J* = 4 Hz) ppm.

The spectroscopic data are in accordance with those reported in literature.^[51]

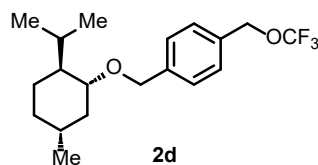
(1-(trifluoromethoxy)ethyl)benzene **2c**

Product **4c** (227 mg, 1.19 mmol, 44%) was prepared according to the general procedure from (1-bromoethyl)benzene **S1** (500 mg, 2.70 mmol, 1.0 equiv) and 0.6 M Ag[OCF₃] in MeCN (6.75 mL, 4.05 mmol, 1.5 equiv) and was obtained after flash column chromatography (SiO₂, *n*-pentane 100%) as a colorless liquid.

¹H NMR (400 MHz, Chloroform-*d*): δ = 7.41 – 7.31 (m, 5H), 5.30 (q, *J* = 6.6 Hz, 1H), 1.64 (d, *J* = 6.6, 3H) ppm. **¹⁹F NMR** (376 MHz, CDCl₃): δ = –57.9 (s, 3F, OCF₃) ppm. **¹³C{¹H} NMR** (176 MHz, CDCl₃): δ 140.8, 129.00, 128.8, 126.1, 122.0 (q, *J* = 255 Hz), 23.7 ppm.

The spectroscopic data are in accordance with those reported in literature.^[52]

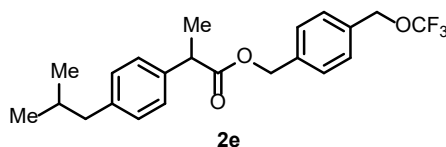
1-(((1*R*,2*S*,5*R*)-2-isopropyl-5-methylcyclohexyl)oxy)methyl)-4-(trifluoromethoxy)methyl)benzene **2d**



Product **4d** (120 mg, 0.348 mmol, 70%) was prepared according to the general procedure from 1-(bromomethyl)-4-(((1*R*,2*S*,5*R*)-2-isopropyl-5-methylcyclohexyl)oxy)methyl)benzene **S3** (170 mg, 0.500 mmol, 1.0 equiv) and 0.65 M Ag[OCF₃] in MeCN (1.15 mL, 0.750 mmol, 1.5 equiv) and was obtained after filtration and evaporation of the solvent under reduced pressure as yellowish oil.

¹H NMR (600 MHz, CDCl₃): δ = 7.38 (d, *J* = 8.2 Hz, 2H), 7.34 (d, *J* = 8.2 Hz, 2H), 4.97 (s, 2H), 4.67 (d, *J* = 11.7 Hz, 1H), 4.41 (d, *J* = 11.7 Hz, 1H), 3.18 (td, *J* = 10.6, 4.1 Hz, 1H), 2.29 (septd, *J* = 7.0, 3.0 Hz, 1H), 2.18 (m, 1H), 1.65 (m, 2H), 1.36 (m, 1H), 1.30 (ddt, *J* = 13.3, 10.3, 3.1 Hz, 1H), 0.99 – 0.86 (m, 9H), 0.72 (d, *J* = 6.9 Hz, 3H) ppm. **¹⁹F NMR** (565 MHz, CDCl₃): δ = –60.1 (s, 3F, OCF₃) ppm. **¹³C{¹H} NMR** (151 MHz, CDCl₃): δ = 140.5, 133.3, 128.5, 128.4, 122.01 (q, *J* = 255 Hz), 79.3, 70.3, 48.7, 40.6, 34.9, 31.9, 25.9, 23.6, 22.7, 21.4, 16.4 ppm. **IR (ATR)**: $\tilde{\nu}$ = 2956, 2923, 2869, 1455, 1265, 1214, 1143, 751 cm⁻¹. **HRMS (EI)**: *m/z* calculated for [C₁₉H₂₇F₃O₂]⁺ ([M]⁺): 344.1958, measured: 344.1976.

4-((trifluoromethoxy)methyl)benzyl 2-(4-isobutylphenyl)propanoate **2e**

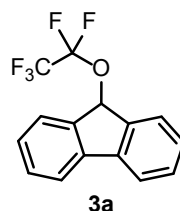


Product **4e** (116 mg, 0.294 mmol, 59%) was prepared according to the general procedure from 4-(bromomethyl)benzyl 2-(4-isobutylphenyl)propanoate **S4** (195 mg, 0.500 mmol, 1.0 equiv) and 0.65 M Ag[OCF₃] in MeCN (1.15 mL, 0.750 mmol, 1.5 equiv) and was obtained after filtration and evaporation of the solvent under reduced pressure as colorless oil.

¹H NMR (600 MHz, CDCl₃): δ = 7.30 (d, *J* = 8.2 Hz, 2H), 7.24 (d, *J* = 8.2 Hz, 2H), 7.19 (d, *J* = 8.1 Hz, 2H), 7.09 (d, *J* = 8.0 Hz, 2H), 5.11 (s, 2H), 4.96 (s, 2H), 3.75 (q, *J* = 7.2 Hz, 1H), 2.45 (d, *J* = 7.2 Hz, 2H), 1.85 (sept *J* = 6.8 Hz, 1H), 1.51 (d, *J* = 7.2 Hz, 3H), 0.91 (s, 3H), 0.90 (s, 3H) ppm. **¹⁹F NMR** (565 MHz, CDCl₃): δ = –60.2 (s, 3F, OCF₃) ppm. **¹³C{¹H} NMR** (151 MHz, CDCl₃): δ = 174.8, 141.0, 137.8, 137.3, 133.9, 129.7, 128.4, 128.3, 127.5, 122.0 (q, *J* = 256 Hz) 69.0, 66.1, 45.5, 45.4, 30.5, 22.7, 18.7 ppm. **IR (ATR)**: $\tilde{\nu}$ = 2956, 2933, 2869, 1734, 1513,

1464, 1262, 1202, 1147, 908, 731 cm^{-1} . **HRMS (EI)**: m/z calculated for $[\text{C}_{22}\text{H}_{25}\text{F}_3\text{O}_3]^+$ ($[\text{M}]^+$): 394.1750, measured: 395.1803.

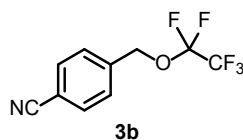
9-(perfluoroethoxy)-9H-fluorene **3a**



Product **5a** (122 mg, 0.41 mmol, 82%) was prepared according to the general procedure from 9-bromofluorene (127 mg, 0.500 mmol, 1.5 equiv) and obtained after flash column chromatography (SiO_2 , *n*-pentane 100%) as a white solid.

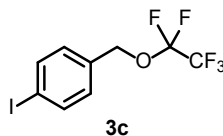
^1H NMR (400 MHz, CDCl_3): δ = 7.67 (d, J = 7.5 Hz, 2H), 7.58 (d, J = 7.5 Hz, 2H), 7.45 (t, J = 7.6 Hz, 2H), 7.35 (td, J = 7.5, 1.1 Hz, 2H), 6.21 (s, 1H) ppm. **^{19}F NMR** (376 MHz, CDCl_3): δ = -85.1 (s, 2F, OCF_2), -85.6 (s, 3F, CF_3) ppm. **$^{13}\text{C}\{^1\text{H}\}$ NMR** (151 MHz, CDCl_3) δ = 141.0, 140.3, 130.3, 128.3, 126.1, 120.3, 116.9 (qt, J = 285, 45 Hz), 116.1 (tq, J = 272, 42 Hz), 77.5 (t, J = 5 Hz) ppm. **IR (ATR)**: $\tilde{\nu}$ = 3278, 2921, 1204, 1087 cm^{-1} . **HRMS (EI)**: m/z calculated for $[\text{C}_{15}\text{H}_9\text{F}_5\text{O}]^+$ ($[\text{M}]^+$): 300.0568, measured: 300.0585.

4-((perfluoroethoxy)methyl)benzonitrile **3b**



Product **5b** (77 mg, 0.31 mmol, 61%) was prepared according to the general procedure from 4-(bromomethyl)benzonitrile (99.0 mg, 0.500 mmol, 1.0 equiv) and obtained after flash column chromatography (SiO_2 , *n*-pentane/ Et_2O , 10:1) as a yellowish liquid.

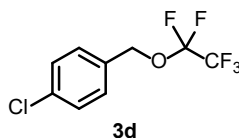
^1H NMR (700 MHz, CDCl_3): δ = 7.71 – 7.69 (m, 2H), 7.48 – 7.47 (m, 2H), 5.10 (s, 2H) ppm. **^{19}F NMR** (565 MHz, CDCl_3): δ = -85.8 (s, 3F, CF_3), -90.4 (s, 2F, OCF_2) ppm. **$^{13}\text{C}\{^1\text{H}\}$ NMR** (176 MHz, CDCl_3): δ = 139.4, 132.9, 128.3, 118.6, 113.2, 66.1 (t, J = 6 Hz), 116.9 (qt, J = 285, 45 Hz), 115.6 (tq, J = 272, 42 Hz) ppm. **IR (ATR)**: $\tilde{\nu}$ = 2967, 1741, 1365, 1216 cm^{-1} . **HRMS (APCI)**: m/z calculated for $[\text{C}_{10}\text{H}_7\text{F}_5\text{NO}]^+$ ($[\text{M}+\text{H}]^+$): 252.0442, measured: 252.0426.

1-iodo-4-((perfluoroethoxy)methyl)benzene **3c**

Product **5c** (77.0 mg, 0.220 mmol, 44%) was prepared according to the general procedure from 1-(bromomethyl)-4-iodobenzene (150 mg, 0.500 mmol, 1.0 equiv) and obtained after flash column chromatography (Si₂O, *n*-pentane 100%) as a colorless liquid.

¹H NMR (600 MHz, CDCl₃): δ = 7.75 – 7.73 (m, 2H), 7.11 (d, *J* = 8.4 Hz, 2H), 4.98 (s, 2H) ppm. **¹⁹F NMR** (376 MHz, CDCl₃) δ = –85.8 (s, 3F, CF₃), –90.1 (s, 2F, OCF₂) ppm. **¹³C{¹H} NMR** (176 MHz, CDCl₃): δ = 138.3, 133.9, 130.1, 117.0 (qt, *J* = 285, 45 Hz), 115.6 (tq, *J* = 271, 42 Hz), 95.1, 66.7 (t, *J* = 6 Hz) ppm.

The spectroscopic data are in accordance with those reported in literature.^[53]

1-chloro-4-((perfluoroethoxy)methyl)benzene **3d**

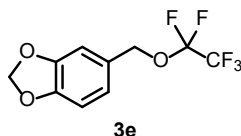
Product **5d** (101 mg, 0.390 mmol, 77%) was prepared according to the general procedure from 1-(bromomethyl)-4-chlorobenzene (104 mg, 0.500 mmol, 1.0 equiv) and obtained after flash column chromatography (SiO₂, *n*-pentane 100%) as a colorless liquid.

Gram-scale

Product **5d** (1.22 g, 4.68 mmol, 80%) was prepared according to the general procedure from 1-(bromomethyl)-4-chlorobenzene (1.20 g, 5.84 mmol, 1.0 equiv) using 1 M Ag[OC₂F₅] in MeCN (8.76 mL, 8.76 mmol, 1.5 equiv) and obtained after flash column chromatography (SiO₂, *n*-pentane 100%) as a colorless liquid.

¹H NMR (700 MHz, CDCl₃): δ = 7.39 – 7.37 (m, 2H), 7.31 – 7.29 (m, 2H), 5.01 (s, 2H) ppm. **¹⁹F NMR** (565 MHz, CDCl₃): δ = –85.8 (s, 3F, CF₃), –90.1 (s, 2F, OCF₂) ppm. **¹³C{¹H} NMR** (176 MHz, CDCl₃): δ = 135.3, 132.7, 129.7, 129.4, 117.0 (qt, *J* = 285, 45 Hz), 115.6 (tq, *J* = 271, 42 Hz), 66.6 (t, *J* = 6 Hz) ppm. **IR (ATR):** $\tilde{\nu}$ = 2916, 2850, 1733, 1715, 1464, 1219, 769 cm⁻¹. **HRMS (EI):** *m/z* calculated for [C₉H₆ClF₅O]⁺ ([M]⁺): 260.0022, measured: 260.0054.

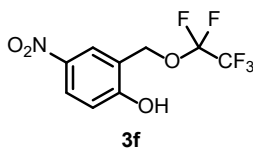
5-((perfluoroethoxy)methyl)benzo[d][1,3]dioxole **3e**



Product **5e** (75 mg, 0.28 mmol, 55%) was prepared according to the general procedure from 5-(bromomethyl)benzo[d][1,3]dioxole **S2** (107 mg, 0.500 mmol, 1.0 equiv) and obtained after flash column chromatography (SiO₂, *n*-pentane 100%) as a colorless liquid.

¹H NMR (700 MHz, CDCl₃): δ = 6.86 – 6.83 (m, 2H), 6.81 (dd, *J* = 7.8, 0.5 Hz, 1H), 5.99 (s, 1H), 4.94 (s, 1H) ppm. **¹⁹F NMR** (376 MHz, CDCl₃): δ = –85.8 (s, 3F, CF₃), –89.8 (s, 2F, OCF₂) ppm. **¹³C{¹H} NMR** (176 MHz, CDCl₃): δ = 148.6, 148.4, 127.9, 122.8, 117.1 (qt, *J* = 284, 45 Hz), 115.5 (tq, *J* = 271, 42 Hz), 109.2, 108.7, 101.7, 67.6 (t, *J* = 6 Hz) ppm. **IR (ATR):** $\tilde{\nu}$ = 2908, 1494, 1192, 1090, 1040, 935 cm⁻¹. **HRMS (EI):** *m/z* calculated for [C₁₀H₇F₅O₃]⁺ ([M]⁺): 270.0310, measured: 270.0290.

4-nitro-2-((perfluoroethoxy)methyl)phenol **3f**

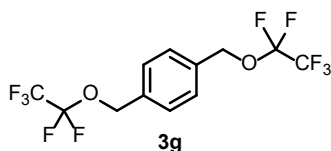


Product **5f** (81 mg, 0.28 mmol, 57%) was prepared according to the general procedure from 2-(bromomethyl)-4-nitrophenol (115 mg, 0.500 mmol, 1.0 equiv) and obtained after two flash column chromatographies (SiO₂, *n*-pentane/Et₂O, 4:1) as a yellowish solid.

¹H NMR (700 MHz, CDCl₃): δ = 8.30 (s, 1H), 8.21 (d, *J* = 8.9 Hz, 1H), 6.98 (d, *J* = 8.8 Hz, 1H), 6.62 (s, 1H), 5.19 (s, 2H) ppm. **¹⁹F NMR** (376 MHz, CDCl₃): δ = –85.7 (s, 3F, CF₃), –90.8 (s, 2F, OCF₂) ppm. **¹³C{¹H} NMR** (176 MHz, CDCl₃): δ = 159.6, 141.9, 126.7, 126.1, 122.3, 117.0

(qt, $J = 285, 45$ Hz), 116.2, 115.6 (tq, $J = 272, 42$ Hz), 62.0 (t, $J = 6$ Hz) ppm. **HRMS (EI)**: m/z calculated for $[C_{12}H_8F_{10}O_2]^+$ ($[M]^+$): 287.0212, measured: 287.0220.

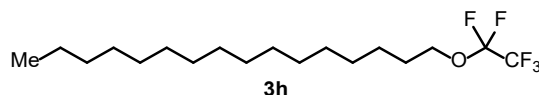
1,4-bis((perfluoroethoxy)methyl)benzene **3g**



Product **5g** (58.0 mg, 0.160 mmol, 32%) was prepared according to the general procedure from 1,4-bis(bromomethyl)benzene (130 mg, 0.500 mmol, 1.0 equiv) using 1.0 M $Ag[OC_2F_5]$ (1.25 mL, 1.25 mmol, 2.5 equiv) and obtained after flash chromatography (SiO_2 , n -pentane 100%) as colorless liquids.

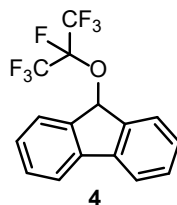
1H NMR (600 MHz, $CDCl_3$): $\delta = 7.40$ (s, 4H), 5.06 (s, 4H) ppm. **^{19}F NMR** (376 MHz, $CDCl_3$): $\delta = -85.8$ (s, 3F, CF_3), -90.1 (s, 2F, OCF_2) ppm. **$^{13}C\{^1H\}$ NMR** (176 MHz, $CDCl_3$): $\delta = 135.1$, 128.7, 117.1 (qt, $J = 284, 45$ Hz), 115.7 (tq, $J = 271, 42$ Hz), 66.9 (t, $J = 6$ Hz) ppm. **IR (ATR)**: $\tilde{\nu} = 2915, 1194, 1090$ cm^{-1} . **HRMS (EI)**: m/z calculated for $[C_{12}H_8F_{10}O_2]^+$ ($[M]^+$): 374.0359, measured: 374.0364.

1-(perfluoroethoxy)hexadecane **3h**



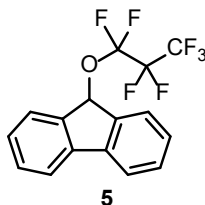
Product **5h** (42 mg, 0.12 mmol, 24%, 41% brsm) was prepared according to the general procedure from 1-iodohexadecane (175 mg, 0.500 mmol, 1.0 equiv) and obtained after two flash column chromatographies (SiO_2 , n -pentane 100%) as a colorless liquid.

1H NMR (600 MHz, $CDCl_3$): $\delta = 4.00$ (t, $J = 6.6$ Hz, 2H), 1.71 – 1.67 (m, 2H), 1.40 – 1.35 (m, 2H), 1.32 – 1.26 (m, 23H), 0.87 (t, $J = 7.0$ Hz, 3H) ppm. **^{19}F NMR** (376 MHz, $CDCl_3$): $\delta = -86.0$ (s, 3F, CF_3), -90.5 (s, 2F, OCF_2) ppm. **$^{13}C\{^1H\}$ NMR** (176 MHz, $CDCl_3$): $\delta = 117$ (qt, $J = 285, 46$ Hz), 115.6 (tq, $J = 269, 42$ Hz), 65.9 (t, $J = 5$ Hz), 32.3, 30.1, 30.1, 30.0, 30.0, 30.0, 29.9, 29.8, 29.7, 29.4, 29.2, 25.8, 23.1, 14.5 ppm. **IR (ATR)**: $\tilde{\nu} = 2927, 1218, 903, 723$ cm^{-1} . **HRMS (EI)**: m/z calculated for $[C_{16}H_{29}F_5O]^+$ ($[M]^+$): 360.2446, measured: 360.2488.

9-((perfluoropropan-2-yl)oxy)-9H-fluorene **4**

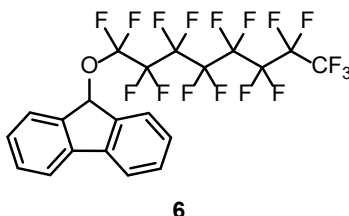
Product **6** (108 mg, 0.310 mmol, 62%) was prepared according to the general procedure from 9-bromofluorene (127 mg, 0.500 mmol, 1.0 equiv) and obtained after flash column chromatography (SiO₂, *n*-pentane 100%) as a white solid.

¹H NMR (400 MHz, CDCl₃): δ = 7.66 (d, *J* = 7.6 Hz, 2H), 7.59 (d, *J* = 7.5 Hz, 2H), 7.45 (t, *J* = 7.5 Hz, 2H), 7.35 (td, *J* = 7.5, 1.2 Hz, 2H), 6.19 (s, 1H) ppm. **¹⁹F NMR** (376 MHz, CDCl₃): δ = -79.3 (d, *J* = 3 Hz, 6F, CF₃), -137.1 (m, 1F, OCF) ppm. **¹³C{¹H} NMR** (151 MHz, CDCl₃): δ = 140.8, 140.7, 130.2, 128.3, 125.9, 120.3, 119.2 (qd, *J* = 289 Hz), 102.8 (dsept, *J* = 251 Hz), 79.4 (d, *J* = 6 Hz) ppm. **IR (ATR)**: $\tilde{\nu}$ = 3278, 2942, 1209, 1085 cm⁻¹. **HRMS (EI)**: *m/z* calculated for [C₁₆H₉F₇O]⁺ ([M]⁺): 350.0536, measured: 350.0538.

9-(perfluoroproxy)-9H-fluorene **5**

Product **7** (84.0 mg, 0.240 mmol, 48%) was prepared according to the general procedure from 9-bromofluorene (127 mg, 0.500 mmol, 1.0 equiv) and obtained after flash column chromatography (SiO₂, *n*-pentane 100%) as a white solid.

¹H NMR (400 MHz, CDCl₃): δ = 7.67 (d, *J* = 7.5 Hz, 2H), 7.56 (d, *J* = 7.5 Hz, 2H), 7.45 (t, *J* = 7.5 Hz, 2H), 7.35 (t, *J* = 7.5 Hz, 2H), 6.24 (s, 1H) ppm. **¹⁹F NMR** (376 MHz, CDCl₃): δ = -80.9 (sext, *J* = 7 Hz, 2F, OCF₂), -81.0 (t, *J* = 7 Hz, 3F, CF₃), -129.0 (t, *J* = 4 Hz, 2F, CF₂) ppm. **¹³C{¹H} NMR** (151 MHz, CDCl₃): δ = 141.0, 140.2, 130.3, 128.3, 126.0, 120.3, 117.7 (qt, *J* = 287, 33 Hz), 117.4 (tt, *J* = 274, 30 Hz), 77.7 (t, *J* = 5 Hz) ppm. **IR (ATR)**: $\tilde{\nu}$ = 3279, 2944, 1206, 1086 cm⁻¹. **HRMS (EI)**: *m/z* calculated for [C₁₆H₉F₇O]⁺ ([M]⁺): 350.0536, measured: 350.0555.

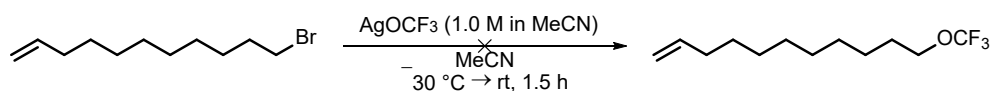
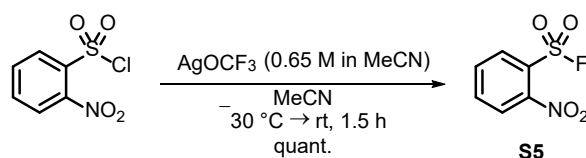
9-((perfluorooctyl)oxy)-9H-fluorene **6**

Product **8** (217 mg, 0.360 mmol, 72%) was prepared according to the general procedure from 9-bromofluorene (127 mg, 0.500 mmol, 1.0 equiv) and obtained after flash column chromatography (SiO₂, *n*-pentane 100%) as a white solid.

¹H NMR (400 MHz, CDCl₃): δ = 7.67 (d, *J* = 7.4 Hz, 2H), 7.57 (d, *J* = 7.6 Hz, 2H), 7.45 (t, *J* = 7.0 Hz, 2H), 7.35 (td, *J* = 7.5, 1.1 Hz, 2H), 6.25 (s, 1H) ppm. **¹⁹F NMR** (565 MHz, CDCl₃): δ = -79.4 (s, 2F, OCF₂), -80.7 (t, *J* = 10 Hz, 3F, CF₃), -121.6 – -122.0 (m, 6F, CF₂), -122.7 – -122.8 (m, 2F, CF₂), -124.6 – -124.7 (m, 2F, CF₂), -126.1 – -126.2 (m, 2F, CF₂) ppm. **¹³C{¹H} NMR** (151 MHz, CDCl₃): δ = 141.0, 140.2, 130.3, 128.3, 126.1, 120.3, 120.0 – 106.9 (m, C₈F₁₇), 77.8 (t, *J* = 5 Hz) ppm. **IR (ATR)**: $\tilde{\nu}$ = 3279, 2956, 1196, 1091 cm⁻¹. **HRMS (EI)**: *m/z* calculated for [C₂₁H₉F₁₇O]⁺ ([M]⁺): 600.0376, measured: 600.0334.

Limitation of the scope

1-Bromo-10-undecen

2-nitrobenzenesulfonyl fluoride **S5**

Instead of the desired trifluoromethoxylation, the corresponding sulfonyl fluoride **S5** was obtained.

¹H NMR (600 MHz, CDCl₃): δ = 8.25 (d, J = 7.9 Hz, 1H), 8.05 (d, J = 8.0 Hz, 1H), 7.98 – 7.94 (m, 1H), 7.89 (tt, J = 7.6, 1.0 Hz, 1H) ppm. **¹⁹F NMR** (565 MHz, CDCl₃): δ = 65.2 (s, 1F, SF) ppm. **¹³C{¹H} NMR** (151 MHz, CDCl₃): δ = 136.9, 133.6, 132.2, 126.2 ppm.

The spectroscopic data are in accordance with those reported in literature.^[54]

X-Ray Crystallography

Crystallographic Data

Table S 1: Crystal data and refinement details for the analysis of the molecular structures in the solid state of [Au(OPPh₃)(OTeF₅)₃], [NEt₃Me][Au(OTeF₅)₄] and [NMe₄][AuCl₃(OTeF₅)].

	[Ag(MeCN) ₂ (OCF ₃) _n]	[Ag(bpy) ₂][OCF ₃]	[Ag(EtCN) ₂ (OC ₂ F ₅) ₂]
Empirical formula	C ₅ H ₆ AgF ₃ N ₂ O	C ₄₈ H ₃₈ Ag ₂ F ₆ N ₁₁ O ₂	C ₁₆ H ₂₀ Ag ₂ F ₁₀ N ₄ O ₂
Formula weight	274.99	1130.636	706.10
Temperature/K	100.00	125.00	100.00
Crystal system	monoclinic	monoclinic	monoclinic
Space group	<i>P</i> 2 ₁ / <i>c</i>	<i>C</i> 2	<i>C</i> 2/ <i>c</i>
<i>a</i> /Å	7.5588(4)	32.8096(11)	18.2518(12)
<i>b</i> /Å	15.2738(7)	7.3577(2)	10.0889(7)
<i>c</i> /Å	7.5868(4)	25.2359(14)	15.2086(17)
<i>α</i> /°	90	90	90
<i>β</i> /°	91.354(2)	130.459(1)	120.039(2)
<i>γ</i> /°	90	90	90
Volume/Å ³	875.66(8)	4635.2(3)	2424.4(4)
<i>Z</i>	4	4	4
$\rho_{\text{calc}}/\text{cm}^3$	2.086	1.620	1.935
μ/mm^{-1}	2.306	0.922	1.712
<i>F</i> (000)	528.0	2262.6	1376.0
Crystal size/mm ³	0.49 × 0.441 × 0.405	0.506 × 0.113 × 0.099	0.626 × 0.562 × 0.431
Radiation	MoK α (λ = 0.71073)	MoK α (λ = 0.71073)	MoK α (λ = 0.71073)
2 θ range for data collection/°	5.39 to 61.046	4.92 to 58.28	4.79 to 56.574
Index ranges	-10 ≤ <i>h</i> ≤ 10, -21 ≤ <i>k</i> ≤ 21, -10 ≤ <i>l</i> ≤ 10	-44 ≤ <i>h</i> ≤ 44, -10 ≤ <i>k</i> ≤ 10, -34 ≤ <i>l</i> ≤ 34	-24 ≤ <i>h</i> ≤ 24, -13 ≤ <i>k</i> ≤ 12, -20 ≤ <i>l</i> ≤ 20
Reflections collected	52271	51778	36086
Independent reflections	2681 [R _{int} = 0.0274, R _{sigma} = 0.0113]	12372 [R _{int} = 0.0334, R _{sigma} = 0.0306]	3015 [R _{int} = 0.0337, R _{sigma} = 0.0155]
Data/restraints/parameters	2681/76/168	12372/1/659	3015/0/156
Goodness-of-fit on <i>F</i> ²	1.185	1.095	1.084
Final <i>R</i> indexes [<i>I</i> > 2 σ (<i>I</i>)]	<i>R</i> ₁ = 0.0190, <i>wR</i> ₂ = 0.0441	<i>R</i> ₁ = 0.0332, <i>wR</i> ₂ = 0.0729	<i>R</i> ₁ = 0.0199, <i>wR</i> ₂ = 0.0454
Final <i>R</i> indexes [all data]	<i>R</i> ₁ = 0.0202, <i>wR</i> ₂ = 0.0445	<i>R</i> ₁ = 0.0492, <i>wR</i> ₂ = 0.0858	<i>R</i> ₁ = 0.0227, <i>wR</i> ₂ = 0.0464
Largest diff. peak/hole / e Å ⁻³	0.32/-0.84	0.56/-1.12	0.43/-0.59
Flack parameter		0.021(7)	
CCDC deposition number	2326777	2326778	2326776

	[Ag(EtCN) ₂ (O ⁻ C ₃ F ₇) ₂]	[Cu(MeCN) ₄][OCF ₃]	[Cu(MeCN) ₄][OC ₂ F ₅]
Empirical formula	C ₁₂ H ₁₅ AgF ₇ N ₃ O	C ₉ H ₁₂ CuF ₃ N ₄ O	C ₂₈ H ₃₆ Cu ₂ F ₁₀ N ₁₂ O ₂
Formula weight	458.14	312.77	889.77
Temperature/K	100.00	100.00	100.00
Crystal system	triclinic	orthorhombic	monoclinic
Space group	<i>P</i> -1	<i>Pna</i> 2 ₁	<i>Cc</i>
<i>a</i> /Å	8.8040(14)	23.6318(14)	17.4471(10)
<i>b</i> /Å	9.0244(9)	8.2908(4)	17.5147(9)
<i>c</i> /Å	11.8303(18)	20.2482(12)	15.8138(9)
<i>α</i> /°	72.493(5)	90	90
<i>β</i> /°	79.437(5)	90	123.482(2)
<i>γ</i> /°	73.868(4)	90	90
Volume/Å ³	856.0(2)	3967.2(4)	4030.5(4)
<i>Z</i>	2	12	4
$\rho_{\text{calc}}/\text{cm}^3$	1.778	1.571	1.466
μ/mm^{-1}	1.252	1.681	1.143
<i>F</i> (000)	452.0	1896.0	1808.0
Crystal size/mm ³	0.919 × 0.559 × 0.391	0.41 × 0.395 × 0.178	0.393 × 0.248 × 0.23
Radiation	MoK α (λ = 0.71073)	MoK α (λ = 0.71073)	MoK α (λ = 0.71073)
2 θ range for data collection/°	4.846 to 61.13	3.992 to 56.592	4.652 to 58.276
Index ranges	-12 ≤ <i>h</i> ≤ 12, -11 ≤ <i>k</i> ≤ 12, -16 ≤ <i>l</i> ≤ 16	-30 ≤ <i>h</i> ≤ 31, -11 ≤ <i>k</i> ≤ 11, -27 ≤ <i>l</i> ≤ 26	-23 ≤ <i>h</i> ≤ 23, -23 ≤ <i>k</i> ≤ 23, -21 ≤ <i>l</i> ≤ 21
Reflections collected	38967	65336	82766
Independent reflections	5226 [<i>R</i> _{int} = 0.0264, <i>R</i> _{sigma} = 0.0172]	9732 [<i>R</i> _{int} = 0.0408, <i>R</i> _{sigma} = 0.0295]	10799 [<i>R</i> _{int} = 0.0343, <i>R</i> _{sigma} = 0.0268]
Data/restraints/parameters	5226/4/249	9732/12/520	10799/2/500
Goodness-of-fit on <i>F</i> ²	1.104	1.145	1.045
Final <i>R</i> indexes [<i>I</i> > 2 σ (<i>I</i>)]	<i>R</i> ₁ = 0.0183, <i>wR</i> ₂ = 0.0426	<i>R</i> ₁ = 0.0329, <i>wR</i> ₂ = 0.0712	<i>R</i> ₁ = 0.0238, <i>wR</i> ₂ = 0.0523
Final <i>R</i> indexes [all data]	<i>R</i> ₁ = 0.0198, <i>wR</i> ₂ = 0.0432	<i>R</i> ₁ = 0.0374, <i>wR</i> ₂ = 0.0726	<i>R</i> ₁ = 0.0288, <i>wR</i> ₂ = 0.0541
Largest diff. peak/hole / e Å ⁻³	0.54/-0.67	0.36/-0.56	0.21/-0.24
Flack parameter		0.409(15)	
CCDC deposition number	2326775	2326772	2326773

	[Cu ^I (MeCN) ₄] ₂ [Cu ^{II} {OC(CF ₃) ₂ -O-C(CF ₃) ₂ O} ₂]
Empirical formula	C ₃₆ H ₄₀ Cu ₃ F ₂₄ N ₈ O ₆
Formula weight	1327.38
Temperature/K	100.00
Crystal system	Monoclinic
Space group	C2/c
a/Å	26.1022(12)
b/Å	14.6566(6)
c/Å	15.6084(6)
α/°	90
β/°	119.3010(10)
γ/°	90
Volume/Å ³	5207.3(4)
Z	4
ρ _{calc} /cm ³	1.693
μ/mm ⁻¹	1.349
F(000)	2652.0
Crystal size/mm ³	0.299 × 0.253 × 0.23
Radiation	MoKα (λ = 0.71073)
2θ range for data collection/°	5.012 to 50.738
Index ranges	-31 ≤ h ≤ 31, -17 ≤ k ≤ 17, -18 ≤ l ≤ 18
Reflections collected	60852
Independent reflections	4772 [R _{int} = 0.0396, R _{sigma} = 0.0168]
Data/restraints/parameters	4772/0/353
Goodness-of-fit on F ²	1.054
Final R indexes [I >= 2σ (I)]	R ₁ = 0.0344, wR ₂ = 0.0899
Final R indexes [all data]	R ₁ = 0.0372, wR ₂ = 0.0918
Largest diff. peak/hole / e Å ⁻³	0.81/-0.34
Flack parameter	
CCDC deposition number	2326774

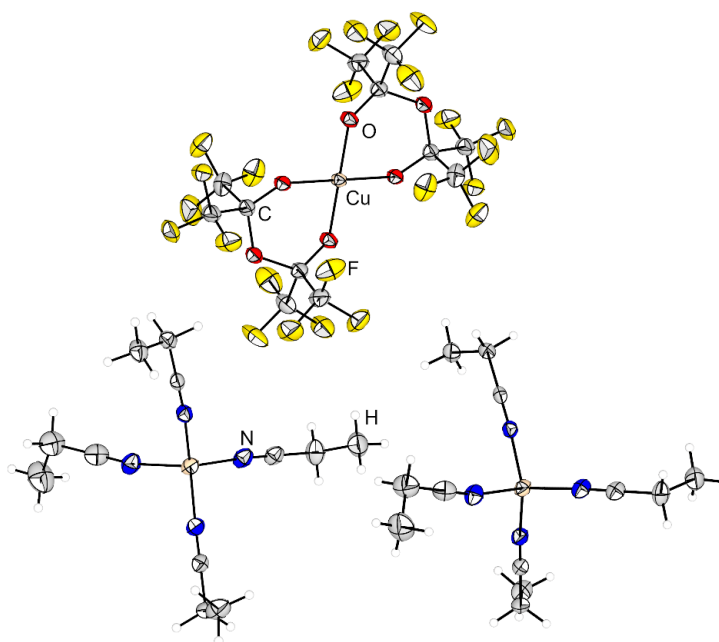


Figure S 1. Molecular structure of $[\text{Cu}^{\text{I}}(\text{MeCN})_4]_2[\text{Cu}^{\text{II}}\{\text{OC}(\text{CF}_3)_2\text{-O-C}(\text{CF}_3)_2\text{O}\}_2]$ in the solid state. Thermal ellipsoids are set at 50 % probability.

Quantum Chemical Calculations - Optimized Minimum Structures

xyz-Coordinates [Å] of CF₂O on PW6B95-D3BJ/def2-QZVPP Level

O	-0.00000019179894	-0.00000015108077	1.25979562663391
C	0.00000006924917	0.00000037908065	0.09476748891065
F	1.05560652189863	-0.00000011399994	-0.67721670842533
F	-1.05560639934885	-0.00000011399994	-0.67721640711923

xyz-Coordinates [Å] of [CF₃O]⁻ on PW6B95-D3BJ/def2-QZVPP Level

O	0.00088964221438	-0.00000058615103	-1.35703492046306
C	0.00037154525382	-0.00000008490690	-0.14712814806285
F	-0.63335836481404	1.09461657703949	0.50188794510718
F	-0.63335906812348	-1.09461653492732	0.50188689969993
F	1.26545624546932	0.00000062894575	0.50038822371879

xyz-Coordinates [Å] of CF₃CF(O) on PW6B95-D3BJ/def2-QZVPP Level

O	1.39989919396921	-0.99037829563030	-0.78232810903681
C	0.88691628989574	-0.17097538743992	-0.12634194585253
C	-0.62581238248575	0.05670362891498	0.03620106673778
F	-0.94487719083294	1.28096827374868	-0.36682503476334
F	-1.29873857846219	-0.81885437963619	-0.68070159328740
F	-0.96440880734428	-0.07247964170093	1.31475055561540
F	1.54702247526021	0.71501580174368	0.60524606058690

xyz-Coordinates [Å] of [C₂F₅O]⁻ on PW6B95-D3BJ/def2-QZVPP Level

O	-1.34635686573683	-1.20427205260787	-0.00000715064916
C	-0.82002553062300	-0.10583218312550	-0.00000068297839
C	0.73308396263707	-0.05309921210902	0.00000036913975
F	1.25435435118986	1.18500628137729	-0.00000629665203
F	1.23805535946094	-0.67841411737272	-1.07602520558410
F	1.23805695704424	-0.67840371219866	1.07603170598172
F	-1.14858435985885	0.76750103403028	1.10936641385485
F	-1.14858487411344	0.76750896200620	-1.10935915311263

xyz-Coordinates [Å] of CF₃CF₂CF(O) on PW6B95-D3BJ/def2-QZVPP Level

O	1.98806204908839	1.24793731323279	-0.57435481307076
C	1.40711253924214	0.39228030106909	-0.03156853752339
C	0.11807851375965	-0.28177819305016	-0.53146323991299
C	-1.09767830847025	-0.01418830837611	0.39031810835232
F	-1.15997503521236	1.28582441600799	0.66146008339213
F	-0.97643892539118	-0.68462074459938	1.52328195886975
F	-2.21388000474180	-0.38503433315622	-0.21026311501192
F	-0.16219477360674	0.19037090882340	-1.74301850926050
F	0.31139528278892	-1.60626665797666	-0.60583207023136
F	1.78551766254323	-0.14452670197475	1.12143613439672

xyz-Coordinates [Å] of [n-C₃F₇O]⁻ on PW6B95-D3BJ/def2-QZVPP Level

O	-1.41840126090305	-0.80920440401214	-1.26863309705099
C	-1.32850798607188	-0.07985228582619	-0.29625206453377
F	-2.32492841514490	-0.25749110369867	0.73636255303259
F	-1.46972067760380	1.33833803198249	-0.54324856030439
C	-0.01049803273616	-0.14294869080144	0.53223846512610
F	0.12202990101568	-1.37102958875307	1.08704623642252
F	0.03077969165021	0.75426262694407	1.54526067416043
C	1.28058238779578	0.08734121246852	-0.27802852333588
F	1.32508554837433	1.30108981429652	-0.81813521284201
F	2.34444070725850	-0.01389877733368	0.54370125010202
F	1.44913813636530	-0.80660883526643	-1.24031272077662

xyz-Coordinates [Å] of CF₃C(O)CF₃ on PW6B95-D3BJ/def2-QZVPP Level

O	0.36559238819335	-0.62219085239798	-1.71786874224463
C	0.13590626278961	-0.22375301251027	-0.62884181050801
C	1.26013497350697	0.03969890373664	0.40263073260496
F	1.47682689158805	1.34963825745930	0.49449955820667
F	2.37703213444383	-0.54897731047735	0.02535173645581
F	0.91212631253494	-0.41938244953621	1.60167284264062

C	-1.31200006480649	0.05390762062463	-0.15412951826076
F	-1.78719246776821	-1.03408638313685	0.44729881347099
F	-2.08278789849564	0.34490011979395	-1.18307092236673
F	-1.34563753198642	1.06024510644414	0.71245931000107

xyz-Coordinates [Å] of $[i\text{-C}_3\text{F}_7\text{O}]^-$ on PW6B95-D3BJ/def2-QZVPP Level

O	1.80977578228355	0.09713605398406	0.00000184006600
C	0.58834935875661	0.30766645666847	0.00000040146113
C	-0.15599198217792	-0.15055444281869	1.29592243244706
F	-1.47661773058393	0.10368646428024	1.32745843550995
F	0.37655497164951	0.44288152004541	2.36621263953793
F	-0.02939721067631	-1.47727796365360	1.48462391724316
C	-0.15598986087490	-0.15055719530956	-1.29592227720119
F	0.37654307955103	0.44289251725071	-2.36621174601702
F	-1.47661994837479	0.10366219276462	-1.32745337362833
F	-0.02937559398822	-1.47727717465395	-1.48463073078250
F	0.17276713443537	1.75774257144230	-0.00000153863619

xyz-Coordinates [Å] of $\text{C}_7\text{F}_{15}\text{CF}(\text{O})$ on PW6B95-D3BJ/def2-QZVPP Level

C	-3.79695709214773	0.53764673267526	0.00382615792976
C	-2.57081307665924	0.27088601036548	-0.90738358749279
C	-1.34573774286424	-0.27259990528748	-0.12500174183903
C	-0.03540787125617	-0.17773969447819	-0.94833916452813
C	1.17222611081642	-1.04086963872810	-0.47692931928215
C	1.78178626421626	-0.84576347117631	0.93729515149368
C	2.48162782674701	0.50677223542706	1.25829628156250
C	3.61840030307247	0.88545157161442	0.28736352105797
O	4.69941415516769	0.44332705447804	0.33105848286013
F	3.22475337837113	1.78956867228130	-0.59487247254179
F	3.03172346006943	0.35122921554058	2.46726081672668
F	1.56625478252817	1.47567912135700	1.33097354672997
F	0.83652305216826	-1.03950157758313	1.86011121458888
F	2.70948376664214	-1.80046946535783	1.06453274010467

F	2.16215975483337	-0.78618336702434	-1.35317050313283
F	0.83335816882030	-2.32538595404084	-0.58363841647016
F	0.35915139755186	1.09510831974361	-0.99682092840626
F	-0.30197372325026	-0.59413981079389	-2.19419515669433
F	-1.57749048268834	-1.54855592717312	0.19245854406877
F	-1.20714171391232	0.44364422673253	0.99611695806394
F	-2.23710095281330	1.41965079422656	-1.50582752785931
F	-2.92920330320770	-0.62308346430512	-1.83002436991204
F	-3.59252822004166	1.60206185659866	0.76084692689700
F	-4.01962852961913	-0.51595914330019	0.77753968334048
F	-4.86288071254441	0.74922760820805	-0.75147683726560

xyz-Coordinates [Å] of $[n\text{-C}_8\text{F}_{16}\text{O}]^-$ on PW6B95-D3BJ/def2-QZVPP Level

O	3.75131581334966	2.35212864221478	0.62369447928200
C	3.31417532164299	1.51747601747661	-0.14437720968517
F	2.60716461268058	2.01326183337580	-1.30096749333797
F	4.27965790494835	0.65968560989264	-0.78480003708858
C	2.27598469792693	0.50445660709796	0.46361864795109
F	1.14185213136577	1.18795953698058	0.75147376164367
F	2.75200223531420	0.00675359006849	1.62660093226812
C	1.86584598414330	-0.73052634428794	-0.36928328904978
F	1.53223391954958	-0.37809502106467	-1.61728231590312
F	2.89762339943683	-1.57682015286695	-0.43993231749832
C	0.65972158252752	-1.56671327327076	0.23307598379905
F	1.03714439244763	-2.85693079530292	0.27609783010941
F	0.37071140295245	-1.19971527464574	1.48758531715219
C	-0.68499716470806	-1.61315545867950	-0.55709647841766
F	-1.45094512570364	-2.52899417762919	0.06803223773744
F	-0.43857855060730	-2.07757433249383	-1.78862299166181
C	-1.58109828353857	-0.34666135862512	-0.73925206927767
F	-0.89252008657915	0.62802347226108	-1.32262151455841
F	-2.56102485488046	-0.73599738177265	-1.58274853762376
C	-2.28971633643183	0.24320671477140	0.51086165597125

F	-2.97621166045078	-0.70857015245455	1.15987727007297
F	-1.39519462857635	0.77605366011060	1.33432275210140
C	-3.31859802599854	1.35905131760149	0.16901631686042
F	-3.77225403235676	1.86330314055886	1.31221681516809
F	-2.76880794182892	2.33358187374347	-0.53243705376814
F	-4.35548770662541	0.87481170694005	-0.50320069224670

Calorimetric Measurements

Setup



Solvation Enthalpy of CO₂ in Acetonitrile

A 100 mL reactor vessel was charged with 40 mL of MeCN and equipped with a calibration heater and a thermal sensor of the EasyMax 102 system. The reactor vessel was connected to a vacuum line and a 5 L pressure equalising vessel filled with CO₂ (1.25 bara, 3 mol). The equalising vessel was used to apply the same pressure of CO₂ to the system with a remaining pressure after the reaction of more than 1 bara. Then a predesigned program was run, including the removal of the gas phase using vacuum and addition of CO₂ (1 bara). Using the EasyMax 102 software, the reaction energy was determined.

Program



#	Action / Note / Sample	Start Time	End Time
1	Start of experiment on 3/11/2022 at 12:53:16 with thermostat off and R set to 200 rpm, Acetonitrile=60 ml	00:00:00	00:00:05
2	Ramp stirrer speed to 200 rpm over 10 sec	00:00:06	00:00:17
3	Heat Tr to 22 °C as fast as possible	00:00:06	00:01:35
4	Wait 10 min	00:00:17	00:10:17
5	Record virtual volume in reactor	00:10:25	
6	U - cpr - U determination with 15 min waiting time and Δ Tr of 3 K	00:10:25	01:55:20
7	Cool Tr to 22 °C as fast as possible	01:55:21	01:56:41
8	Wait 20 min and remove the gas Phase using vacuum	01:56:41	02:16:41
9	Wait 10 min	02:16:41	02:26:41
10	Wait 10 min	02:26:41	02:36:41
11	Add carbonyl fluoride at once	02:36:41	02:36:59
12	Wait 45 min	02:36:59	03:21:59
13	Record virtual volume in reactor	03:22:35	
14	U - cpr - U determination with 15 min waiting time and Δ Tr of 3 K	03:22:35	05:07:40
15	Ramp stirrer speed to 0 rpm	05:10:30	05:10:36
16	End of experiment	05:41:16	05:41:16

Obtained Values

Table S 2. Determined values for the solvation energy of COF₂ in acetonitrile.

Measurement	<i>E</i> [kJ]
1	0.29311
2	0.30707
3	0.29713
Average	0.29910

Trends

Trend	Color	Units
Tr-Tj		K
qr_hf		W

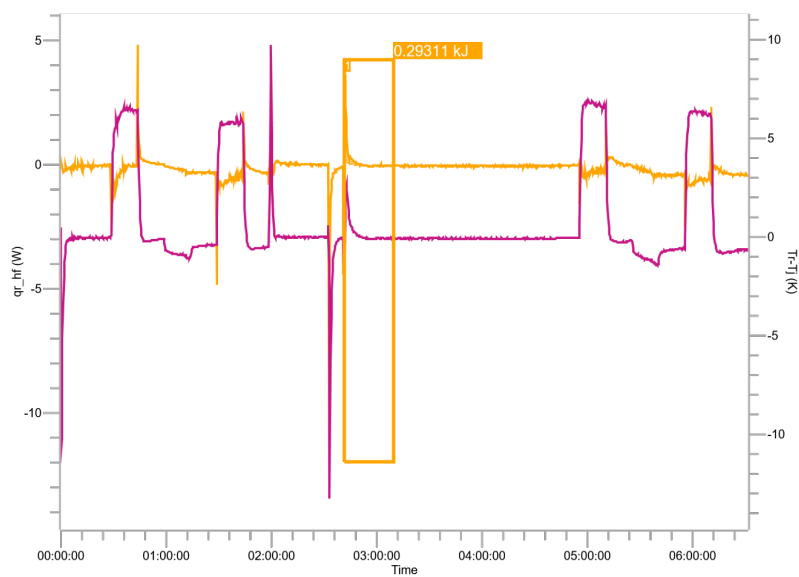


Figure S 2. Temperature curve and heat flow for the addition of COF₂ to 60 mL of acetonitrile (Measurement 1).

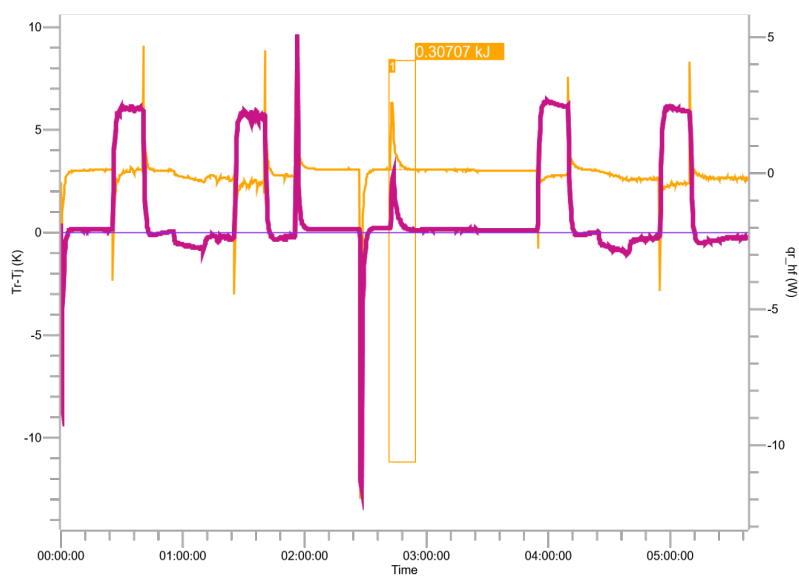


Figure S 3. Temperature curve and heat flow for the addition of COF₂ to 60 mL of acetonitrile (Measurement 2).

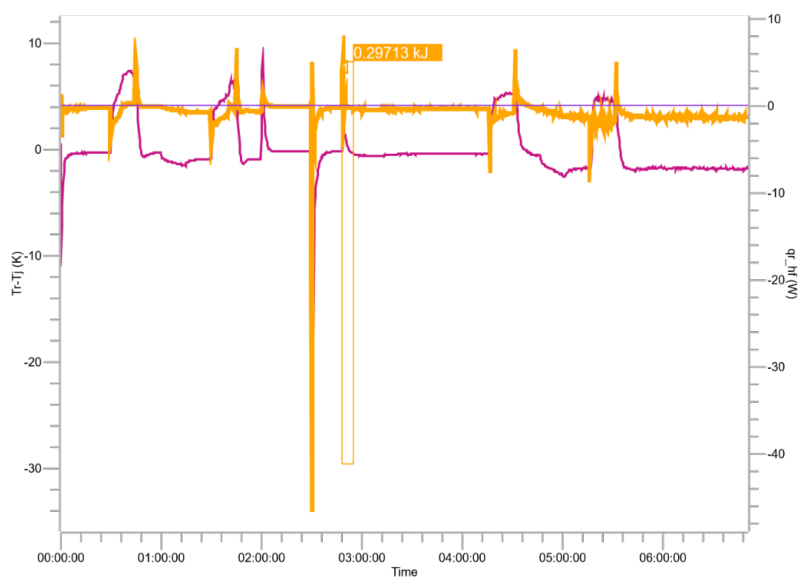


Figure S 4. Temperature curve and heat flow for the addition of COF_2 to 60 mL of acetonitrile (Measurement 3).

Calorimetric Calculations

Measurement 1

Integral Results

Trend	Name	Start Time	End Time	Integral	Baseline Type	ΔT_{ad}
qr_hf	1	02:41:23	03:09:51	0.29311 kJ	Proportional To Conversion	2.3045 K

Virtual Volume (Vv)

Time	Vv (used)	Interpolation
00:00:06	60 ml	Proportional to Vr
00:13:46	65 ml	Proportional to Vr
04:40:04	65 ml	Constant offset

Heat Transfer Coefficient (U)

Time	U (used)	UA	Calculated by	Tr	Interpolation
00:36:18	119.74 W/K*m ²	0.79071 W/K	Standard method	22.69 °C	Proportional to Vv_observed
01:36:22	121.50 W/K*m ²	0.80233 W/K	Standard method	25.61 °C	Proportional to Vv_observed
05:02:36	112.00 W/K*m ²	0.73960 W/K	Standard method	22.69 °C	Proportional to Vv_observed
06:02:40	110.35 W/K*m ²	0.72868 W/K	Standard method	25.69 °C	Hold value

Specific Heat (cpr)

Time	cpr (used)	Calculated by	Tr	Interpolation
01:06:18	2.3001 J/g*K	Standard method	23.11 °C	Proportional to Mr
05:32:36	2.7016 J/g*K	Standard method	23.06 °C	Hold value

Selected reactor inserts

EasyMax calibration heater, C22, 10W
Pt100 temperature sensor, EasyMax, FEP-coated, 175mm
Magnetic stir bar, cross-shaped, PTFE coated, 38mm

Specific Heat of Reactor Inserts (Cpi)

	Cpi at Min. Working Vol.	Cpi per cm
At start of experiment	10.92 J/K	1.079 J/K*cm
Total	10.92 J/K	1.079 J/K*cm

Various Parameters

qr definition	$qr_{hf} = q_{flow_{hf}} - q_c + q_{accu}$
Reactor Time Constant	15 s
ΔT_{ad} calculation	Use mr and cpr at the end of the integral

Measurement 2

Integral Results

Trend	Name	Start Time	End Time	Integral	Baseline Type	ΔT_{ad}
qr_hf	1	02:41:49	02:54:32	0.30707 kJ	Proportional To Conversion	2.6333 K

Virtual Volume (Vv)

Time	Vv (used)	Interpolation
00:00:06	60 ml	Proportional to Vr
00:10:22	65 ml	Proportional to Vr
03:39:16	65 ml	Constant offset

Heat Transfer Coefficient (U)

Time	U (used)	UA	Calculated by	Tr	Interpolation
00:32:54	131.53 W/K*m ²	0.86853 W/K	Standard method	22.61 °C	Proportional to Vv_observed
01:32:56	126.38 W/K*m ²	0.83452 W/K	Standard method	25.56 °C	Proportional to Vv_observed
04:01:50	124.09 W/K*m ²	0.81943 W/K	Standard method	22.62 °C	Proportional to Vv_observed
05:01:54	121.46 W/K*m ²	0.80204 W/K	Standard method	25.62 °C	Hold value

Specific Heat (cpr)

Time	cpr (used)	Calculated by	Tr	Interpolation
01:02:54	1.3580 J/g*K	Standard method	23.15 °C	Proportional to Mr
04:31:50	2.4769 J/g*K	Standard method	23.11 °C	Hold value

Selected reactor inserts

EasyMax calibration heater, C22, 10W
Pt100 temperature sensor, EasyMax, FEP-coated, 175mm
Magnetic stir bar, cross-shaped, PTFE coated, 38mm

Specific Heat of Reactor Inserts (Cpi)

	Cpi at Min. Working Vol.	Cpi per cm
At start of experiment	10.92 J/K	1.079 J/K*cm
Total	10.92 J/K	1.079 J/K*cm

Various Parameters

qr definition	$qr_{hf} = q_{flow_{hf}} - q_c + q_{accu}$
Reactor Time Constant	15 s
ΔT_{ad} calculation	Use mr and cpr at the end of the integral

Measurement 3

Integral Results

Trend	Name	Start Time	End Time	Integral	Baseline Type	ΔT_{ad}
qr_hf	1	02:48:04	02:55:05	0.29713 kJ	Proportional To Conversion	1.5452 K

Virtual Volume (Vv)

Time	Vv (used)	Interpolation
00:00:06	60 ml	Proportional to Vr
00:14:42	65 ml	Proportional to Vr
04:01:06	65 ml	Constant offset

Heat Transfer Coefficient (U)

Time	U (used)	UA	Calculated by	Tr	Interpolation
00:37:14	112.91 W/K*m ²	0.74557 W/K	Standard method	22.93 °C	Proportional to Vv_observed
01:37:18	125.39 W/K*m ²	0.82804 W/K	Standard method	25.60 °C	Proportional to Vv_observed
04:23:38	125.71 W/K*m ²	0.83015 W/K	Standard method	22.62 °C	Proportional to Vv_observed
05:23:40	113.03 W/K*m ²	0.74636 W/K	Standard method	25.65 °C	Hold value

Specific Heat (cpr)

Time	cpr (used)	Calculated by	Tr	Interpolation
01:07:16	2.5628 J/g*K	Standard method	23.04 °C	Proportional to Mr
04:53:38	4.0845 J/g*K	Standard method	22.92 °C	Hold value

Selected reactor inserts

EasyMax calibration heater, C22, 10W
Pt100 temperature sensor, EasyMax, FEP-coated, 175mm
Magnetic stir bar, cross-shaped, PTFE coated, 38mm

Specific Heat of Reactor Inserts (Cpi)

	Cpi at Min. Working Vol.	Cpi per cm
At start of experiment	10.92 J/K	1.079 J/K*cm
Total	10.92 J/K	1.079 J/K*cm

Various Parameters

qr definition	$qr_{hf} = q_{flow_{hf}} - q_c + q_{accu}$
Reactor Time Constant	15 s
ΔT_{ad} calculation	Use mr and cpr at the end of the integral

Reaction of AgF with COF₂ in Acetonitrile

A 100 mL reactor vessel was charged with AgF (amount see Table S 3) and 40 mL of MeCN and equipped with a calibration heater and a thermal sensor of the EasyMax 102 system. The reactor vessel was connected to a vacuum line and a 5 L pressure equalising vessel filled with COF₂ (1.25 bara, 3 mol). The equalising vessel was used to apply the same pressure of COF₂ to the system with a remaining pressure after the reaction of more than 1 bara. Then a predesigned program was run, including the removal of the gas phase using vacuum and addition of COF₂. Using the EasyMax 102 software, the reaction energy was determined.

Program

#	Action / Note / Sample	Start Time	End Time
1	Start of experiment on 3/11/2022 at 12:53:16 with thermostat off and R set to 200 rpm, Acetonitrile=60 ml; silver(I) fluoride=5 g	00:00:00	00:00:05
2	Ramp stirrer speed to 200 rpm over 10 sec	00:00:06	00:00:17
3	Heat Tr to 22 °C as fast as possible	00:00:06	00:01:35
4	Wait 10 min	00:00:17	00:10:17
5	Record virtual volume in reactor	00:10:25	
6	U - cpr - U determination with 15 min waiting time and Δ Tr of 3 K	00:10:25	01:55:20
7	Cool Tr to 22 °C as fast as possible	01:55:21	01:56:41
8	Wait 20 min and remove the gas Phase using vacuum	01:56:41	02:16:41
9	Wait 10 min	02:16:41	02:26:41
10	Wait 10 min	02:26:41	02:36:41
11	Add carbonyl fluoride at once	02:36:41	02:36:59
12	Wait 45 min	02:36:59	03:21:59
13	Record virtual volume in reactor	03:22:35	
14	U - cpr - U determination with 15 min waiting time and Δ Tr of 3 K	03:22:35	05:07:40
15	Ramp stirrer speed to 0 rpm	05:10:30	05:10:36
16	End of experiment	05:41:16	05:41:16

Obtained Values

Table S 3. Determined values for the reaction energy of AgF with COF₂.

Measurement	m _{AgF} [g]	m _{AgF} [mol]	E [kJ]	E _{solv} [kJ mol ⁻¹]
1	5.10	0.0402	2.996	74,57
2	5.05	0.0398	2.940	73,86
3	5.05	0.0398	2.955	74,24
Average	5,07	0.0399	2.964	74,22

Trends

Trend	Color	Units
Tr		°C
qr_hf		W

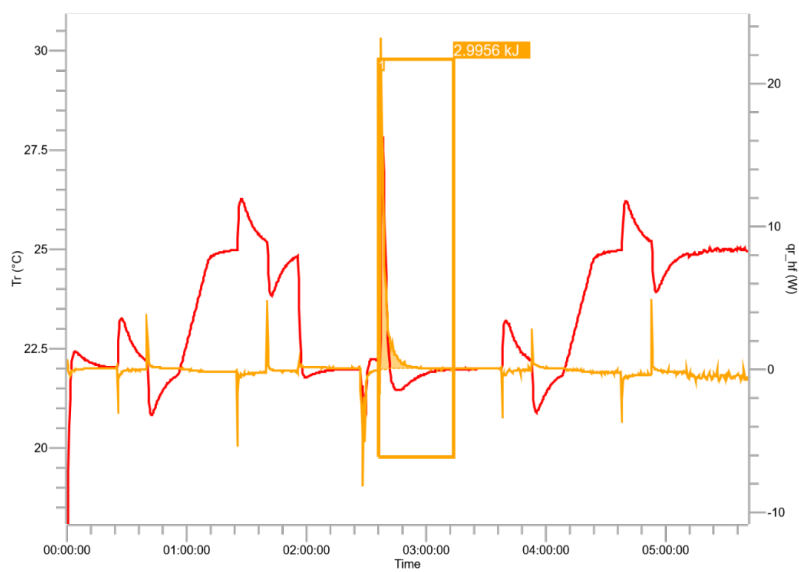


Figure S 5. Reactor temperature curve and heat flow for the reaction of AgF with COF₂ in 60 ml acetonitrile (Measurement 1).

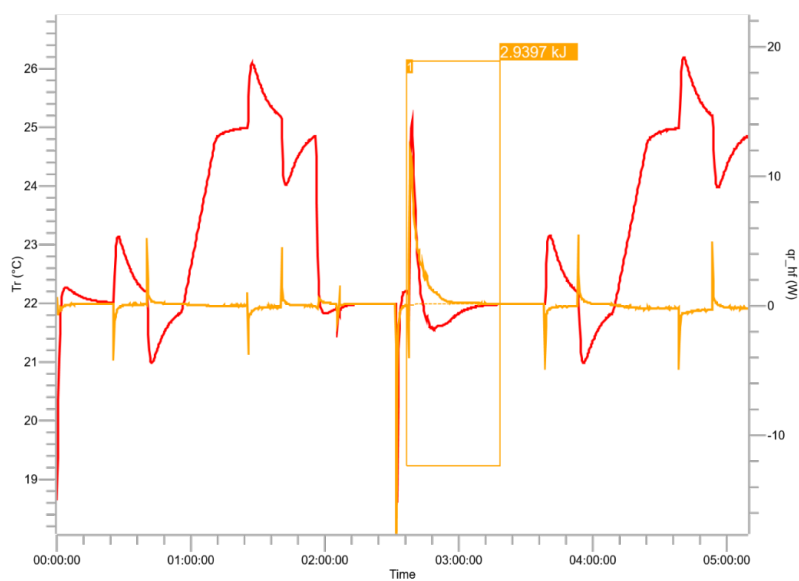


Figure S 6. Reactor temperature curve and heat flow for the reaction of AgF with COF₂ in 60 ml acetonitrile (Measurement 2).

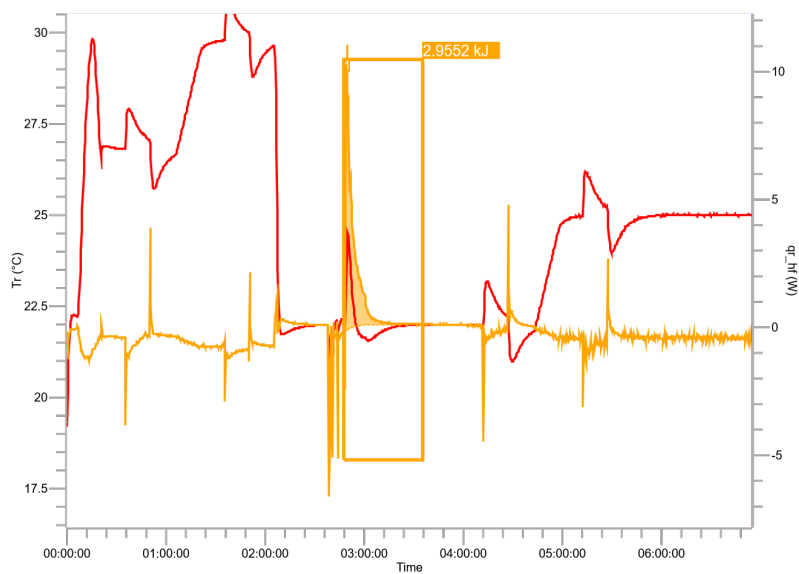


Figure S 7. Reactor temperature curve and heat flow for the reaction of AgF with COF₂ in 60 ml acetonitrile (Measurement 3).

Calorimetric Calculations

Measurement 1

Integral Results

Trend	Name	Start Time	End Time	Integral	Baseline Type	ΔT_{ad}
qr_hf	1	02:36:07	03:13:41	2.9956 kJ	Proportional To Conversion	22.842 K

Virtual Volume (Vv)

Time	Vv (used)	Interpolation
00:00:06	60 ml	Proportional to Vr
00:10:26	65 ml	Proportional to Vr
03:22:36	65 ml	Constant offset

Heat Transfer Coefficient (U)

Time	U (used)	UA	Calculated by	Tr	Interpolation
00:32:52	120.28 W/K*m ²	0.79427 W/K	Standard method	22.63 °C	Proportional to Vv_observed
01:32:48	120.14 W/K*m ²	0.79337 W/K	Standard method	25.63 °C	Proportional to Vv_observed
03:45:06	122.73 W/K*m ²	0.81044 W/K	Standard method	22.63 °C	Proportional to Vv_observed
04:45:10	124.05 W/K*m ²	0.81915 W/K	Standard method	25.62 °C	Hold value

Specific Heat (cpr)

Time	cpr (used)	Calculated by	Tr	Interpolation
01:02:44	2.3783 J/g*K	Standard method	23.13 °C	Proportional to Mr
04:15:08	2.7857 J/g*K	Standard method	23.12 °C	Hold value

Selected reactor inserts

EasyMax calibration heater, C22, 10W
Pt100 temperature sensor, EasyMax, FEP-coated, 175mm
Magnetic stir bar, cross-shaped, PTFE coated, 38mm

Specific Heat of Reactor Inserts (Cpi)

	Cpi at Min. Working Vol.	Cpi per cm
At start of experiment	10.92 J/K	1.079 J/K*cm
Total	10.92 J/K	1.079 J/K*cm

Various Parameters

qr definition	$qr_{hf} = q_{flow_{hf}} - q_c + q_{accu} + q_{dos}$
qdos averaged	yes
Reactor Time Constant	15 s
ΔT_{ad} calculation	Use mr and cpr at the end of the integral

Measurement 2

Integral Results

Trend	Name	Start Time	End Time	Integral	Baseline Type	ΔT_{ad}
qr_hf	1	02:36:28	03:18:26	2.9397 kJ	Proportional To Conversion	24.152 K

Virtual Volume (Vv)

Time	Vv (used)	Interpolation
00:00:08	60 ml	Proportional to Vr
00:10:24	65 ml	Proportional to Vr
03:23:14	65 ml	Constant offset

Heat Transfer Coefficient (U)

Time	U (used)	UA	Calculated by	Tr	Interpolation
00:32:56	133.82 W/K*m ²	0.88367 W/K	Standard method	22.60 °C	Proportional to Vv_observed
01:33:00	137.23 W/K*m ²	0.90619 W/K	Standard method	25.55 °C	Proportional to Vv_observed
03:45:46	127.89 W/K*m ²	0.84448 W/K	Standard method	22.60 °C	Proportional to Vv_observed
04:45:48	125.43 W/K*m ²	0.82827 W/K	Standard method	25.61 °C	Hold value

Specific Heat (cpr)

Time	cpr (used)	Calculated by	Tr	Interpolation
01:02:56	2.2102 J/g*K	Standard method	23.17 °C	Proportional to Mr
04:15:46	2.5854 J/g*K	Standard method	23.12 °C	Hold value

Selected reactor inserts

EasyMax calibration heater, C22, 10W
Pt100 temperature sensor, EasyMax, FEP-coated, 175mm
Magnetic stir bar, cross-shaped, PTFE coated, 38mm

Specific Heat of Reactor Inserts (Cpi)

	Cpi at Min. Working Vol.	Cpi per cm
At start of experiment	10.92 J/K	1.079 J/K*cm
Total	10.92 J/K	1.079 J/K*cm

Various Parameters

qr definition	$qr_{hf} = q_{flow_{hf}} - q_c + q_{accu} + q_{dos}$
qdos averaged	yes
Reactor Time Constant	15 s
ΔT_{ad} calculation	Use mr and cpr at the end of the integral

Measurement 3

Integral Results

Trend	Name	Start Time	End Time	Integral	Baseline Type	ΔT_{ad}
qr_hf	1	02:47:51	03:35:23	2.9552 kJ	Proportional To Conversion	20.929 K

Virtual Volume (Vv)

Time	Vv (used)	Interpolation
00:00:06	60 ml	Proportional to Vr
00:20:24	65 ml	Proportional to Vr
03:56:52	65 ml	Constant offset

Heat Transfer Coefficient (U)

Time	U (used)	UA	Calculated by	Tr	Interpolation
00:42:56	126.61 W/K*m ²	0.83604 W/K	Standard method	27.42 °C	Proportional to Vv_observed
01:43:00	133.35 W/K*m ²	0.88057 W/K	Standard method	30.35 °C	Proportional to Vv_observed
04:19:24	119.49 W/K*m ²	0.78907 W/K	Standard method	22.64 °C	Proportional to Vv_observed
05:19:28	120.32 W/K*m ²	0.79453 W/K	Standard method	25.61 °C	Hold value

Specific Heat (cpr)

Time	cpr (used)	Calculated by	Tr	Interpolation
01:12:56	2.7035 J/g*K	Standard method	27.91 °C	Proportional to Mr
04:49:26	2.9992 J/g*K	Standard method	23.07 °C	Hold value

Selected reactor inserts

EasyMax calibration heater, C22, 10W
Pt100 temperature sensor, EasyMax, FEP-coated, 175mm
Magnetic stir bar, cross-shaped, PTFE coated, 38mm

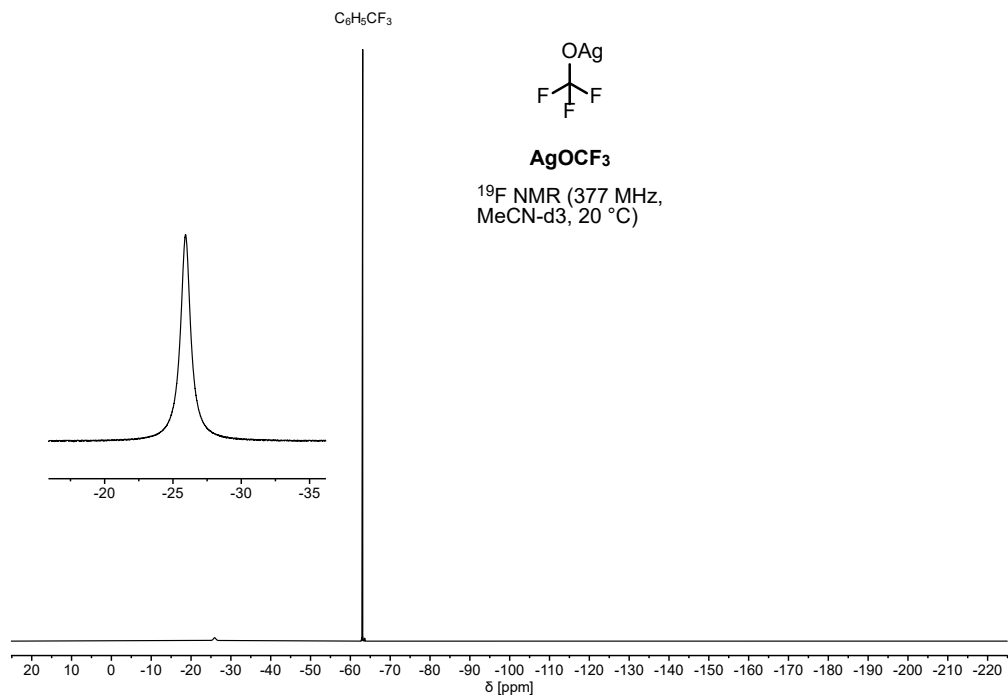
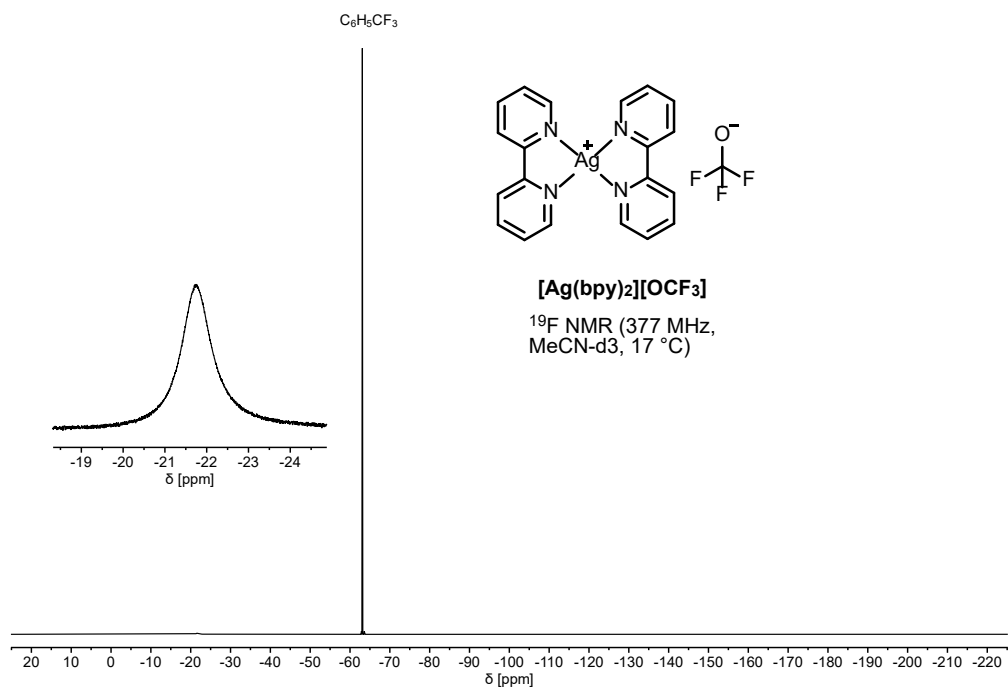
Specific Heat of Reactor Inserts (Cpi)

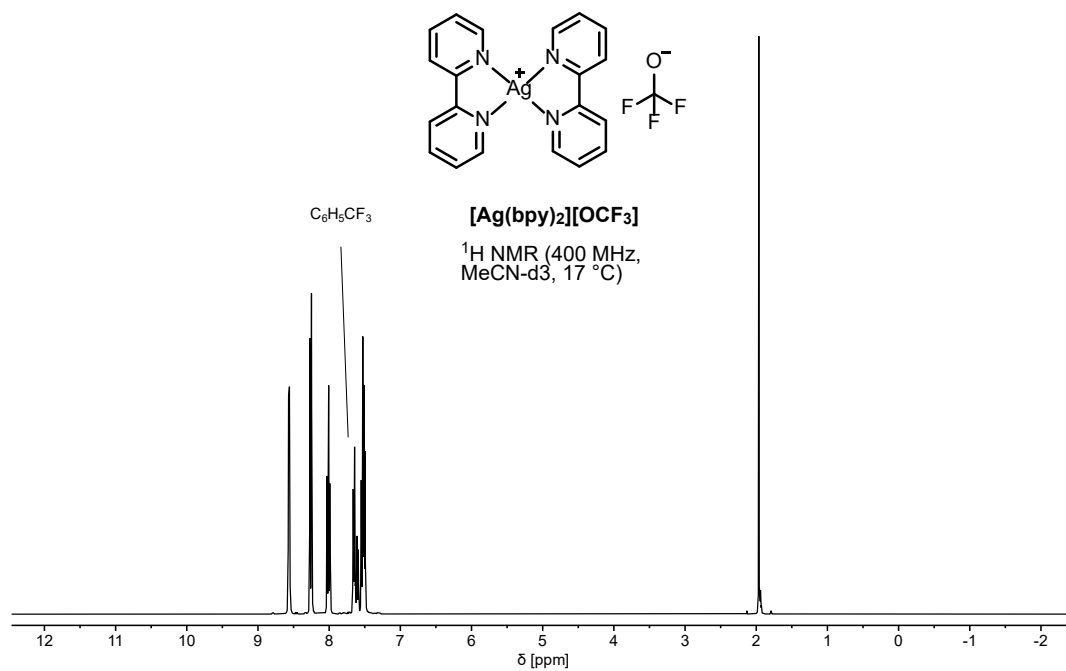
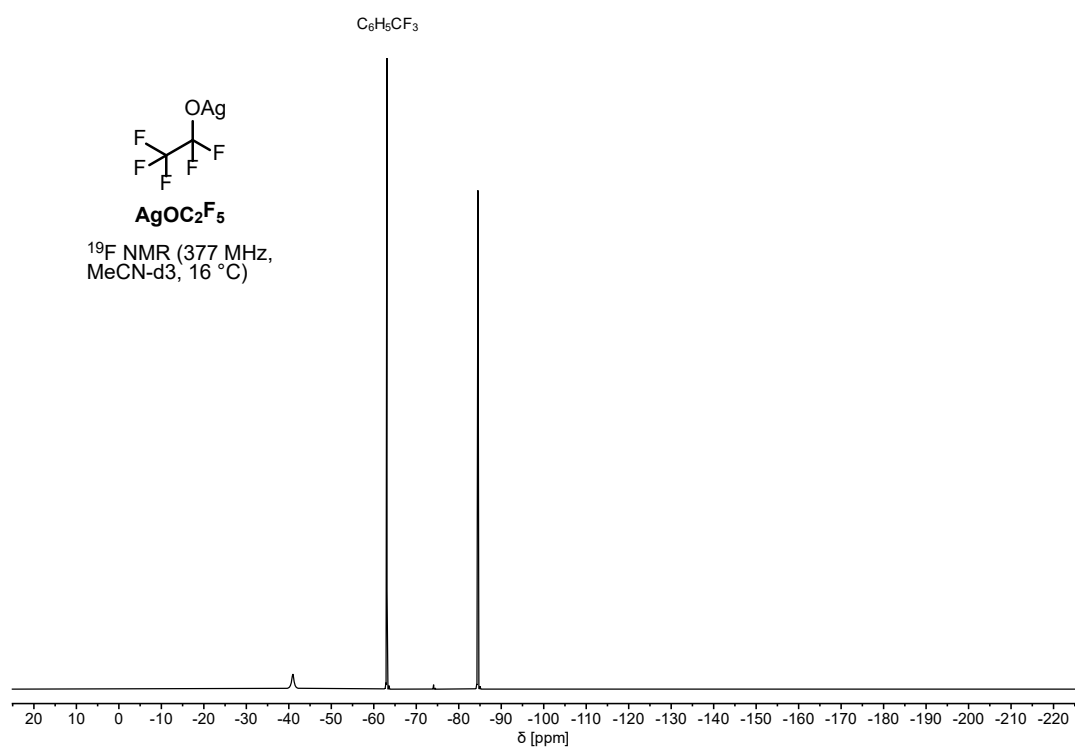
	Cpi at Min. Working Vol.	Cpi per cm
At start of experiment	10.92 J/K	1.079 J/K*cm
Total	10.92 J/K	1.079 J/K*cm

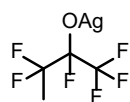
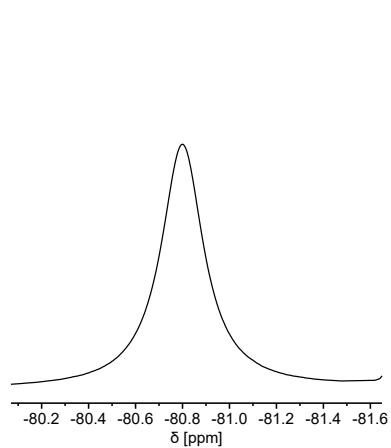
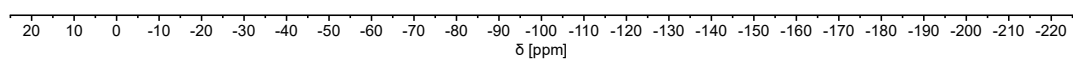
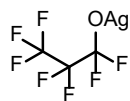
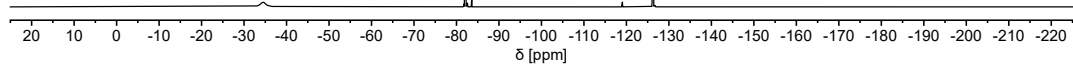
Various Parameters

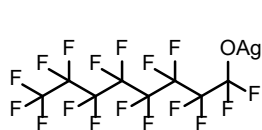
qr definition	$qr_{hf} = q_{flow_{hf}} - q_c + q_{accu} + q_{dos}$
qdos averaged	yes
Reactor Time Constant	15 s
ΔT_{ad} calculation	Use mr and cpr at the end of the integral

NMR Spectra

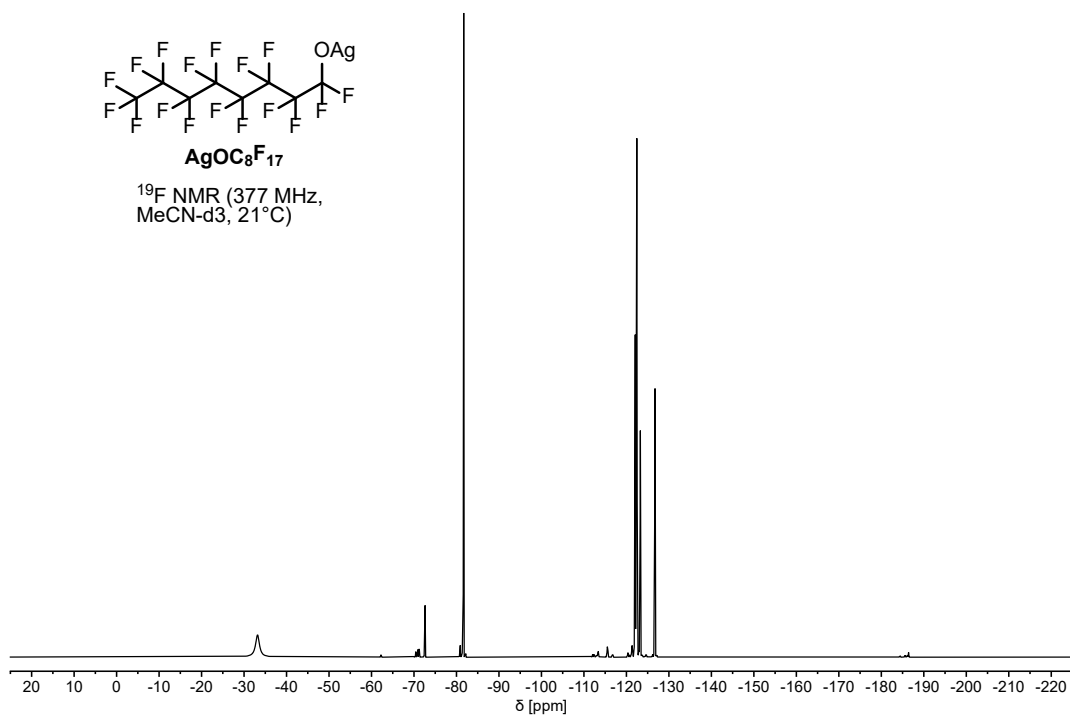
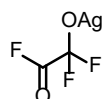
Ag[OCF₃][Ag(bpy)₂][OCF₃]

**Ag[OC₂F₅]**

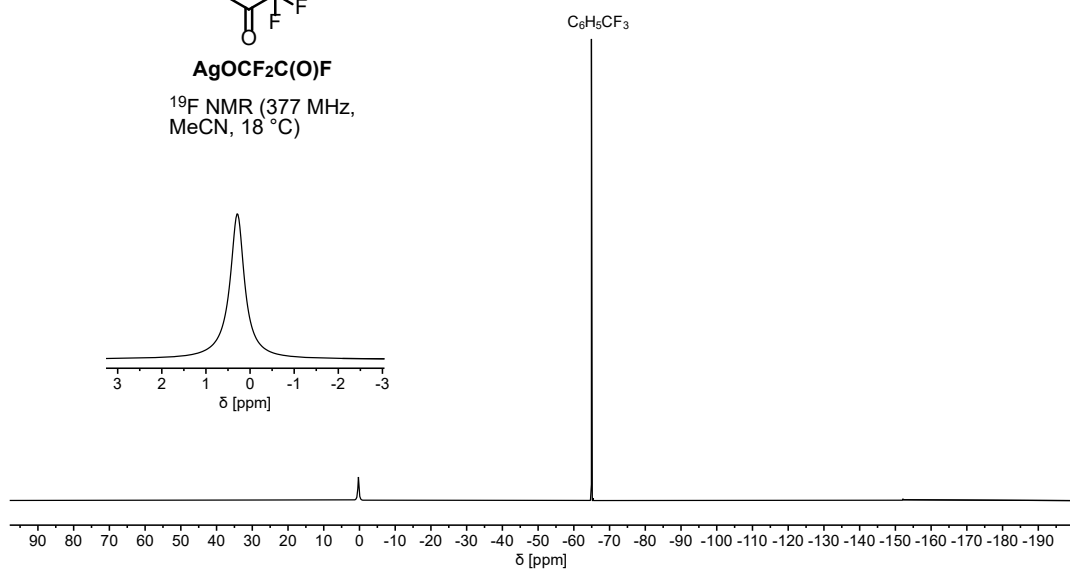
$\text{Ag}[\text{O}^i\text{C}_3\text{F}_7]$ **Ag-i-OC₂F₅** ^{19}F NMR (377 MHz,
MeCN-d₃, 21 °C) $\text{Ag}[\text{O}^n\text{C}_3\text{F}_7]$ **Ag-n-OC₃F₇** ^{19}F NMR (377 MHz,
MeCN-d₃, 21 °C)

$\text{Ag}[\text{OC}_8\text{F}_{17}]$  $\text{AgOC}_8\text{F}_{17}$

^{19}F NMR (377 MHz,
MeCN-d₃, 21°C)

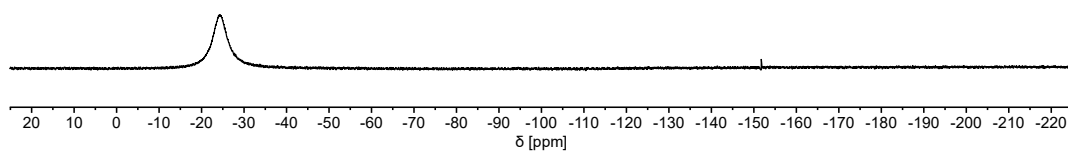
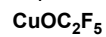
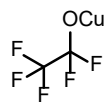
 $\text{Ag}[\text{OCF}_2\text{C}(\text{O})\text{F}]$  $\text{AgOCF}_2\text{C}(\text{O})\text{F}$

^{19}F NMR (377 MHz,
MeCN, 18 °C)

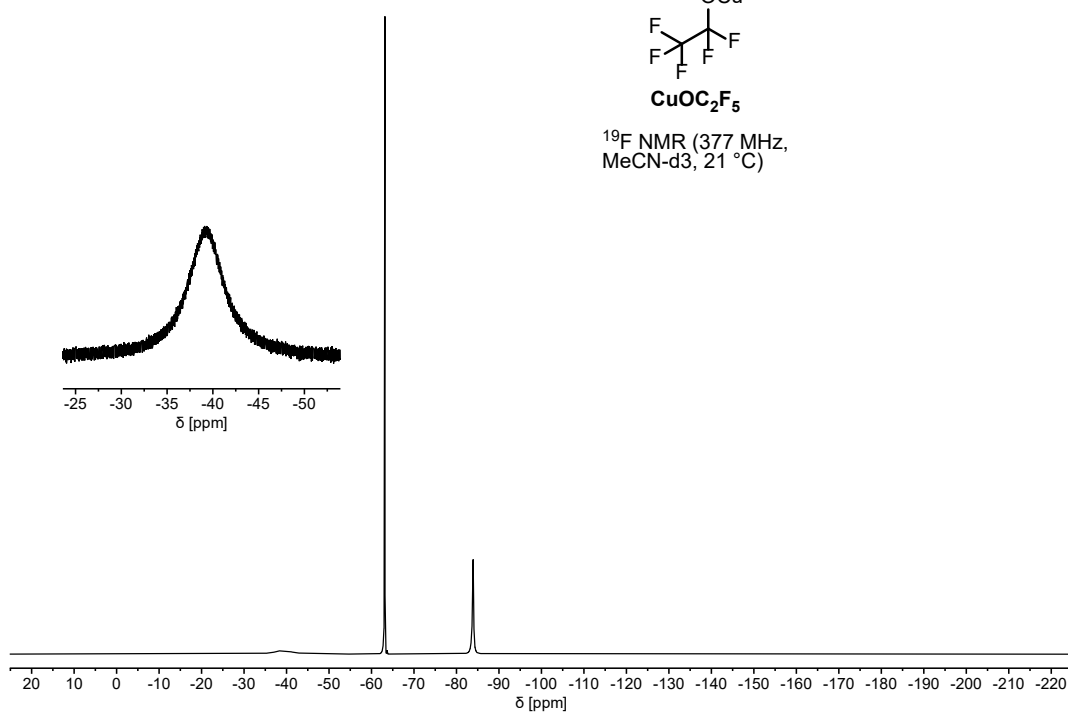


Cu[OCF₃]

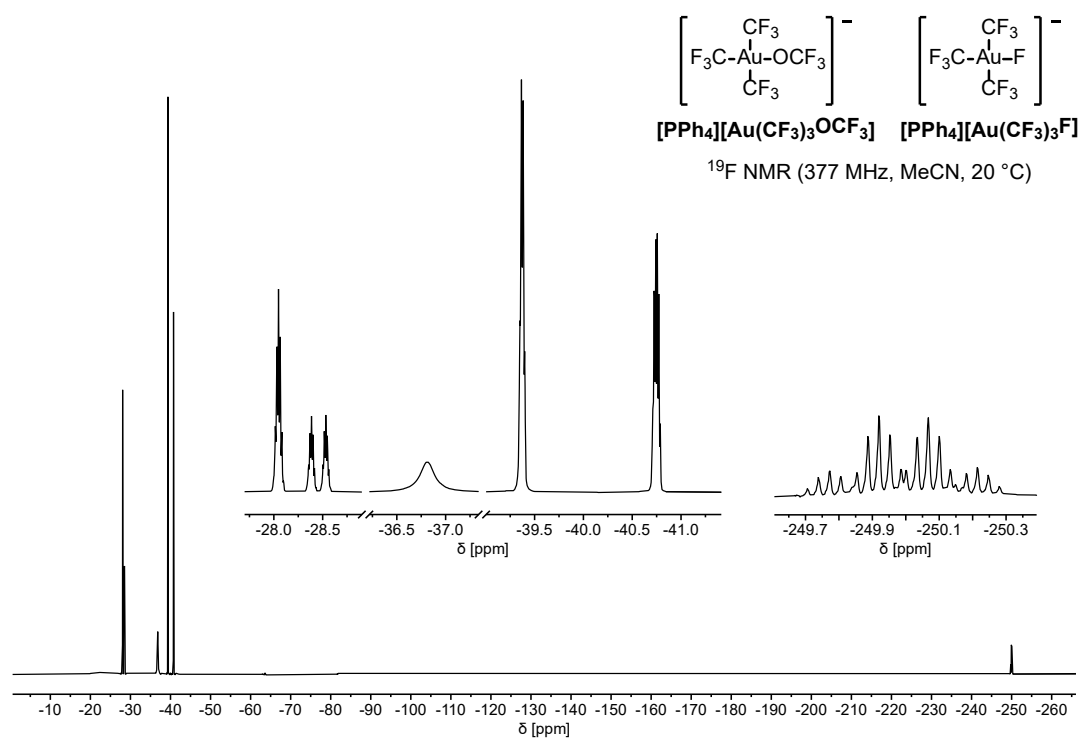
¹⁹F NMR (377 MHz,
MeCN-d₃, 21 °C)

Cu[OC₂F₅]

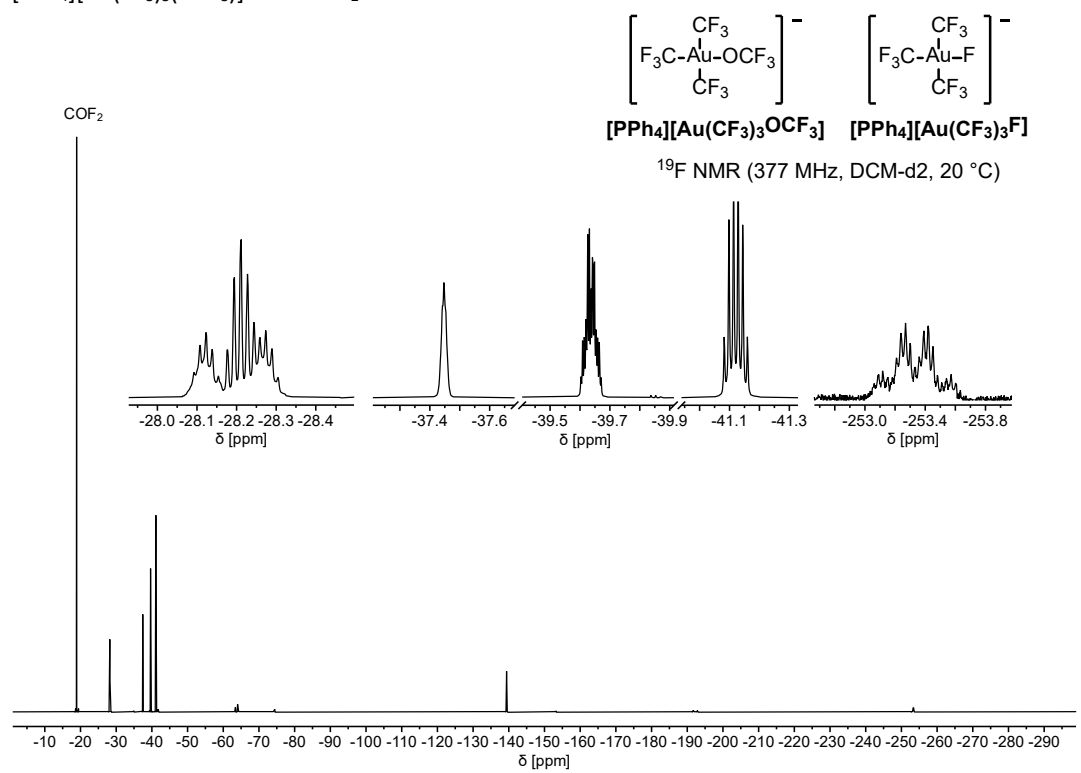
¹⁹F NMR (377 MHz,
MeCN-d₃, 21 °C)

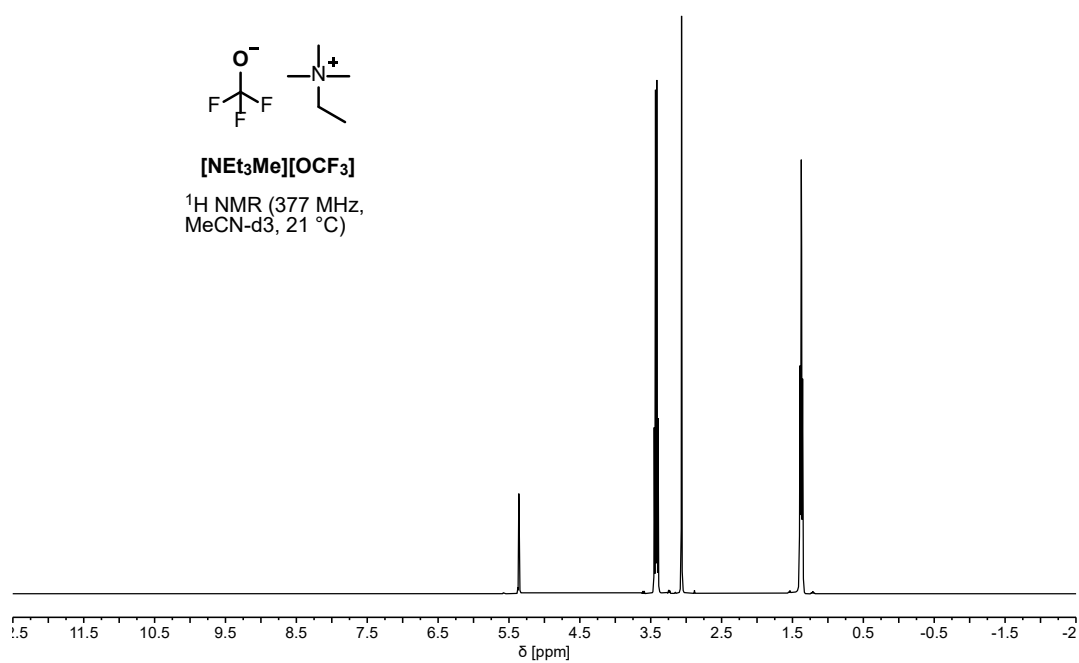
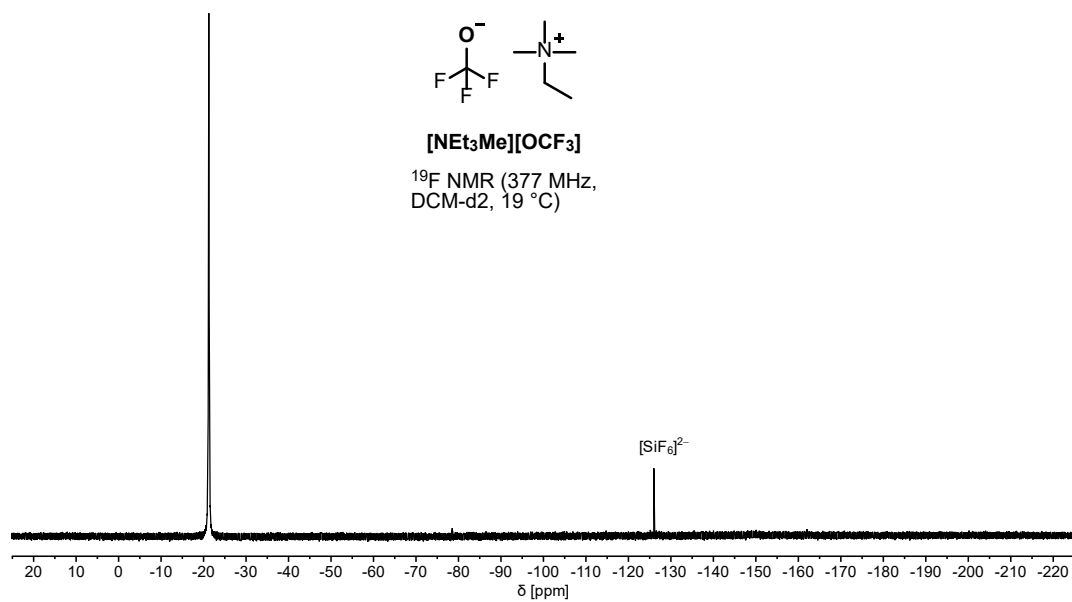


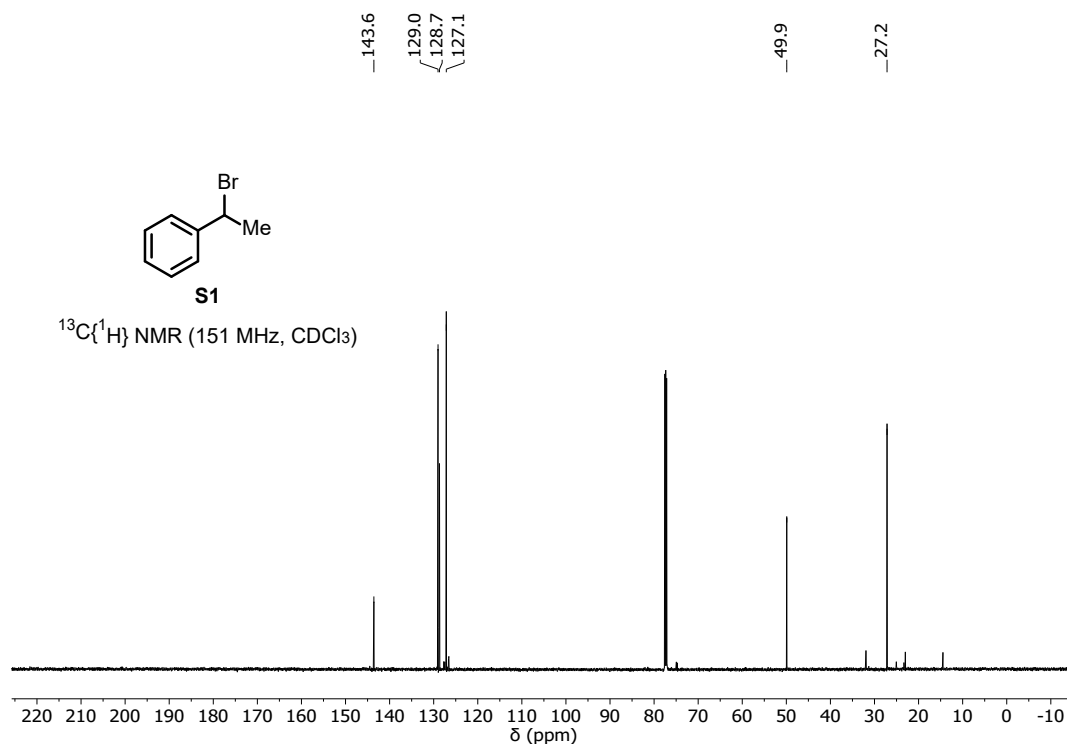
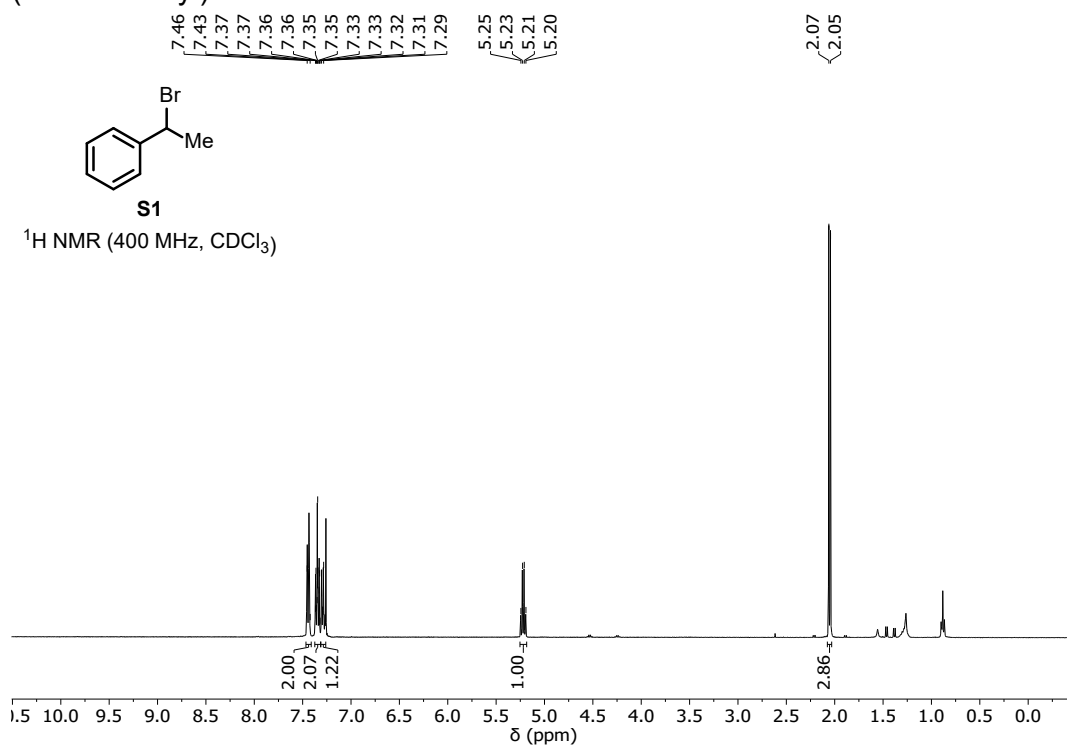
[PPh₄][Au(CF₃)₃(OCF₃)] from AgOCF₃

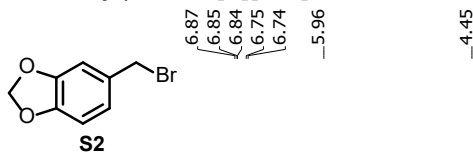
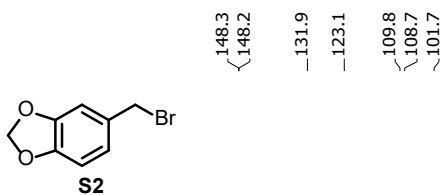
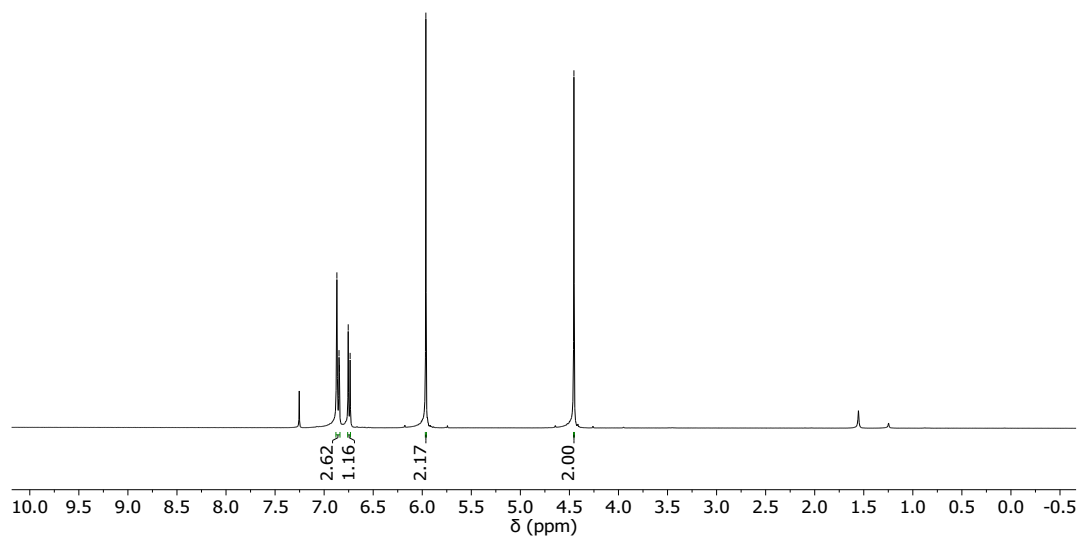
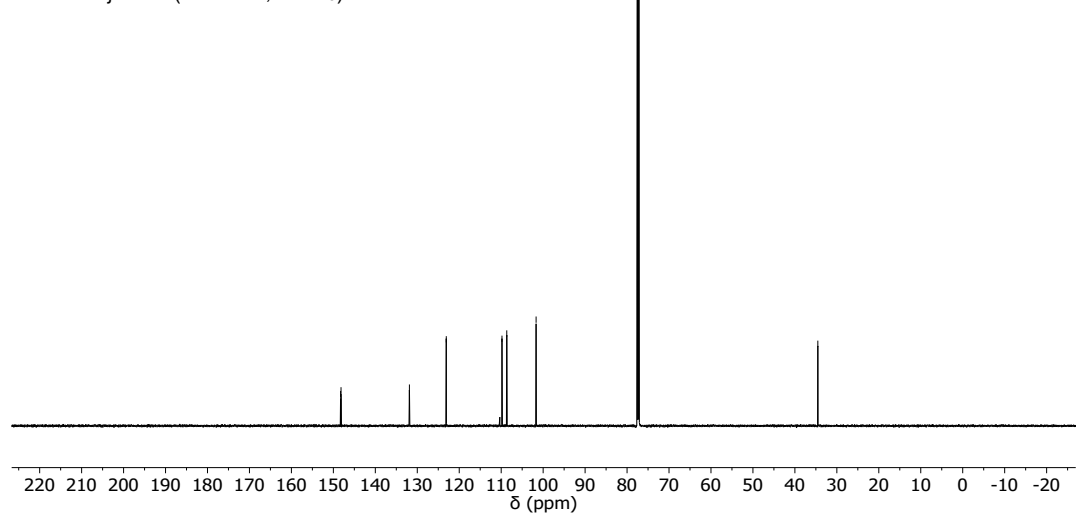


[PPh₄][Au(CF₃)₃(OCF₃)] from COF₂

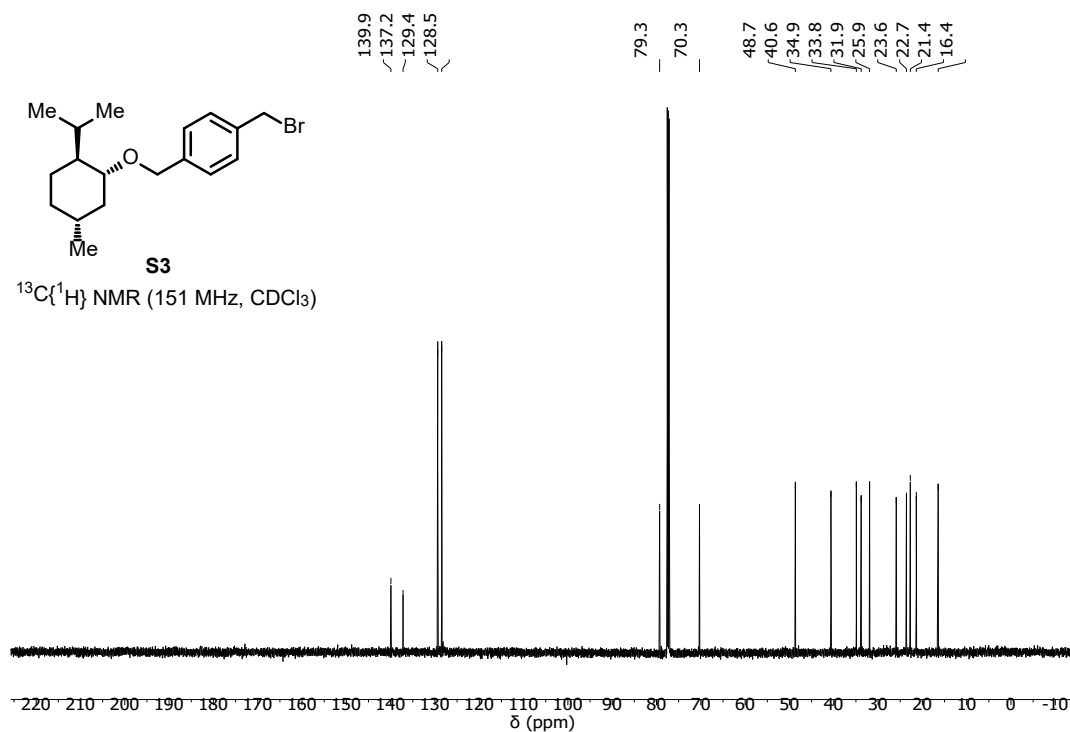
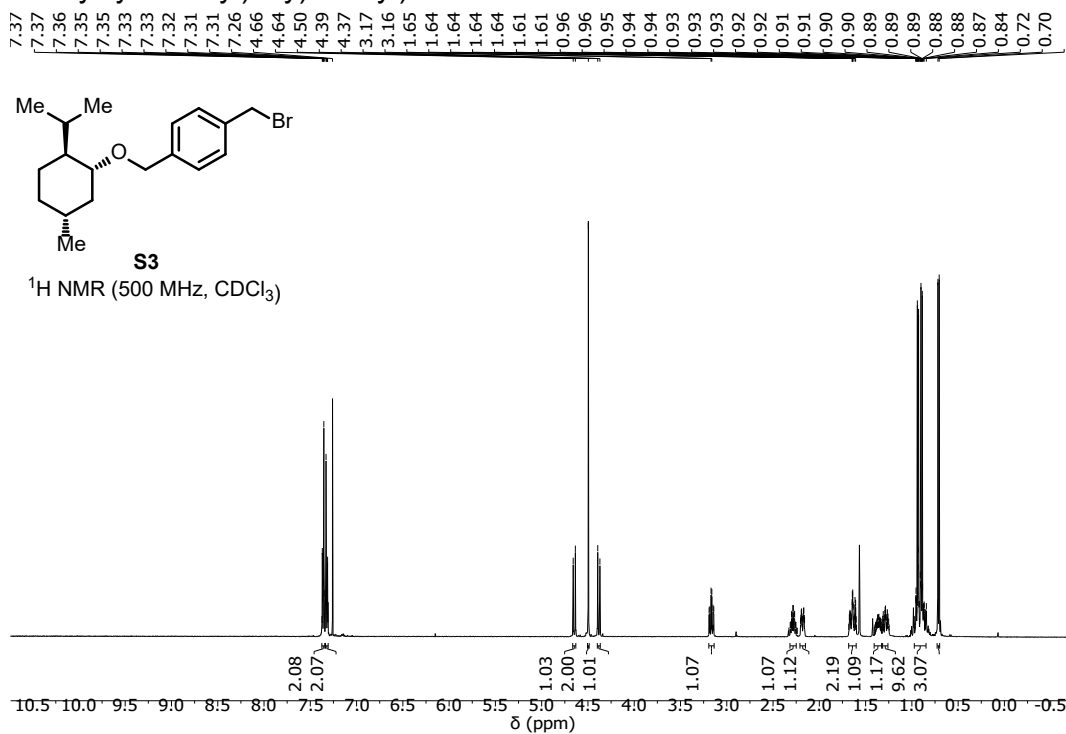


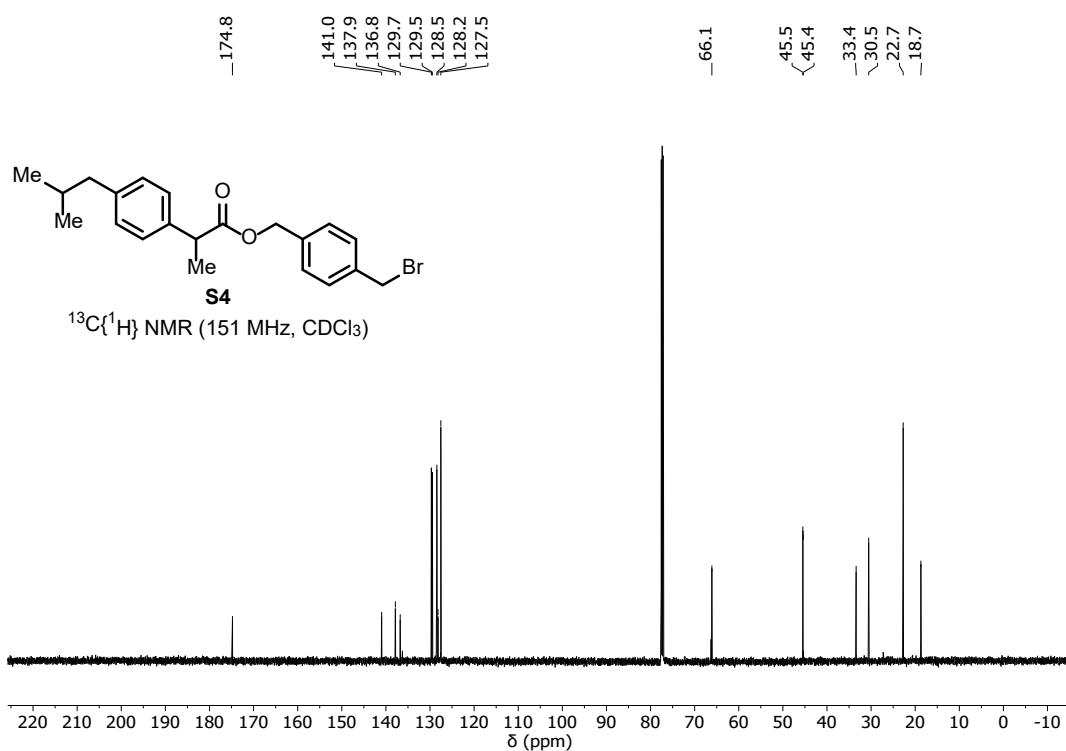
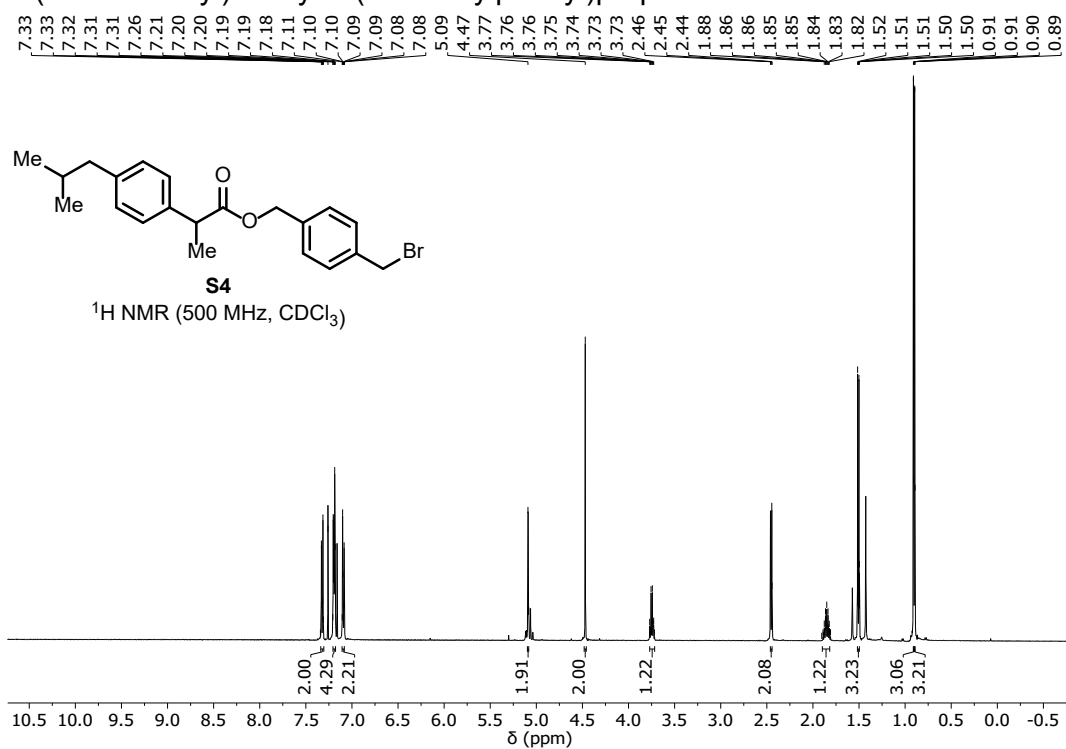


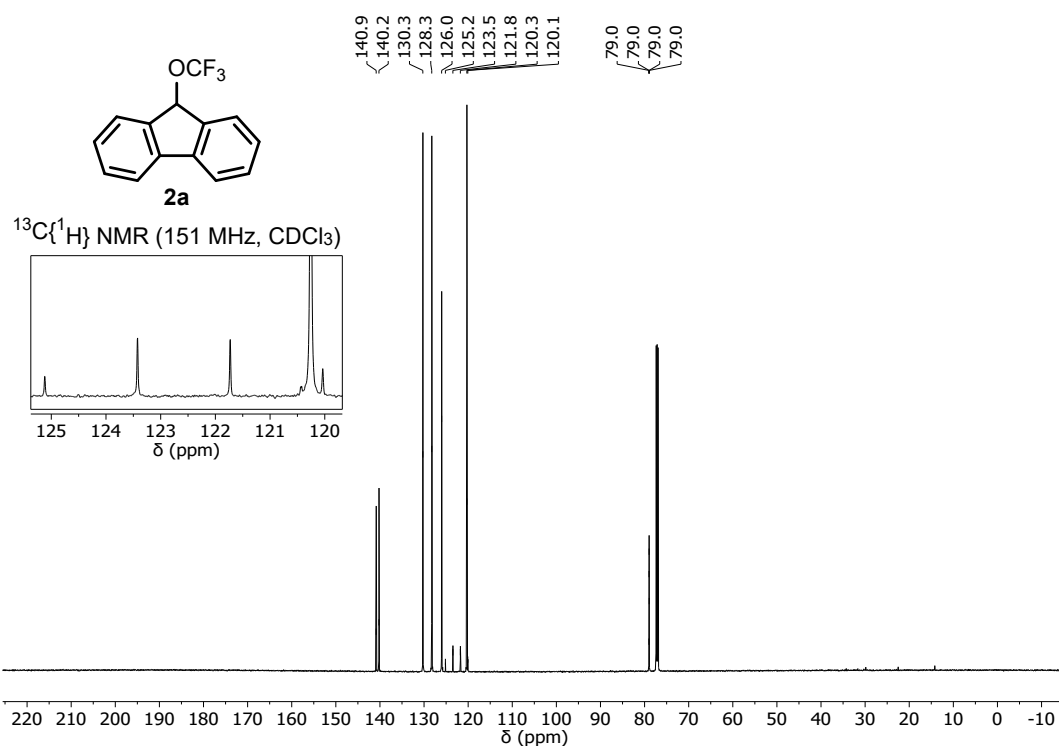
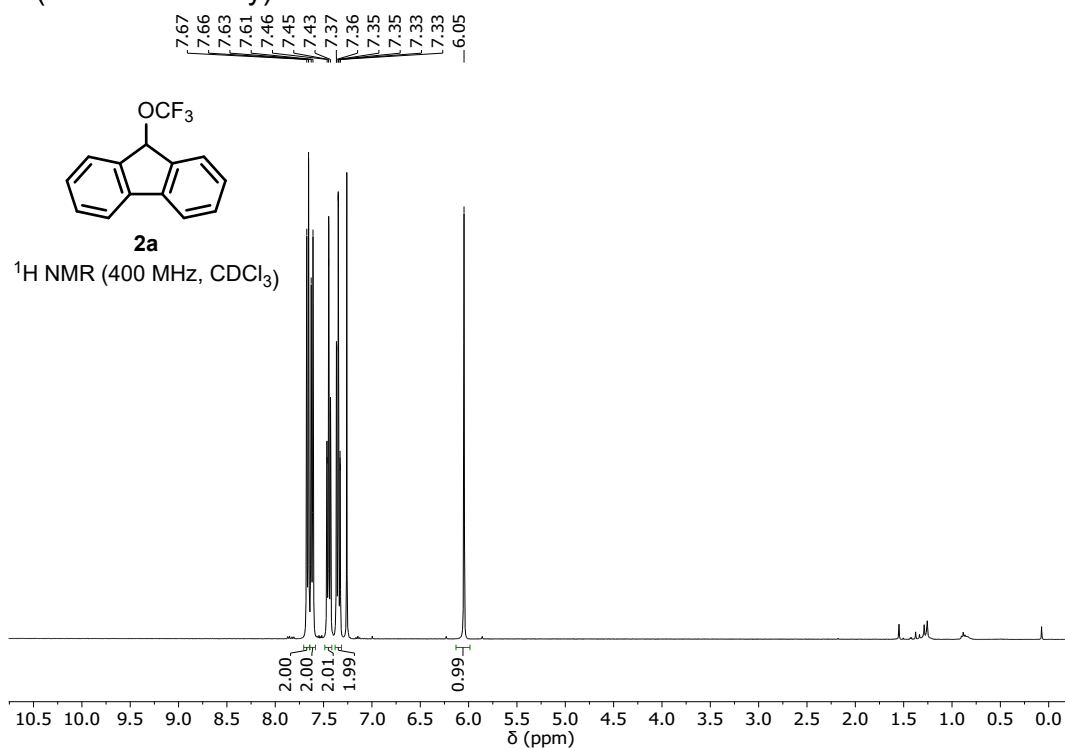
(1-bromoethyl)benzene **S1**

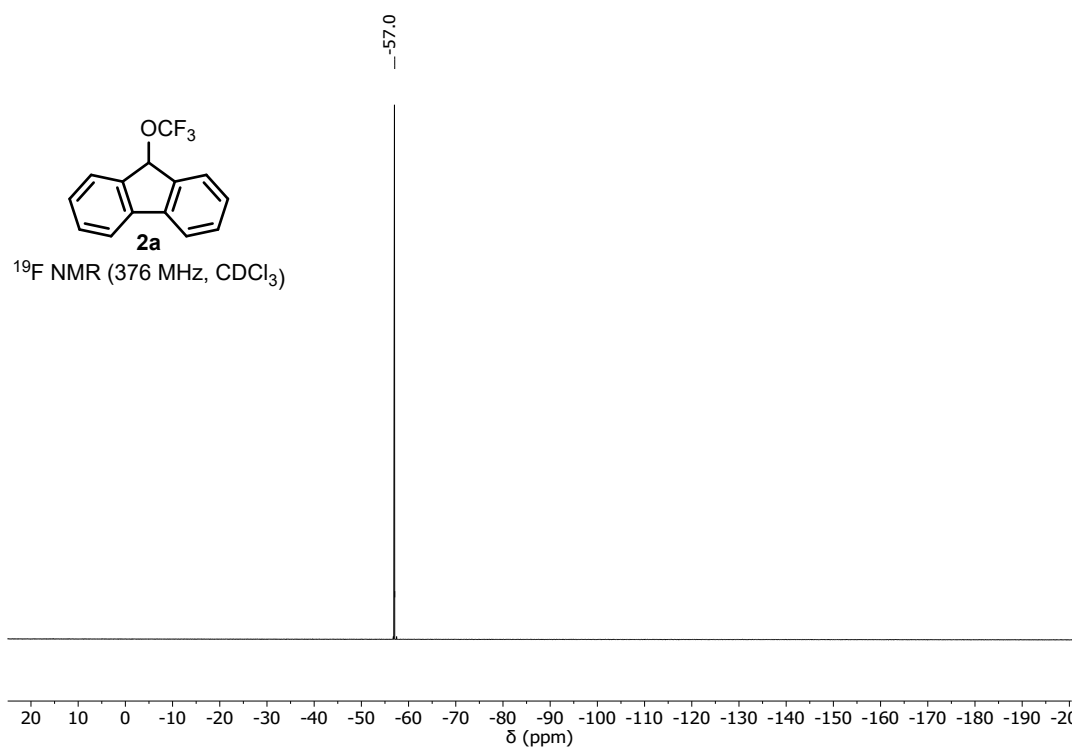
5-(bromomethyl)benzo[d][1,3]dioxole **S2**¹H NMR (400 MHz, CDCl₃)¹³C{¹H} NMR (176 MHz, CDCl₃)

1-(bromomethyl)-4-(((1*R*,2*S*,5*R*)-2-isopropyl-5-methylcyclohexyl)oxy)methyl)benzene **S3**

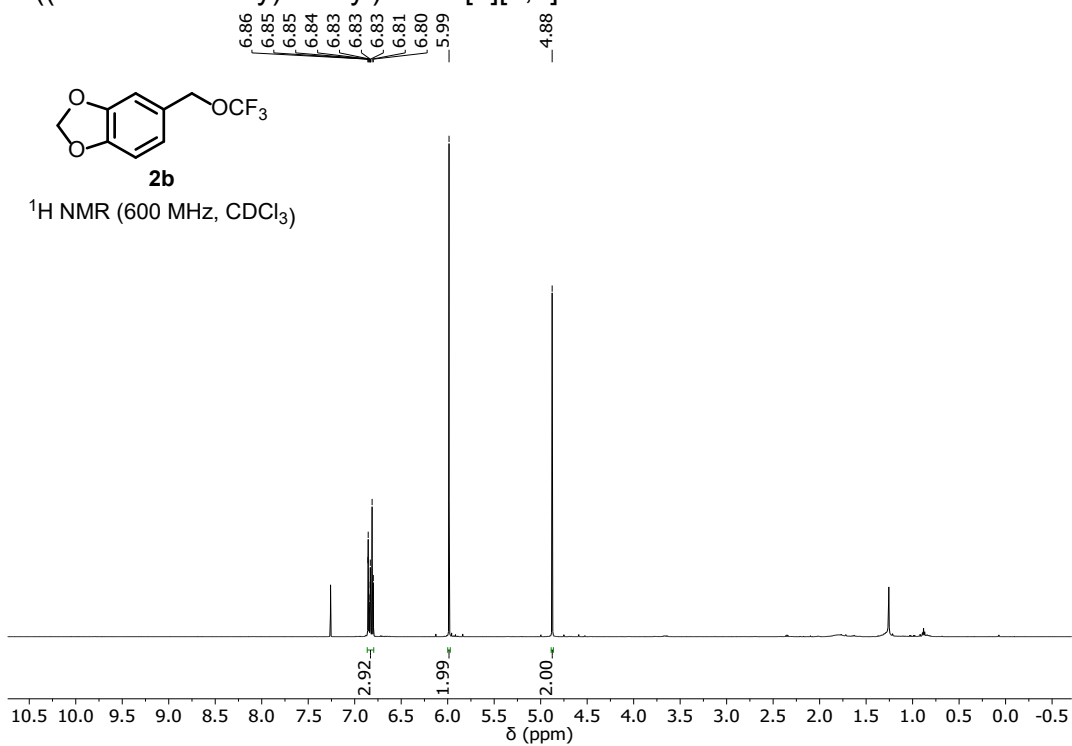


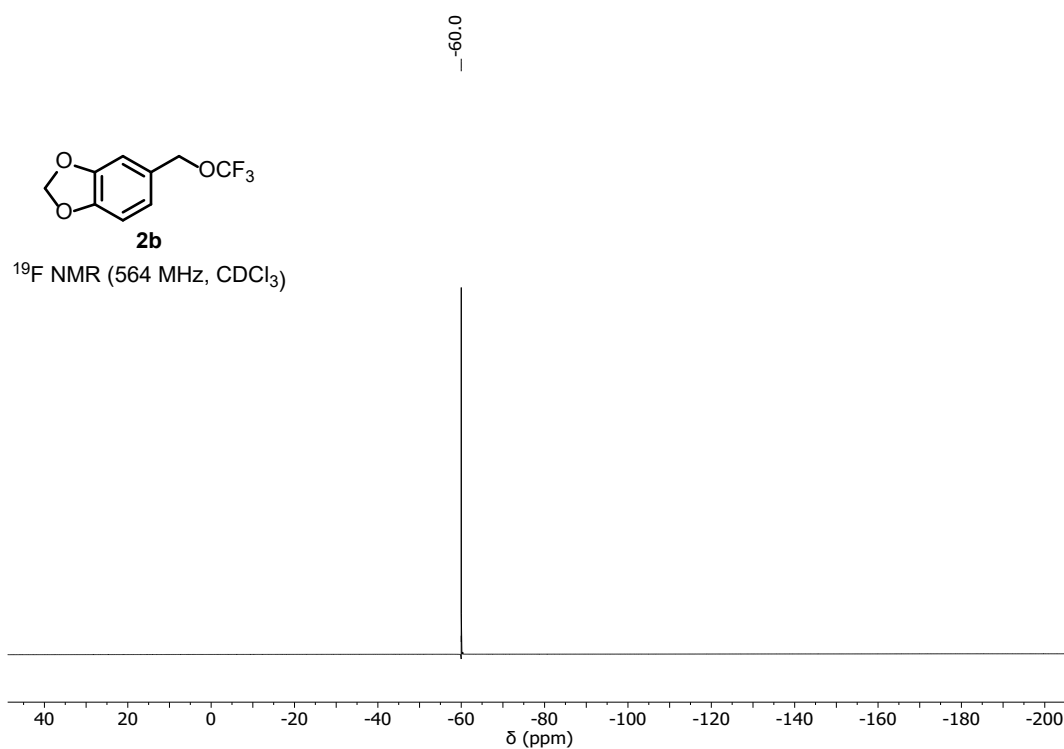
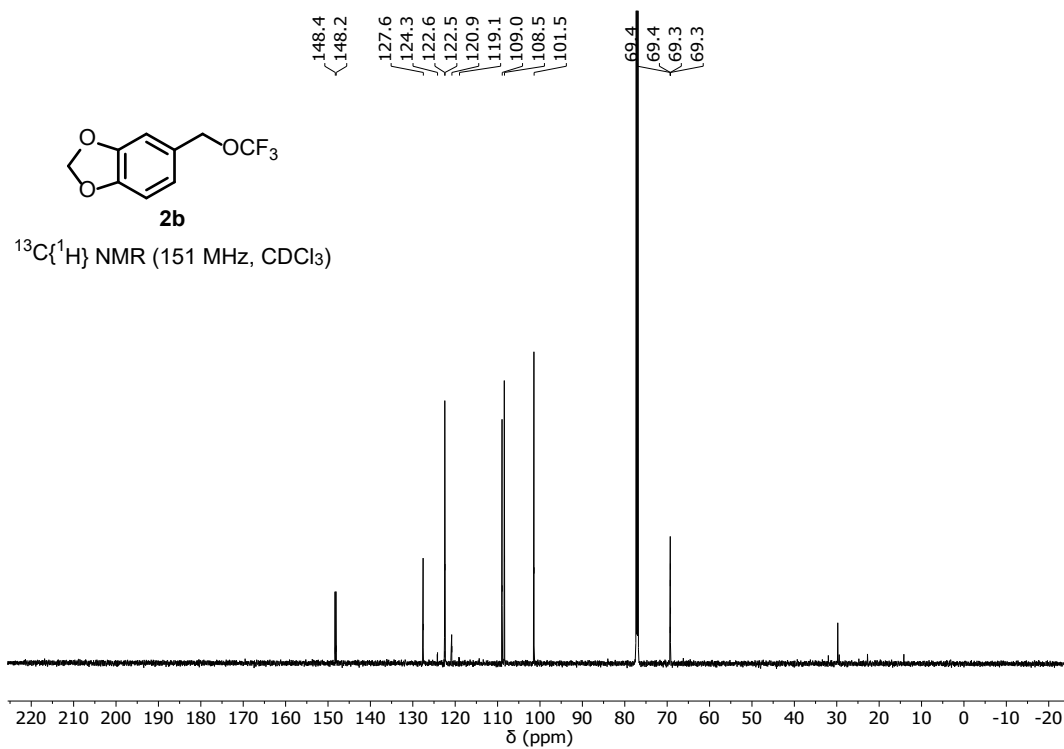
4-(bromomethyl)benzyl 2-(4-isobutylphenyl)propanoate **S4**

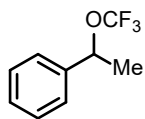
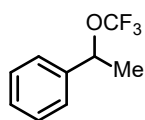
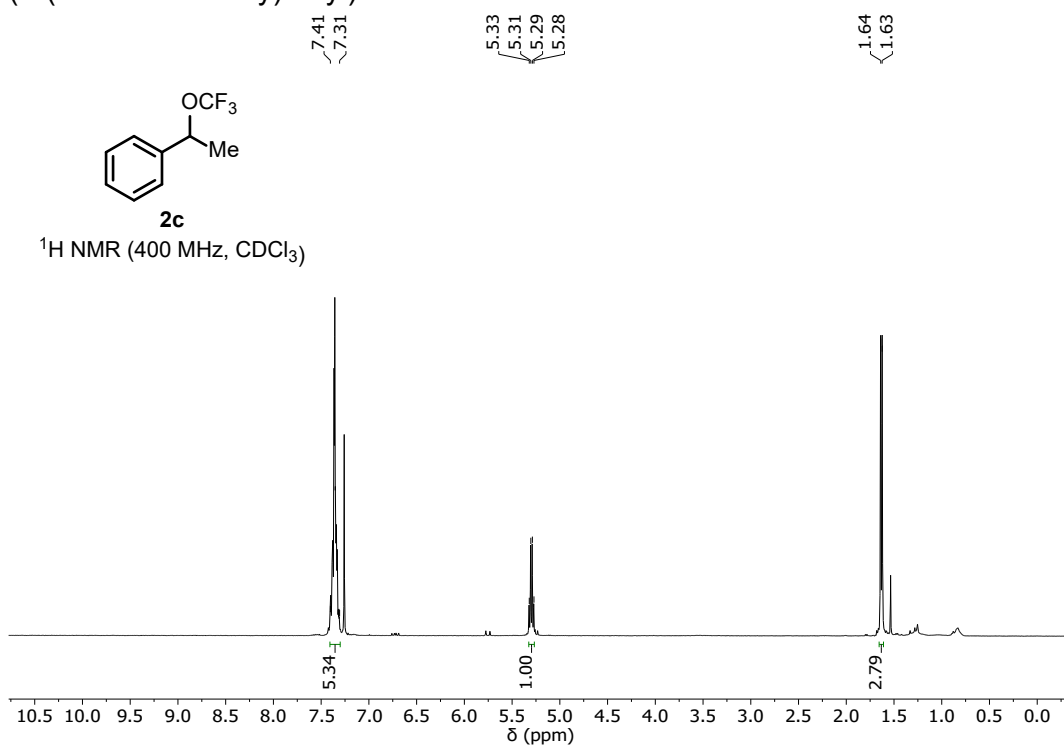
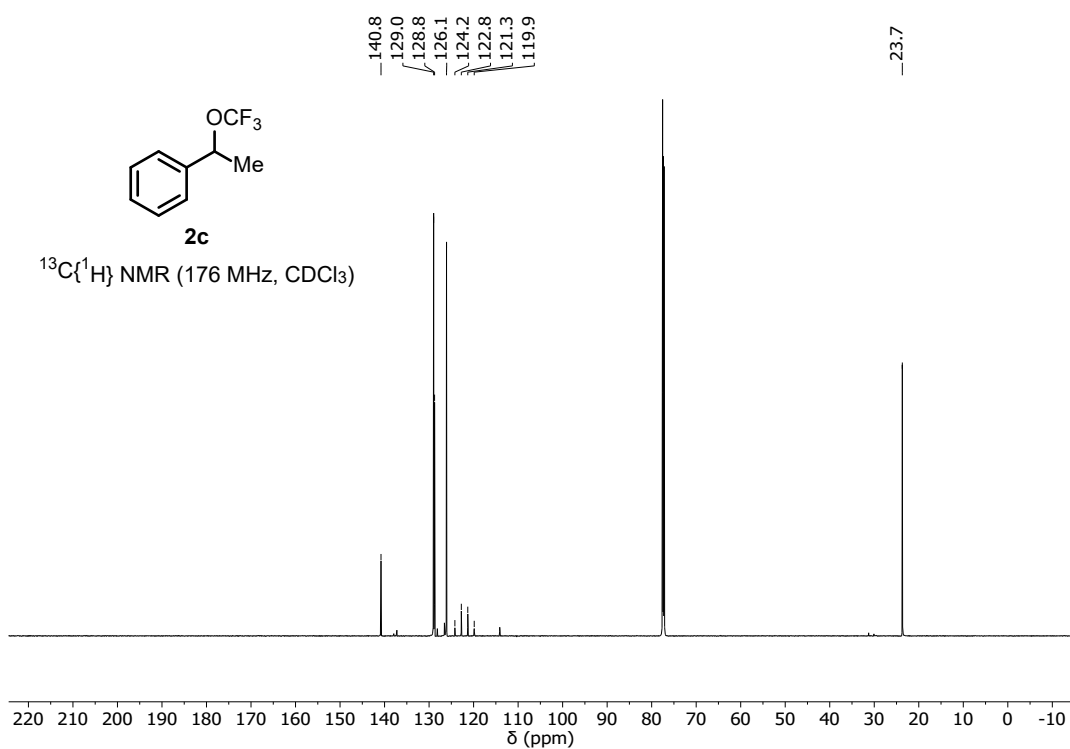
9-(trifluoromethoxy)-9H-fluorene **2a**

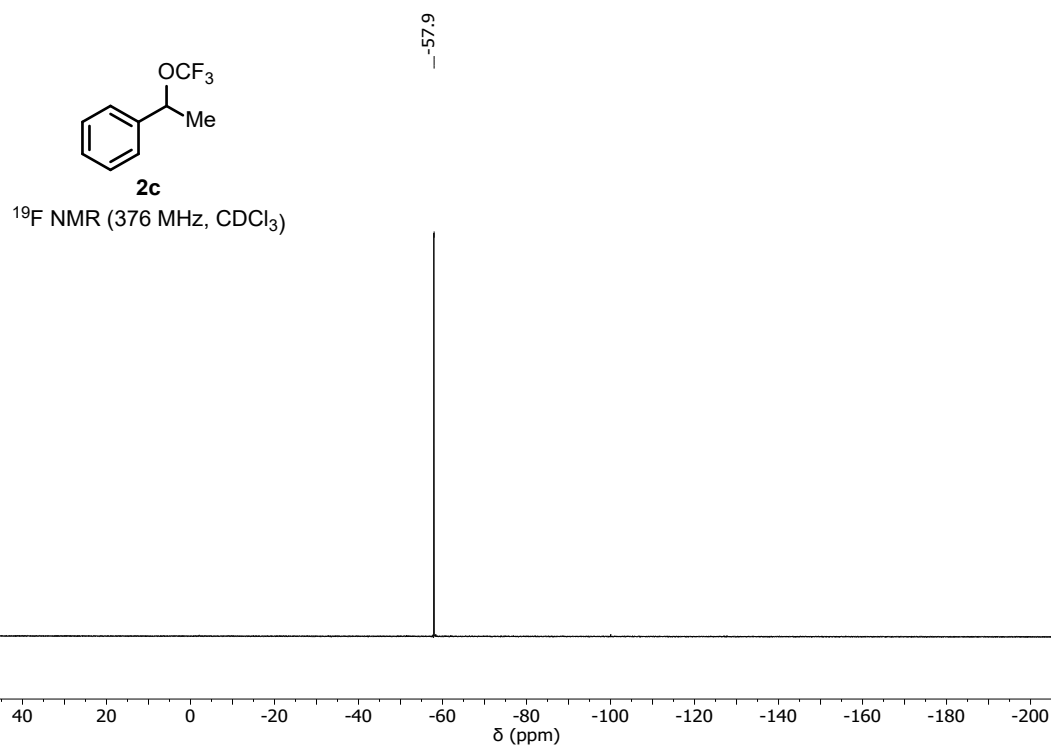


5-((trifluoromethoxy)methyl)benzo[d][1,3]dioxole 2b



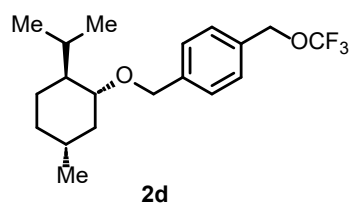


(1-(trifluoromethoxy)ethyl)benzene **2c****2c** $^1\text{H NMR}$ (400 MHz, CDCl_3)**2c** $^{13}\text{C}\{^1\text{H}\}$ NMR (176 MHz, CDCl_3)

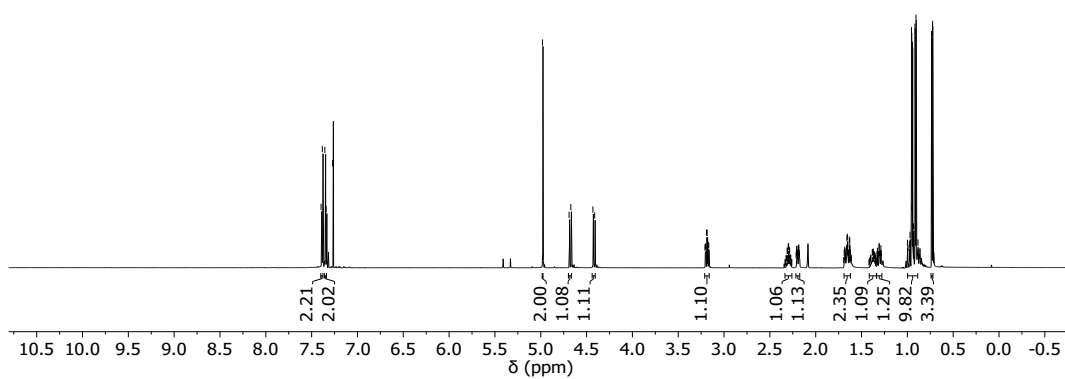


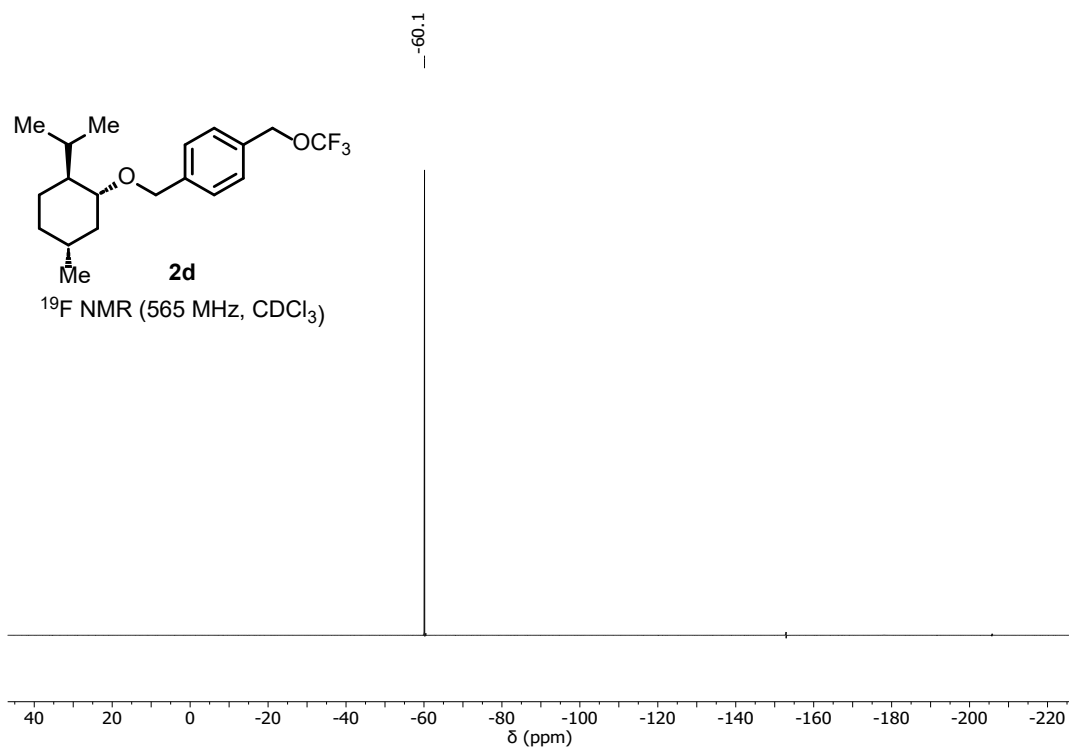
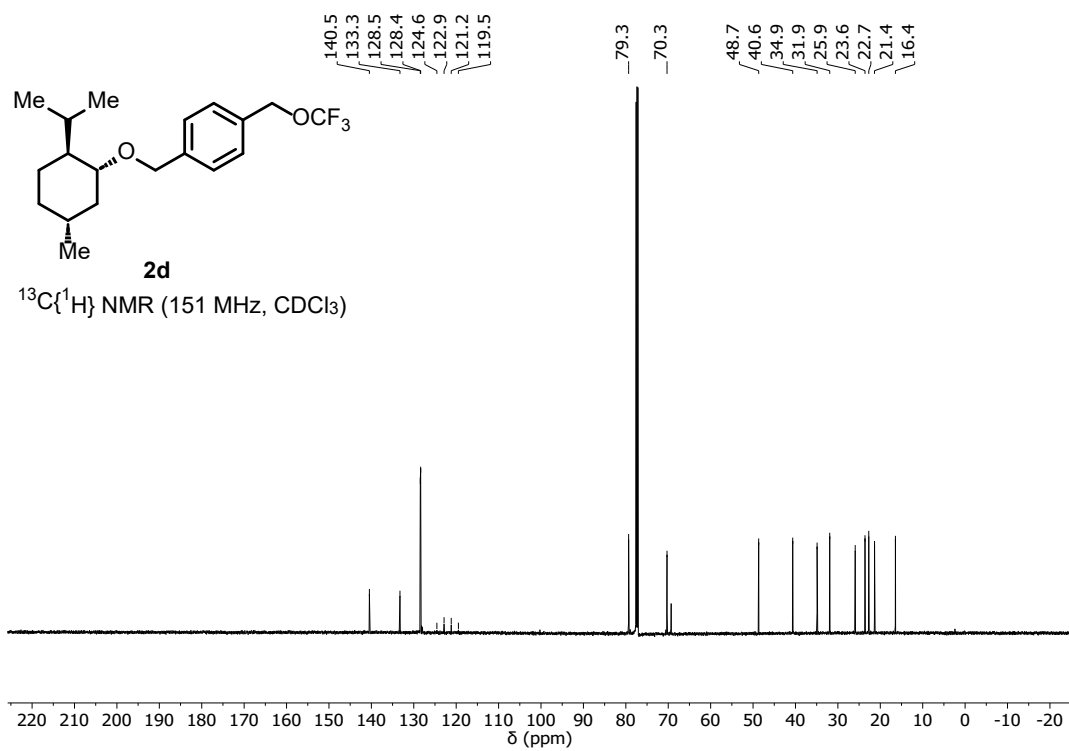
1-(((1*R*,2*S*,5*R*)-2-isopropyl-5-methylcyclohexyl)oxy)methyl)-4-(trifluoromethoxy)methyl)benzene **2d**

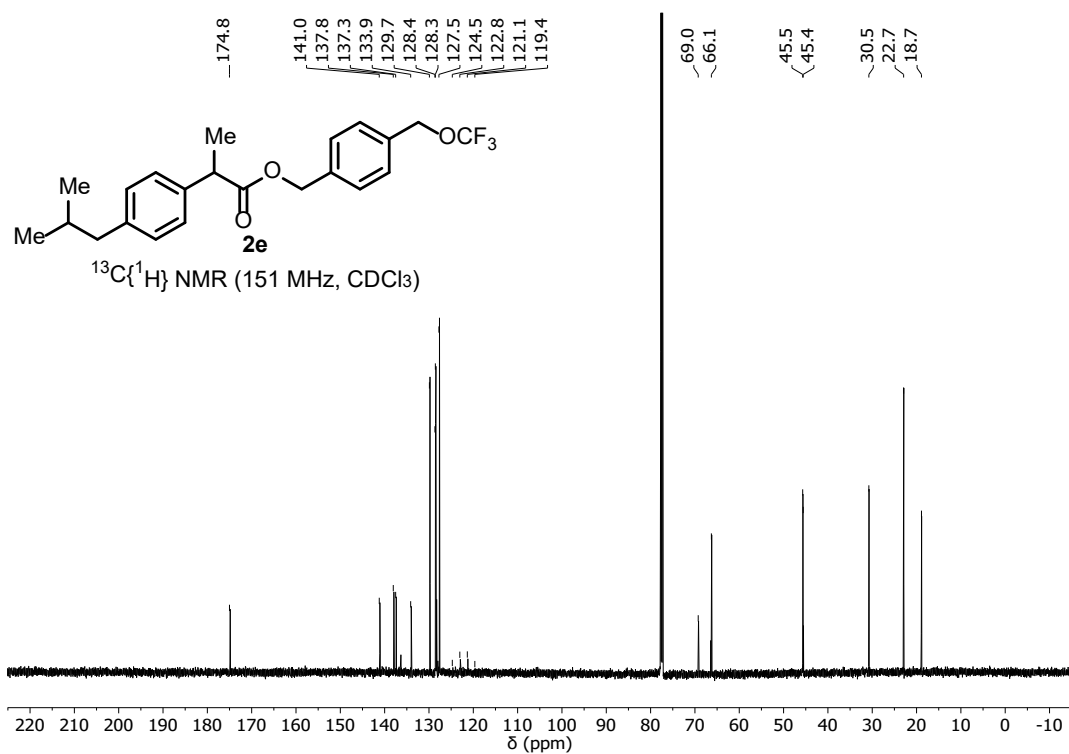
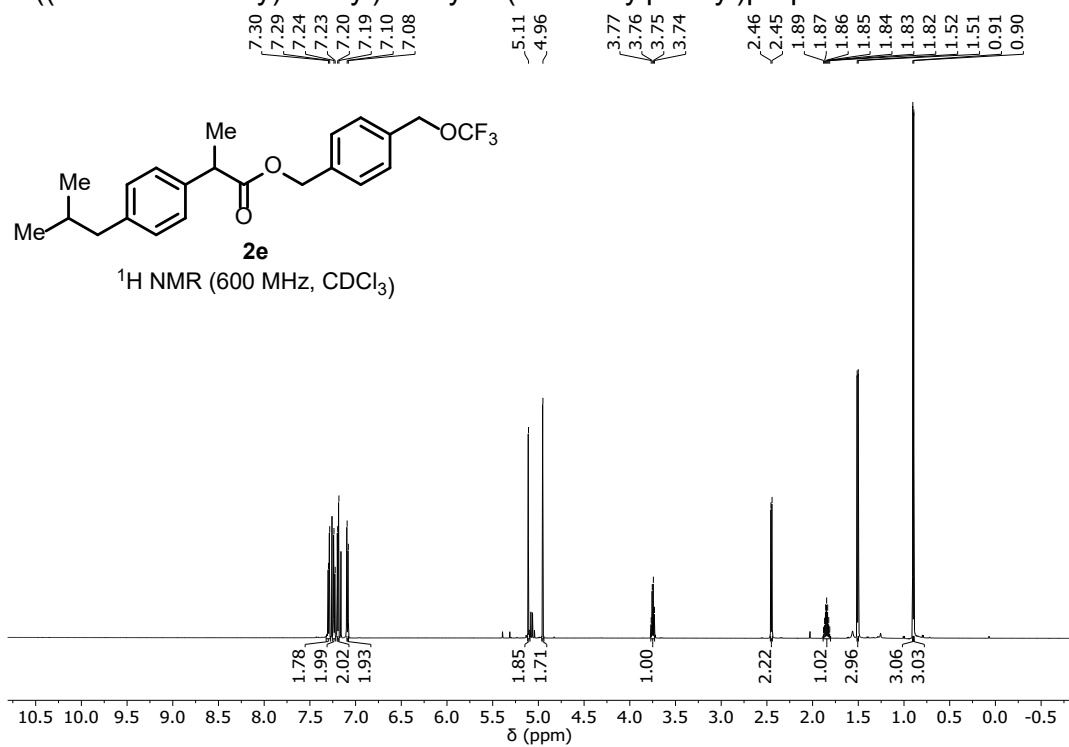
7.39, 7.37, 7.34, 7.33, 7.26, 4.97, 4.68, 4.66, 4.42, 4.40, 3.20, 3.19, 3.18, 3.17, 3.16, 3.16, 2.30, 2.29, 2.28, 2.28, 2.27, 2.20, 2.19, 2.18, 2.17, 1.67, 1.65, 1.65, 1.64, 1.64, 1.62, 1.62, 1.30, 1.30, 1.30, 1.28, 0.99, 0.98, 0.97, 0.96, 0.94, 0.94, 0.93, 0.92, 0.91, 0.90, 0.87, 0.73, 0.71

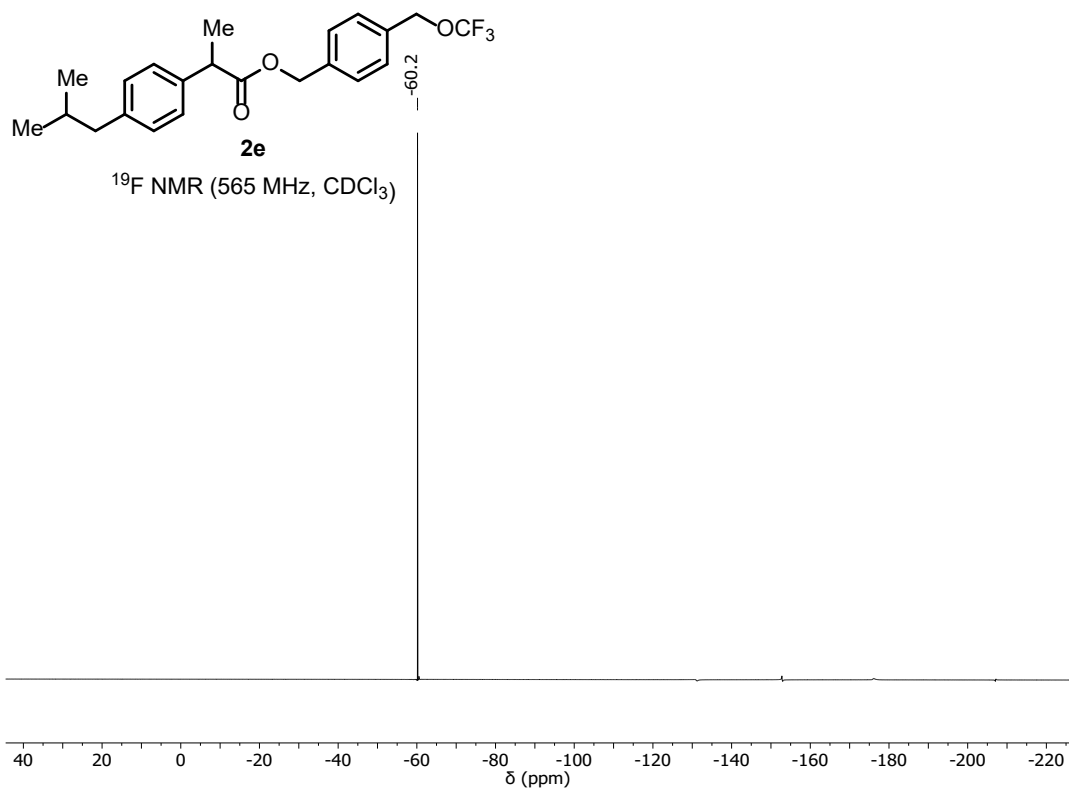


¹H NMR (600 MHz, CDCl₃)

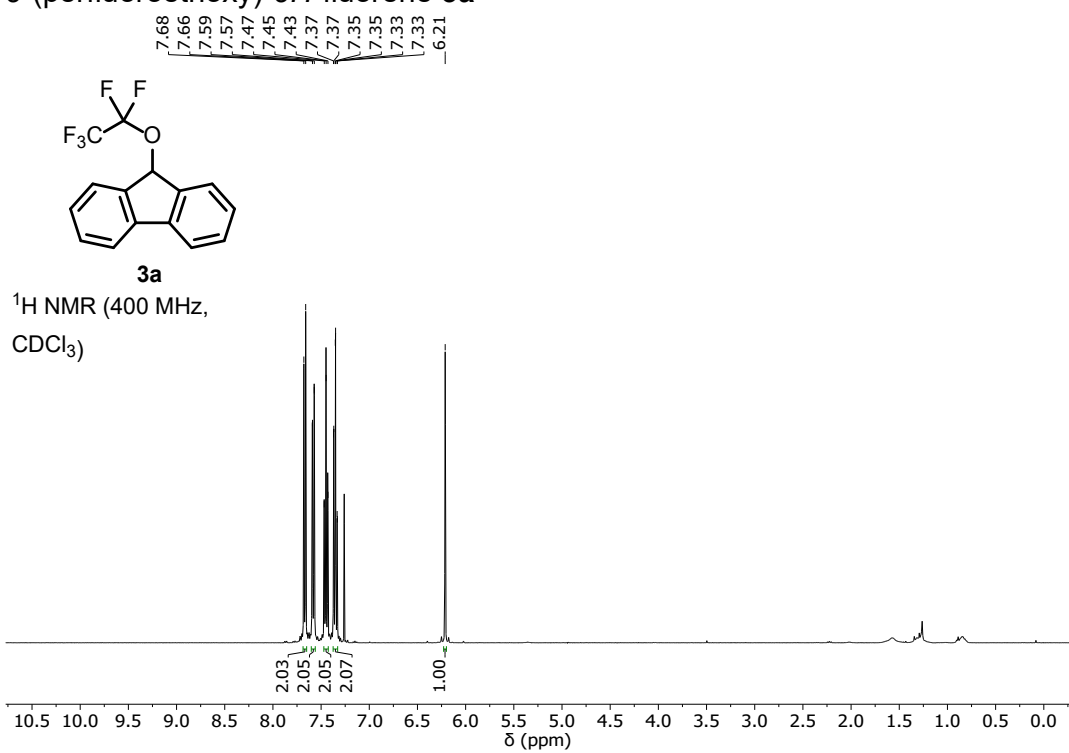


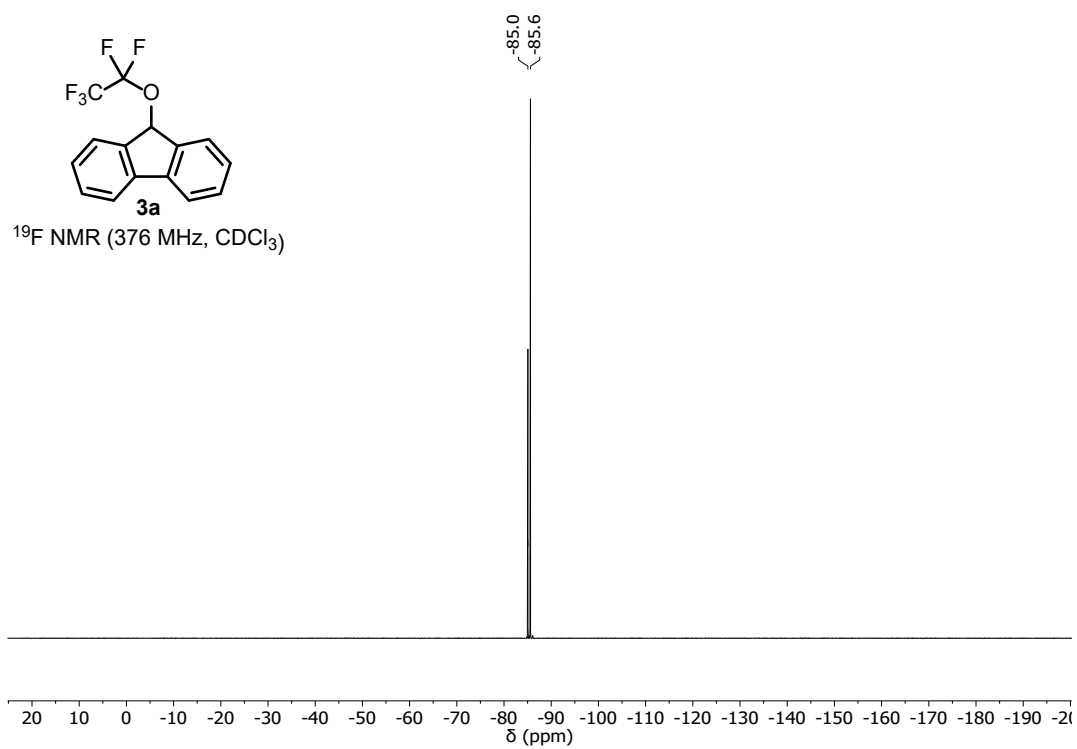
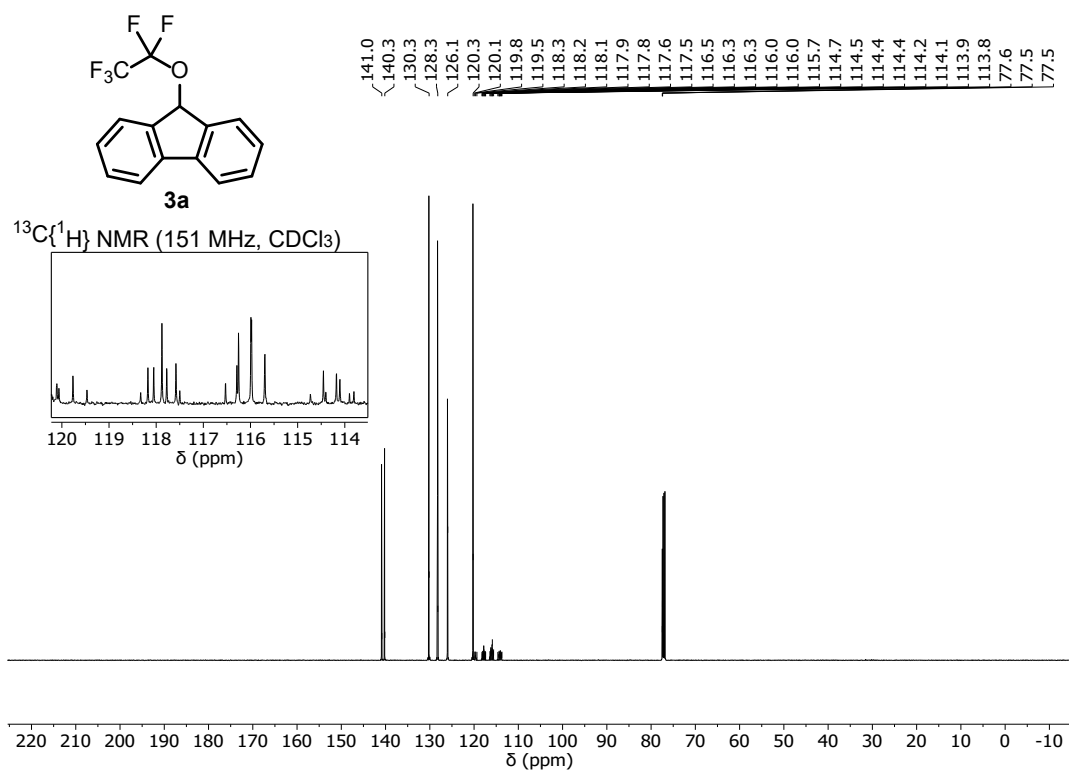


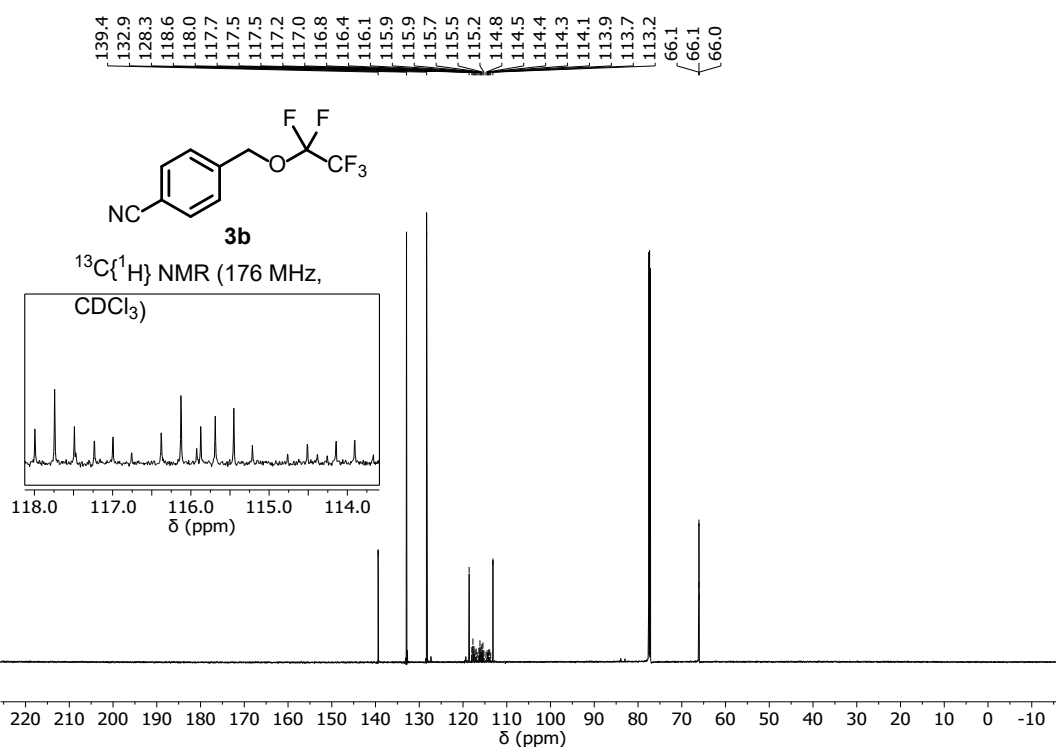
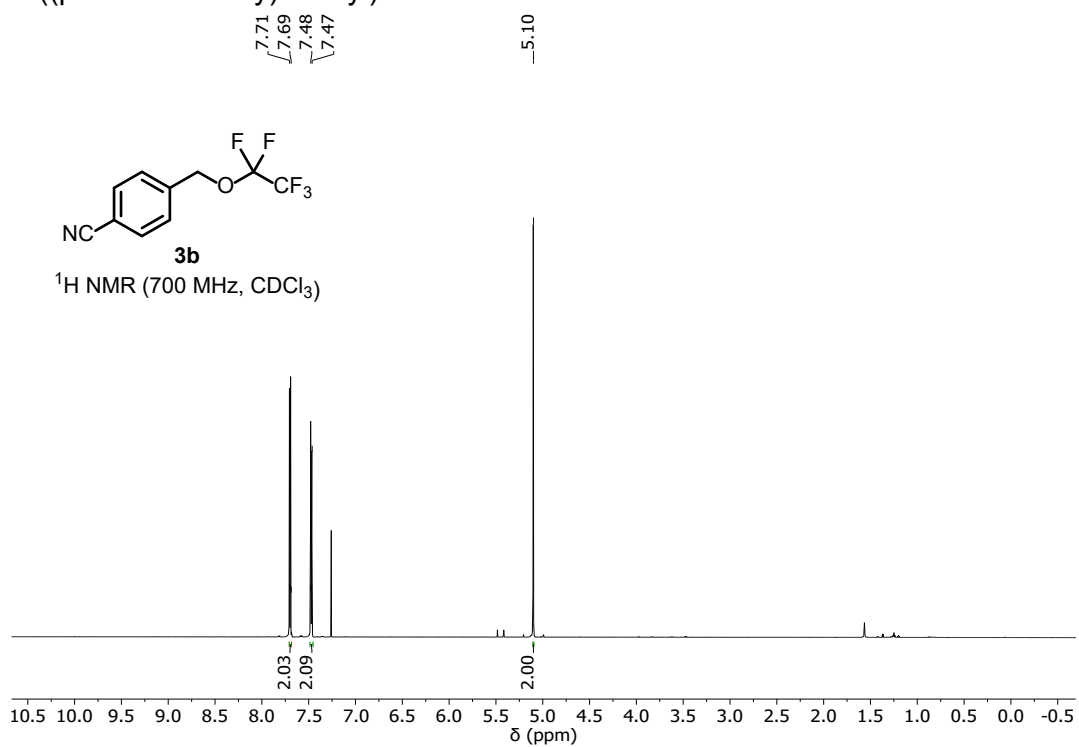
4-((trifluoromethoxy)methyl)benzyl 2-(4-isobutylphenyl)propanoate **2e**

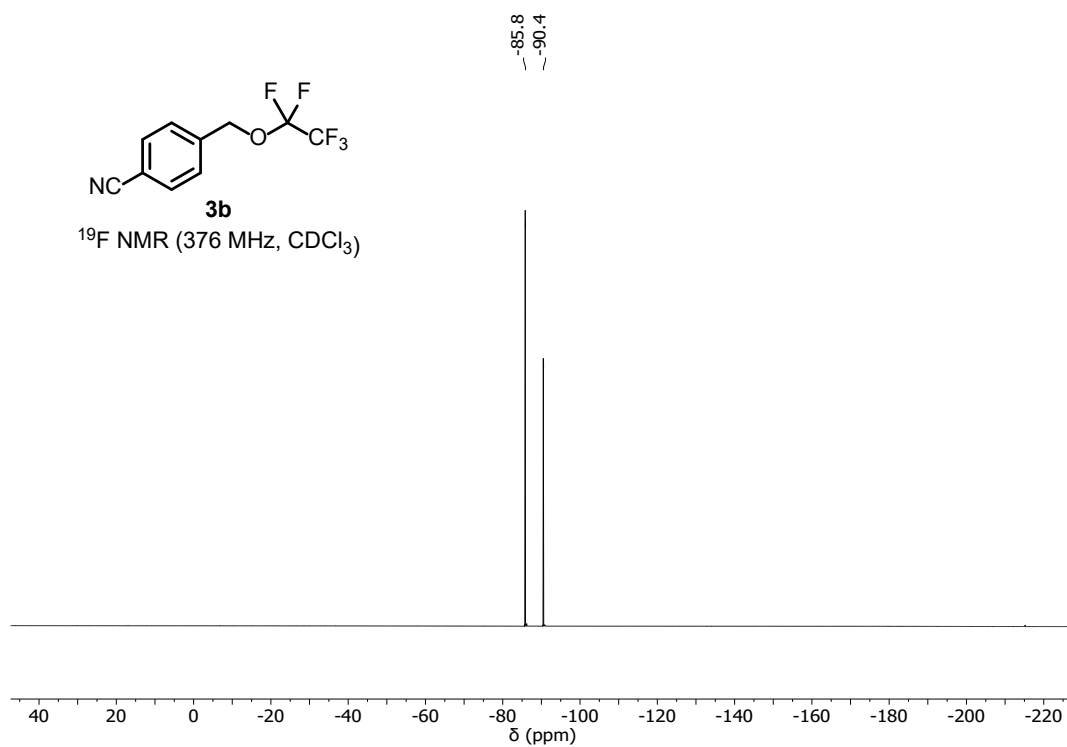


9-(perfluoroethoxy)-9H-fluorene 3a

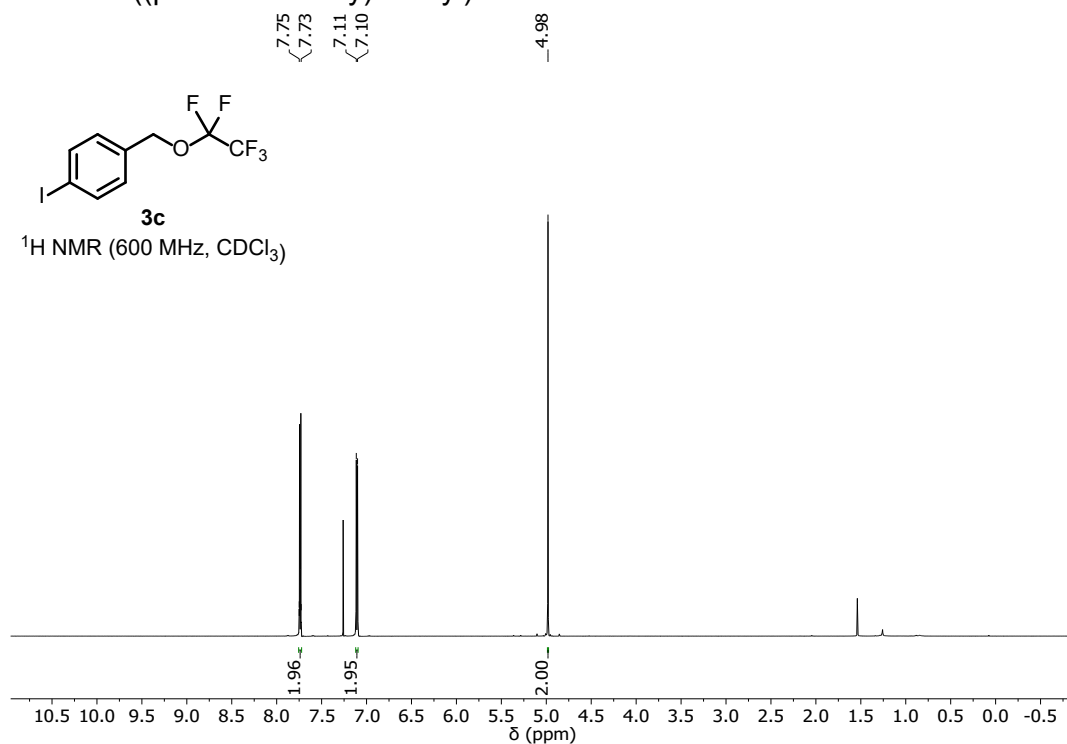


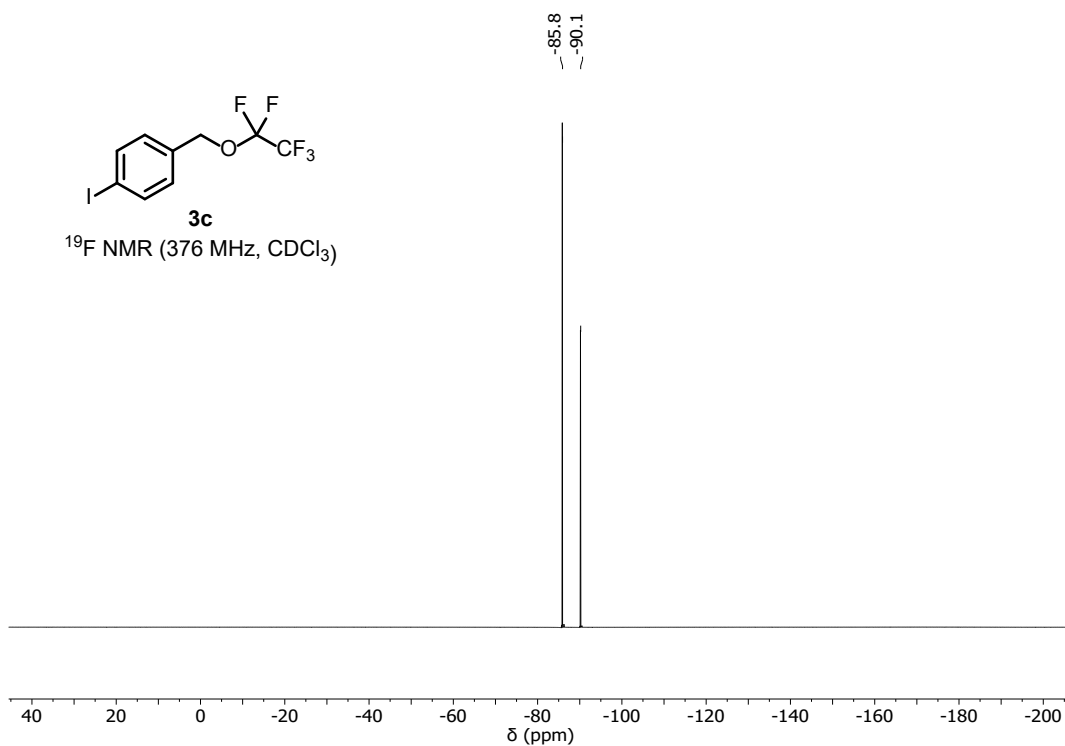
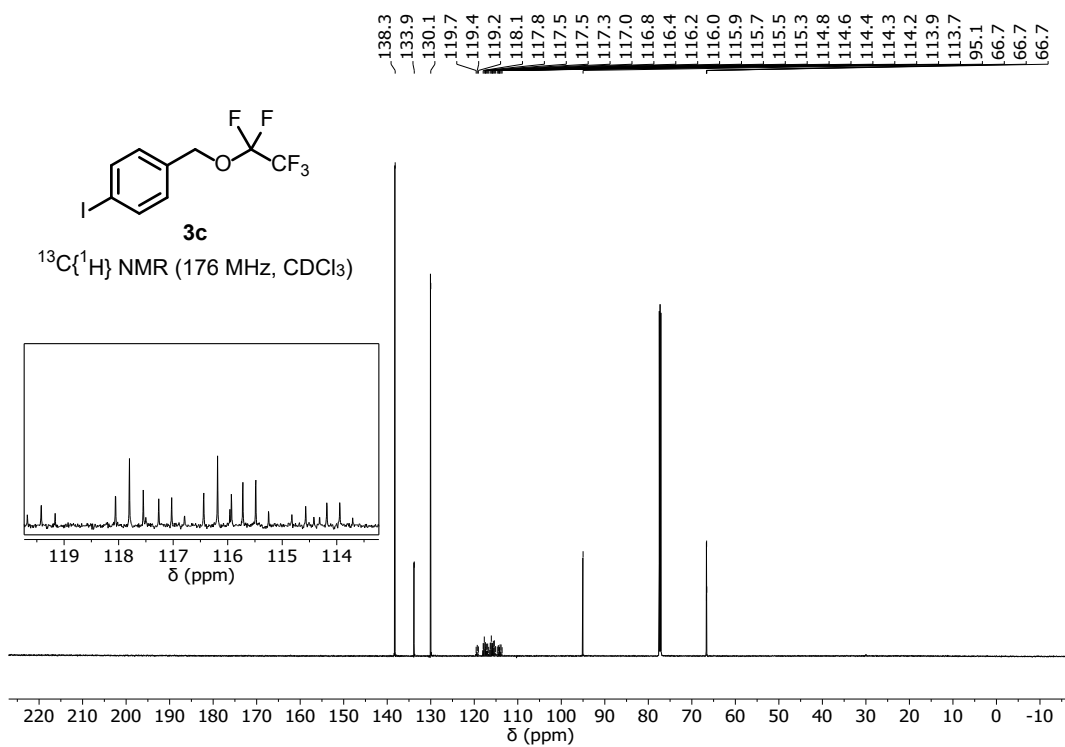


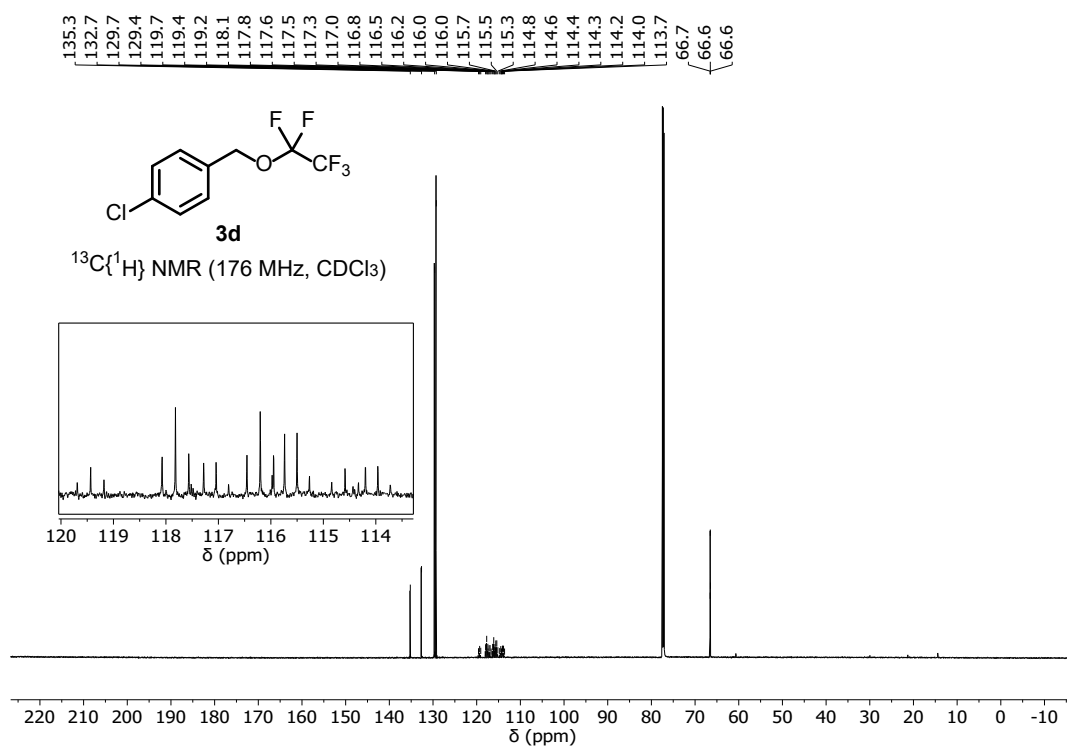
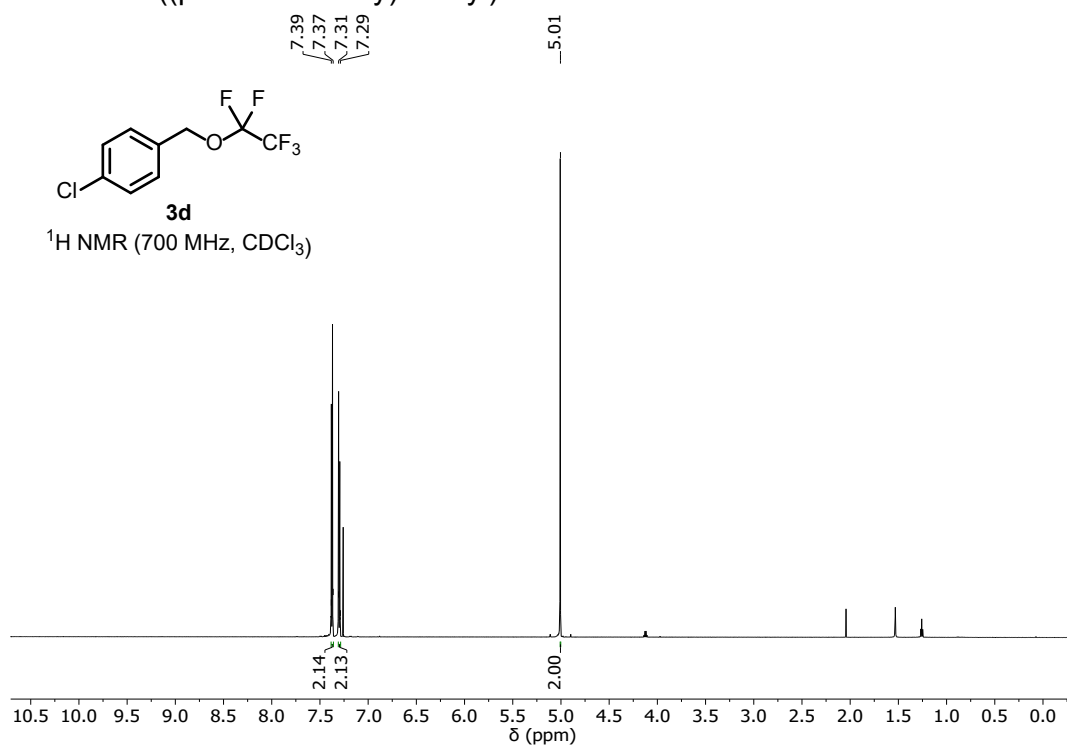
4-((perfluoroethoxy)methyl)benzonitrile **3b**

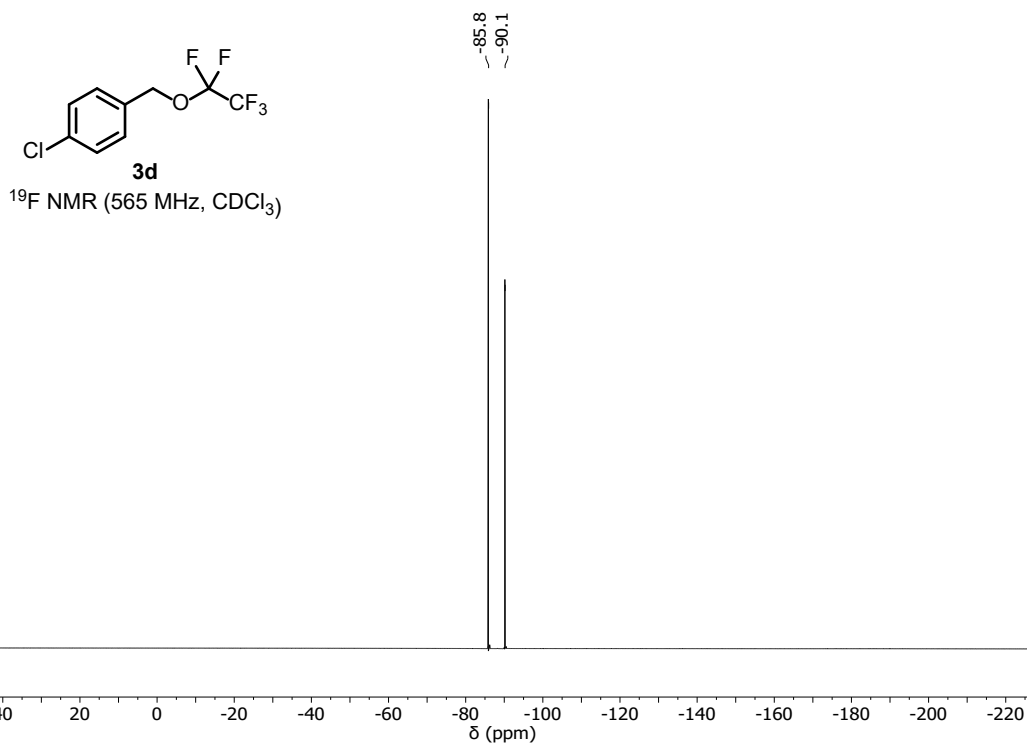


1-iodo-4-((perfluoroethoxy)methyl)benzene **3c**

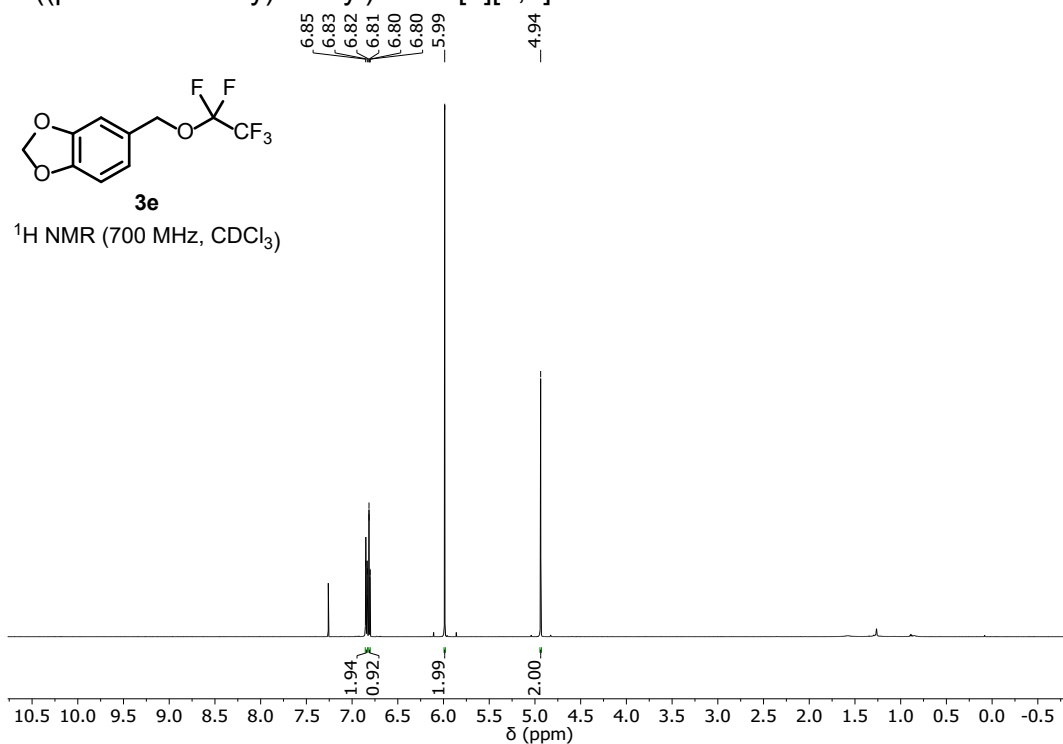


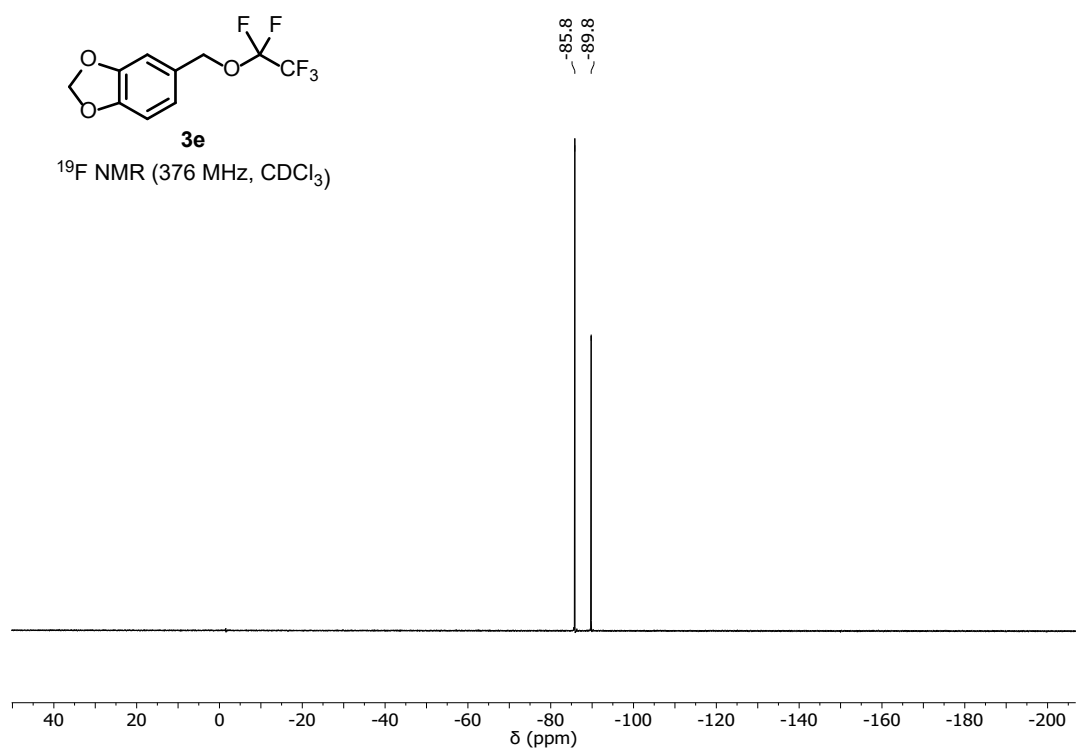
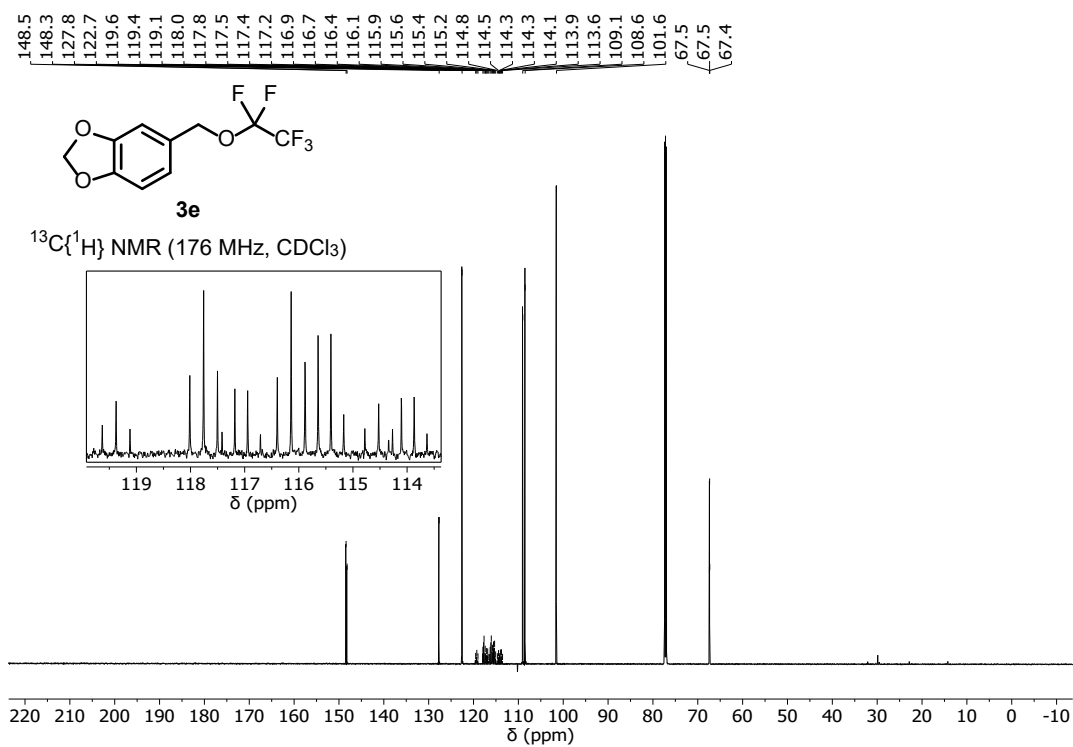


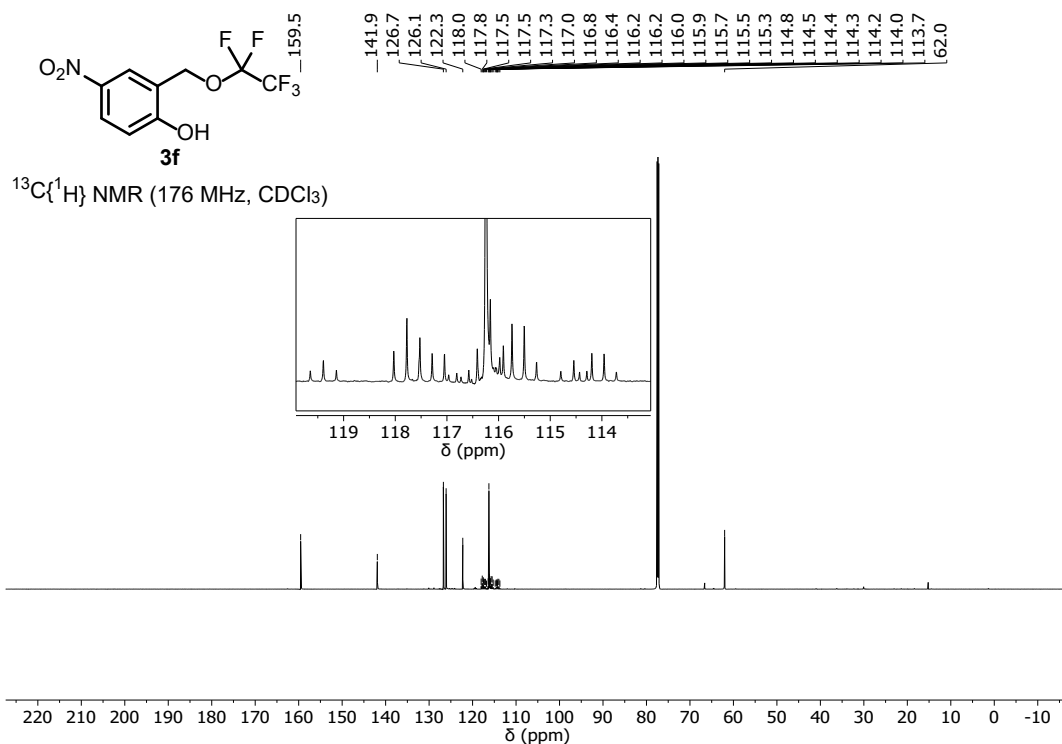
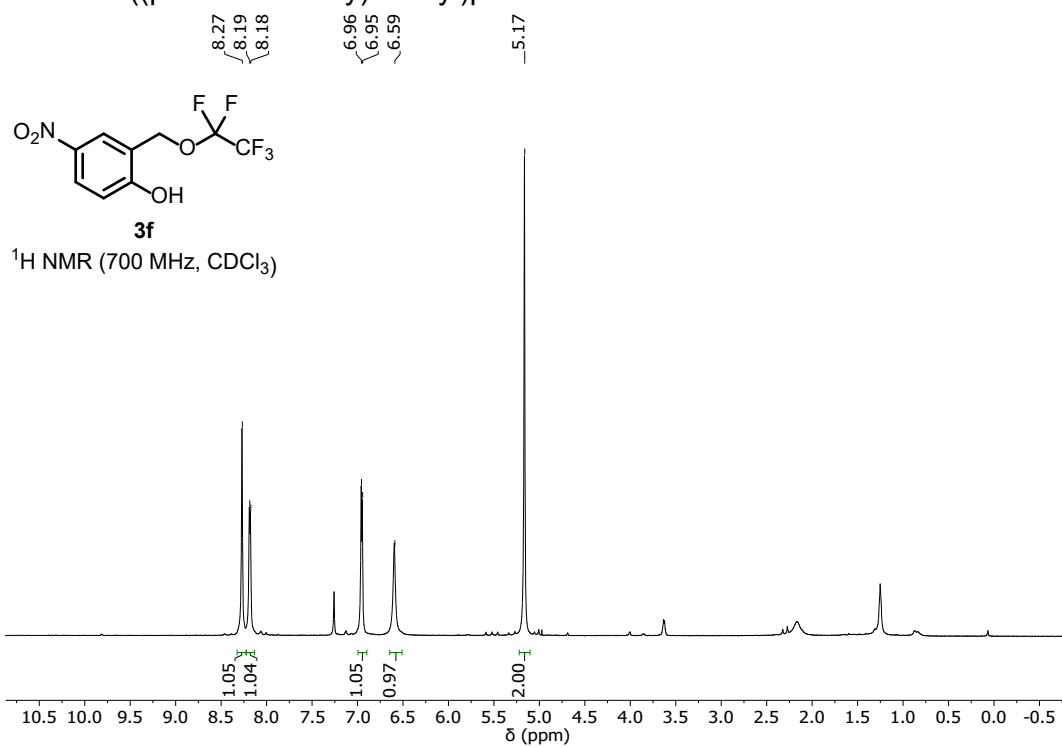
1-chloro-4-((perfluoroethoxy)methyl)benzene **3d**

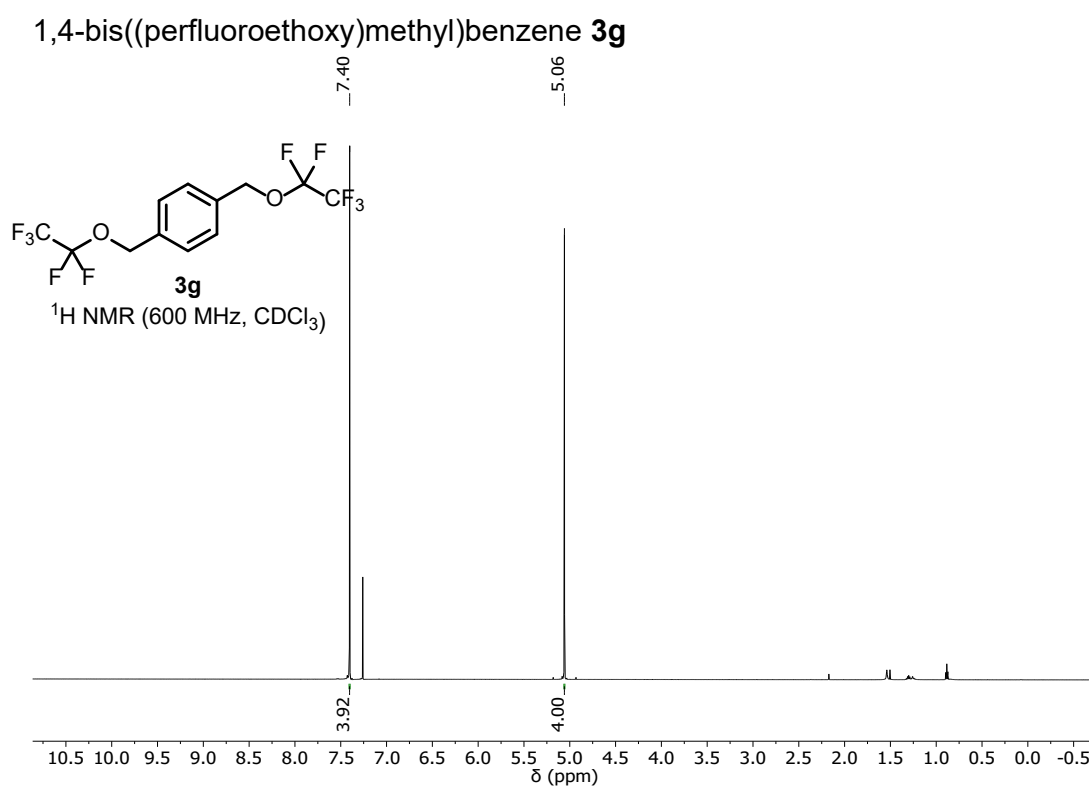
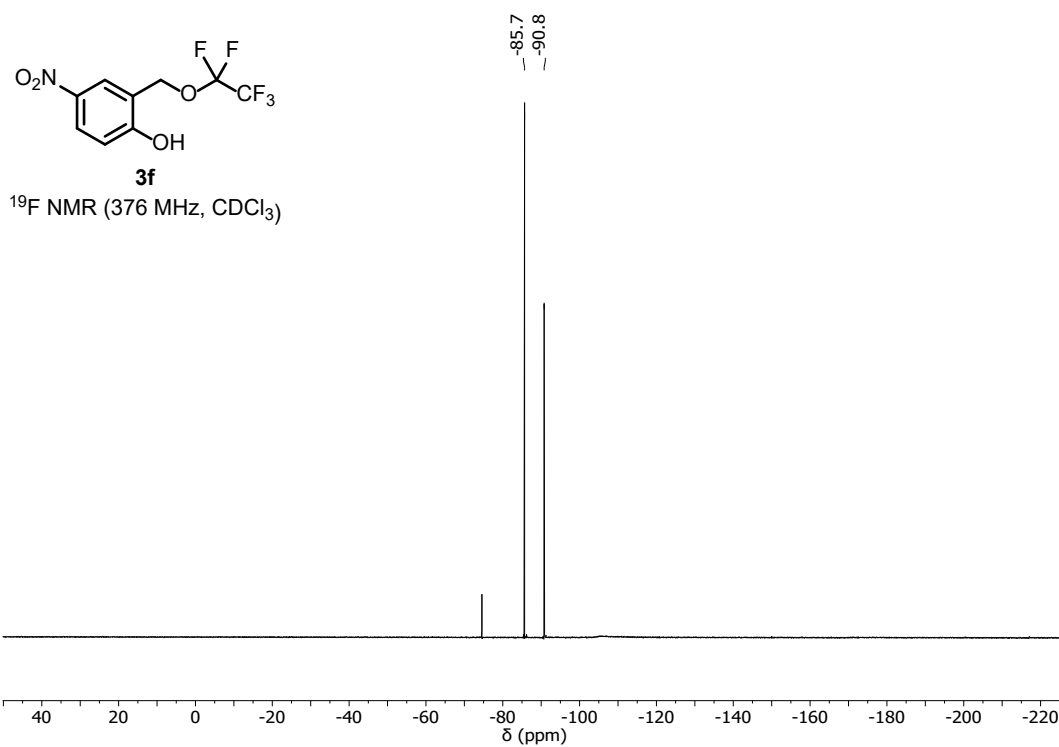


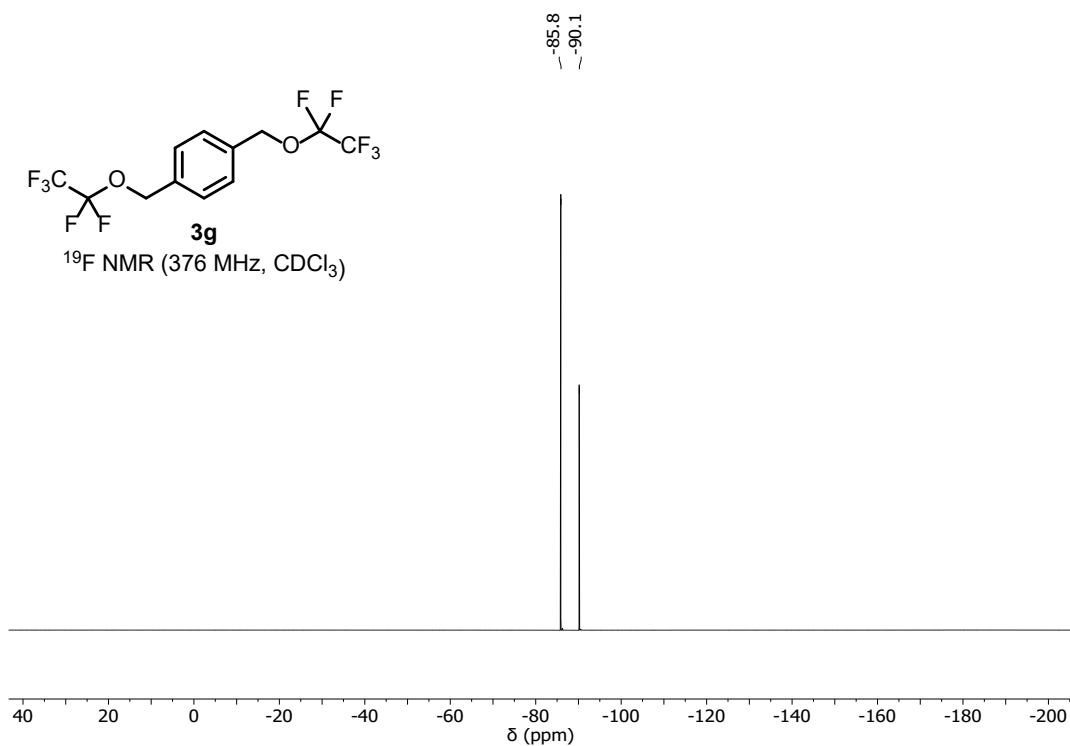
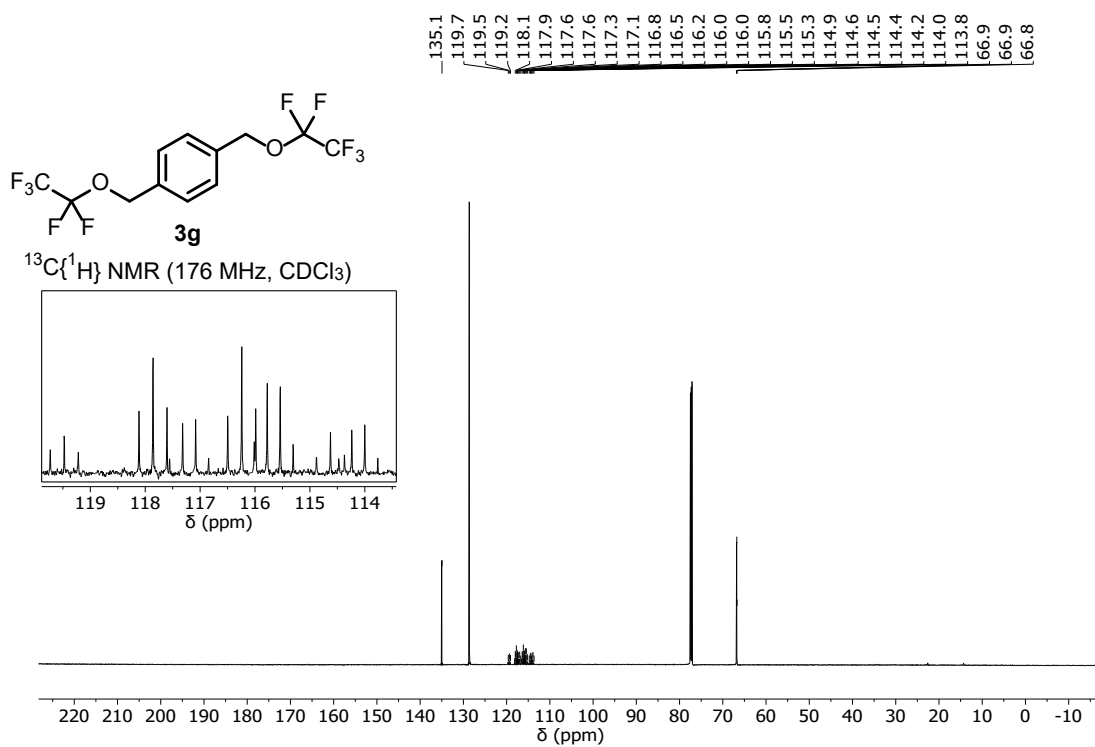
5-((perfluoroethoxy)methyl)benzo[d][1,3]dioxole **3e**

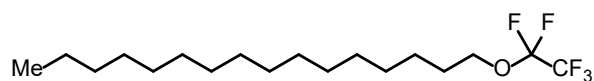
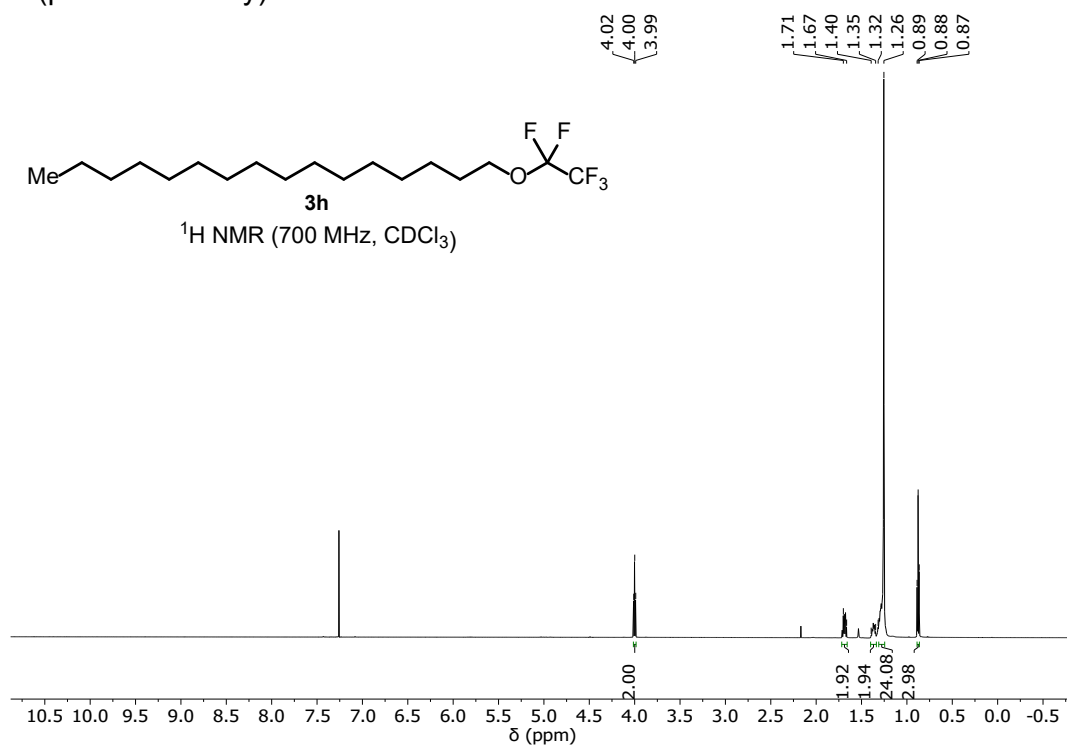




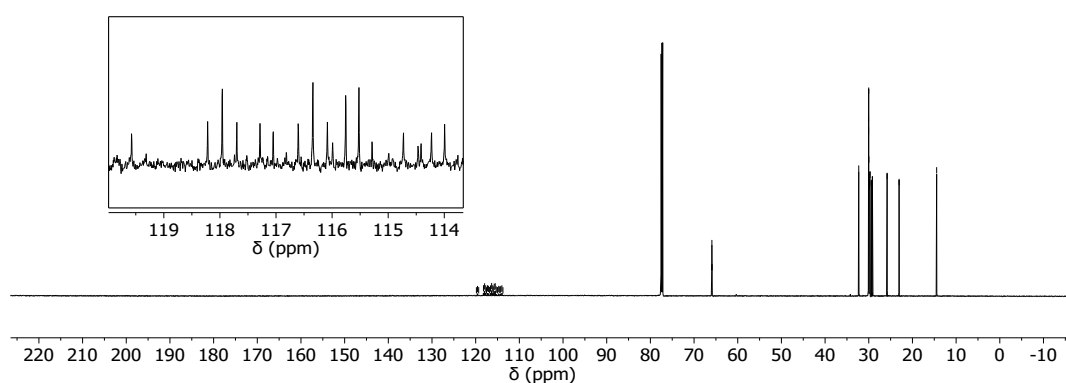
4-nitro-2-((perfluoroethoxy)methyl)phenol **3f**

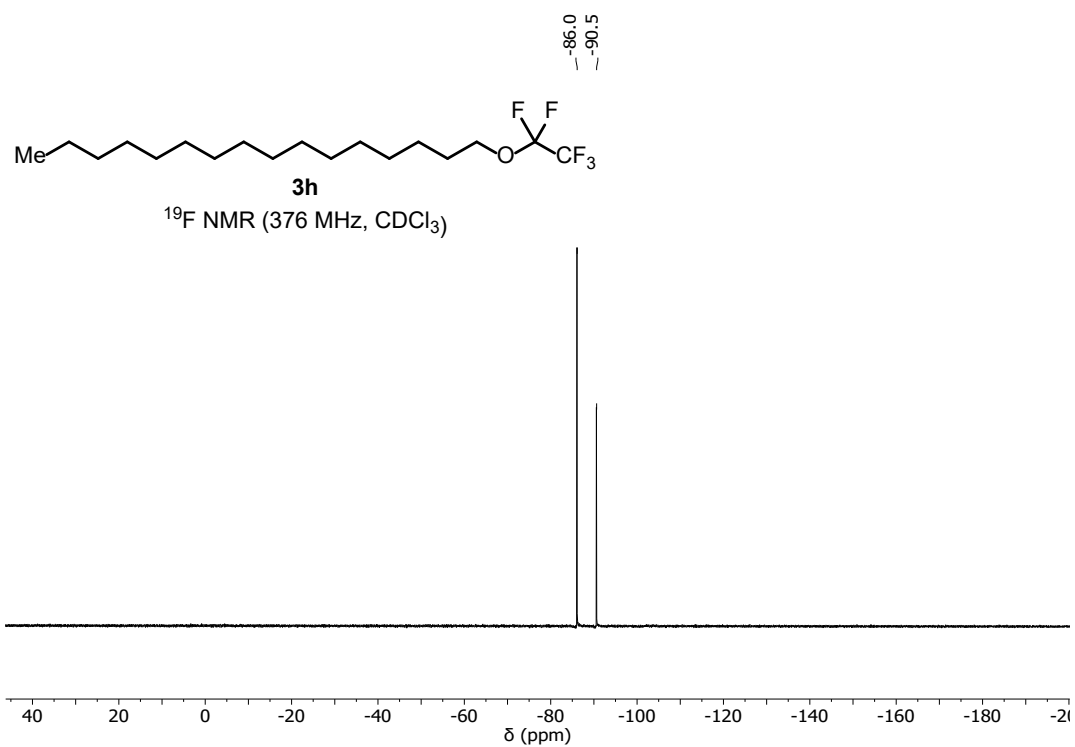




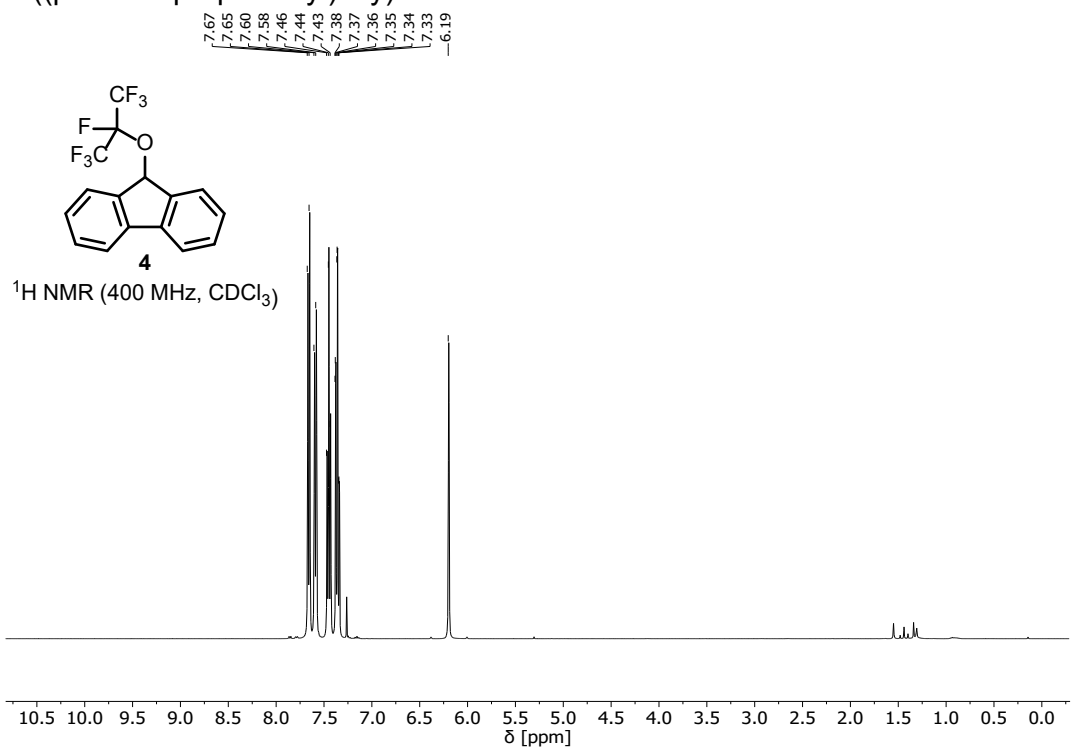
1-(perfluoroethoxy)hexadecane **3h**

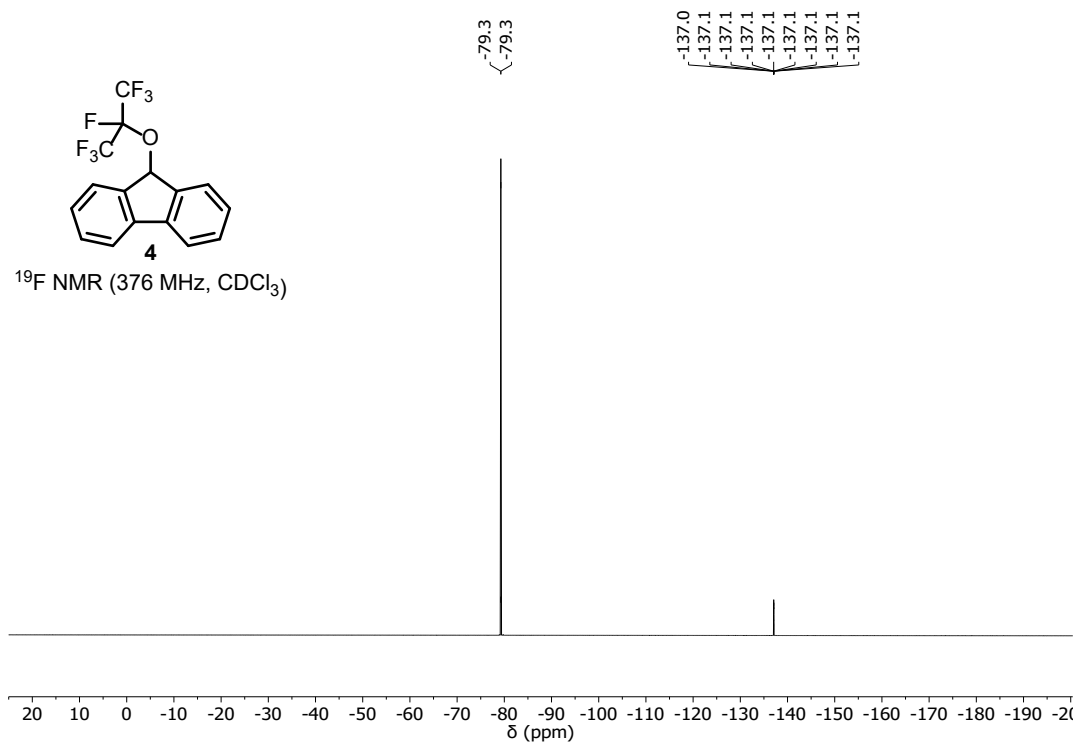
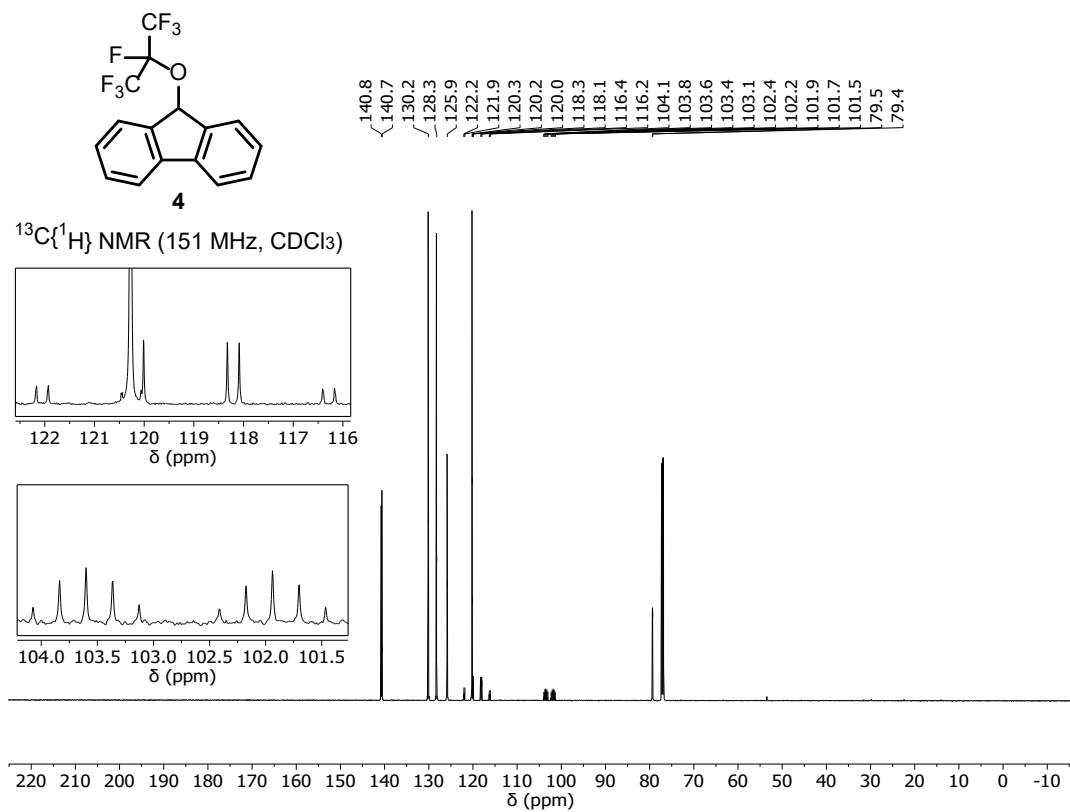
$^{13}\text{C}\{^1\text{H}\}$ NMR (176 MHz, CDCl_3)

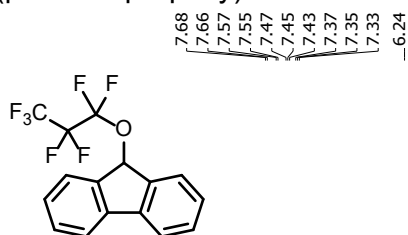
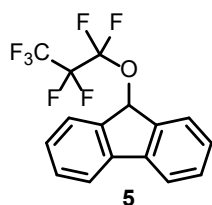
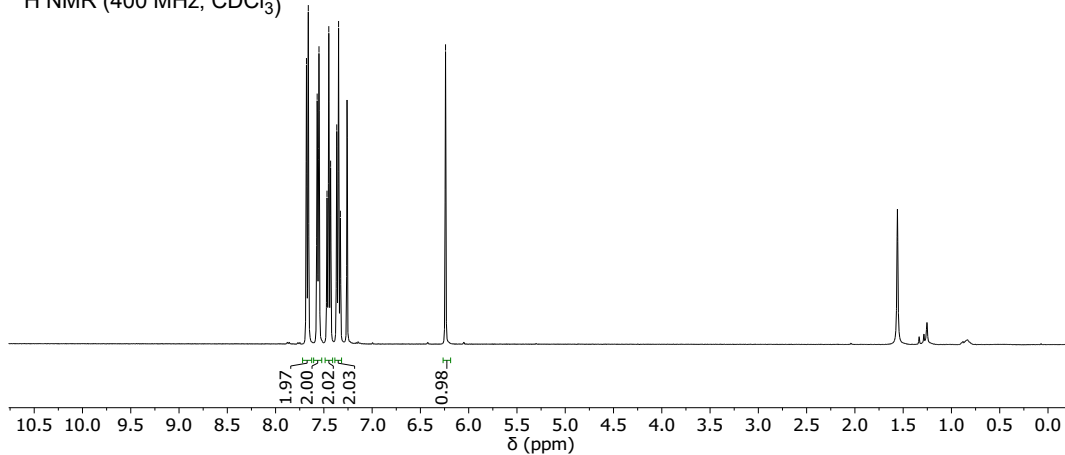
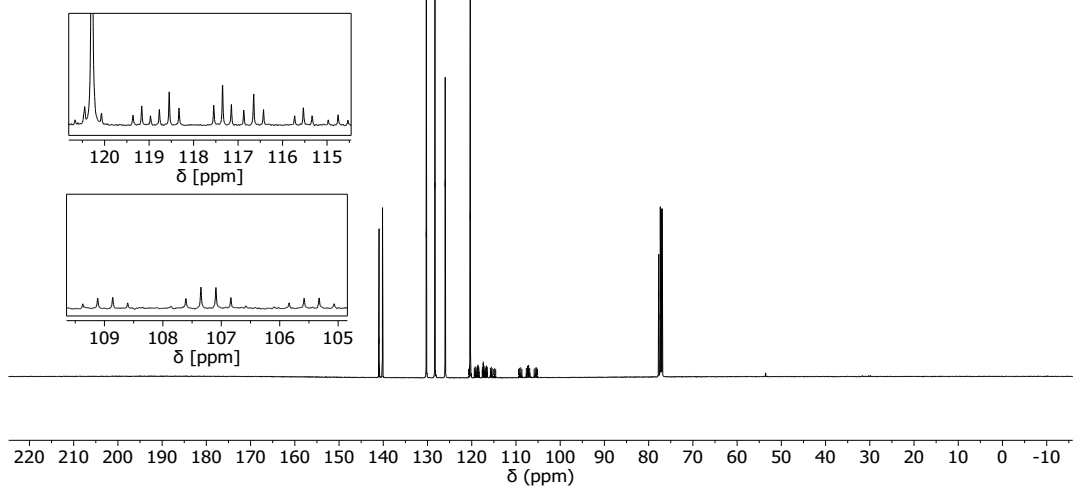


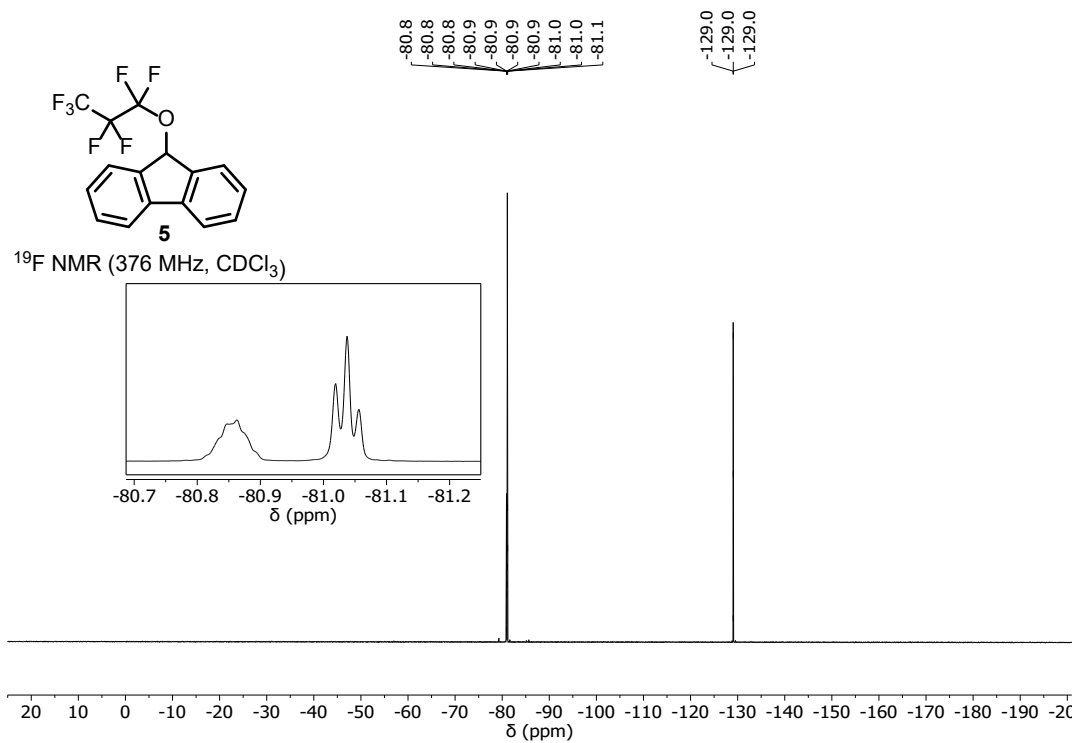


9-((perfluoropropan-2-yl)oxy)-9H-fluorene 4

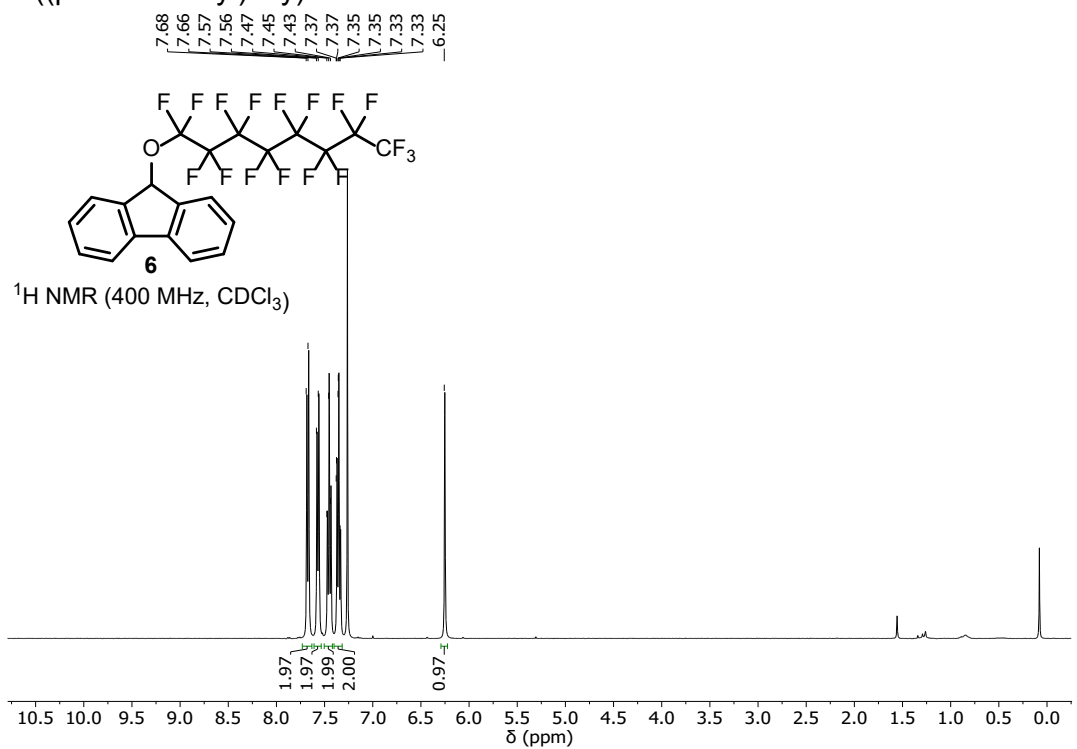


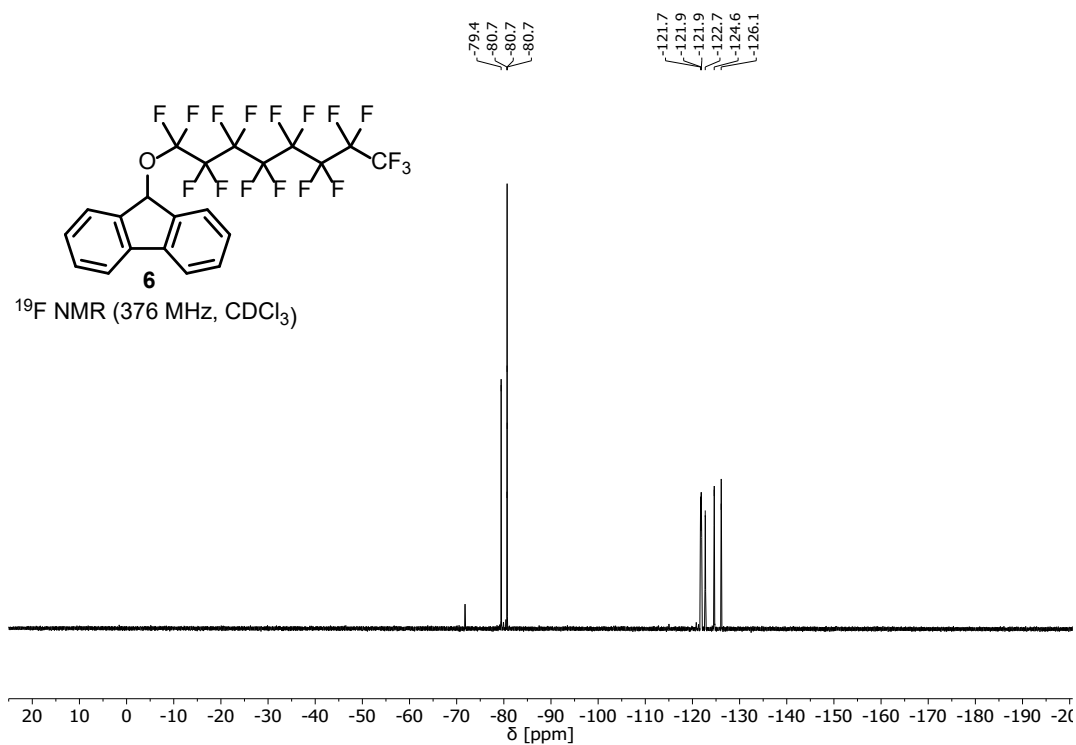
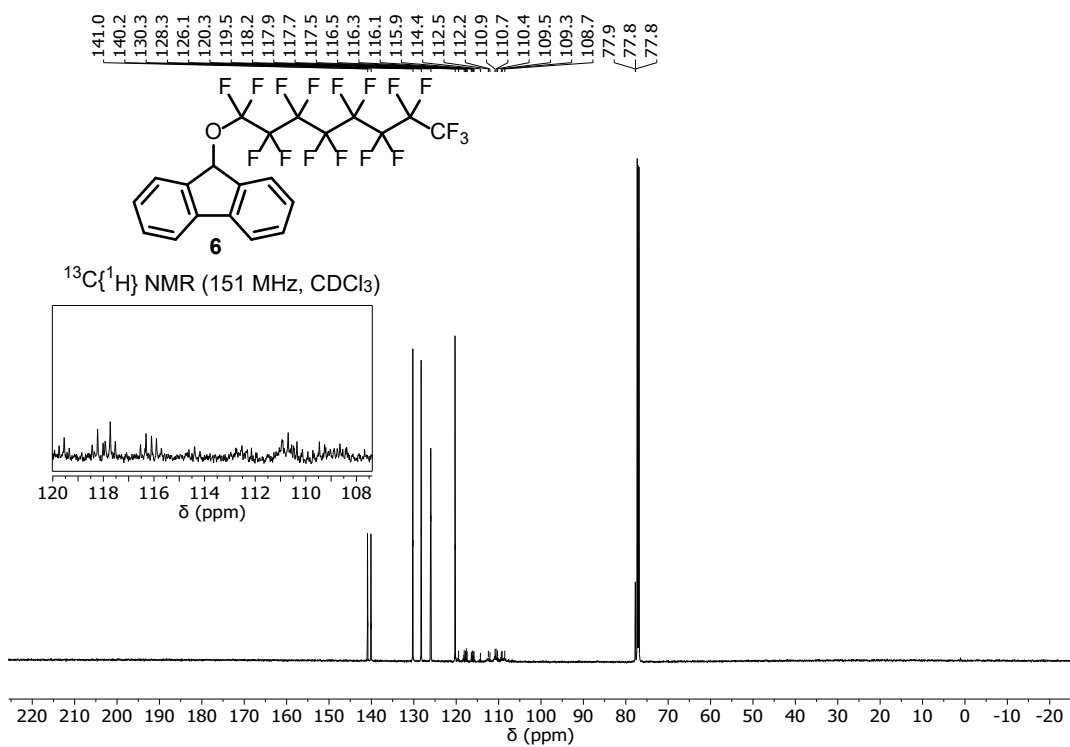


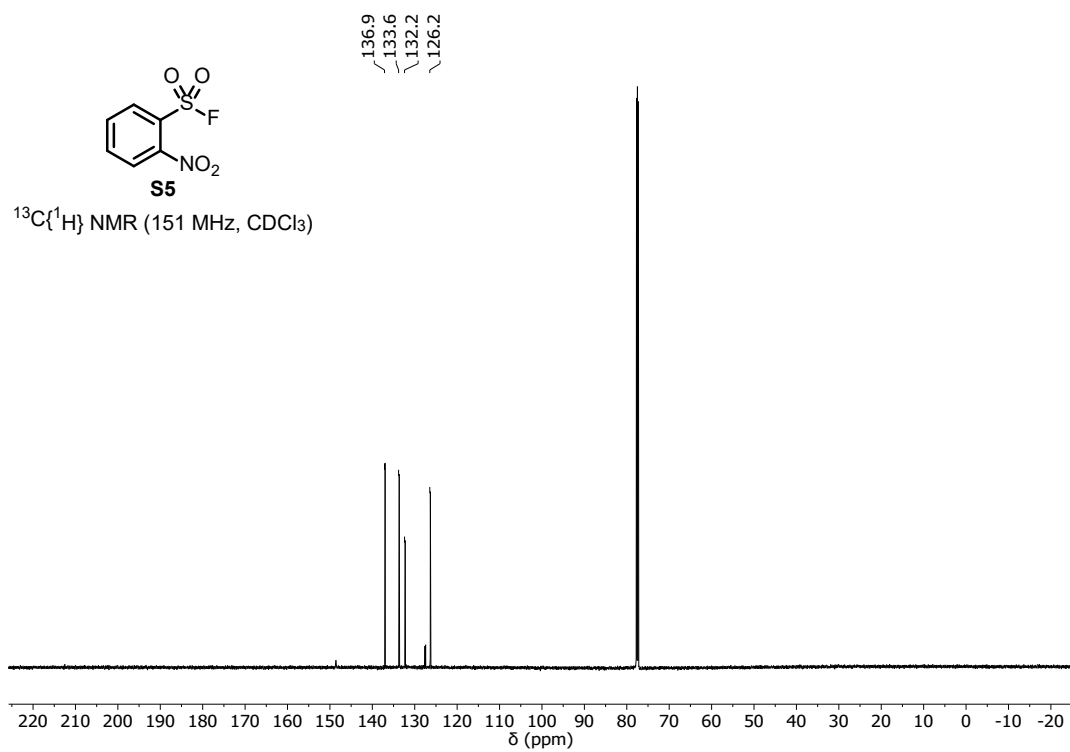
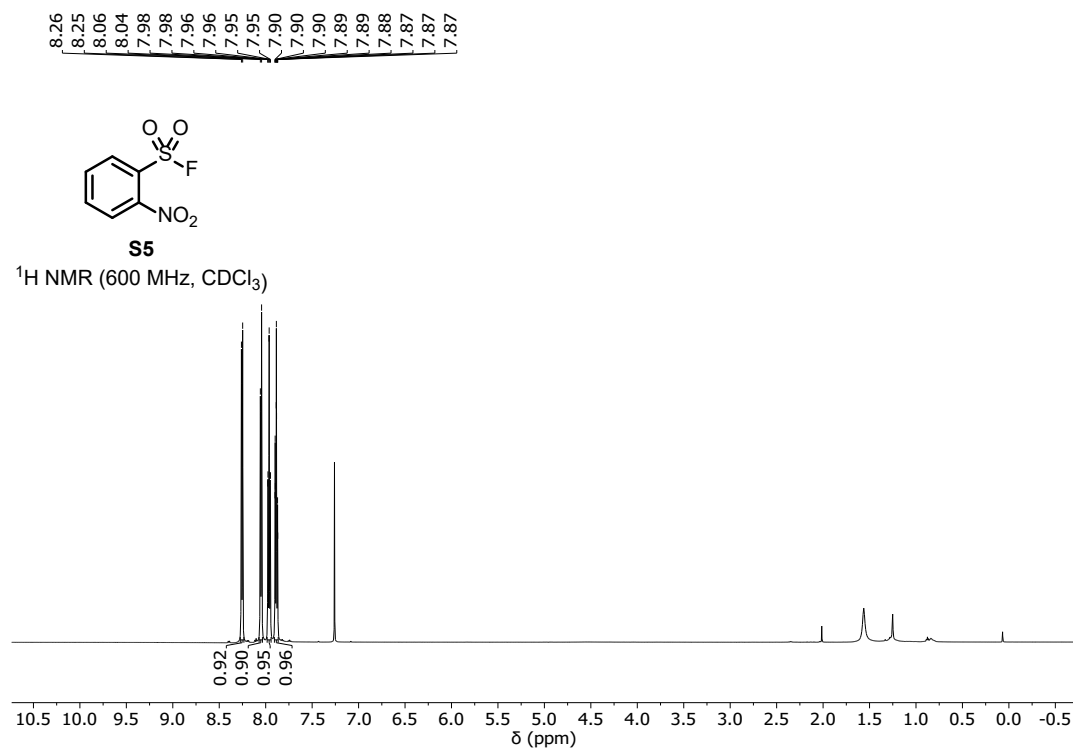
9-(perfluoropropoxy)-9H-fluorene **5****5** ^1H NMR (400 MHz, CDCl_3)**5** $^{13}\text{C}\{^1\text{H}\}$ NMR (151 MHz, CDCl_3)

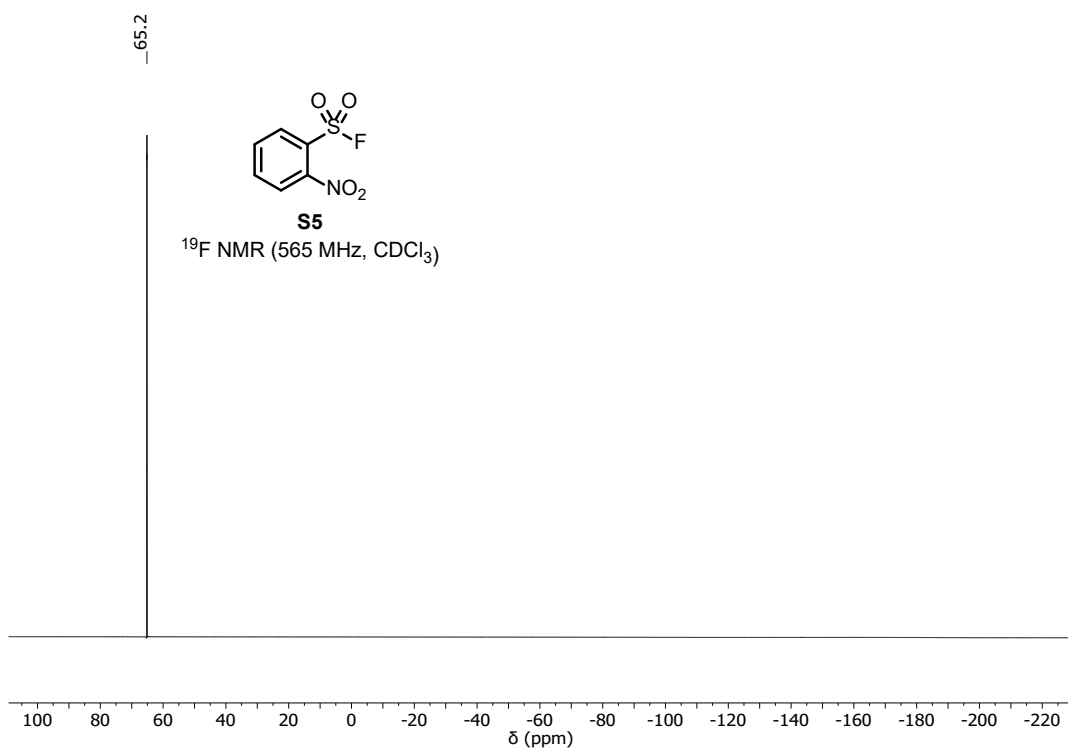


9-((perfluorooctyl)oxy)-9H-fluorene 6





2-nitrobenzenesulfonyl fluoride **S5**



References

- [47] A. López-Pérez, J. Adrio, J. C. Carretero, *Org. Lett.* **2009**, *11*, 5514.
- [48] C. J. J. Hall, I. S. Marriott, K. E. Christensen, A. J. Day, W. R. F. Goundry, T. J. Donohoe, *Chem. Commun.* **2022**, *58*, 4966.
- [49] X. Zhu, M. Jiang, X. Li, E. Zhu, Q. Deng, X. Song, J. Lv, D. Yang, *Org. Chem. Front.* **2022**, *9*, 347.
- [50] M. Yang, J. Fang, H. Liu, X. Lu, J. Zhou, Z. Mou, H. Wang, *Adv. Synth. Catal.* **2023**, *365*, 1806.
- [51] W. Zhang, J. Chen, J.-H. Lin, J.-C. Xiao, Y.-C. Gu, *iScience* **2018**, *5*, 110.
- [52] O. Marrec, T. Billard, J.-P. Vors, S. Pazenok, B. R. Langlois, *J. Fluorine Chem.* **2010**, *131*, 200.
- [53] M.-L. Fu, J.-B. Liu, X.-H. Xu, F.-L. Qing, *J. Org. Chem.* **2017**, *82*, 3702.
- [54] D. Louvel, A. Chelagha, J. Rouillon, P.-A. Payard, L. Khrouz, C. Monnereau, A. Tlili, *Chem. Eur. J.* **2021**, *27*, 8704.

8.2 SI of Trifluoromethyl Fluorosulfonate (CF₃OSO₂F) and Trifluoromethoxy Sulfur Pentafluoride (CF₃OSF₅) – Two Gaseous Sulfur(VI) Compounds with Insulating Properties

Paul Golz[†], Gesa H. Dreyhsig[†], Holger Pernice, Thomas Drews, Jan H. Nissen, Helmut Beckers, Simon Steinhauer, Anja Wiesner, and Sebastian Riedel*

[†] These authors have contributed equally.

Chem. Eur. J. **2024**, *30*, e202400258.

<https://doi.org/10.1002/chem.202400258>

© 2024 The Authors. Published by Wiley-VCH Verlag GmbH.

Chemistry–A European Journal

Supporting Information

Trifluoromethyl Fluorosulfonate (CF₃OSO₂F) and Trifluoromethoxy Sulfur Pentafluoride (CF₃OSF₅) – Two Gaseous Sulfur(VI) Compounds with Insulating Properties

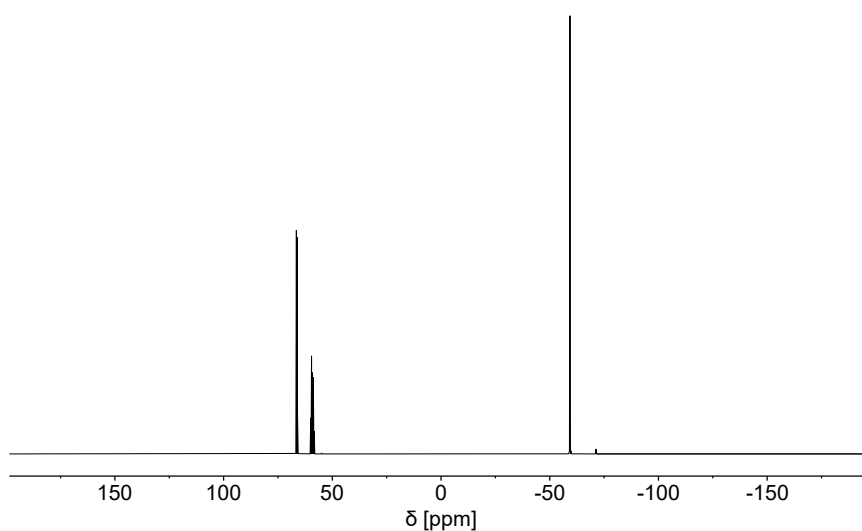
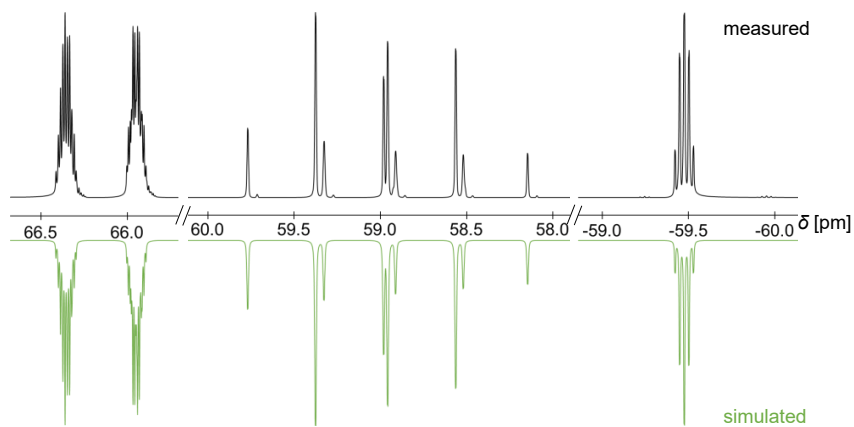
Paul Golz, Gesa H. Dreyhsig, Holger Pernice, Thomas Drews, Jan H. Nissen, Helmut Beckers,
Simon Steinhauer, Anja Wiesner, and Sebastian Riedel*

Table of Contents

Table of Contents	1
1. NMR Spectra	2
1.1. CF ₃ OSF ₅	3
¹⁹ F	3
¹³ C	4
¹⁷ O	4
1.2. CF ₃ OSO ₂ F	5
¹⁹ F	5
¹³ C	5
¹⁷ O	6
2. IR Spectra	7
2.1. CF ₃ OSF ₅	7
1.1. CF ₃ OSO ₂ F	7
2. X-Ray Crystallography	9
3. Quantum Chemical Calculations - Optimized Minimum Structures	10
xyz-Coordinates [Å] of CF ₃ OSO ₂ F on B3LYP-D3/def2-TZVP Level	10
xyz-Coordinates [Å] of [CF ₃ OSO ₂ F] ⁻ on BP86-D3/def2-QZVPP Level	10
xyz-Coordinates [Å] of CF ₃ OSO ₂ F on BP86-D3/def2-QZVPP Level	11
xyz-Coordinates [Å] of [CF ₃ OSO ₂ F] ⁺ on BP86-D3/def2-QZVPP Level	11
xyz-Coordinates [Å] of CF ₃ OSF ₅ on B3LYP-D3/def2-TZVP Level	12
xyz-Coordinates [Å] of [CF ₃ OSF ₅] ⁻ on BP86-D3/def2-QZVPP Level	12
xyz-Coordinates [Å] of CF ₃ OSF ₅ on BP86-D3/def2-QZVPP Level	13
xyz-Coordinates [Å] of [CF ₃ OSF ₅] ⁺ on BP86-D3/def2-QZVPP Level	13
xyz-Coordinates [Å] of CF ₂ O on B3LYP-D3/def2-TZVP Level	13
xyz-Coordinates [Å] of CF ₃ OF on B3LYP-D3/def2-TZVP Level	14
xyz-Coordinates [Å] of SF ₄ on B3LYP-D3/def2-TZVP Level	14
xyz-Coordinates [Å] of SF ₆ on B3LYP-D3/def2-TZVP Level	14
xyz-Coordinates [Å] of SO ₂ on B3LYP-D3/def2-TZVP Level	14
xyz-Coordinates [Å] of SO ₂ F ₂ on B3LYP-D3/def2-TZVP Level	15
4. Determination of Critical Parameters	16
5. Determination of Melting Point	18
6. Determination of Gas Densities	18
7. Determination Vapor Pressures and Boiling Points	19
8. Determination of Dielectric Properties and Breakdown Voltages	21
9. Stability of Dielectric Gases during Breakdown	23
10. Decomposition Products	25

10.1. $\text{CF}_3\text{OSO}_2\text{F}$	25
10.2. CF_3OSF_5	26
10.3. References	27

1. NMR Spectra

1.1. CF_3OSF_5 ^{19}F Figure S 1: ^{19}F NMR spectrum (377 MHz, neat, external capillary, 21 °C) of CF_3OSF_5 .Figure S 2. ^{19}F NMR spectrum (377 MHz, neat, external capillary, 21 °C) of CF_3OSF_5 compared to the simulated spectrum (bottom, green). NMR spectroscopical parameters used in the simulation: $\delta(\text{F}_A) = 58.9$ ppm, $\delta(\text{F}_B) = 66.1$ ppm, $^2J(^{19}\text{F}, ^{19}\text{F}) = 153$ Hz, $^4J(^{19}\text{F}_A, ^{19}\text{F}_{\text{CF}}) = 1.4$ Hz, $^4J(^{19}\text{F}_B, ^{19}\text{F}_{\text{CF}}) = 10.0$ Hz.

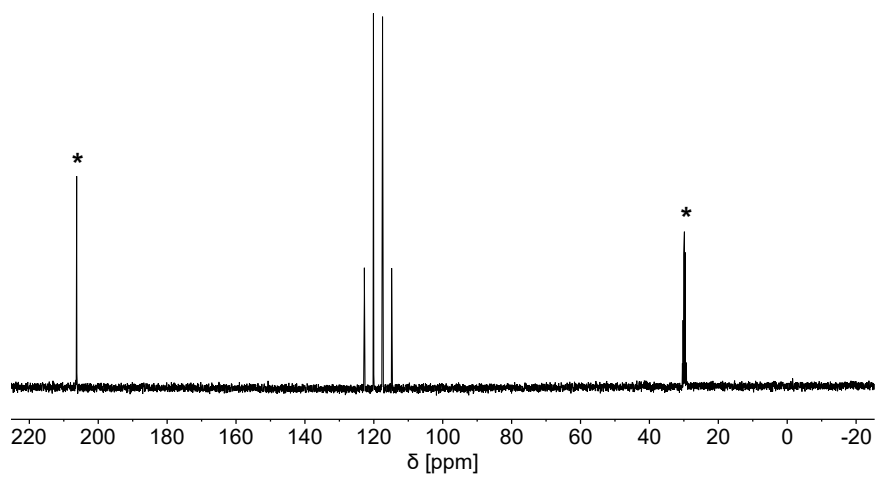
^{13}C 

Figure S 3. ^{13}C $\{^1\text{H}\}$ NMR spectrum (101 MHz, neat, external capillary*, 20 °C) of CF_3OSF_5 .

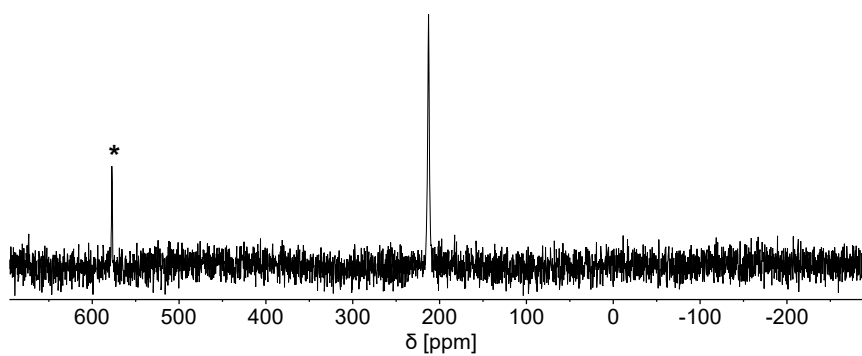
 ^{17}O 

Figure S 4. ^{17}O NMR spectrum (54 MHz, neat, external capillary*, 21 °C) of CF_3OSF_5 .

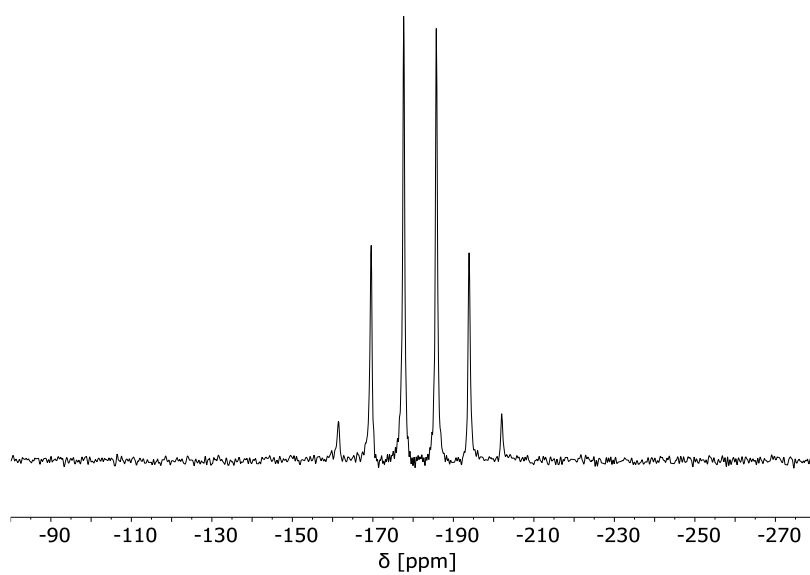
^{33}S 

Figure S 5. ^{33}S NMR spectrum (31 MHz, neat, external capillary, 21 °C) of CF_3OSF_5 .

1.2. $\text{CF}_3\text{OSO}_2\text{F}$
 ^{19}F

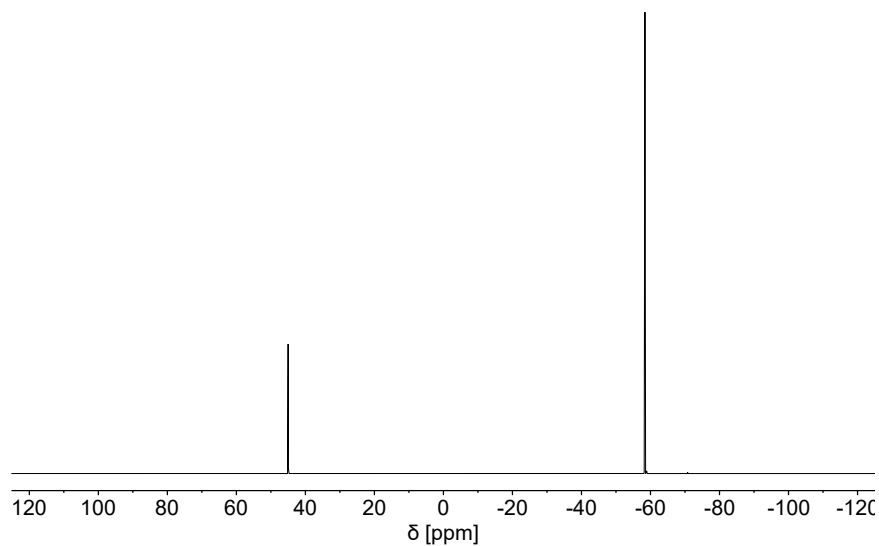


Figure S 6. ^{19}F NMR spectrum (377 MHz, neat, external capillary, 22 °C) of $\text{CF}_3\text{OSO}_2\text{F}$.

^{13}C

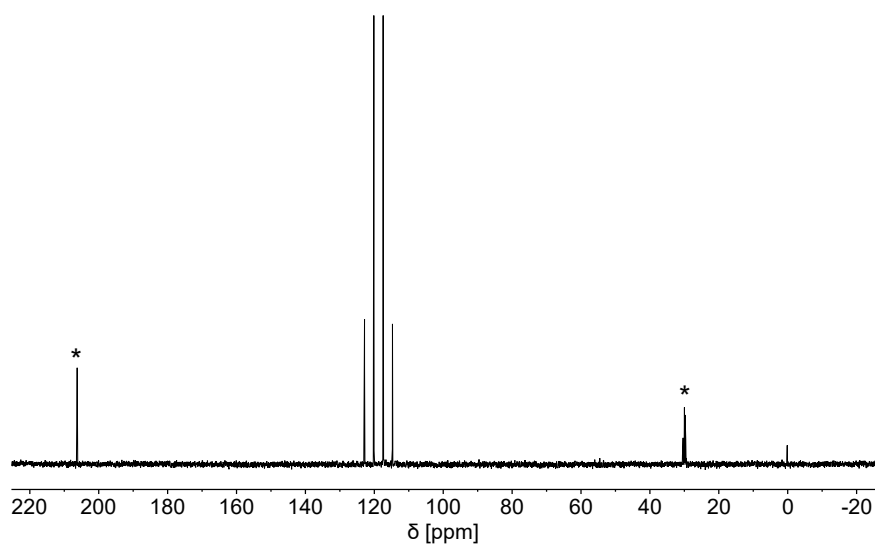


Figure S 7. ^{13}C { ^1H } NMR spectrum (101 MHz, neat, external capillary*, 20 °C) of $\text{CF}_3\text{OSO}_2\text{F}$.

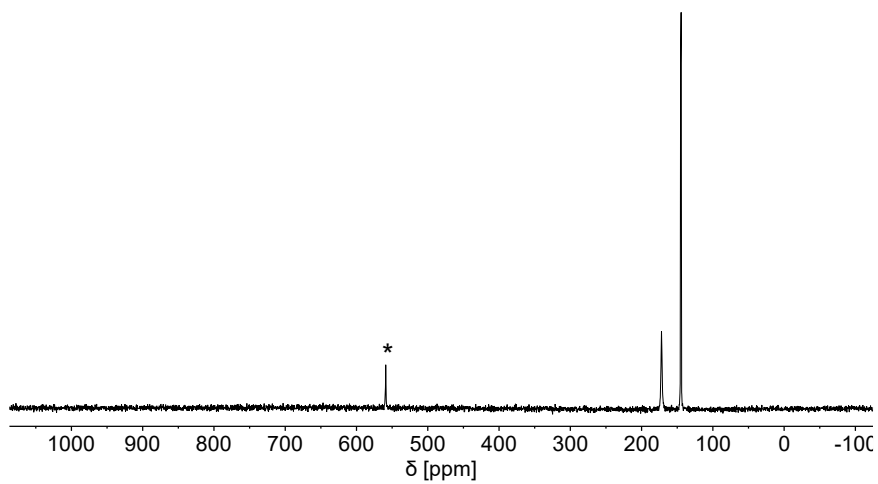
^{17}O 

Figure S 8. ^{17}O NMR spectrum (54 MHz, neat, external capillary*, 20 °C) of $\text{CF}_3\text{OSO}_2\text{F}$.

2. IR Spectra

2.1. CF_3OSF_5

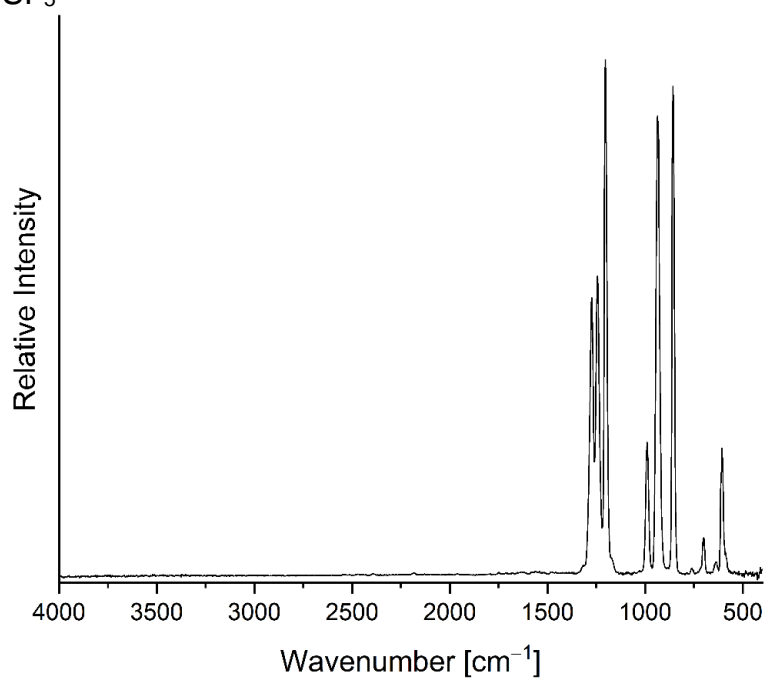


Figure S 9: Gas phase IR spectrum of CF_3OSF_5 .

1.1. $\text{CF}_3\text{OSO}_2\text{F}$

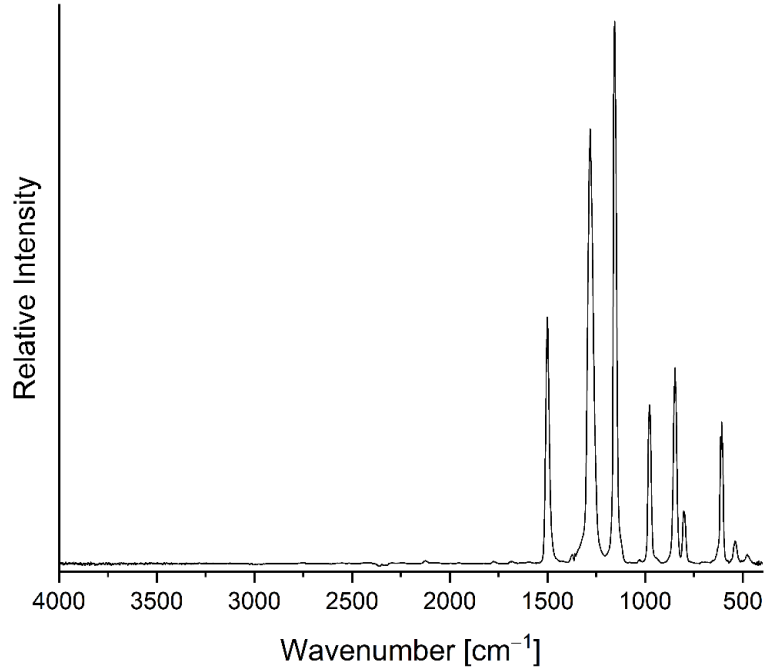


Figure S 10: Gas phase IR spectrum of $\text{CF}_3\text{OSO}_2\text{F}$.

Table S 1: Recorded and calculated (B3LYP-D3/def2-TZVP level of theory) gas phase IR bands [cm^{-1}] of CF_3OSF_5 and $\text{CF}_3\text{OSO}_2\text{F}$ with assignments.

Experimental		Calculated	Mode
$\text{CF}_3\text{OSO}_2\text{F}$			
1500	m	1498	$\nu_{\text{as}} \text{SO}_2$
1283	m	1265	$\nu_{\text{s}} \text{SO}_2$
1278	sh	1260	$\nu_{\text{as}} \text{CF}_3$
		1231	$\nu_{\text{as}} \text{CF}_3$
1155	vs	1128	νCO
978	m	958	$\nu_{\text{as}} \text{COS}$ & $\nu_{\text{s}} \text{CF}_3$
846	m	821	νSF
800	w	785	$\nu_{\text{s}} \text{COS}$ νSO
		618	δ
608	m	599	δ
540	w	531	δ
		523	δ
		465	δ
CF_3OSF_5			
1273	m	1246	$\nu_{\text{as}} \text{CF}_3$
1244	m	1209	$\nu_{\text{as}} \text{CF}_3$
1203	s	1175	νCO
990	m	974	$\nu_{\text{as}} \text{COS}$ & $\nu_{\text{s}} \text{CF}_3$
937	s	917	$\nu_{\text{as}} \text{SF}_4$
933	sh	901	$\nu_{\text{as}} \text{SF}_4$
857	s	832	$\nu_{\text{as}} \text{SF}_3\text{O}$ & νSO
760	w	735	$\nu_{\text{s}} \text{SF}_5\text{O}$ & $\nu_{\text{s}} \text{COS}$
700	w	682	δ
636	w	630	δ
607	m	586	δ
		577	δ
		519	δ

2. X-Ray Crystallography

The molecular structure in the solid state was determined by single-crystal X-ray diffraction using *in-situ* crystallization. The compounds of interest were condensed in capillaries with a diameter of $d_{\text{cap}} = 50 \mu\text{m}$ and a length of $l_{\text{cap}} = 3 \text{ cm}$. The substances were frozen inside the capillaries installed on the diffractometer and selectively melted to obtain a single crystal. The achieved crystals were measured in a cooled nitrogen stream with a temperature of -148°C for $\text{CF}_3\text{OSO}_2\text{F}$ and -147°C for CF_3OSF_5 .

Table S 2: Crystal data and refinement details for the analysis of the molecular structures in the solid state of $\text{CF}_3\text{OSO}_2\text{F}$ and CF_3OSF_5 .

	CF₃OSO₂F	CF₃OSF₅
Empirical formula	CF ₄ O ₃ S	CF ₃ OS
Formula weight	168.07	212.07
Temperature/K	128.90	125.00
Crystal system	monoclinic	orthorhombic
Space group	P2 ₁ /n	Pnma
a/Å	6.8807(4)	7.4421(2)
b/Å	8.1434(5)	5.89030(10)
c/Å	9.3004(6)	12.8423(3)
α/°	90	90
β/°	110.102(3)	90
γ/°	90	90
Volume/Å³	489.38(5)	562.96(2)
Z	4	4
ρ_{calc}/g/cm³	2.281	2.502
μ/mm⁻¹	6.509	6.642
F(000)	328.0	408.0
Crystal size/mm³	0.874 × 0.288 × 0.22	0.392 × 0.227 × 0.2
Radiation	CuKα (λ = 1.54178)	CuKα (λ = 1.54178)
2θ range for data collection/°	13.968 to 161.2	13.752 to 148.662
Index ranges	-8 ≤ h ≤ 8, -10 ≤ k ≤ 10, -11 ≤ l ≤ 11	-9 ≤ h ≤ 8, -7 ≤ k ≤ 6, -16 ≤ l ≤ 15
Reflections collected	5799	7778
Independent reflections	1043 [R _{int} = 0.0554, R _{sigma} = 0.0420]	633 [R _{int} = 0.0241, R _{sigma} = 0.0138]
Data/restraints/parameters	1043/0/82	633/0/62
Goodness-of-fit on F²	1.138	1.242
Final R indexes [I > 2σ (I)]	R ₁ = 0.0481, wR ₂ = 0.1366	R ₁ = 0.0439, wR ₂ = 0.1305
Final R indexes [all data]	R ₁ = 0.0548, wR ₂ = 0.1437	R ₁ = 0.0446, wR ₂ = 0.1317
Largest diff. peak/hole / e Å⁻³	0.56/-0.50	0.76/-0.76
CCDC deposition number	2308232	2308230

3. Quantum Chemical Calculations - Optimized Minimum Structures

xyz-Coordinates [Å] of CF₃OSO₂F on B3LYP-D3/def2-TZVP Level

S	-3.99703321494703	3.53569919774162	3.47641283955595
O	-5.39273595534200	2.85519613947360	3.90176977064325
F	-4.18649750625725	3.45450368853997	1.92913198369881
C	-6.58600799985127	3.58010111292198	3.97022674071594
F	-6.59001482793648	4.39555511319380	5.01406801604545
F	-7.54615198795166	2.68197930713037	4.10887026558564
F	-6.79268387701663	4.28626940430214	2.86322636375212
O	-3.00493578874805	2.59969882796162	3.83089484161348
O	-3.98101884194961	4.90520720873489	3.82378917838933

xyz-Coordinates [Å] of [CF₃OSO₂F]⁻ on BP86-D3/def2-QZVPP Level

F	3.87479790143556	-0.09027315984337	-0.76910725721708
C	3.57806979214112	1.06395774523025	-1.51998521730455
O	2.83965573167668	1.92146754554210	-0.95111048400381
S	0.76375391849021	0.89373633575350	-0.04783376015248
O	-0.10320699959446	-0.01083049926135	-0.81266592225728
O	0.84540849422793	0.71389349600876	1.40389910548237
F	0.01334445182321	2.38839888657699	-0.21512696605277
F	4.84540422885135	1.57769906824847	-1.86445866023341
F	3.09442248094838	0.53597058174464	-2.73333083826096

xyz-Coordinates [Å] of CF₃OSO₂F on BP86-D3/def2-QZVPP Level

F	3.83185774285207	1.24044750021112	-0.09585988552288
C	3.38885787006413	0.93080931011047	-1.32241180876397
O	2.06200629138057	1.36273690573310	-1.52572871992415
S	0.87936769469387	1.00276002157193	-0.45850098878081
O	-0.33005602222941	1.28619222196982	-1.15006809465314
O	1.16474213182260	-0.20878748130535	0.23635671882253
F	1.13513444541098	2.19251405878409	0.55326010438954
F	4.11631229269778	1.57469748361968	-2.23653184753897
F	3.50342755330739	-0.38735002069487	-1.51023547802812

xyz-Coordinates [Å] of [CF₃OSO₂F]⁺ on BP86-D3/def2-QZVPP Level

F	4.26148548377448	0.54641182215577	-0.42586665243002
C	3.56463193002232	0.82121810965548	-1.47266176097340
O	2.28070988822956	1.74753413641451	-0.83275686453001
S	0.97030195617486	1.17702319845019	-0.33217887332317
O	0.11097641900740	0.61181483256538	-1.37098730339831
O	1.09806137014146	0.18489905476560	0.73309316643974
F	0.34135836094616	2.45828737566850	0.21727240359611
F	4.07802342270916	1.68339297706382	-2.27033906452284
F	3.01406116899457	-0.20029150673925	-2.04429505085808

xyz-Coordinates [Å] of CF₃OSF₅ on B3LYP-D3/def2-TZVP Level

S	-0.65309547847796	1.95302997785704	0.56102372039177
F	0.41842797192561	0.89188342245286	0.08442689838631
O	-1.78817914218044	3.01209529132683	1.15010515872484
F	-1.78824134528219	1.09087653943528	-0.12969844723089
F	-0.44860541122662	2.75012546404490	-0.79308670734100
F	0.50871797087847	2.80030079243104	1.22465165487973
F	-0.84601346961892	1.15246950640472	1.90201366949548
C	-2.27741062483405	4.12365054932428	0.49672371724136
F	-3.17427821426885	4.64712754567607	1.32349346520782
F	-2.87814961339460	3.81914004492243	-0.65244944829407
F	-1.33232264352045	5.03136086612454	0.25740631853865

xyz-Coordinates [Å] of [CF₃OSF₅]⁻ on BP86-D3/def2-QZVPP Level

F	4.07784733106796	0.60367597758396	0.19993191540969
C	3.94602494768586	-0.24530732711732	1.30088767138274
O	2.83080332544127	-0.86158817159534	1.40566854654689
S	0.87770695525496	0.35680830883468	1.59499346914114
F	0.98712033432626	0.35543499023372	3.29121836170640
F	1.56270869530945	1.91491568696357	1.55108609386001
F	-0.58279368421438	1.05492133485579	1.73806313324291
F	0.67555064879643	0.39683848998190	-0.09252180471641
F	0.10987670984936	-1.15238115970833	1.64744885306799
F	5.01581563344217	-1.14828563875050	1.16996811793694
F	4.30819910304065	0.55757750871786	2.38602564242167

xyz-Coordinates [Å] of CF₃OSF₅ on BP86-D3/def2-QZVPP Level

F	3.90736624985309	0.66492370465285	0.21040348972718
C	3.76172938784777	-0.08535871214240	1.31553544674370
O	2.48677891946524	-0.62752207124046	1.43608126710733
S	1.06512514541972	0.26401853943088	1.57936330793209
F	1.20026802862411	0.25621782879666	3.17522349580303
F	1.80744143553605	1.68256536908107	1.53127007239425
F	-0.33875178060889	1.01532572625577	1.71995599911922
F	0.90579818819270	0.30270530822796	-0.01387553377305
F	0.31824907607332	-1.13963342739374	1.62807121088495
F	4.57407309166788	-1.14716191049937	1.22728266220073
F	4.12078225792900	0.64652964483079	2.38345858186055

xyz-Coordinates [Å] of [CF₃OSF₅]⁺ on BP86-D3/def2-QZVPP Level

F	3.84419431322391	0.69319435538249	0.24788021218014
C	3.95922593475488	-0.13281776367966	1.26153045483457
O	2.67941109319456	-0.58649805234590	1.77263203388483
S	0.83419380187997	0.37214343270406	1.60917587793310
F	0.95065465578178	0.33490951698148	3.17261619545325
F	1.62342778197362	1.72949759411629	1.60594829765353
F	-0.55958656086975	1.00265361453584	1.54965657472306
F	1.04812742619846	0.26374976903284	0.05825109308105
F	0.34493180506598	-1.11448587019341	1.62489084359033
F	4.63707227081601	-1.20772676049050	0.94164600012170
F	4.44720747798052	0.47799016395648	2.34854241654442

xyz-Coordinates [Å] of CF₂O on B3LYP-D3/def2-TZVP Level

C	-6.36049706486716	3.70633270722660	3.79556997979831
F	-6.39962168780350	4.75566754084975	4.59390096220196
F	-7.28622750223421	2.85878609079663	4.20125269259897
O	-5.63476374509512	3.55458366112702	2.88972636540075

xyz-Coordinates [Å] of CF₃OF on B3LYP-D3/def2-TZVP Level

F	-4.37696735038760	3.49245995300293	3.50524651764912
O	-5.43740290190848	2.74356974062012	4.08719325429226
C	-6.57600890569536	3.53063130152157	3.92478869236919
F	-6.47038097544015	4.69753415263530	4.54666232311017
F	-7.53523584806347	2.80112521308967	4.47894930301599
F	-6.85112401850493	3.75433963913041	2.64666990956327

xyz-Coordinates [Å] of SF₄ on B3LYP-D3/def2-TZVP Level

S	-0.90935838422390	2.04412929575756	0.57165916299697
F	0.38349990547637	1.27469710291719	-0.14785225250728
F	-2.27558639840450	2.83821621515271	1.10569356002533
F	-1.85057525075288	1.11798762076301	-0.27024966372584
F	-0.68230987209509	3.22883976540953	-0.42663080678917

xyz-Coordinates [Å] of SF₆ on B3LYP-D3/def2-TZVP Level

S	-0.78656163332748	2.12706183050449	0.55415791406485
F	0.30545910295515	1.15180443119114	-0.03639939513938
F	-1.87858570617542	3.10231859553818	1.14471647117897
F	-1.92294784270048	1.26103910403461	-0.11733146631277
F	-0.69540207543395	3.01669339595124	-0.74704338801010
F	0.34982187026544	2.99308303027275	1.22564844442572
F	-0.87772371558325	1.23742961250760	1.85536141979271

xyz-Coordinates [Å] of SO₂ on B3LYP-D3/def2-TZVP Level

S	-3.89290559658771	-0.16240315145485	0.02217967335872
O	-2.45891062918165	-0.08592865822493	-0.06755336003146
O	-4.48206377423064	-1.01386819032022	1.02126368667275

xyz-Coordinates [Å] of SO₂F₂ on B3LYP-D3/def2-TZVP Level

S	0.42294258675863	0.42294262494574	-0.0000000618518
F	-0.59703273528630	-0.03550521291870	1.07915000665349
F	-0.03550514614596	-0.59703273116361	-1.07914995510455
O	1.71354305501558	0.05292220621350	0.43045431156562
O	0.05292223965805	1.71354311292307	-0.43045435692939

4. Determination of Critical Parameters

The critical point was determined optically by observing an opalescence between the liquid and the gas phase of the substance of interest, realized by using a pressure-resistant fused quartz tube containing a sample of the investigated gas (Figure S 11). The tube was located inside an autoclave with a transpicuous window connected to an adjustable thermostat (*RTE-101*, NESLAB INSTRUMENTS Inc. Newington, NH, USA) containing a heat transfer fluid. Two thermocouples were used to determine the temperature of the heating reagent at the thermostat and at the sample. The vapor pressure was measured using a pressure sensor (*PMP 41-RE13S1A11MA*, 40 bar, Endress+Hauser AG, Reinach, Switzerland), which was directly connected to the fused quartz tube. The used equipment was evacuated using a vacuum pump (*XDS10*, Edwards Ltd, Burgess Hill, United Kingdom). The resulting vacuum can be checked by a further pressure sensor (*Type 3247.069.192*, 1 bar, KOBOLD Messring GmbH, Hofheim am Taunus, Germany). To fill the tube with the substance of interest, it was possible to connect the tube to a gas supply like a gas cylinder. Several regulating valves were used to separate different parts of the system from each other.

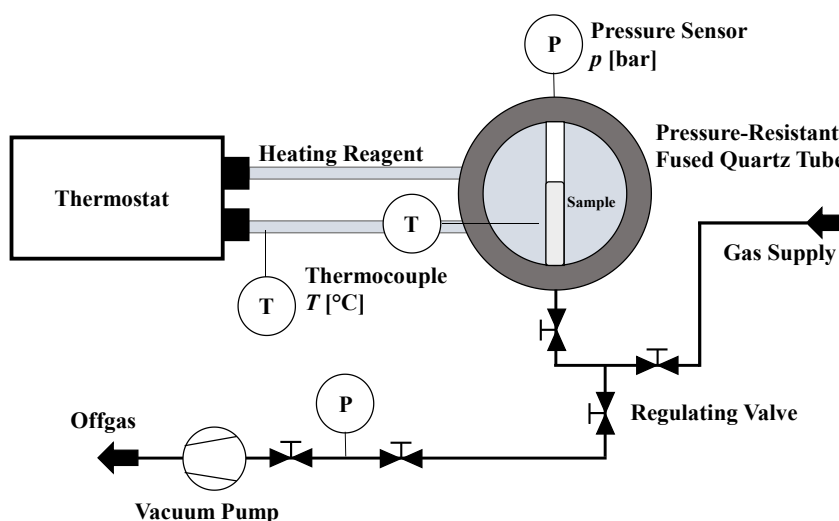


Figure S 11. Schematic representation of the used equipment for the determination of the critical point of gases

The used equipment enabled the measurement of the vapor pressure curve by a slow increase of the temperature of the system resulting in an additional pressure increase. After observing an opalescence, the measured pressure and temperature were checked by observing the opalescence at this point several times. The critical temperature T_{crit} and the critical pressure p_{crit} were determined by averaging the measured values (Table S 3).

Table S 3. Measured and averaged values of the critical temperature T_{crit} [°C] and the critical pressure p_{crit} [bar] of CF_3OSO_2F and CF_3OSF_5 .

Substance	Measurement Number	T_{crit} [°C]	p_{crit} [bar]
CF_3OSO_2F	1	123.0	32.9
	2	123.3	31.9
	3	123.4	32.1
	4	123.6	32.1
	5	123.7	32.2
	6	123.8	32.1
	Average	123.5	32.2
CF_3OSF_5	1	110.4	28.6
	2	110.5	28.6
	3	110.6	28.7
	4	110.7	28.7
	5	110.8	28.6
	6	111.0	28.8
	Average	110.7	28.7

The *Van Der Waals*-constants a and b of the gases were determined from their critical temperatures T_{crit} and critical pressures p_{crit} (Table S 4) by use of Equation 1 - 3.

$$p = \frac{nRT}{V - nb} - \frac{n^2a}{V^2} \quad (1)$$

$$a = \frac{27(RT_{crit.})^2}{64 p_{crit}} \quad (2)$$

$$b = \frac{RT_{crit.}}{8 p_{crit}} \quad (3)$$

To validate the applied method, the critical point of SF_6 was measured and the VAN DER WAALS-constants a and b were calculated using the corresponding equations. The values were compared to the literature-known values of SF_6 (Table S 4).

Table S 4: Critical temperature T_{crit} [°C], critical pressure p_{crit} [bar] and *Van der Waals*-constants a [bar L² mol⁻²] and b [L mol⁻¹] for CF_3OSO_2F and CF_3OSF_5 .¹⁾

	CF_3OSO_2F	CF_3OSF_5	SF_6
T_{crit} [°C]	123.5 ± 0.5	110.7 ± 0.5	45.8 ± 0.5 (45.5)
p_{crit} [bar]	32.2 ± 0.2	28.7 ± 0.2	37.6 ± 0.2 (37.5)
a [bar L ² mol ⁻²]	14.239	14.980	7.893 (7.857)
b [L mol ⁻¹]	0.128	0.139	0.088 (0.088)

1) Values known from Literature^[44] are given in parentheses.

5. Determination of Melting Point

The melting points of $\text{CF}_3\text{OSO}_2\text{F}$ ($-4.2\text{ }^\circ\text{C}$ ^[24]) and CF_3OSF_5 ($-10\text{ }^\circ\text{C}$ ^[23]) were re-examined. The measurements were performed by using fused glass capillaries filled with the investigated gas. The substance was frozen using liquid nitrogen and put inside a cooling bath containing liquified propane tempered with liquid nitrogen. The temperature of the bath was measured using a thermocouple (*GTH 175/Pt 1000*, GHM GROUP – Greisinger, Regenstauf, Germany).

While the cooling mixture warmed up slowly the temperature at the beginning of the optically observed liquification of the solid sample was recorded. The observed melting points of $\text{CF}_3\text{OSO}_2\text{F}$ and CF_3OSF_5 were -156.5 ± 0.5 and -161.6 ± 0.5 [$^\circ\text{C}$], respectively.

6. Determination of Gas Densities

The density ρ was determined by weighing the mass of the gas m in a defined volume as a function of the pressure p and the temperature T of the gas. A 500 mL round bottom flask with a RETTBERG-PTFE Valve and a determined gas volume of 540.4 mL was used in these experiments. The flask was tempered by a water bath heated with an electric magnetic stirrer (*IKA® RCT standard safety control*, IKA-Werke, Staufen im Breisgau, Germany) and the mass of the gas was determined by an analytical balance (*LA 314i*, VWR International, Radnor, PA, USA). The temperature was measured using a thermocouple (*GTH 175/Pt 1000*, GHM GROUP – Greisinger, Regenstauf, Germany). Each measurement carried out at least three times. The densities ρ_{ext} were determined by extrapolation of the measured values to the atmospheric pressure $p_0 = 1.013$ bar (Table S 5).

Table S 5: Estimation of gas densities ρ_0 [kg m^{-3}] of $\text{CF}_3\text{OSO}_2\text{F}$ and CF_3OSF_5 .¹⁾

Measured gas mass m [kg], measured temperature of external heat supply T [$^\circ\text{C}$], measured gas pressure p [bar] and measured ρ_{meas} [kg m^{-3}] and extrapolated ρ_{ext} gas density of $\text{CF}_3\text{OSO}_2\text{F}$ and CF_3OSF_5

Substance	T [$^\circ\text{C}$]	p [bar]	m [1×10^{-3} kg]	ρ_{meas} [kg m^{-3}]	ρ_0 [kg m^{-3}]
$\text{CF}_3\text{OSO}_2\text{F}$	26.0	1.009	3.802	7.04	7.07 ± 0.07
		1.000	3.770	6.98	
		1.000	3.767	6.97	
	27.2	1.019	3.845	7.12	7.10 ± 0.07
		1.013	3.837	7.10	
		1.005	3.816	7.06	
CF_3OSF_5	26.0	1.017	4.831	8.90	8.88 ± 0.09
		1.019	4.849	8.97	
		1.027	4.882	9.03	

1) m [kg] gas mass, T [$^\circ\text{C}$] temperature of external heating medium, p [bar] gas pressure, ρ_{meas} [kg m^{-3}] measured gas density, ρ_{ext} gas density extrapolated to $p_0 = 1.013$ bar. Literature known gas density of $\text{CF}_3\text{OSO}_2\text{F}$ $\rho = 7.46\text{ kg m}^{-3}$ at $20\text{ }^\circ\text{C}$.^[24]

7. Determination Vapor Pressures and Boiling Points

The vapor pressure p_v was measured in a small stainless-steel vessel (~10 mL) equipped with a pressure sensor (*SolidSenseII-GFD00B5PSF*, 2 bar, Brooks Instruments, USA). The vessel was tempered in an ethanol cooling bath connected to an adjustable thermostat (CC-902, Peter Huber Kaeltemaschinenbau SE, Germany) with an external PT100 thermocouple (Figure S 12). The gasses ~5 mL (liquid) were condensed into the vessel by use of liquid nitrogen and the vessel was then transferred into the cooling bath. p_v was determined in several heating or cooling cycles at temperatures around the expected boiling point with temperature steps of 1K. Each measurement was carried out at least three times. The vapor pressure curves were fitted by using a multiple linear regression (Equation 4) where a_0 , a_1 , and a_2 are constants from which the Antoine parameters A , B , and C were calculated (Table S 7, Equations 5 to 7). The boiling points (Table S 7) were calculated at atmospheric pressure $p_0 = 1.013$ bar using the Antoine parameters.

$$\log(p_v) = a_0 + a_1 \cdot \frac{1}{T} + a_2 \cdot \frac{\log(p_v)}{T} \quad (4)$$

$$A = a_0 \quad (5)$$

$$B = a_0 \cdot a_2 - a_1 \quad (6)$$

$$C = -a_2 \quad (7)$$

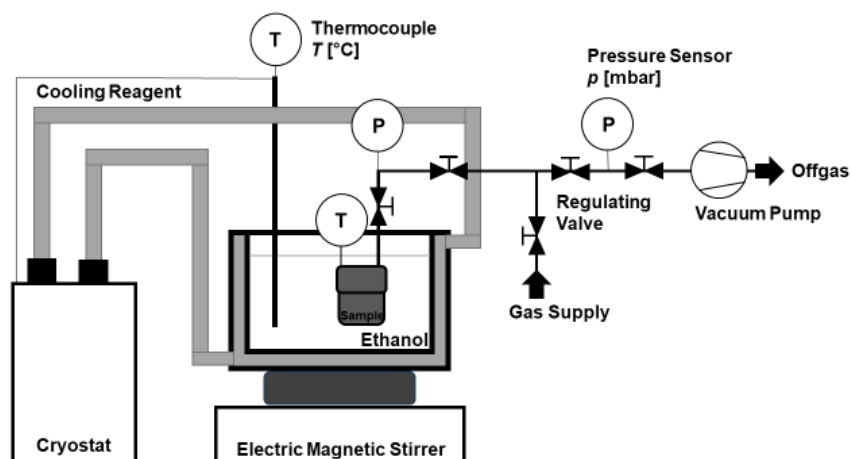


Figure S 12 Schematic representation of the equipment used for the determination of the vapor pressure of gases.

Table S 6: Averaged vapor pressures p_v of CF_3OSF_5 and $\text{CF}_3\text{OSO}_2\text{F}$.

CF_3OSF_5			$\text{CF}_3\text{OSO}_2\text{F}$		
T [K]	T [°C]	p_v [bar]	T [K]	T [°C]	p_v [bar]
257.15	-16.0	0.805	263.15	-10.0	0.837
258.15	-15.0	0.839	264.15	-9.0	0.869
259.15	-14.0	0.875	265.15	-8.0	0.908
260.15	-13.0	0.912	266.15	-7.0	0.949
261.15	-12.0	0.952	267.15	-6.0	0.981
262.15	-11.0	0.992	268.15	-5.0	1.028
263.15	-10.0	1.034	269.15	-4.0	1.069
264.15	-9.0	1.077	270.15	-3.0	1.115
265.15	-8.0	1.120	271.15	-2.0	1.160
266.15	-7.0	1.166	272.15	-1.0	1.199
267.15	-6.0	1.212	273.15	0.0	1.253

Table S 7: Determined Antoine parameters A, B, C¹⁾ and boiling points b.p [°C]²⁾ of CF_3OSF_5 and $\text{CF}_3\text{OSO}_2\text{F}$.¹⁾

Substance	CF_3OSF_5	$\text{CF}_3\text{OSO}_2\text{F}$
A	3.5546	1.0319
B	709.9924	59.2839
C	-62.6017	-209.9254
Temperature Range ΔT [K]	257.15 – 267.15	263.15 – 273.15
b.p. [°C]	-10.5 ± 0.5	-5.5 ± 0.5

1) Antoine parameters are valid for the equation $\log_{10}(p_v) = A - \frac{B}{(T+C)}$ where p_v [bar] and T [K], 2) at atmospheric pressure $p_0 = 1.013$ bar.

8. Determination of Dielectric Properties and Breakdown Voltages

The electrical discharge properties of SF_6 , $\text{CF}_3\text{OSO}_2\text{F}$, and CF_3OSF_5 were determined by measuring their breakdown voltages U_{BD} at different electrode distances $d_{\text{el.dist.}}$ and an initial pressure of $p_i = 0.1$ bara. The measurements were performed using an adjusted 250 mL round bottom flask equipped with a YOUNG valve and two adapters for the electrodes (Figure S 13). The flask was connected to a glass line equipped with a pressure sensor (626BX13MDE, 1000 mbar, MKS Instruments Deutschland GmbH, Munich, Germany) a infrared cell with silicon windows with an additional pressure sensor (626AX12MDE, 100 mbar, MKS Instruments Deutschland GmbH, Munich, Germany) and gas supply cylinders. The Infrared cell was placed in the sample compartment of a FT IR spectrometer (Vector 22, Bruker Corporation, Billerica, MA, USA). A vacuum pump (TRIVAC D4B, Leybold GmbH, Cologne, Germany) was used to evacuate the system. The used electrodes were made of stainless steel in a cylindrical shape with a diameter of $d = 0.5$ cm and were connected to a transformer consisting of two electromagnetic inductors (562 14, 500 coils and 562 17, 23000 coils, both Leybold GmbH, Cologne, Germany). The transformer amplified the voltage U from a power supply (E401HB/080, 0 – 260 V, FILEC, Uden, Netherlands) by a factor of 46. A multimeter (0330HD Digital Multimeter, Dominique DUTSCHER SAS, Bernolsheim, France) was used to determine the applied voltage U .

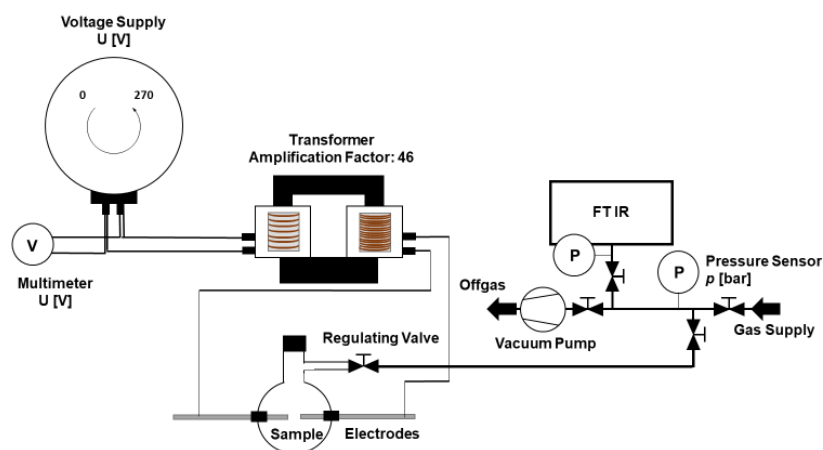


Figure S 13: Schematic representation of the equipment used for the determination of the dielectric discharge and breakdown properties of gases.

The breakdown voltage U_{BD} was measured at least three times for each selected electrode distance $d_{el.dist.}$ and averaged (Table S 8). The relative dielectric strengths (DS) compared to SF_6 of CF_3OSO_2F , and CF_3OSF_5 were calculated from the averaged values for U_{BD} at the selected $d_{el.dist.}$ (Table S 9).

Table S 8: Measured breakdown voltage U_{BD} [kV] for selected electrode distance $d_{el.dist.}$ [cm] of SF_6 , CF_3OSO_2F and CF_3OSF_5 .

$d_{el.dist.}$ [cm]	SF_6		CF_3OSO_2F		CF_3OSF_5	
	U_{BD} [kV]	av. U_{BD} [kV]	U_{BD} [kV]	av. U_{BD} [kV]	U_{BD} [kV]	av. U_{BD} [kV]
0.2	1.8 ± 0.2		2.9 ± 0.2		3.0 ± 0.2	
	1.9 ± 0.2	1.9 ± 0.2	2.7 ± 0.2	2.7 ± 0.2	2.9 ± 0.2	3.0 ± 0.2
	2.1 ± 0.2		2.6 ± 0.2		3.1 ± 0.2	
0.3	2.5 ± 0.2		3.4 ± 0.2		4.3 ± 0.2	
	2.7 ± 0.2	2.6 ± 0.2	3.5 ± 0.2	3.5 ± 0.2	4.1 ± 0.2	4.2 ± 0.2
	2.7 ± 0.2		3.5 ± 0.2		4.3 ± 0.2	
0.4	3.9 ± 0.2		4.4 ± 0.2		5.0 ± 0.2	
	4.0 ± 0.2	3.9 ± 0.2	4.5 ± 0.2	4.5 ± 0.2	4.8 ± 0.2	4.9 ± 0.2
	3.8 ± 0.2		4.5 ± 0.2		4.8 ± 0.2	
0.5	4.3 ± 0.2		5.4 ± 0.2		5.6 ± 0.2	
	4.5 ± 0.2	4.4 ± 0.2	5.3 ± 0.2	5.3 ± 0.2	5.8 ± 0.2	5.8 ± 0.2
	4.5 ± 0.2		5.3 ± 0.2		6.0 ± 0.2	
0.8	5.7 ± 0.2		8.1 ± 0.2		7.4 ± 0.2	
	6.0 ± 0.2	5.9 ± 0.2	8.4 ± 0.2	8.2 ± 0.2	7.8 ± 0.2	7.6 ± 0.2
	5.9 ± 0.2		8.1 ± 0.2		7.5 ± 0.2	
1	6.8 ± 0.2		9.5 ± 0.2		10.3 ± 0.2	
	6.8 ± 0.2	6.8 ± 0.2	9.5 ± 0.2	9.4 ± 0.2	9.1 ± 0.2	9.7 ± 0.2
	6.9 ± 0.2		9.3 ± 0.2		9.6 ± 0.2	

Table S 9: Dielectric strength DS relative to SF_6 of CF_3OSO_2F and CF_3OSF_5 at selected electrode distances $d_{el.dist.}$ [cm] and averaged.

$d_{el.dist.}$ [cm]	DS relative to SF_6		
	SF_6	CF_3OSO_2F	CF_3OSF_5
0.2	1.0	1.4 ± 0.2	1.6 ± 0.2
0.3	1.0	1.3 ± 0.2	1.6 ± 0.2
0.5	1.0	1.2 ± 0.2	1.3 ± 0.2
0.8	1.0	1.2 ± 0.2	1.3 ± 0.2
1.0	1.0	1.4 ± 0.2	1.3 ± 0.2
Av.	1.0	1.3 ± 0.2	1.4 ± 0.2

9. Stability of Dielectric Gases during Breakdown

The gases $\text{CF}_3\text{OSO}_2\text{F}$ and CF_3OSF_5 were exposed to an electric arc for a time-period of 10 s and then analyzed using IR spectroscopy. The experimental set-up shown in Figure S 13 was used. The initial gas pressure was adjusted to $p_i = 0.1$ bara and the undecomposed dielectric amount φ [%] was estimated from its partial pressure p_{rem} direct after the arc exposition, which was obtained by integration of the area of a characteristic band in the IR spectrum (Table S 10). IR spectra of $\text{CF}_3\text{OSO}_2\text{F}$ and CF_3OSF_5 were recorded at different pressures as reference (Figure S 14 -Figure S 15). Each measurement was performed a at least three times.

Table S 10: Estimated partial pressure p_{rem} [mbar] and relative amount of undecomposed dielectric φ [%] of $\text{CF}_3\text{OSO}_2\text{F}$ and CF_3OSF_5 .

$d_{el.dist.}$ [cm]	$\text{CF}_3\text{OSO}_2\text{F}$			CF_3OSF_5		
	p_{rem} [mbar]	φ [%]	av. φ [%]	p_{rem} [mbar]	φ [%]	av. φ [%]
0.2	3.487	98.2	99.5	3.278	92.6	93.9
	3.505	100.1		3.307	92.9	
	3.55	100.0		3.392	96.1	
0.3	3.494	98.7	97.8	2.715	76.5	80.4
	3.433	97.8		2.766	78.4	
	3.4	96.9		3.074	86.3	
0.4	3.233	91.1	89.4	1.69	47.5	48.0
	3.26	90.6		1.56	45.1	
	3.102	86.4		1.815	51.4	
0.5	2.911	82.7	83.5	0.879	25.3	24.1
	3	84.0		0.823	23.7	
	3.002	83.9		0.818	23.4	
0.8	1.874	53.1	48.0	0.721	20.5	18.6
	1.572	44.8		0.57	16.0	
	1.642	46.2		0.682	19.3	
1	1.473	41.8	41.9	0.671	19.3	18.0
	1.415	40.2		0.614	17.7	
	1.541	43.5		0.596	17.0	

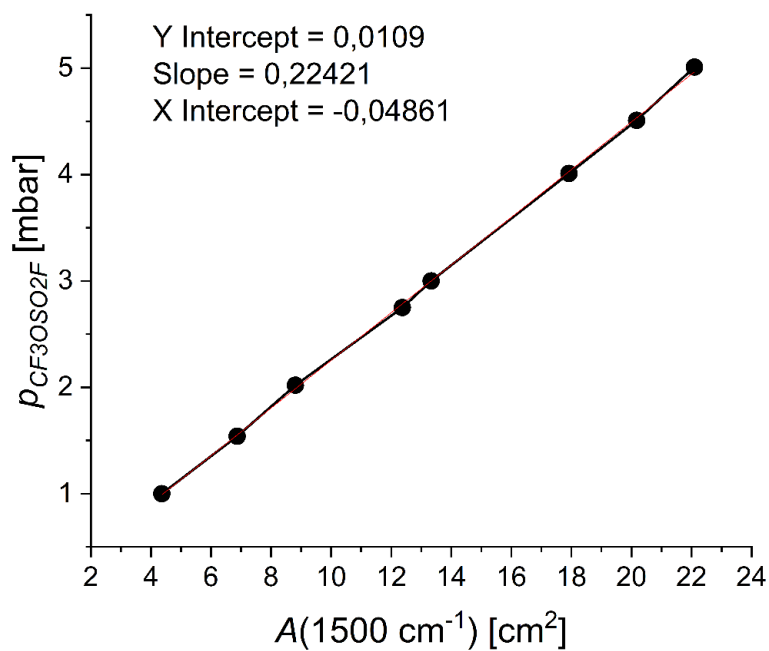


Figure S 14: Relation between the area of the characteristic peak $A(1500\text{ cm}^{-1})$ [cm²] and the measured partial pressure $p(\text{CF}_3\text{OSO}_2\text{F})$ [mbar] to calculate the remaining relative dielectric amount φ [%] of trifluoromethyl fluorosulfonate ($\text{CF}_3\text{OSO}_2\text{F}$).

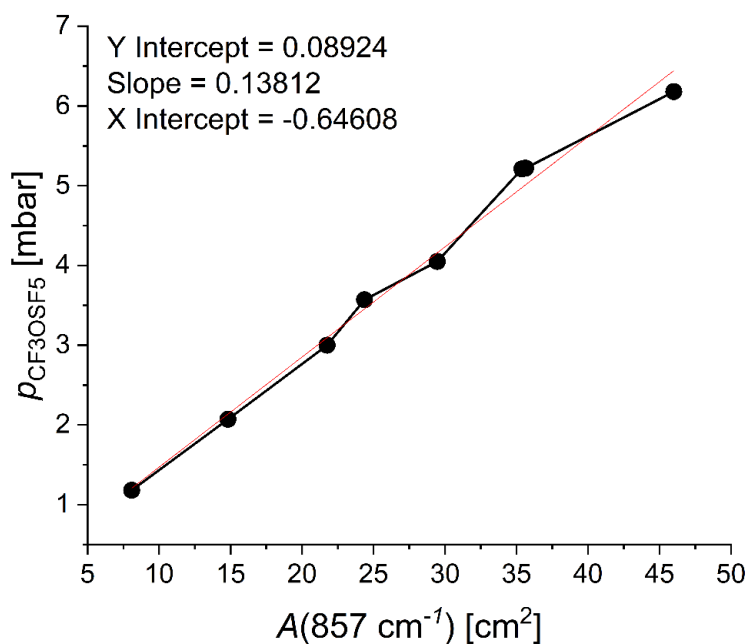


Figure S 15: Relation between the area of the characteristic peak $A(857\text{ cm}^{-1})$ [cm²] and the measured partial pressure $p(\text{CF}_3\text{OSF}_5)$ [mbar] to calculate the remaining relative dielectric amount φ [%] of trifluoromethoxy sulfur pentafluoride (CF_3OSF_5).

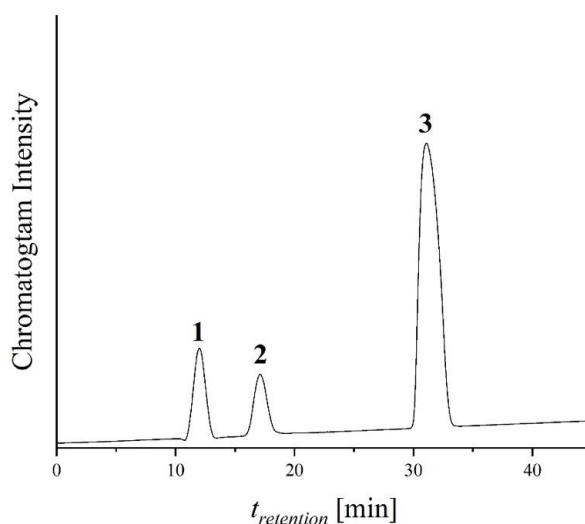
10. Decomposition Products

The substance mixtures obtained after several breakdown measurements of $\text{CF}_3\text{OSO}_2\text{F}$ and CF_3OSF_5 were collected and characterized by separating the individual components using a GCIR system, which was equipped with a TG-SQC GC-column (*TraceGOLD*TM, Thermo Fisher Scientific, Waltham, MA, USA), and operated with a controlled temperature gradient as shown in (8).

$$T_1 = 35\text{ }^\circ\text{C} \xrightarrow{t=3\text{ min}} T_2 = 95\text{ }^\circ\text{C} \xrightarrow{t=15\text{ min}} T_3 = 140\text{ }^\circ\text{C} \xrightarrow{t=10\text{ min}} T_4 = 180\text{ }^\circ\text{C} \xrightarrow{t=2\text{ min}} T_5 = 200\text{ }^\circ\text{C} \quad (8)$$

10.1. $\text{CF}_3\text{OSO}_2\text{F}$

Table S 11: Gas chromatogram of the gas mixtures collected after exposure of $\text{CF}_3\text{OSO}_2\text{F}$ to an electric arc. Signals are assigned to CF_2O (1), SO_2F_2 (2) and $\text{CF}_3\text{OSO}_2\text{F}$ (3). Retention times, $t_{\text{retention}}$ [min], and characteristic FTIR band positions, $\tilde{\nu}$ [cm^{-1}], are given below.



Peak	$t_{\text{retention}}$ [min]	Compound
1	12.018	CF_2O
2	17.141	SO_2F_2
3	31.119	$\text{CF}_3\text{OSO}_2\text{F}$

IR (FTIR), Peak 1: $\tilde{\nu} = 2499$ (vw), 2359 (s), 2322 (m), 2183 (vw), 1958 (s), 1929 (s), 1555 (vw), 1280 (m), 1256 (vs), 1231 (s), 1027 (vs), 978 (w), 959 (w), 799 (vw), 774 (w), 750 (vw) cm^{-1} .

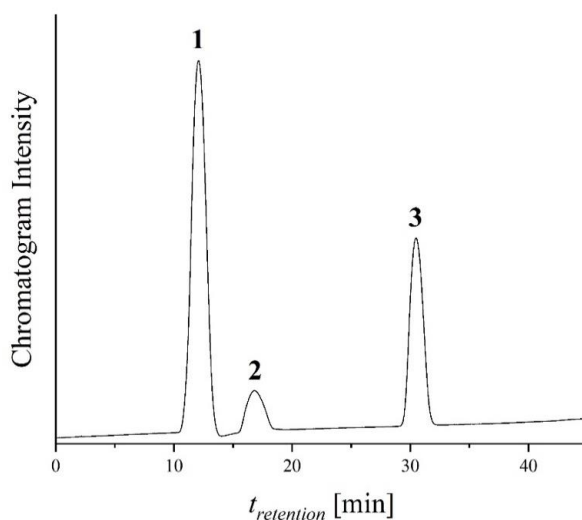
IR (FTIR), Peak 2: $\tilde{\nu} = 1517$ (m), 1502 (vs), 1488 (m), 1338 (w), 1283 (m), 1268 (s), 1027 (vw), 944 (w), 898 (m), 883 (s), 865 (s), 846 (s), 807 (m), 807 (w), 744 (w) cm^{-1} .

IR (FTIR), Peak 3: $\tilde{\nu} = 1497$ (vs), 1284 (vs), 1271 (vs), 1157 (vs), 1149 (vs), 977 (s), 846 (s), 798 (w) cm^{-1} .

1) Relative IR band intensities are given in parentheses: vw = very weak, m = medium, s = strong, vs = very strong.

10.2. CF₃OSF₅

Table S 12: Gas chromatogram of the gas mixtures collected after exposure of CF₃OSF₅ to an electric arc. Signals are assigned to CF₂O (1), SF₆ (2) and CF₃OSF₅ (3). Retention times, $t_{\text{retention}}$ [min], and characteristic FTIR band positions, $\tilde{\nu}$ [cm⁻¹], are given below.



Peak	$t_{\text{retention}}$ [min]	Compound
1	12.169	CF ₂ O
2	16.872	SF ₆
3	30.528	CF ₃ OSF ₅

IR (FTIR), Peak 1: $\tilde{\nu}$ = 2476 (vw), 2359 (w), 2323 (w), 2183 (vw), 1958 (s), 1928 (vs), 1558 (vw), 1539 (vw), 1279 (ws), 1256 (ws), 1238 (ws), 1027 (m), 977 (w), 959 (w), 798 (vw), 774 (w), 750 (vw) cm⁻¹.

IR (FTIR), Peak 2: $\tilde{\nu}$ = 981 (vw), 943 (vs) cm⁻¹.

IR (FTIR), Peak 3: $\tilde{\nu}$ = 1269 (m), 1244 (m), 1200 (s), 988 (w), 933 (vs), 855 (s), 759 (vw), 700 (w) cm⁻¹.

1) Relative IR band intensities are given in parentheses: vw = very weak, m = medium, s = strong, vs = very strong.

10.3. References

- [23] G. Pass, H. L. Roberts, *Inorg. Chem.* **1963**, 2, 1016.
- [24] W. P. van Meter, G. H. Cady, *J. Am. Chem. Soc.* **1960**, 82, 6005.
- [44] a) D. Atack, W. G. Schneider, *J. Phys. Chem.* **1951**, 55, 532, b) A. Diefenbacher, M. Türk, *Fluid Phase Equilib.* **2001**, 182, 121; c) K. Morofuji, K. Fujii, M. Uematsu, K. Watanabe, *Int. J. Thermophys.* **1986**, 7, 17.